THE STEADY PERFORMANCE OF COMPLIANT-SURFACE AEROSTATIC THRUST BEARINGS

by

Milan Stanojevic M.Sc.

A Thesis submitted in fulfilment of the requirements for the Degree of Doctor of Philosophy

Department of Mechanical Engineering
The University of Aston in Birmingham

July 1976

LAYOUT OF THE THESIS

Title Page

Summary

Motto of the Thesis

Dedication

Acknowledgements

Notation

List of Photographs

Contents

Eight Chapters

Four Appendices

List of References

SUMMARY

The object of the research is to predict and confirm the predicted steady performance of aerostatic compliant surface thrust bearings. The use of a compressible lubricant (air) instead of an incompressible lubricant (oil) forms a natural extension of previous work, on hydrostatic bearings [201] to [205] .

The design of the main experimental apparatus was assisted by the theory of Dowson and Taylor [201] modified for compressible lubricants.

A subsidiary experimental apparatus to determine the bulk modulus of the elastomers to be used was also constructed and the design was similar in principle of operation to one described by Rightmire [305].

Experiments were first performed on rigid bearings to develop the rig. A method of predicting load capacity was developed which was considerably simpler than previous theory [108]. The theory lines agreed well with the experiments if the experimentally determined discharge coefficient and the roughness of bearing surfaces are taken into account.

Experimental determination of elastomer properties, i.e. bulk modulus and elastic modulus, indicated that the former is several orders of magnitude larger than the latter. This means that the Poisson's ratio of these elastomers is very close to 0.5 and the governing elastic equations, obtained by

extending Dowson's theory, had to be modified further to account for nearly incompressible or completely incompressible elastomers. A mathematical model has therefore been established and an attempt has been made to solve the equations by finite difference methods.

The performance of various elastomers bonded to one rigid surface with varying aspect ratio and hardness was compared with the performance of unbonded elastomers and to rigid bearing performance. It was discovered that the unbonded elastomers have inferior performance to bonded ones, but they are superior to rigid bearings and they also have advantages such as quick removal and easy exchange of damaged compliant layers.

" The philosopher may be delighted with the extent of his views, the artificer with the readiness of his hands, but let the one remember that without mechanical performance, profound speculation is but an idle dream, and the other that without theoretical prediction dexterity is little more than brute instinct."

Dr. S. Johnson

To My Wife Bruna

ACKNOWLEDGEMENTS

I would like to express my gratitude to the University of Aston for the award of a postgraduate studentship in Tribology which made this work possible.

My profound thanks are conveyed to Dr. G.K. Lewis, my Supervisor, for his creative thinking and constant help throughout this project.

My sincere appreciation is given to the laboratory staff of the Mechanical Engineering Department for their excellent work in making and rectifying experimental facilities for this research project, particularly to Messrs. Pratt, Green, Pizer, Smith and Holtom.

I would like to thank Messrs. Hopkins and Burton of the Metrology Laboratory for providing help in using measuring instruments.

My thanks are given to Mr. J.E. Stuckey of the Chemistry Department for providing an elastomer formula and to Mr. Hughes for his help in making rubber components.

I would also like to thank Mr. T.H. Richards for his excellent set of lectures in Solid Mechanics and to Messrs. Ohuonu, Taylor, Tahan, Jliev, Rakić, Gligić and Holliday for discussions and encouragement.

Special thanks are conveyed to Mrs. M. Bellamy for her patience in typing the manuscript.

NOTATION

Symbol	Name	Dimension
A_r	Restrictor area	L^2
A_p	Cross sectional area of the perspex tube	L^2
A_2	Parameter	-
A	Bearing area	L^2
C_D	Discharge coefficient	-
$C_{ijk\ell}$	Elastic constants tensor	F/L^2 or $M/(LT^2)$
D	Effective bearing diameter	L
E	Elastic modulus	F/L^2 or $M/(LT^2)$
E^1	Equivalent elastic modulus in Dowson's theory	F/L^2 or $M/(LT^2)$
F	Absolute film pressure squared	F^2/L^4 or $M^2/(L^2T^4)$
G	Modulus of elasticity in shear (one of the Lamé constants)	F/L^2 or $M/(LT^2)$
$\bar{H}=\frac{h}{h_o}$	Dimensionless film thickness for compliant bearings	—
$H=\frac{h}{r_o}$	Dimensionless film thickness for rigid bearings	—
I	Integral in the expression for load	—
J	Integer number	—
K	Bulk modulus	F/L^2 or $M/(LT^2)$
L	Bearing parameter in modified Dowson's theory	—
L_C	Capillary length	L
M	Mass flow rate	FT/L or M/T
$\bar{M}$	Dimensionless mass flow	—
P	Dimensionless pressure	—

Symbol	Name	Dimension
P_p	Dimensionless port pressure	-
P_s	Dimensionless supply pressure	-
Q	Volumetric flow	L^3/T
Q_a	Volumetric flow at outer bearing radius r_o	L^3/T
Q_p	Volumetric flow at inlet radius r_p	L^3/T
R	Dimensionless radius	-
R_p	Dimensionless port radius	-
R_a	Gas constant for air	$L^2 (T^2 {}^oK)$
Re	Reynolds number	-
S	Stiffness	F/L or M/T^2
$\bar{S}$	Dimensionless stiffness	-
S_e	Elastomer shape factor	-
SF	Surface roughness effects	L
T_a	Ambient and film air temperature	^oK
V	Elastomer volume	L^3
W	Bearing load	F or ML/T^2
$\bar{W}$	Dimensionless load	-
$\bar{W}_e$	Dimensionless load calculated by error functions	-
$\bar{W}_s$	Dimensionless load calculated by Sympson's Rule	-
b	Elastomer thickness in a contact problem (fig.4)	L
c	Cylinder radius (fig.4)	L
$c^1=\frac{h_a G}{tp_a}$	Dimensionless apparent film thickness	-

Symbol	Name	Dimension
$c_u(i)$	Coetficient of u in finite difference expression	–
$c_w(i)$	Coefficient of w in finite difference expression	–
d	Diameter of the capillary or orifice	L
d_o	Outer bearing diameter	L
d_p	Inner diameter of perspex tube	L
e_r	Radial strain	–
e_θ	Circumferential strain	–
e_z	Axial strain	–
$e_{r\theta}$	Strain in r, θ plane	–
$e_{\theta z}$	Strain in θ, z plane	–
e_{zr}	Strain in z, r plane	–
e_{ij}	Strain in subscript notation	–
$\hat{e}_{ij}$	Strain deviator	–
e_{kk}	$(= e_r+e_\theta+e_z)$ volumetric strain	–
g	Acceleration	–
h	Film thickness	L
h_o	Uniform bearing clearance as if there is no deformation of the elastomer	L
h_a	Apparent film thickness	L
h_m	Measured film thickness	L
k	A factor used to calculate compression characteristics of elastomers	–
k_c	Capillary coefficient	L^3

Symbol	Name	Dimension
p_g	Gauge film pressure	F/L^2 or $M/(LT^2)$
p	Absolute film pressure	F/L^2 or $M/(LT^2)$
p_a	Ambient pressure	"
p_p	Absolute port pressure	"
p_s	Absolute supply pressure	"
q	Flow parameter	—
q_r	Volumetric flow per unit length	L^2/T
r	Radial coordinate	L
r_p	Port radius	L
r_o	Outer bearing radius	L
t	Elastomer thickness	L
t_o	Initial elastomer thickness	L
u	Elastomer displacement in the radial direction	L
u_e	Preload deflection (ref. [219])	L
v_{mean}	Mean flow velocity (= Q/A)	L/T
v_r	Radial velocity of fluid	"
v_θ	Circumferential velocity of fluid	"
v_z	Axial velocity of fluid	"
w_g	Load parameter	—
w	Elastomer displacement in the axial direction	L
z	Axial coordinate	L
ΔH_S	Real displacement of water level under given pressure with elastomer in rig	L
ΔH_D	Real displacement of water level under given pressure with dummy steel disc in rig	L
$\Delta H_S(T)$	Theoretical displacement	L
$\Delta H_D(T)$	Theoretical displacement	L

Symbol	Name	Dimension
ΔV_S	Volume change of the elastomer due to pressurization	L^3
ΔV_D	Volume change of the steel disc	L^3
Δr	Radial increment	L
Δz	Axial increment	L
Δt	Elastomer compression	L
δ	Elastic compression of the bearing liner (from Dowson's theory, ref. [201]	L
δ_e	Dimensional deflection at exit (ref [219])	L
η	Film viscosity	FT/L^2 or $M/(LT)$
μ	Coefficient of friction	—
λ	One of the Lamé constants	F/L^2 or $M/(LT^2)$
ν	Poisson's ratio	—
ρ	Density of elastomer or fluid	FT^2/L^4 or M/L^3
σ_r	Radial stress	F/L^2 or $M/(LT^2)$
σ_θ	Circumferential stress	"
σ_z	Axial stress	"
$\tau_{r\theta}$	Shear stress in r, θ plane	"
$\tau_{\theta z}$	Shear stress in θ, z plane	"
τ_{zr}	Shear stress in z, r plane	"
τ_{ij}	Stress in subscript notation	"
$\hat{\tau}_{ij}$	Stress deviator	"

General suffices

D	Discharge
a	Ambient
c	Compression
e	Elastomer
m	Measured
o	Outer radius
p	Inner radius
r	Radial
s	Supply
z	Axial
θ	Circumferential

LIST OF PHOTOGRAPHS

CONTENTS

I INTRODUCTION

Fluid film bearings operate with a layer of liquid or gas effectively separating the bearing surfaces. The load capacity derived from the pressure within the lubricating film may be generated by the relative motion of the converging bearing surfaces, or by external pressurization, or by a combination of both actions. Friction forces arise from shearing of fluid between the bearing surfaces.

The purpose of this work is to study the steady performance of externally pressurized compliant thrust bearings lubricated by air. One of the surfaces of these bearings is compliant and the other is of rigid geometry. In order to see how these bearings behave when compared to bearings where both surfaces are rigid, Appendix I, "Rigid Bearing Theory" is presented.

Because of the many engineering applications, circular-step thrust bearings are an important class of the thrust bearing family and this geometry has been chosen for investigations. Consider a circular thrust bearing geometry, fig.1, where a rigid bearing of outside radius r_o and inner radius r_p is shown. The lubricant is supplied to the film at pressure p_p into the bearing clearance h_o. Pressure distribution in the film follows a logarithmic law, see equation I - 8, Appendix I, falling to ambient pressure p_a at outer radius r_o.

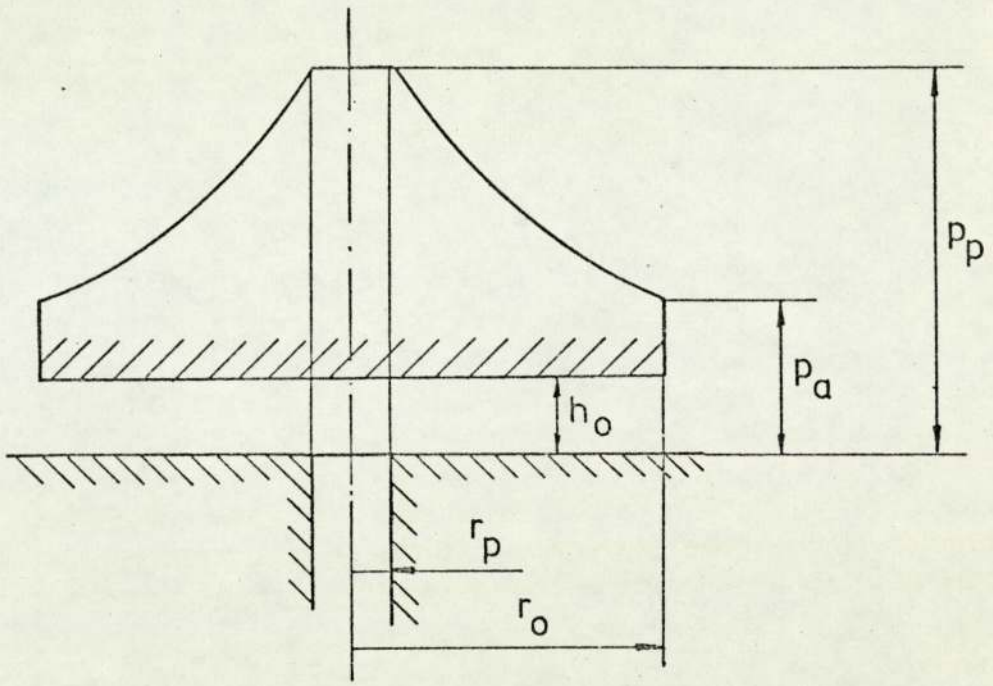

RIGID CIRCULAR AEROSTATIC THRUST BEARING

FIG 1

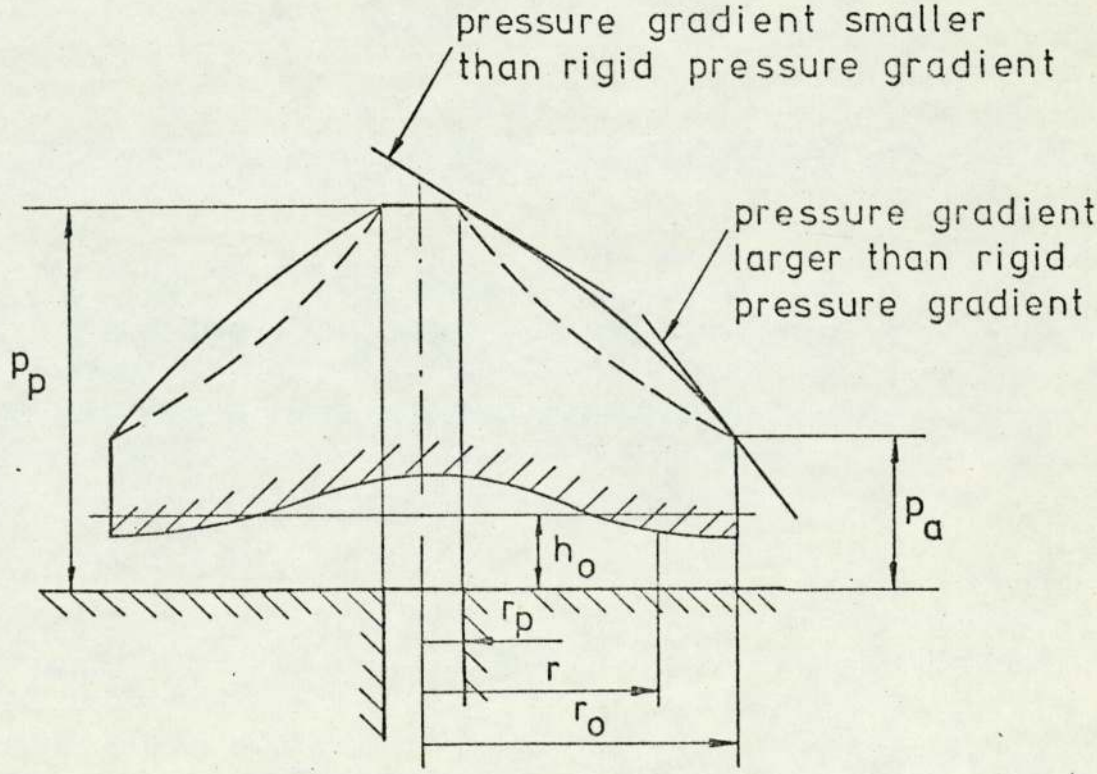

COMPLIANT CIRCULAR AEROSTATIC THRUST BEARING

FIG 2

The load capacity of plane thrust bearings can be determined by summing all pressure forces in the bearing film within the bearing area, so that for circular thrust bearings:

$$W = 2\pi \int_{o}^{r_o} prdr - \pi r_o^2 p_a \qquad (1)$$

In the bearing shown in fig. 1 the load capacity

$$W_1 = 2\pi \int_{o}^{r_p} p_p \, rdr + 2\pi \int_{r_p}^{r_o} prdr - \pi r_o^2 p_a$$

$$= \pi r_p^2 p_p + 2\pi \int_{r_p}^{r_o} prdr - \pi r_o^2 p_a \qquad (2)$$

i.e. it is determined by the pressure p_p at the inlet of the bearing film.

Now consider a circular externally pressurized thrust bearing where the upper surface is compliant, see fig. 2. Suppose that the same pressure p_p is admitted to the bearing clearance with the mean value h_o the same as the rigid film thickness. Due to the compliant surface, the thickness of the film varies with film pressure and thus with radius. The film is largest where the largest pressure (p_p) exists.

The compliance of one of the bearing surfaces is achieved by elastomers which adhere to the rigid backing plate. These

materials are almost incompressible i.e. their volume is nearly constant whilst their profile changes as different inlet pressures are admitted to the film. As pressure p_p is admitted to the film, parts of the film, in the centre of the bearing, are larger than the mean film thickness h_o and parts of the film, on the periphery, are smaller than the mean.

Consider that the mass flow through the compliant bearing, fig. 2 is the same as in the rigid bearing on fig. 1. For isothermal flow through the film:

$$Q_p \, p_p = Q_a \, p_a \tag{3}$$

From (I-3), Appendix I, volumetric flow at any radius r ($r_o > r > r_p$) is given by

$$Q = - \frac{\pi r \frac{d}{dr} (p^2) h^3}{12 \eta p} \tag{4}$$

so that mass flow at radius r becomes:

$$M = \frac{p Q}{R_a T_a} = - \frac{\pi}{12 \eta R_a T_a} \, r \, \frac{d}{dr} (p^2) h^3 \tag{5}$$

The minus sign in equations (4) and (5) signifies that the pressure gradient $\frac{d}{dr}(p^2)$ is negative. Both (4) and (5) are valid for rigid and compliant bearings lubricated isothermically by a perfect gas.

For given mass flow along the compliant bearing radius, it is clear from equation (5) that at any radius where the film is smaller than h_o (the rigid bearing film), the local

pressure gradient is larger than the corresponding rigid bearing pressure gradient. Therefore at the film exit, where the film is smaller than the corresponding rigid case, the pressure gradient is larger, and at entrance, where the film is larger than the corresponding rigid case, the pressure gradient is smaller, see fig. 2.

These two boundary values of pressure gradient dictate a modified pressure distribution for compliant bearings as shown in fig. 2. This is an improved pressure distribution compared with the rigid case as the area under the pressure curve is increased. The load capacity as before is given by

$$W_2 = \pi r_p^2 p_p + 2\pi \int_{r_p}^{r_o} prdr - \pi r_o^2 p_a \qquad (6)$$

but now the integral of equation (6) has a larger value than the integral of equation (2). Thus

$$W_2 > W_1 \qquad (7)$$

i.e. for the same mass flow rate the load capacity of compliant bearings is superior to that of rigid bearings. This in turn implies that the compliant bearing can support the same load as the rigid bearing but with smaller flow rates.

The superior performance as compared with rigid bearings is a characteristic feature of compliant bearings. This is the major reason for their investigation. The interest of researchers

and engineers in these bearings is also aroused by other factors such as:

It some impurities are admitted accidently into the bearing clearance, this is not so critical as with rigid bearings, because they can be "accommodated" by the elastomer.

Tolerances of both compliant and of rigid surfaces in compliant bearings need not be so small as when both surfaces are rigid.

Consider a compliant thrust bearing geometry, fig. 3. It is convenient to take the origin of the co-ordinate system at the centre of the elastomer disc and at the point where the elastomer is touching its backing plate. This origin is then stationary relative to the elastomer and the backing plate. The experimental set-up is such that the z-axis points downwards. (It is more convenient in the theoretical analysis to turn the bearing upside down, so that the z-axis is pointing upwards, see chapter III).

After this brief introduction about the compliant bearings, it is necessary to search the relevant literature and see what is already known about them so that the gaps in the knowledge can be discovered.

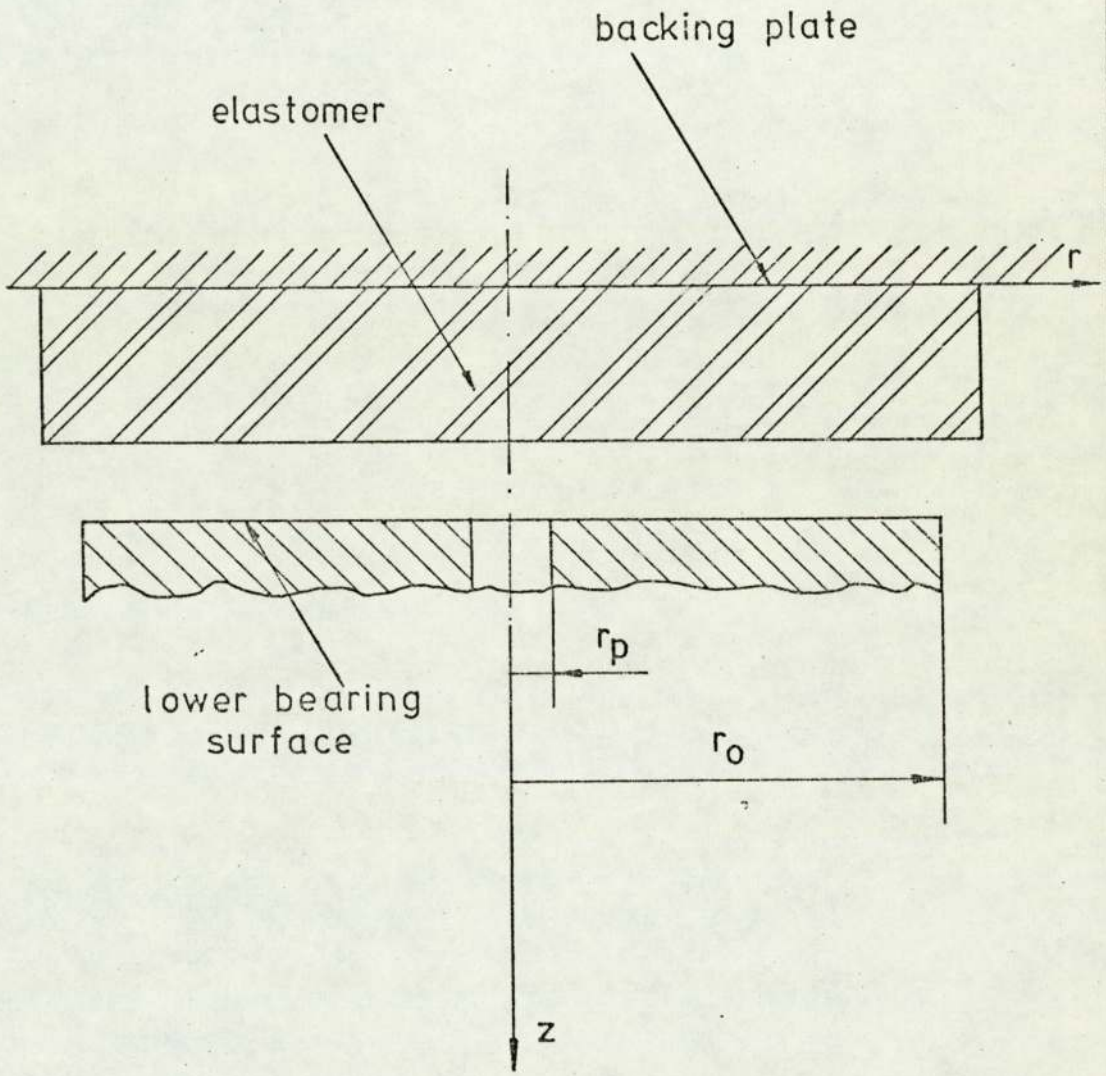

COMPLIANT CIRCULAR AEROSTATIC THRUST BEARING GEOMETRY

FIG 3

II REVIEW OF RELEVANT LITERATURE

2.1 Rigid Bearings

Although this research project does not directly concern rigid bearings, it is desirable to be aware of the theoretical background and performance of such bearings. A further understanding of compliant surface bearings may be achieved by a knowledge of work done with rigid bearings.

Fuller [101] gives a concise guide to hydrostatic and hydrodynamic lubrication and the many examples in his work give the reader a clear picture about both journal and thrust bearings lubricated by oil or air. His simple formula about the one-dimensional flow of viscous liquid through a slot is developed at the very beginning of the book and used repeatedly throughout. The formula states:

$$Q = \frac{\Delta p b_o h^3}{12 \eta \ell}$$

The width of slot b_o is assumed to be large compared to film thickness h so that one-dimensional flow Q results. A pressure difference Δp is the cause of flow Q of the lubricant of absolute viscosity η.

When this equation is applied to a circular hydrostatic bearing of circumference $2\pi r$ and length dr there follows:

$$Q = - \frac{dp \times 2\pi r \times h^3}{12 \eta dr}$$

By integrating this expression with respect to r, the quantity of flow needed to maintain the film h in a circular bearing of outer radius r_o and inner radius r_p and using incompressible lubricant becomes:

$$Q = \frac{(p_p - p_a)\ \pi h^3}{6\eta\ \ell n\ (r_o/r_p)} \qquad (1)$$

In the same reference [101], Fuller shows that for a compressible lubricant, the volume rate of flow at inlet is

$$Q_p = \frac{\pi h^3}{6\eta\ \ell n(r_o/r_p)} \left[\frac{p_p^2 - p_a^2}{2p_p}\right] \qquad (2)$$

Equation (1) can be used for air "if the pressures involved are not greater than a few pounds per square inch. Where greater loads are carried and unit pressures are higher, the analysis must include the compressibility effect due to significant changes in volume as the air passes through the bearing, "so that equation (2) is then used.

The incompressible flow assumption leads to an underprediction of the bearing performance.

Elwell and Sternlicht [102] analyse circular hydrostatic thrust bearings both experimentally and theoretically using incompressible lubricants. Load carrying capacity, stiffness and flow rate are evaluated for three different types of flow restrictors. While equations (1) and (2) concern the bearing film only, equations in [102] consider a flow restrictor and bearing film together as a unique bearing element. A reasonable agreement between theory and experiments is achieved.

Comolet [103] studies air flow between parallel flat plates and unlike the previous references includes inertia effects. Turbulence for longitudinal flow occurs at Reynolds number based on film thickness of about 1000 and for radial flow, laminar flow transforms to turbulent at Re = 550 approx. In radial flow, supersonic flow can sometimes exist over a part of a bearing film. This supersonic flow transforms to subsonic through a shock wave. Entrance length is a value of radius from which the developed formulae apply. This entrance length is smaller for smaller film thicknesses.

Powell, Moye and Dwight [105] study both thrust and journal air bearings. A linear pressure distribution which gives an analytic solution for load capacity is assumed for thrust bearings. It is shown that for the geometry chosen, validity of this assumption is satisfied. The author of this thesis cannot use this assumption because, for the geometry of the experiments, see Appendix I, errors in load capacity are as high as 40-50%. Coefficients of discharge of the feed hole was measured experimentally with varying supply pressure and keeping the bearing load constant [105]. The agreement between load-clearance experiments and theory taking experimental discharge coefficients into account is good. A simple orifice feed hole of area $A_r = \pi d^2/4$ (where d is the feed hole diameter) and annular feed hole $A_r = \pi dh$ (where h is the bearing clearance) are considered.

Grassam and Powell in [106] and [107] have given design procedures of aerostatic thrust and journal bearings for maximum stiffness assuming incompressible flow through the bearing element. Their design procedures utilate Kg, a gauge

pressure ratio of film entry and supply pressures.

Gross [108] gives a comprehensive theoretical analysis about hydrodynamic and hydrostatic compressible lubrication. Laminar viscous flow theory is initially used, but also inertia effects and supersonic effects, i.e. presence of shock waves within the bearing film is analysed. Gas bearing Design Manual of MTI [109] consists of similar analysis, given in more detail and with a lot of references. Tang and Gross [104] considered orifice and inherently compensated gas thrust bearings. They presented design graphs of load capacity assuming laminar viscous flow in the bearing and taking compressibility of the gas into account. In particular Tang and Gross [104] derived a bearing load in terms of two error functions to evaluate expressions for stiffness. They assumed a constant value for the discharge coefficient of the restrictor.

Dudgeon and Lowe [110], [111], [112] and [144] also considered both orifice and inherent compensation. They gave a design procedure for maximum stiffness assuming compressible flow through the bearing. Unlike Tang and Gross [104] their value of empirical discharge coefficient is not constant but depends upon the ratio of film entry pressure to supply pressure [144]. The discharge coefficient occurs in their expression for restrictor flow.

The author of this report has determined the discharge coefficient of an inherently compensated thrust bearing experimentally, see Chapter VI. Discharge coefficients of other restrictors can be obtained in a similar manner. The

expression for bearing load given by Gross [108] is also modified. It is shown, see Appendix I, that the load is given with sufficient accuracy by means of one error function only. In the same appendix the analytic expressions for bearing stiffness for all three types of restrictor are presented. Stiffness expressions for the orifice and the inherent restrictor take into account the variation of the coefficient of discharge with the ratio of film entry pressure to supply pressure.

Various authors [113] to [120] have been concerned with inertia effects(with or without rotation)and supersonic flow in aerostatic thrust bearings. It has been shown in chapter VI that Reynolds numbers rapidly decrease as bearing radius increases. These effects are therefore localised and can be neglected for the range of flow rates and film thicknesses investigated in this project [103],[143].

Lewis [121]shows that for incompressible fluids the flow and load characteristics can be conveniently expressed as non-dimensional parameters i.e. as shown in Appendix I, a flow parameter.

$$q = \frac{Q\eta}{(p_p - p_a)h^3}$$

and load parameter

$$w_g = \frac{W}{A(p_p - p_a)}$$

For uniform-film bearings using incompressible lubricants, load parameter w_g and flow parameter q are constant. They do

not depend upon film thickness but only upon bearing geometry. For the case of a circular step bearing:

$$q = \frac{\pi}{6\ell n(d_o/d)}$$

$$w_g = \frac{[1-(d/d_o)^2]}{2\ell n(d_o/d)}$$

These parameters can be written in terms of bearing geometry only also for compressible lubricants as shown in section AI.4 of Appendix I.

Stiffness, which is the change of applied load W with film thickness h, $-\frac{\partial W}{\partial h}$ is another important bearing parameter. Stiffness depends on the type of compensating element. It is shown by Lewis [121] that for journal bearings, stiffness can be expressed in terms of the load and flow parameters w_g and q and their derivatives with respect to film thickness h. If the stiffness is equal to or less than zero, the shaft will not be able to support any load so that these derived expressions show when the bearings are statically unstable. Ling [122], Malanoski and Loeb [123] and Lewis and Scouller [124] are concerned with variations of stiffness depending upon the restrictor used. Wunsch and Scoles [125] show how stiffness can be improved by automatically varying the supply pressure as bearing load changes.

In [126] Kilmister shows that two factors determine the load that the bearing will support: maximum pressure in the film and the shape of pressure profile. The relationship

between the load and the film (i.e. the stiffness) can be improved by adjusting the relationship between the thickness of the film and either the maximum fluid pressure or the shape of the pressure profile. It is shown that a certain degree of stiffness will be achieved if bearing surfaces can be arranged so that pockets will develop on the bearing surfaces as the load on the bearing is increased. This can be achieved by a metallic concave profile diaphragm in one of the bearing surfaces. The operation of this bearing is thus similar to operation of compliant surface bearings.

In [127] a rectangular thrust bearing is analysed. Dimensionless stiffness is given as a function of dimensionless bearing parameter and it is shown that stiffness is a maximum when this parameter is slightly larger than 1.

Effects of non-parallel bearing surfaces are discussed in [119], [128] and [129]. Load and flow rates increase with tilt but stiffness can increase or decrease according to geometry [129].

The effects of surface roughness are discussed in [130] and [131]. Bailey [131] claims that the largest gaps in the separation of the surfaces dominate the flow, i.e. in case of scraped surfaces the hollows define the surface, rather than flat portions which may be ground and lapped. References [132] and [133] show how a statistical roughness theory can be applied to various lubrication modes. Papers [134], [135] and [136] also deal with surface roughness effects.

The author of this report has shown that it is necessary to take the roughness of the bearing surfaces into

account in describing the bearing performance, see chapter VI.

2.2 Compliant Bearings

Solutions for film pressure and load by Dowson and Taylor [201] are given as pressures and load for rigid bearings times a corresponding multiplying factor. Although this is a simplified theory, it has its merits of clearly showing how compliant bearing solutions depart from rigid bearing solutions. In this way this paper may be thought of as a crossing between rigid and compliant lubrication and as an introduction to compliant bearings. Their solution assumes that elastomer strain is only in the axial direction, i.e. in the direction of the applied load. As circular sections are considered, the theory assumes axial symmetry and also that elastomer thickness is much smaller than the radius so that the elastic compression of the liner is given as

$$\delta = \frac{p_g t}{E'} \qquad \text{where}$$

p_g is gauge film pressure, t is elastomer thickness and E' is an equivalent elastic modulus. This means that film pressure and elastomer deflection profiles are similar.

Investigations [201] had been initiated because of an interest in animal joints. Those joints are a form of compliant surface in which the rigid bone is lined with relatively soft articular cartilage. Experiments were done on a thrust bearing machine described by Coombs and Dowson [119]. An important feature of this machine is a supporting spherical hydrostatic bearing connected to the lower thrust surface. Thus, the

lower thrust surface aligns itself with the upper surface. Changes of film pressures with radius were measured for bearings lined with discs of nitrile and polyurethane rubbers and using oil as lubricant. Comparisons of experimental pressure profiles with rigid theory showed an improved bearing performance, i.e. increased load capacity.

Dowson's and Taylor's theory [201] breaks down for a completely compliant elastomer with Poisson's ratio of 0.5. In the author's closure of [201], Dowson and Taylor have shown that a column model approximation (which is basically their theory) agrees well with Castelli's et al theory for Poisson's ratio values of up to 0.45.

Subsequently, Castelli et al [202] developed a theory which is not only suitable for lower values of Poisson's ratio but also for values near to completely incompressible case including 0.5.

In their theory, if the rubber is deflected due to the film pressure in the central region of a thrust bearing, radial strain which was neglected in [201] will displace this volume towards the edges of the bearing. There may be "an undershoot" and "an overshoot" along the bearing radius. Apart from [202] this theory is also described in [203], [204], [205] and [206].

Interests in experiments [202],[203], [204]and [205] was aroused by initial tests with plastics like nylon and ptfe. When used on journal bearings, coefficient of friction appeared to be very low even though the oil flow to bearings was very small. This low coefficient of friction indicated

that fluid film lubrication was achieved. Rigid bearings of the same geometry would have required much higher flow rates for similar coefficients of friction.

The theory developed at Columbia University distinguishes between "finite" and "infinite" elastomers. According to [207] in the case of thrust bearings the boundary conditions for "infinite" elastomer case will be satisfied in practice if the elastomer extends about three to five elastomer thicknesses beyond the corresponding rigid mating bearing surface. Experiments of [202] were done on a thrust bearing where the diameter of a rigid lower plate was 101.6mm. and upper compliant discs were 127mm dia. Neoprene rubbers with thicknesses 3.18mm, 4.87mm and 9.47mm were used. Whilst the first two cases can be taken as "infinite", the third thickness does not satisfy the empirical requirement of [207], although it was reported as an infinite case. In [202] entrance effects are neglected and the film entry pressure is taken to be the measured supply pressure.

In [205] an improved version of the test rig is reported which allows measurements of the film entry pressure and film thickness. In both [202] and [205] tests are arranged in order of increasing compliance - from the thinnest specimen of the hardest rubber to the thickest specimen of the softest rubber. In the case of [205] discs of butadiene acrylnitrile (paracril) were used both as "finite" and "infinite" cases. In [202] radial pressure distribution, supply pressure, average oil temperature and flow rate were recorded. These results showed better load capacity when compared to the prediction of rigid bearing theory. They also related the load

capacity with thickness and hardness of the compliant layer, the inverse dependence of load on flow rate and the dependence of pressure profile on recess pressure. Reference [205] shows both experimentally and theoretically better load capacity for the 'infinite' case. For a given recess (port) pressure both bearings carry several times more load than the equivalent rigid bearing. The oil flow rate is reported to be less than for an equivalently loaded rigid bearing. For bearings fed with oil, temperature effects are important. Performance of these bearings depends on the elastomer thermal expansion, change of the characteristic modulus of the elastomer and change of oil viscosity.

In the case of gas compliant lubrication [206] theory showed that for constant recess pressure there is an increased load capacity of compressible films compared to incompressible films similarly as with rigid bearings. Also, this is because the gas behaves as a secondary elastomer, enhancing the beneficial effects derived from the compliant bearing itself.

References [208] and [209] develop theoretical solutions for the infinite width slider and infinite length journal bearing. The governing fluid-film equation used is the incompressible form of the Reynolds equation given in [137] and [138]. The elastomer is defined as a linearly elastic homogeneous isotropic body characterized by equations of motion in terms of displacements [208] and the equations of stress equilibrium and a linear viscoelastic stress-strain relation [209]. In both cases body forces are neglected.

According to [209] a three element linear elastic model shown in the sketch below, is accurate for elastomers such as rubbers. This model is also known as a three-parameter solid [11].

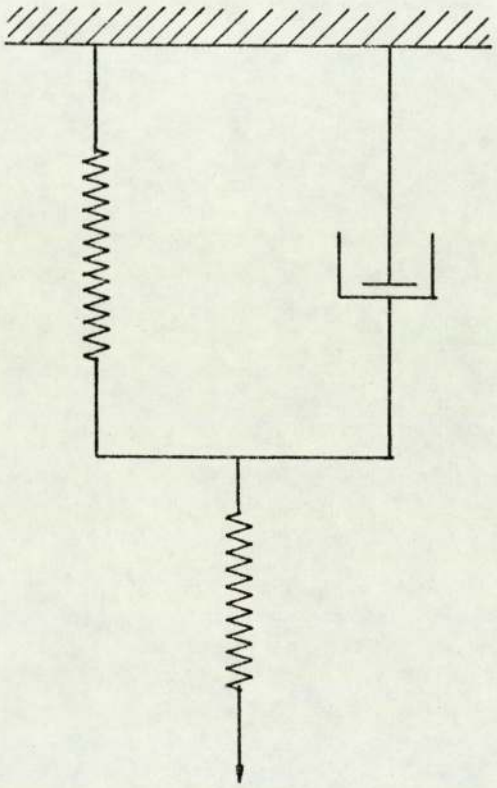

Investigations [210] and [211] were set up in order to prove experimentally theory [206]. Theory [206] does not say anything about the effect of compensating elements at the entrance to the bearing film, and subsequently Lowe's experiments were performed on an inherently compensated bearing. The diameter of the bearing inlet hole was 6.35mm and the outside diameter was 101.6mm which corresponds to a

radius ratio of 0.0625. This is one of the radius ratios investigated by Castelli and Pirvics [206] theoretically. Pressure toppings were very near to the inlet hole in order to establish the pressures immediately after the entrance to the clearance space. The resulting pressure distribution (spaced within 1mm from the edge of the inlet hole) showed a pressure depression similar in shape as with rigid bearings [112] and maybe smaller in magnitude. The pressure ratio at the edge of the inlet was than extrapolated from those pressure readings from the outer toppings where there were no pressure depressions. The film static pressure immediately at the entry to the bearing film (after the inherent 'curtain' area of $2\pi r_p h$) represents the theoretical recess pressure of reference [206].

In his experiments Lowe used natural rubber discs with three various hardnesses and four various thicknesses. Lowe's radius/thickness ratios closely corresponded to those of reference [206]. Lowe has showed that there is a reasonable agreement between theory and experiments at low values of the equivalent thickness whereas a departure occurred at larger equivalent film thicknesses.

Pneumatic hammer instability was also reported by Lowe who showed that the region of stable operation is enlarged when the elastomer becomes thinner and harder, i.e. when the behaviour of compliant bearings approaches the behaviour of inherently compensated rigid bearings.

It was generally concluded [210] and [211] that the load capacity increases with supply pressure and with elastomer thickness and decreases with increasing elastomer hardness. When compared to rigid bearings not only is the load capacity increased but the stiffness remains essentially constant which is not the case with rigid bearings. The flowrates, however, are higher than with corresponding rigid bearings. Therefore there are two reasons for operating these bearings at low clearances: the first is small flow rates, about the same or slightly higher than rigid bearings and second is that at small clearances stiffness is about the same as for large clearances, whereas for rigid thrust bearings stiffness approaches zero as film thickness approaches zero. Lowe has compared flow rates against film thickness at the same supply pressures as rigid bearings and he found that they are higher for compliant bearings.

Lowe has plotted these flow rates against the apparent clearance, by using the original elastomer thickness in an unstressed state. The upper or moving bearing element contains film thickness probes outside the bearing area, and they measure distances to parts of the lower rigid bearing element, also outside the bearing area. In this way the measured film thickness is an apparent value and it represents the clearance between the lower thrust pad and the plane of the undeflected elastomer surface. This apparent value of film thickness is taken to be positive if the deflection of the elastomer is smaller than the mean film thickness, and the apparent value of film thickness is taken to be negative if the deflection of the elastomer is greater than the mean film thickness.

In their paper [212] Lau and Harman have analysed surface roughness effects in compliant bearing both theoretically and experimentally. They have considered a square slider bearing with a small round centre recess (port). In their analysis film thickness consists of three parts: the first is nominal film thickness assuming both surfaces are smooth and rigid, the second the film thickness contribution resulting from the deflection of the compliant surface and the third is contribution from surface roughness. The contribution from the deflection of compliant surface is taken to be $\frac{t}{E^1} \times p(x,y)$ where t is the elastomer thickness in the unstressed state, $p(x,y)$ is the film pressure and E^1 is the equivalent elastic modules. This modulus can be taken to be equal to the average slope of the stress-strain curve of the compliant material for a particular bearing. The contribution of surface roughness to the film thickness is given by a random variable considered to be of approximately Gaussian distribution. This random variable has negligible effect on pressure gradients in the Reynolds equation because the roughness is considered to be uniform and two-dimensional. Bulges of this two-dimensional roughness offer almost no resistance to flow so that pressure gradients are hardly affected. The authors indicate however that one-dimensional roughness offers large flow resistances so that pressure gradients might be affected. Christensen and Tønder [136] have simplified the problem of random analysis through the introduction of polynomial distribution and because of its simplicity their formula is used here. The analysis is based on isoviscous and incompressible lubricants although air

is used as a lubricant in experiments. Gauge supply pressure is low (0.85 bar) and according to [101] this is probably justified, see the beginning of this chapter.

The purpose of investigations [212] is to study a potential application of compliant bearings where the rigid mating surface can have certain uneveness for example in the transportation of unmachined castings. Tne authors give the example of a guideway that might be used for high speed ground transportation vehicles. The author of this thesis has noted that the authors of reference [212]have taken only a rigid bearing member to be rough - a compliant member is assumed to be smooth.

The purpose of investigations [213] and [214] is to develop the "self-caging" spherical bearing for directional gyroscopes. Caging refers to the ability of the compliant spherical bearing to hold the rotor when the hydrostatic bearing pressure is removed.

It was found that it is better to bond the elastomers to the rotating bearing element because of the undesirable bearing squeal-high pitched audible frequency - if the elastomer is bonded to the stator. As the elastomer is rotating and the load is stationary, an observer positioned on the elastomer would experience a relative load movement. Castelli and Pirvics [208] and [209] have investigated these situations theoretically.

In investigations [213] and [214] silicone rubbers of various hardnesses and thicknesses between 0.5 and 1.5mm. are used. Rotor speeds of 40000 rpm are reported. One test rig

was designed to study gyroscope rotors moulded with silicone rubber. The second test rig provided characteristics of pressure, film and flow of silicone rubber.

Theoretically coupled elasticity and hydrodynamic, both incompressible and compressible, equations are solved for a plane externally pressurized bearing consisting of a flat elastomer bonded to a semi-infinite rigid body. The lift-off pressure is determined for any given preload deflection. Pressure and deflection profiles are obtained experimentally and theoretically. This lift-off pressure is sensitive to various values of Poisson's ratio. It is shown that if the ratio of a characteristic dimension of a rigid surface (say radius in the case of circular thrust bearings) and the elastomer thickness is large, then a simple algebraic relationship determines the lift-off pressure. This relationship is:

$$p_p - p_a = \frac{\pi E u_e}{2t(1-\nu^2)\delta_e}$$

Also for this case the deflection at the centre is twice that at the edge.

Pressure profiles within the flat bearing were found to be highly flattened near the supply port and steep at the bearing edge when the compliant material was soft, the supply pressure was high or the initial bearing gap was small. Displacements were found to contain large dips near the bearing edge and bulges outside it for these same conditions. It appears that large pressure gradients near the bearing edge correspond to large displacement gradients at these places. The highest initial gradients occur when the initial gap is

zero or negative (i.e. preloaded elastomers).

The authors of references [213], [214] and [219] in the conclusion about the future work, see a need to investigate the unbonded elastomers because of the ease of replacement of the damaged elastomer layers. This author has tested a number of unbonded elastomers and compared them with the performance of bonded elastomers and also with the rigid bearing theory, see chapter VII.

References [215] and [216] deal with bearings where the lubricant is in contact with metal surfaces only. Anderson [215] describes a foil sector shaped pad thrust bearing. This bearing does not contain any elastomers and it is analysed as a square slider bearing. Dayson [216] describes a stepped sliding thrust bearing where the step is mounted on an elastic foundation so that step height can be changed according to varying loading conditions. Anderson's and Dayson's bearings are similar to a bearing described by Kilmister [126] where the compliance effect of the bearing was achieved by a metallic concave profile diaphragm and the bearing did not contain any elastomers. This author has, however, chosen to study bearings lined with various elastomers.

Reference [217] refers to a bonded assembly of elastomeric material and interspersed metal shims which support high compression loads and allow much more displacement in shear. Stiffness in compression can be up to 1000 times the stiffness in shear. These assemblies are successfully applied to helicopter rotor systems where oscillating motion is required. This reference is not related to the author's work but is given

here for completion of the compliant bearing references read by the author.

2.3 Elastomer Properties

From compliant bearing references it can be seen that authors have assumed small deformations of the elastomer, i.e. the external forces producing deformation do not exceed a certain limit. With the removal of the forces, deformations disappear completely i.e. elastomers undergoing external loading and pressurization in bearings are perfectly elastic. They are also homogeneous (the smallest element of the elastomer possesses the same physical properties as the bulk of the elastomer) and isotropic (properties are the same in all directions). There is only one exception among the compliant bearing references when Pirvics and Castelli [209] looked theoretically into the viscoelastic effects of the compliant material.

Materials with the above assumptions are described in many books and papers concerning the theory of elasticity, for example, [301], [302] and [303]. From these references elastic materials are described by five elastic constants or properties, which are interrelated. They are: modulus of elasticity (or Young's modulus) E, bulk modulus K, Lamé's constants, λ and G and Poisson's ratio ν. These five constants are interrelated in such a way that if any two constants are known, the other three can be determined.

Looking through various equations of compliant bearing references it can be seen that in order to calculate pressure distribution and load capacity of such bearings, two elastic

constants must be known. These two constants are usually λ and G, E and ν, or K and E. The study [304] was undertaken in order to determine the shape of filler particles on properties of compounded rubber. Test specimens were mounted in a suitable stretching frame where elongations up to 300% could be achieved. Poisson's ratio was calculated with respect to two lateral dimensions and from the change of volume measurements. It was found that volumetric Poisson's ratio is approximately the average value between two lateral Poisson's ratios for a given rubber. All three values of Poisson's ratio decreased with increasing strain. Poisson's ratio calculated from volumetric measurements was about 0.5 for strains up to 50%.

Higginson [218] quotes values of Poisson's ratio about 0.3 for metals, about 0.35 for perspex and in the range of 0.4 to 0.5 for rubbers. In the discussion of [201] Castelli and Rightmire quote values of Poisson's ratio in the range 0.47 to 0.50 for elastomers of engineering interest. It is also shown [201], [202], [203] and [205] that bearing performance is sensitive to small changes of this elastomer property, particularly when its value is close to 0.5. Detailed investigation of this property [305] revealed that its range is between 0.495 and 0.50 for various rubbers. Nylon sample value was however $\nu = 0.417$.

Rightmire [305] has measured bulk modulus K and shear modulus G of various elastomers for small strains so that Poisson's ratio could be calculated. He has also done a comprehensive error analysis of his measurements. Lowe [210] and [211] has used Rightmire's results of elastomer properties

when comparing his own experimental results with Castelli's theory.

Testing of physical properties of rubber is described in British and American Standards [309] and [310]. These tests are specified at high strains, so it is doubtful it they are suitable for evaluating rubber properties as encountered in compliant bearings.

References [306], [307] and [308] give a lot of information about elastomer properties,about applications and general data about various elastomers. Theoretical derivation of compression characteristics of bonded rubber blocks as found in [307] and [308] is quite useful, when assessing shape factors of rubbers in a given situation. Because rubbers are almost incompressible, the compression characteristics are not the same if one rubber disc is bonded to metal by one side, or by both sides or, if it is not bonded at all. Also compression characteristics of an unbonded rubber disc, when pressed between two metal plates, depend upon the amount of friction between rubber and metal. They depend upon the extent by which rubber is allowed to flow sideways when compressed.

Reference [305] determines bulk modulus and shear modulus of elastomers and references [311] and [312] describe the determination of Young's modulus. The theory of the latter two papers is a modified theory of contacts originally given by Hertz [12].

Drutowski [311] and Finkin [312] explain that hardness is the ability of material to sustain deformation. When talking

of metals this deformation is permanent i.e. plastic flow occurs, but in the case of elastomers it is an elastic deformation. Finkin states that rubber hardness depends upon a more fundamental property, Young's modulus, and he develops a formula for Young's modulus in terms of either indentor penetration or contact radius of a spherical indentor. Herts's theory assumes an infinite depth and therefore his equations do not include elastomer thickness whilst equations of Finkin do.

2.4 Areas of Investigation

The preceding account is a brief guide to the available knowledge of compliant lubrication. Lines of investigation in this report should include something that has not been done so far.

It is noticed that so far theoretical and experimental work on compliant bearings has been done for steady-state operation. Time-dependent solutions are an extension to this work. These solutions exist for rigid bearings, see references [107], [108], [109] and [138]. Dynamic work with compliant bearings is a large new area of investigation, which apart from dynamic performance of these bearings should also include investigations of elastomer properties. Generally the work reported here is limited to steady-state operation though in chapter VIII (Future work) one set of results of elastomer properties under dynamic conditions is included. But dynamic performance of these bearings remains to be studied.

At the beginning of this research project the steady performance of compliant bearings lub ricated by a compressible

fluid had not been done and this was considered to be a major new area of investigation. Previous workers [201] to [205] have investigated incompressible lubricants only.

In the theory of Castelli the governing equations are formulated in terms of a stress function. This formulation allows all values of Poisson's ratio to be used including when ν approaches 0.5. This theory is analytic but the resulting integrals are solved numerically.

At the beginning of this project it was hoped to analyse aerostatic thrust bearings under dynamic conditions. It was thought that a direct numerical solution (rather than semi-analytic, semi-numerical) is easier for the mathematical model under dynamic conditions.

For the direct numerical solution the governing elastic equations are best expressed in terms of displacements, see chapter III and appendices II and III. However, because of the $(1-2\nu)$ appearing in this formulation, a modified form of these equations is required when Poisson's ratio approaches 0.5, see chapter III and Appendix III.

Investigations of elastomer properties, [305] and chapter IV of this thesis, have revealed that these materials are almost incompressible and that these modified forms of elastic equations are of engineering interest.

A first step in the direct numerical solution is to consider steady state operation and completely incompressible elastomers when $\nu = 0.5$.

It was decided to perform some experiments with rigid bearings in order to develop the experimental apparatus. Once confidence with the rig had been gained, experiments with the compliant bearings were to be performed.

So far in the compliant bearing literature elastomers have been bonded to a rigid backing. In this project tests have been carried out with unbonded elastomers. This setup is attractive because damaged elastomer layers can be easily and quickly replaced. Although this advantage may not be very significant for a simple circular thrust bearing geometry, it can be more significant for more complex geometries such as spherical compliant bearings [214] and [219].

It is noticed that throughout the experiments with compliant bearings, elastomer aspect ratio was varied by varying elastomer thickness. In this report elastomers of various thicknesses were tested, but also elastomer diameter was varied for a given thickness. The range of elastomers investigated was extended to include some plastic material.

III THEORETICAL ANALYSIS

Two basic constituents of the theoretical analysis are an elasticity problem and a fluid problem. The fluid problem can be treated as a boundary condition of the elasticity problem.

Circular thrust bearings and journal bearings are most important from an engineering point of view. For both geometries the elasticity problem is described by well-known general elasticity equations in cylindrical polar coordinates. They are [302] :

$$\left.\begin{aligned}
\rho a_r &= \frac{\partial \sigma_r}{\partial r} + \frac{1}{r}\frac{\partial \tau_{r\theta}}{\partial \theta} + \frac{\sigma_r - \sigma_\theta}{r} + \frac{\partial \tau_{rz}}{\partial z} + F_r \\
\rho a_\theta &= \frac{1}{r}\frac{\partial \sigma_\theta}{\partial \theta} + \frac{\partial \tau_{r\theta}}{\partial r} + \frac{2\tau_{r\theta}}{r} + \frac{\partial \tau_{z\theta}}{\partial z} + F_\theta \\
\rho a_z &= \frac{\partial \sigma_z}{\partial z} + \frac{1}{r}\frac{\partial \tau_{z\theta}}{\partial \theta} + \frac{\partial \tau_{zr}}{\partial r} + \frac{\tau_{rz}}{r} + F_z
\end{aligned}\right\} \qquad (1)$$

It is a very elaborate task to solve this three-dimensional problem. In order to simplify it, various assumptions are made. The experimental setup of the project is a dominant factor in determining any departures and simplifications from equations (1).

The main points to be considered in order to arrive at simplifying assumptions are:

1) Whether this is a dynamic or a steady-state problem.
2) Whether body forces can be neglected.
3) Axial symmetry in thrust bearing analysis.
4) Whether the loading arrangement in the bearing is such that plane strain can be assumed.
5) Whether there are any assumptions in the elastomer properties that can simplify equations (1).

The project is concerned with steady state work, so that inertia forces, on the left hand side of equations (1), are equal to zero.

The project is concerned with a thrust bearing of circular geometry and the experimental setup is such that there is no rotation. Furthermore, bearing load is one or two orders of magnitude greater than the elastomer weight. This means that body forces (the last terms on the right hand side of equations (1)) can safely be neglected.

Axial symmetry is a sound assumption for circular compliant surface thrust bearings in which tilt is eliminated. A steady state axisymmetric situation in a solid of revolution and without body forces has been analyzed by the Columbia group [202] to [207], and their experimental results as well as those of Lowe [210] and [211] proved it to be a good mathematical model for circular compliant thrust bearings.

With the first three points considered in order to arrive at the assumptions of a steady state axisymmetric situation in a solid of revolution and without body forces, equations (1)

reduce to:

$$\left.\begin{aligned} \frac{\partial \sigma_r}{\partial r} + \frac{\sigma_r - \sigma_\theta}{r} + \frac{\partial \tau_{rz}}{\partial z} &= 0 \\ \frac{\partial \sigma_z}{\partial z} + \frac{\partial \tau_{rz}}{\partial r} + \frac{\tau_{rz}}{r} &= 0 \end{aligned}\right\} \qquad (2)$$

It is often advantageous to express equations (2) in terms of displacements. In order to do this, firstly one can write general equations of strains in terms of displacements. After that by Hooke's law, stresses are expressed in terms of strains and then in terms of displacements so that the stresses in equations (2) can be substituted by displacements.

Strains in terms of displacements in cylindrical polar coordinates can be written as [302]:

$$\left.\begin{aligned} e_r &= \frac{\partial u}{\partial r} \\ e_\theta &= \frac{u}{r} + \frac{1}{r}\frac{\partial v}{\partial \theta} \\ e_z &= \frac{\partial w}{\partial z} \\ e_{r\theta} &= \frac{1}{2}\left(\frac{1}{r}\frac{\partial u}{\partial \theta} + \frac{\partial v}{\partial r} - \frac{v}{r}\right) \\ e_{\theta z} &= \frac{1}{2}\left(\frac{1}{r}\frac{\partial w}{\partial \theta} + \frac{\partial v}{\partial z}\right) \\ e_{zr} &= \frac{1}{2}\left(\frac{\partial u}{\partial z} + \frac{\partial w}{\partial r}\right) \end{aligned}\right\} \qquad (3)$$

For axial symmetry, equations (3) reduce to:

$$\left.\begin{aligned} e_r &= \frac{\partial u}{\partial r} \\ e_\theta &= \frac{u}{r} \\ e_z &= \frac{\partial w}{\partial z} \\ e_{zr} &= \frac{1}{2}\left(\frac{\partial u}{\partial z} + \frac{\partial w}{\partial r}\right) \end{aligned}\right\} \qquad (4)$$

Hooke's law follows from equations (II-9), Appendix II :

$$\left.\begin{aligned} \sigma_r &= \lambda(e_r + e_\theta + e_z) + 2Ge_r \\ &= (\lambda+2G)e_r + \lambda\, e_\theta + \lambda\, e_z \\ \sigma_\theta &= \lambda(e_r + e_\theta + e_z) + 2G\, e_\theta \\ &= \lambda\, e_r + (\lambda + 2G)\, e_\theta + e_z \\ \sigma_z &= \lambda(e_r + e_\theta + e_z) + 2Ge_z \\ \tau_{rz} &= 2G\, e_{rz} \end{aligned}\right\} \qquad (5)$$

Taking into account equation (4), stresses in terms of displacements become:

$$\left.\begin{aligned}
\sigma_r &= (\lambda + 2G)\frac{\partial u}{\partial r} + \lambda \frac{u}{r} + \lambda \frac{\partial w}{\partial z} \\
\sigma_\theta &= \lambda\frac{\partial u}{\partial r} + (\lambda + 2G) \frac{u}{r} + \lambda\frac{\partial w}{\partial z} \\
\sigma_z &= \lambda\frac{\partial u}{\partial r} + \lambda\frac{u}{r} + (\lambda + 2G)\frac{\partial w}{\partial z} \\
\tau_{rz} &= G\left(\frac{\partial u}{\partial z} + \frac{\partial w}{\partial r}\right)
\end{aligned}\right\} \quad (6)$$

If strains in terms of stresses are desired, from equations (II-10) of Appendix II and taking account of (II-11):

$$e_{ij} = \frac{\tau_{ij}}{2G} - \delta_{ij}\tau_{kk}\frac{\lambda}{2G(3\lambda + 2G)} \quad (7)$$

Equation (7) written in full becomes:

$$\left.\begin{aligned}
e_r &= \frac{1}{2G}\left[\sigma_r \times\frac{2(\lambda+G)}{3\lambda+2G} - (\sigma_\theta + \sigma_z) \times \frac{\lambda}{3\lambda + 2G}\right] \\
e_\theta &= \frac{1}{2G}\left[\sigma_\theta \frac{2(\lambda+G)}{3\lambda+2G} - (\sigma_z + \sigma_r) \frac{\lambda}{3\lambda + 2G}\right] \\
e_z &= \frac{1}{2G}\left[\sigma_z \frac{2(\lambda+G)}{3\lambda +2G} - (\sigma_r + \sigma_\theta) \frac{\lambda}{3\lambda + 2G}\right] \\
e_{zr} &= \frac{\tau_{zr}}{2G}
\end{aligned}\right\} \quad (8)$$

Rather than in terms of Lamé constants λ and G, it is sometimes convenient to write (7) in terms of Young's modulus E and Poisson's ratio ν. Taking into account equations (II-11),

equation (7) can be written as:

$$e_{ij} = \frac{1+\nu}{E} \tau_{ij} - \frac{\nu}{E} \delta_{ij} \tau_{kk} \tag{9}$$

or written in full:

$$\left.\begin{aligned} e_r &= \frac{1}{E}\left[\sigma_r - \nu(\sigma_\theta + \sigma_z)\right] \\ e_\theta &= \frac{1}{E}\left[\sigma_\theta - \nu(\sigma_z + \sigma_r)\right] \\ e_z &= \frac{1}{E}\left[\sigma_z - \nu(\sigma_r + \sigma_\theta)\right] \\ e_{rz} &= \frac{1+\nu}{E} \tau_{rz} \end{aligned}\right\} \tag{10}$$

Going back to equations (2) it is now possible to express the stresses therein in terms of displacements u and w, by means of equations (6). First σ_r is differentiated with respect to r, σ_z with respect to z and τ_{rz} both with respect to r and to z.

$$\frac{\partial \sigma_r}{\partial r} = (\lambda+2G)\frac{\partial^2 u}{\partial r^2} + \lambda\left(\frac{1}{r}\frac{\partial u}{\partial r} - \frac{u}{r^2}\right) + \lambda \frac{\partial}{\partial r}\left(\frac{\partial w}{\partial z}\right)$$

$$\frac{\partial \sigma_z}{\partial z} = \lambda \frac{\partial}{\partial z}\left(\frac{\partial u}{\partial r}\right) + \frac{\lambda}{r}\frac{\partial u}{\partial z} + (\lambda+2G)\frac{\partial^2 w}{\partial z^2}$$

$$\frac{\partial \tau_{rz}}{\partial r} = G \frac{\partial}{\partial r}\left(\frac{\partial u}{\partial z} + \frac{\partial w}{\partial r}\right) = G \frac{\partial}{\partial r}\left(\frac{\partial u}{\partial z}\right) + G \frac{\partial^2 w}{\partial r^2}$$

$$\frac{\partial \tau_{rz}}{\partial z} = G \frac{\partial}{\partial z}\left(\frac{\partial u}{\partial z} + \frac{\partial w}{\partial r}\right) = G \frac{\partial^2 u}{\partial z^2} + \frac{\partial}{\partial z}\left(\frac{\partial w}{\partial r}\right)$$

so that the equations of equilibrium (2) in terms of displacements become :

$$\left.\begin{aligned}(\lambda+2G)\left(\frac{\partial^2 u}{\partial r^2}+\frac{1}{r}\frac{\partial u}{\partial r}-\frac{u}{r^2}\right)+(\lambda+G)\frac{\partial}{\partial r}\left(\frac{\partial w}{\partial z}\right)+G\frac{\partial^2 u}{\partial z^2}&=0\\ (\lambda+2G)\frac{\partial^2 w}{\partial z^2}+G\left(\frac{\partial^2 w}{\partial r^2}+\frac{1}{r}\frac{\partial w}{\partial r}\right)+(\lambda+G)\frac{\partial}{\partial z}\left(\frac{\partial u}{\partial r}+\frac{u}{r}\right)&=0\end{aligned}\right\} \quad (11)$$

Equations (11) can be written slightly differently as:

$$\left.\begin{aligned}(\lambda+2G)\frac{\partial}{\partial r}\frac{1}{r}\frac{\partial(ru)}{\partial r}+G\frac{\partial^2 u}{\partial z^2}+(\lambda+G)\frac{\partial}{\partial z}\left(\frac{\partial w}{\partial z}\right)&=0\\ (\lambda+2G)\frac{\partial^2 w}{\partial z^2}+\frac{G}{r}\left[\frac{\partial}{\partial r}\left(r\frac{\partial w}{\partial r}\right)\right]+(\lambda+G)\frac{\partial}{\partial z}\left[\frac{1}{r}\frac{\partial(ru)}{\partial r}\right]&=0\end{aligned}\right\} \quad (12)$$

It can be seen that the assumptions of steady-state operation, of body forces neglected and of axial symmetry reduce the general equation of equilibrium (1) into equations (2) in terms of stresses or equations (11) or (12) in terms of displacements. It is seen that these equations depend upon coordinates r and z and that both (11) and (12) contain displacements u and w. They are therefore coupled equations.

In the plane strain situation (point four of assumptions), forces are applied at the boundary of a thin plate in the plane of the plate, see sketch.

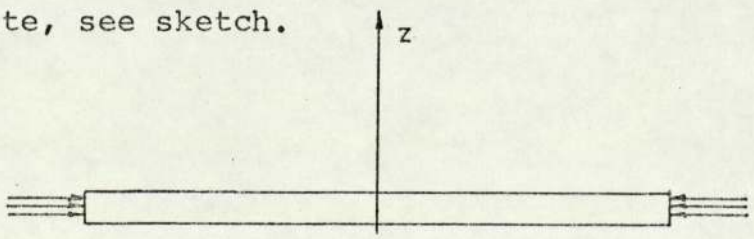

These forces are applied normally to the z-axis and are distributed uniformly along the plate thickness.

If the dimension of the plate in the z-direction is large and the body is loaded by forces normal to and not varying with z, then any plane of such a body normal to the z axis has got the same stress and strain distribution. This situation is described as plane strain.

At this point it is convenient to mention that some authors [314] define plane strain as a state when the axial displacements in the z-direction are zero, whilst others include in this definition the condition when axial displacements are uniform. If the axial displacements are uniform, this means that there is a uniform loading in the z-direction also.

A plane strain situation for steady-state operation and neglecting body forces reduces equations (1) to:

$$\begin{aligned} \frac{\partial \sigma_r}{\partial r} + \frac{1}{r}\frac{\partial \tau_{r\theta}}{\partial \theta} + \frac{\sigma_r - \sigma_\theta}{r} &= 0 \\ \frac{1}{r}\frac{\partial \sigma_\theta}{\partial \theta} + \frac{\partial \tau_{r\theta}}{\partial r} + \frac{2\tau_{r\theta}}{r} &= 0 \end{aligned} \qquad (13)$$

The problem described by equations (13) is analyzed in [203], [214], [219] and [220].

Incidentally Benjamin [203] used an axial wave number K_1 defined by Michell [15]. Benjamin shows that when $K_1=0$, equations (1) reduce to equations (13). This is the first step in Benjamin's solution and it can be considered as a first

approximation of the elasticity problem.

Meijers [220] examined the contact problem of a rigid cylinder against an elastic layer of thickness b, bonded to a rigid base, see fig. 4 . It is assumed that the cylinder is long enough in the direction normal to the plane of fig.4 , It is also assumed that there is no friction between the cylinder and the elastomer layer.

Theoretical solutions of Meijers concern various ratios of half contact zone c and elastomer thickness b. They also include situations when c/b is very small and when c/b is very large. The condition that $c/b \to 0$ means that the problem is near to "a circular disc on a half plane" state.

The condition that $c/b \to \infty$ means that the curvature is very smooth, almost plane, so that one can imagine a plane or a flat stamp in contact with the elastomer.

In the experimental configuration of Gupta and Smith [214] and [219], the ratio of c/b is large, and they have taken the condition of $c/b \to \infty$ as a solution to their elasticity problem.

Their papers concern the transient stage from a complete elastomer contact until the bearing lift-off. Just before the complete lift-off is achieved, a uniform pressure distribution exists in the bearing film(see fig. 5). This uniform pressure distribution means that the axial displacements are uniform. This situation can then be taken to belong to the class of plane strain problems, because the same stress and strain distribution exists in any plane of the elastomer

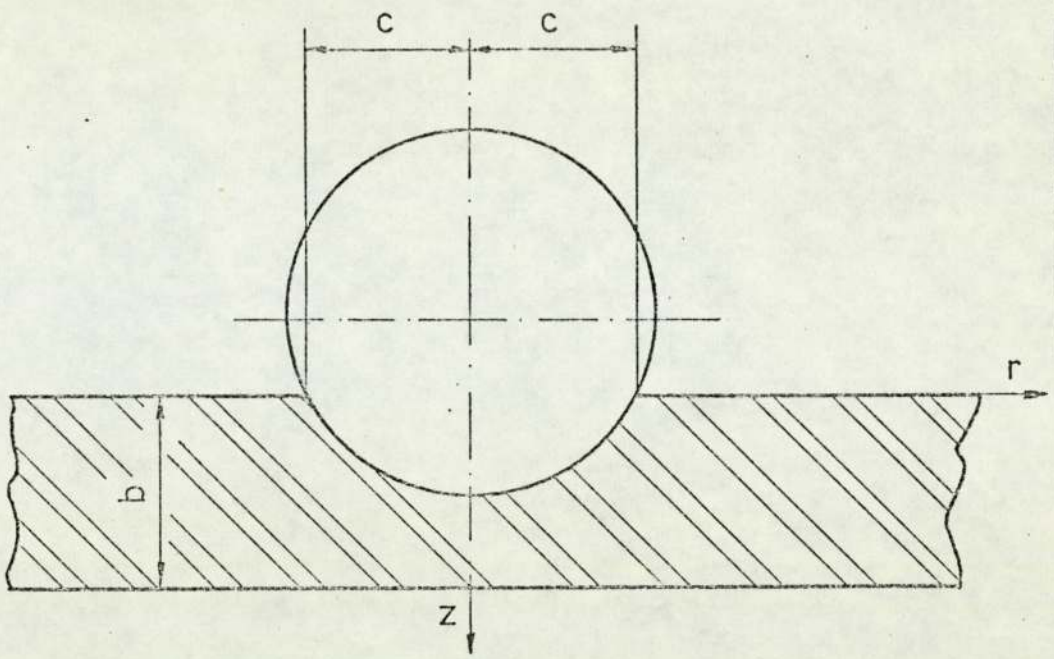

CONTACT PROBLEM OF A RIGID CYLINDER AGAINST AN ELASTIC LAYER

FIG 4

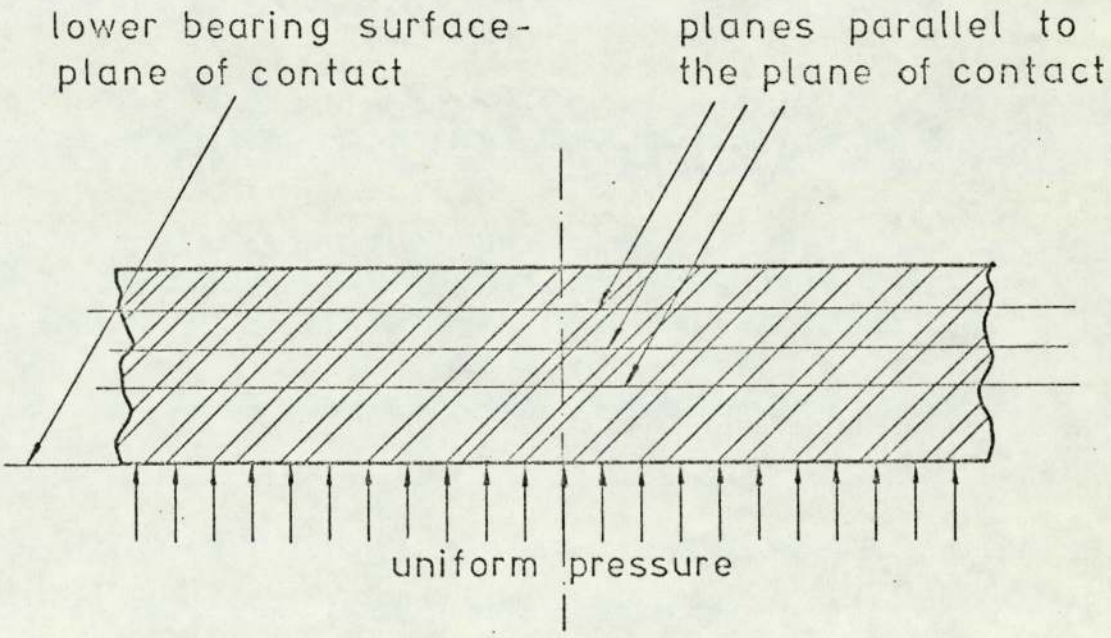

BEARING PRESSURE DISTRIBUTION BEFORE THE LIFT-OFF

FIG 5

parallel to the plane of contact, see fig. 5 .

If plane strain and axial symmetry is assumed, equations (13) reduce to radial equilibrium:

$$\frac{\partial \sigma_r}{\partial r} + \frac{\sigma_r - \sigma_\theta}{r} = 0 \qquad (14)$$

Equation (14) is a starting point in the solution of Kinsman [221]. In his solution radial and circumferential strains e_r and e_θ are given by the first two of equations (4). As equation (14) does not contain z, Kinsman's solution assumes that the radial displacement u is not a function of z. A possible experimental setup for such a theory is that the elastomer is not bonded to its backing and that it is allowed to move uniformly radially outwards.

Dowson and Taylor [201] take radial and circumferential strains to be

$$e_r = e_\theta = 0 \qquad (15)$$

With the axial stress σ_z equal to the gauge film pressure p_g, radial and circumferential stresses in Dowson and Taylor's theory reduce to:

$$\sigma_r = \sigma_\theta = \frac{\nu p_g}{1-\nu} \qquad (16)$$

Now, axial displacement δ is determined by the equation for the axial strain, the third equation of (10), as:

$$e_z = \frac{\delta}{t} = \frac{p_g}{E}\left[1 - \frac{2\nu^2}{1-\nu}\right] \qquad (17)$$

It is seen that for values of Poisson's ratio approaching to $\nu=0.5$, the axial displacement in Dowson's and Taylor's solution approaches zero, no matter what the film pressure is. This is understandable because in this theory no allowance is made for radial displacements. When Poisson's ratio approaches 0.5, elastomers become more and more incompressible, and as nothing is flowing radially outwards, notning will flow axially inwards either.

Clearly, Downson's and Taylor's theory is not suitable for completely incompressible elastomers. As stated in the literature survey, this theory can be used for Poisson's ratio values of up to 0.45,for example for bearings lined with soft metals.

Rightmire [305] has shown that most engineering elastomers have the value of Poisson's ratio in the range of:

$$0.495 < \nu < 0.5 \qquad (18)$$

Equations for stress in terms of strains (II-9), Appendix II, are not suitable for these values of Poisson's ratio because λ becomes very large. For a typical value of elastomer shear modules G=7 bar, reported by Benjamin, Rightmire and Castelli [205], the following table gives an insight into the possible values of Lamé Constant λ

ν	0.4950	0.4975	0.4975	0.4999
λ/G	99	199	499	4999
λ	693	1393	3493	34993

Such large values of λ when Poisson's ratio approaches 0.5 are not desirable when a numerical solution of equations (11) or (12) is required because they can cause an overflow in the computer. Equations (11) and (12) have been developed by starting from (II-9), Appendix II for stresses in terms of strains.

It is necessary to start from the modified form for the stress-strain law equation (III-9), Appendix III, and develop new equations of the type (11) or (12). Written in full, equations (III-9), Appendix III becomes:

$$\left.\begin{aligned}
\sigma_r &= p_m - G(e_r + e_\theta + e_z) + 2Ge_r \\
\sigma_\theta &= p_m - G(e_r + e_\theta + e_z) + 2Ge_\theta \\
\sigma_z &= p_m - G(e_r + e_\theta + e_z) + 2Ge_z \\
\tau_{rz} &= 2Ge_{rz}
\end{aligned}\right\} \qquad (19)$$

If strain-displacement the relationship is now used, equation (4), stresses in terms of displacements become

$$\left.\begin{aligned}
\sigma_r &= p_m - G\left(\frac{\partial u}{\partial r} + \frac{u}{r} + \frac{\partial w}{\partial z}\right) + 2G\frac{\partial u}{\partial r} \\
\sigma_\theta &= p_m - G\left(\frac{\partial u}{\partial r} + \frac{u}{r} + \frac{\partial w}{\partial z}\right) + 2G\frac{u}{r} \\
\sigma_z &= p_m - G\left(\frac{\partial u}{\partial r} + \frac{u}{r} + \frac{\partial w}{\partial z}\right) + 2G\frac{\partial w}{\partial z} \\
\tau_{rz} &= G\left(\frac{\partial u}{\partial z} + \frac{\partial w}{\partial r}\right)
\end{aligned}\right\} \qquad (20)$$

Substituting these values for stresses into the equations of equilibrium (2), the equations of equilibrium in terms of displacements become:

$$\left.\begin{aligned} \frac{\partial p_m}{\partial r} + G\left(\frac{\partial^2 u}{\partial r^2} + \frac{1}{r}\frac{\partial w}{\partial r} - \frac{u}{r^2} + \frac{\partial^2 u}{\partial z^2}\right) &= 0 \\ \frac{\partial p_m}{\partial z} + G\left(\frac{\partial^2 w}{\partial r^2} + \frac{1}{r}\frac{\partial w}{\partial r} + \frac{\partial^2 w}{\partial z^2}\right) &= 0 \end{aligned}\right\} \qquad (21)$$

or

$$\left.\begin{aligned} \frac{\partial p_m}{\partial r} + \frac{E}{2(1+\nu)}\left(\frac{\partial^2 u}{\partial r^2} + \frac{1}{r}\frac{\partial u}{\partial r} - \frac{u}{r^2} + \frac{\partial^2 u}{\partial z^2}\right) &= 0 \\ \frac{\partial p_m}{\partial z} + \frac{E}{2(1+\nu)}\left(\frac{\partial^2 w}{\partial r^2} + \frac{1}{r}\frac{\partial w}{\partial r} + \frac{\partial^2 w}{\partial z^2}\right) &= 0 \end{aligned}\right\} \qquad (22)$$

Similarly, starting from (III-14) and using the condition (III-13), Appendix III, the equations for equilibrium in terms of displacements for an incompressible elastomer become:

$$\left.\begin{aligned} \frac{\partial \tau_{mean}}{\partial r} + \frac{E}{3}\left(\frac{\partial^2 u}{\partial r^2} + \frac{1}{r}\frac{\partial u}{\partial r} - \frac{u}{r^2} + \frac{\partial^2 u}{\partial z^2}\right) &= 0 \\ \frac{\partial \tau_{mean}}{\partial z} + \frac{E}{3}\left(\frac{\partial^2 w}{\partial r^2} + \frac{1}{r}\frac{\partial w}{\partial r} + \frac{\partial^2 w}{\partial z^2}\right) &= 0 \end{aligned}\right\} \qquad (23)$$

Equations (22) are the general field equations for an axisymmetric compliant material for any value of Poisson's ratio ν within its natural limits $0 < \nu < 0.5$.

Equations (23) establish the solution when the elastomer volume does not change, i.e. when $\nu = 0.5$.

Boundary conditions of an axisymmetric solid of revolution specify either displacements or stresses at a particular boundary. Consider the arrangement of an incompressible solid of revolution as shown in fig. 6.

Stresses are given as

$$\left.\begin{aligned} \sigma_r &= \tau_{mean} + 2G\frac{\partial u}{\partial r} \\ \text{or} \quad \sigma_r &= \tau_{mean} - 2G\left(\frac{\partial w}{\partial z} + \frac{u}{r}\right) \end{aligned}\right\} \qquad (24)$$

$$\left.\begin{aligned} \sigma_\theta &= \tau_{mean} + 2G\frac{u}{r} \\ \text{or} \quad \sigma_\theta &= \tau_{mean} - 2G\left(\frac{\partial u}{\partial r} + \frac{\partial w}{\partial z}\right) \end{aligned}\right\} \qquad (25)$$

$$\left.\begin{aligned} \sigma_z &= \tau_{mean} - 2G\left(\frac{\partial u}{\partial r} + \frac{u}{r}\right) \\ \text{or} \quad \sigma_z &= \tau_{mean} + 2G\frac{\partial w}{\partial z} \end{aligned}\right\} \qquad (26)$$

$$\tau_{rz} = G\left(\frac{\partial u}{\partial z} + \frac{\partial w}{\partial r}\right) \qquad (27)$$

Consider fig. 6.

I On this boundary radial stress is zero and because this is a free surface, shear stress is also zero.

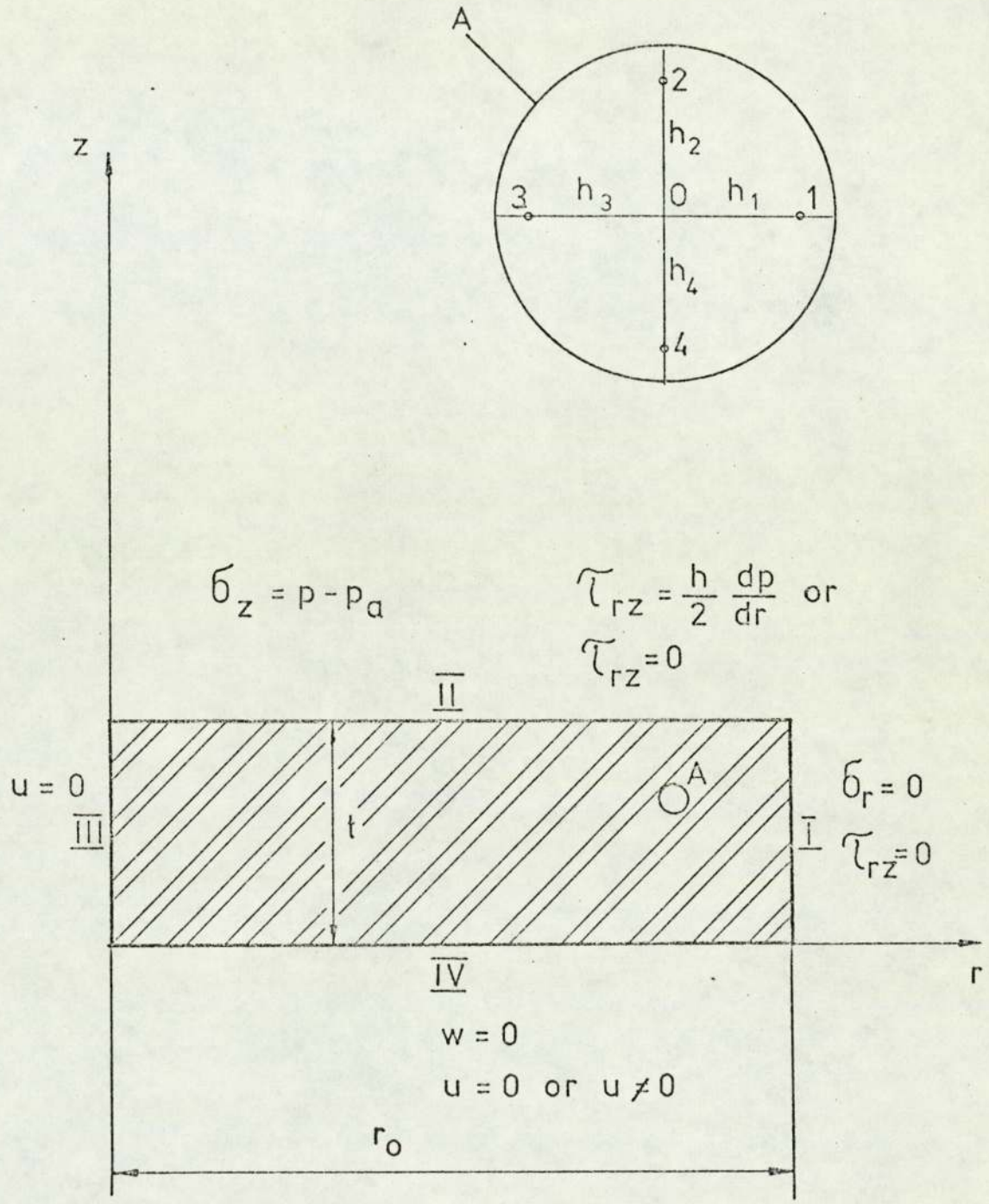

BOUNDARY CONDITIONS FOR
A COMPLIANT BEARING

FIG 6

II Here axial stress σ_z is determined by the gauge film pressure $p-p_a$. Shear stress τ_{rz} is calculated from the requirement that the flow velocity is zero at z=t. Usual assumptions for the Reynolds equation, which is the governing equation for the film pressure distribution, are neglect of body and inertia forces and sometimes neglect of the presence of compressibility effects in the Navier-Stokes equations of motion, from which Reynolds equation is derived, see Appendix I. Depending upon the flow conditions, some of these assumptions may not be true, see for example reference [140]. Velocity gradient, which figures in the expression for shear stress is also derived in Appendix I.

Benjamin and Castelli [204] have shown that in the case of journal bearings shear stresses are negligible compared to normal stresses. Therefore as a first approximation these stresses can be taken to be equal to zero.

III Because of axial symmetry, there is no radial displacement at r=0.

IV On this side there is no axial displacement, but depending whether the elastomer is free or bonded to its backing plate, there may or may not be some radial displacement.

Dowson and Taylor have developed an approximate analytic solution for pressure distribution and bearing load. They have shown that if the elastic compression is small this analytic solution is satisfactory. Otherwise an iterative

procedure is used.

Castelli et al have solved their compliant bearing problem by means of Fourier and Hankel transforms. Initially, their method of solution is analytic, but the resulting integrals are then solved numerically.

The author has attempted a numerical solution with the help of the subroutine "solution of Elliptic Partial Differential Equations" which is available at the University of Manchester Regional Computer Centre. This subroutine consists of 17 "sub-subroutines" out of which the user writes three for a particular problem. This subroutine is based upon finite central difference methods.

The governing elastic equations are transformed into finite difference schemes with the help of the reference (18). Consider an incompressible material and assume that p_m = const. Then from (23), the following equations are obtained:

$$\left.\begin{aligned} \frac{\partial^2 u}{\partial r^2} + \frac{1}{r}\frac{\partial u}{\partial r} - \frac{u}{r^2} + \frac{\partial^2 u}{\partial z^2} &= 0 \\ \frac{\partial^2 w}{\partial r^2} + \frac{1}{r}\frac{\partial w}{\partial r} + \frac{\partial^2 w}{\partial z^2} &= 0 \end{aligned}\right\} \qquad (28)$$

From (24) to (27)

$$\left.\begin{aligned} \frac{\sigma_r}{G} &= \frac{\tau_{mean}}{G} + 2\frac{\partial u}{\partial r} \\ \frac{\sigma_\theta}{G} &= \frac{\tau_{mean}}{G} + 2\frac{u}{r} \\ \frac{\sigma_z}{G} &= \frac{\tau_{mean}}{G} + 2\frac{\partial w}{\partial z} \\ \frac{\tau_{rz}}{G} &= \frac{\partial u}{\partial z} + \frac{\partial w}{\partial r} \end{aligned}\right\} \qquad (29)$$

Consider a point O and the four neighbouring points i (i = 1, 2, 3 and 4), see fig. 6. Distances from O to the neighbouring points are h(i). Then the following expressions can be stated [18] :

$$\left.\begin{aligned}
\frac{\partial^2 u}{\partial r^2} &= \frac{2}{\Delta r^2 h_1 h_3 (h_1+h_3)} \left[h_3 u_1 + h_1 u_3 - (h_1 + h_3) u_o\right] \\
\frac{1}{r}\frac{\partial u}{\partial r} &= \frac{1}{r h_1 h_3 (h_1+h_3) \Delta r} \left[h_3^2 u_1 - h_1^2 u_3 - (h_3^2 - h_1^2) u_o\right] \\
-\frac{u}{r^2} &= -\frac{u_o}{r^2} \\
\frac{\partial^2 u}{\partial z^2} &= \frac{2}{\Delta z^2 h_2 h_4 (h_2+h_4)} \left[h_4 u_2 + h_2 u_4 - (h_2 + h_4) u_o\right] \\
\frac{\partial^2 w}{\partial r^2} &= \frac{2}{\Delta r^2 h_1 h_3 (h_1 + h_3)} \left[h_3 w_1 + h_1 w_3 - (h_1 + h_3) w_o\right] \\
\frac{1}{r}\frac{\partial w}{\partial r} &= \frac{1}{r h_1 h_3 (h_1 + h_3) \Delta r} \left[h_3^2 w_1 - h_1^2 w_3 - (h_3^2 - h_1^2) w_o\right] \\
\frac{\partial^2 w}{\partial z^2} &= \frac{2}{\Delta r^2 h_2 h_4 (h_2+h_4)} \left[h_4 w_2 + h_2 w_4 - (h_2+h_4) w_o\right]
\end{aligned}\right\} \quad (30)$$

and

$$\left.\begin{aligned}
\frac{\partial u}{\partial r} &= \frac{1}{h_1 h_3 (h_1+h_3)\Delta r}\left[h_3^2 u_1 - h_1^2 u_3 - (h_3^2-h_1^2)u_o\right] \\
\frac{u}{r} &= \frac{u_o}{r} \\
\frac{\partial w}{\partial z} &= \frac{1}{h_2 h_4 (h_2+h_4)\Delta z}\left[h_4^2 w_2 - h_2^2 w_4 - (h_4^2-h_2^2)w_o\right] \\
\frac{\partial u}{\partial z} &= \frac{1}{h_2 h_4 (h_2+h_4)\Delta z}\left[h_4^2 u_2 - h_2^2 u_4 - (h_4^2-h_2^2)u_o\right] \\
\frac{\partial w}{\partial r} &= \frac{1}{h_1 h_3 (h_1+h_3)\Delta r}\left[h_3^2 w_1 - h_1^2 w_3 - (h_3^2-h_1^2)w_o\right]
\end{aligned}\right\} \qquad (31)$$

Then at any point O within the plane of the elastomer shown on fig. 6 displacements u and w can be expressed as:

$$\left.\begin{aligned}
u_o &= c_u(1)u_1 + c_u(2)u_2 + c_u(3)u_3 \\
&\quad + c_u(4)u_4 + c_u(5) \\
w_o &= c_w(1)w_1 + c_w(2)w_2 + c_w(3)w_3 \\
&\quad + c_w(4)w_4 + c_w(5)
\end{aligned}\right\} \qquad (32)$$

Coefficients $c_u(i)$ and $c_w(i)$ where $i = 1,4$ depend upon $h(i)$, Δr, Δz. Coefficients $c_u(5)$ and $c_w(5)$ apart from $h(i)$, Δr and Δz can also depend upon u, w, G and $p_g = p - p_a$ at boundaries.

The film pressure p must satisty the Reynolds equation also. This equation is given by equation (I-5), Appendix I which states

$$\frac{d}{dr}\left[r\,\frac{d}{dr}(p^2)\right] = 0 \qquad (33)$$

Equation (33) can be modified to read

$$\frac{d^2(p^2)}{dr^2} + \frac{d(p^2)}{dr}\left(\frac{3}{h}\,\frac{dh}{dr} + \frac{1}{r}\right) = 0 \qquad (34)$$

The film thickness of equation (34) can be described as

$$h = h_o + w \qquad (35)$$

where h_o is a uniform film thickness without elastomer deformation. Now equation (34) can be expressed as

$$\frac{d^2F}{dr^2} + \frac{dF}{dr}\left[\frac{3}{(h_o+w)}\,\frac{dw}{dr} + \frac{1}{r}\right] = 0 \qquad (36)$$

A finite difference form of this equation can be taken to be equal to

$$\frac{F(J+1)-2F(J)+F(J-1)}{\Delta r^2} + \frac{F(J+1)-F(J-1)}{2\Delta r} \times \mathrm{BRACK}(J)=0 \qquad (37)$$

so that pressure squared at any radial position $r=(J-1)\Delta r$ is equal to:

$$F(J) = F(J+1)(1+BRACK(J) \times \Delta r/2)/2 + \\ + F(J-1)(1-BRACK(J) \times \Delta r/2)/2 \qquad (38)$$

Here BRACK (J) is the term in the square bracket of equation (36). In finite central difference form this term is equal to

$$BRACK(J) = \left[\frac{3}{h_o + w(J)} \qquad \frac{w(J+1)-w(J-1)}{2\Delta r} + \frac{1}{r} \right] \qquad (39)$$

Referring to figure (6) a flow diagram of the solution is shown in figure (7).

The programme available at the Manchester Computer Centre is suitable for solving two dimensional second order elliptic partial differential equations with one variable.

Within the elastomer field the governing equations have one variable only (either w or u) but at some boundaries two variables define the problem.

The difficulty lies in modifying the programme to be used at the boundaries and according to the flow chart of fig. 7. Sections 1, 2, and 3 of the flow chart have been written, see Appendix IV. Although these sections work individually, more programme development is needed that they work as a whole unit.

Sections 1 and 2 are written in Fortran and section 3 in Basic.

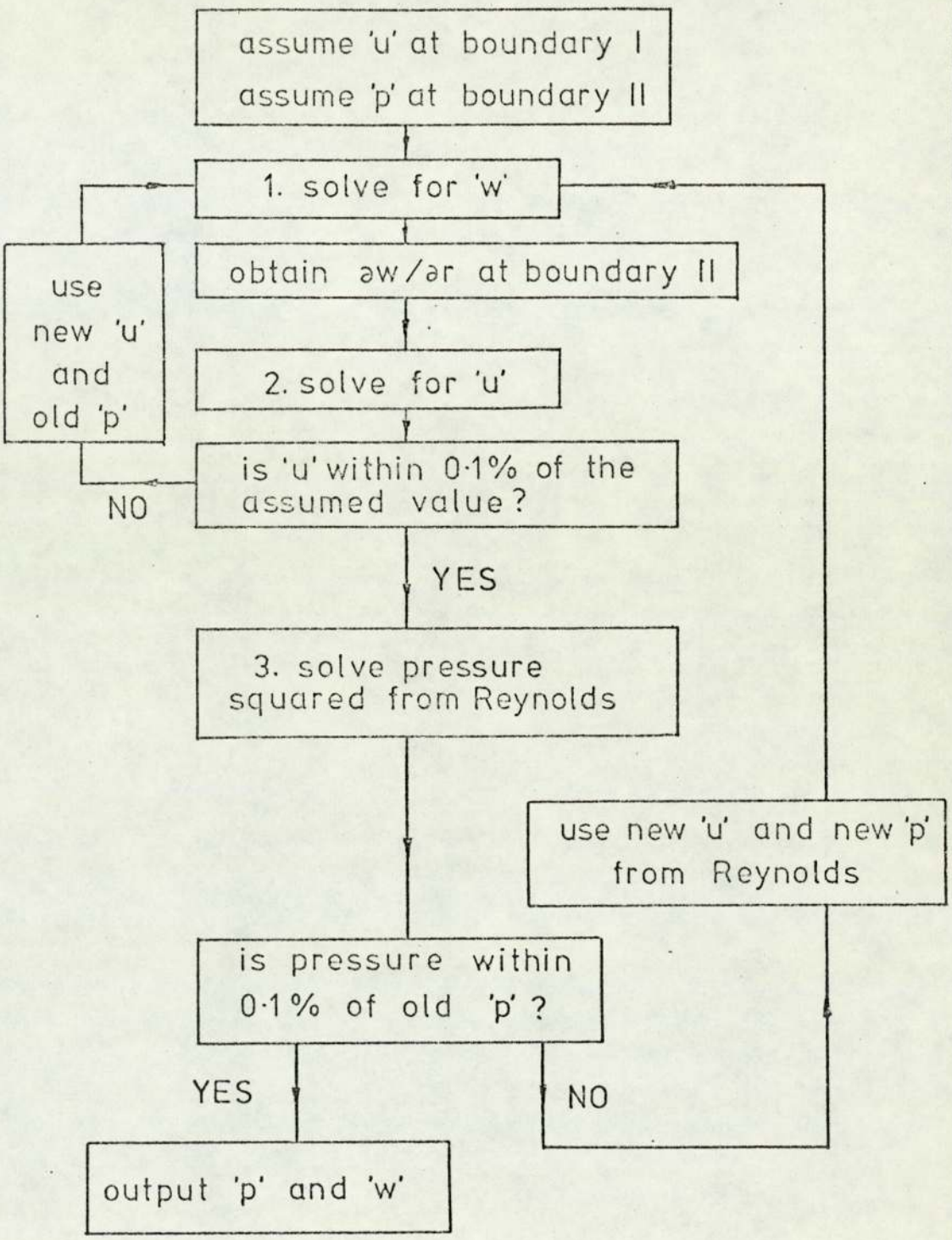

FLOW DIAGRAM FOR THE SOLUTION OF COMPUTER PROGRAMMES PRESENTED IN APPENDIX IV

FIG 7

IV EXPERIMENTAL ANALYSIS OF ELASTOMER PROPERTIES

4.1 Basic relationships

A literature survey has revealed that elastomers used in compliant bearings are taken to be perfectly elastic, homogeneous and isotropic.

In developing stress strain relationships for bearing elastomers, Appendix II it is seen that for a large group of materials named Hookean elastic solids, the stress tensor is proportional to the strain tensor. For these materials, there are in general 21 coefficients of proportionality or elastic constants. The number of elastic constants reduces to two only for perfectly elastic, homogeneous and isotropic materials.

Stress in terms of strain, or vice versa, for these materials can therefore be expressed in terms of two elastic constants. If stress is expressed in terms of strain, Lamé constants λ and G are normally used, see equation (II-9), Appendix II, or equations (5), Chapter III. If strain is expressed in terms of stress, bulk modulus K and shear modules G can be used, see equation (II-10), Appendix II, or Lamé constants λ and G can be used, see equations (7) and (8), Chapter III. It is even more customary to write strain in terms of stress by means of elastic modulus E and Poisson's ratio ν, as shown in equation (9) or (10) of Chapter III. Some of the more important relationships between λ, G, K, E and ν are given by equations (II-11), Appendix II.

In the discussion of Rightmite's paper [305], Dowson and Taylor have given relationships for evaluating Poisson's ratio by means of elastic modulus E, shear modulus G and bulk

modulus K as follows

$$\left.\begin{aligned} \nu &= \frac{E}{2G} - 1 \\ \nu &= \frac{1}{2} - \frac{E}{6K} \\ \nu &= \frac{1}{2} - \frac{G}{2K} \end{aligned}\right\} \qquad (1)$$

The first two of equation (1) follow from elastic relationships, some of which are given by equations (II-11), Appendix II, whilst in evaluating the third of equations (1) it has been assumed that the value of Poisson's ratio is close to 0,5. Rightmire [305] has calculated Poisson's ratio by means of experimentally determined values of shear modulus G and bulk modulus K. The third of equations (1) is his first order solution and in his paper [305] he proved that this solution is accurate enough for the range of elastomer properties investigated.

Poisson's ratio is not a property that can be measured directly, but it is calculated by means of other properties of the material.

Rightmire has chosen to measure bulk modulus K and shear modulus G and then to calculate Poisson's ratio ν.

It is not practical to try and measure elastic modulus E and shear modulus G, because E and G are of the same order of magnitude and this can result in large errors in Poisson's ratio ν.

The author has chosen to measure experimentally the bulk modulus K and the elastic modulus E. Elastic modulus was

chosen rather than shear modulus, because it can be measured conveniently during the bearing tests, see Chapter VII.

In order to make an estimate of the errors in Poisson's ratio ν, when working with the second of the equations (1), the following has been done

The total differential of ν can be written as

$$\Delta\nu = \frac{\partial\nu}{\partial E}\,\Delta E + \frac{\partial\nu}{\partial K}\,\Delta K \qquad (2)$$

When equation (2) is applied to the second equation of (1)

$$\Delta\nu = -\frac{1}{6K}\,\Delta E + \frac{E}{6K^2}\,\Delta K$$

which can be written as

$$\frac{\Delta\nu}{\nu} = -\frac{1}{(\frac{3K}{E}-1)}\,\frac{\Delta E}{E} + \frac{1}{(\frac{3K}{E}-1)}\,\frac{\Delta K}{K} \qquad (3)$$

From equation (II–11), Appendix II

$$\frac{3K}{E} = \frac{1}{1-2\nu}$$

and when this result is substituted into equation (3), this reduces to

$$\frac{\Delta\nu}{\nu} = -(\frac{1}{2\nu}-1)\,\frac{\Delta E}{E} + (\frac{1}{2\nu}-1)\,\frac{\Delta K}{K} \qquad (4)$$

where $\frac{\Delta\nu}{\nu}$, $\frac{\Delta E}{E}$ and $\frac{\Delta K}{K}$ represent errors of ν, E and K respectively.

It is seen that for the range of Poisson's ratios for elastomers $0{,}495 \leq \nu \leq 0{,}50$, the following can be concluded

For $\nu = 0{,}5$, $\frac{\Delta\nu}{\nu} = 0$; i.e. there is no error for all

possible errors in measuring elastic modulus E or bulk modulus K.

If the true value of $\nu = 0,495$, and supposing that the errors in determining E and K are 0,10 and 0,20 respectively, then the error in calculating Poisson's ratio becomes

$$\frac{\Delta\nu}{\nu} = -0,01 \times 0,10 + 0,01 \times 0,020 =$$

$$= -0,001 + 0,002 = 0,001$$

It is shown that even for the relatively large errors of 10% and 20% in E and K, the error in Poisson's ratio is only 0,1%.

If the first of the equations (1) was considered and if similar analysis was performed, it can be shown that the resulting equation of relative errors is

$$\frac{\Delta\nu}{\nu} = -\frac{(1+\nu)}{\nu}\frac{\Delta E}{E} + \frac{(1+\nu)}{\nu}\frac{\Delta G}{G} \qquad (5)$$

For true value of $\nu=0,5$ and for $\frac{\Delta E}{E} = 0,10$ and $\frac{\Delta G}{G} = 0,20$, the error in Poisson's ratio is as high as 30%.

Therefore the use of the second of equations (1) is justified.

4.2 Bulk modulus evaluation

For a body subjected to hydrostatic pressure and from equation (II-8), Appendix I bulk modulus is given by

$$K = \frac{p}{e_{kk}} \qquad (6)$$

where $e_{kk} = \frac{\Delta V}{V}$ is volumetric strain. By knowing the pressure p to which the elastomer sample is subjected and by knowing the volume change incurred, the bulk modulus K is obtained.

An experimental apparatus, to measure volumetric strain and pressure, which is very similar in principle of operation to that of G.K. Rightmire [305] has been developed in the University workshops, see fig. 8 and photograph I .

A perspex tube of 6.35 mm. nominal inside diameter is 'welded'to PVC adaptors. This tube-adaptor assembly is then connected to a container where the elastomer disc is placed. The container with its cover is shown in photograph II .

The container consists of two parts bolted together and sealed with an 'O'ring. The upper part has a vent valve incorporated in its design and this valve is sealed with a "DOWTY" seal. The lower PVC adaptor of the perspex tube is sealed with an "O" ring against the top steel part of the container. The perspex tube-adaptors assembly is secured to the container by means of a steel adaptor bolted to the upper part of the container.

Water coloured with red ink is used as a working liquid in this bulk modulus apparatus. Both the cavity where the elastomer disc is placed and about 3/4 of the height of the perspex tube are filled with this liquid. The vent valve in the upper part of the container is used to eliminate air bubbles trapped by the working liquid during filling. In his apparatus Rightmire [305] has used mercury, but water coloured with red ink is preferred for safety and sensitivity.

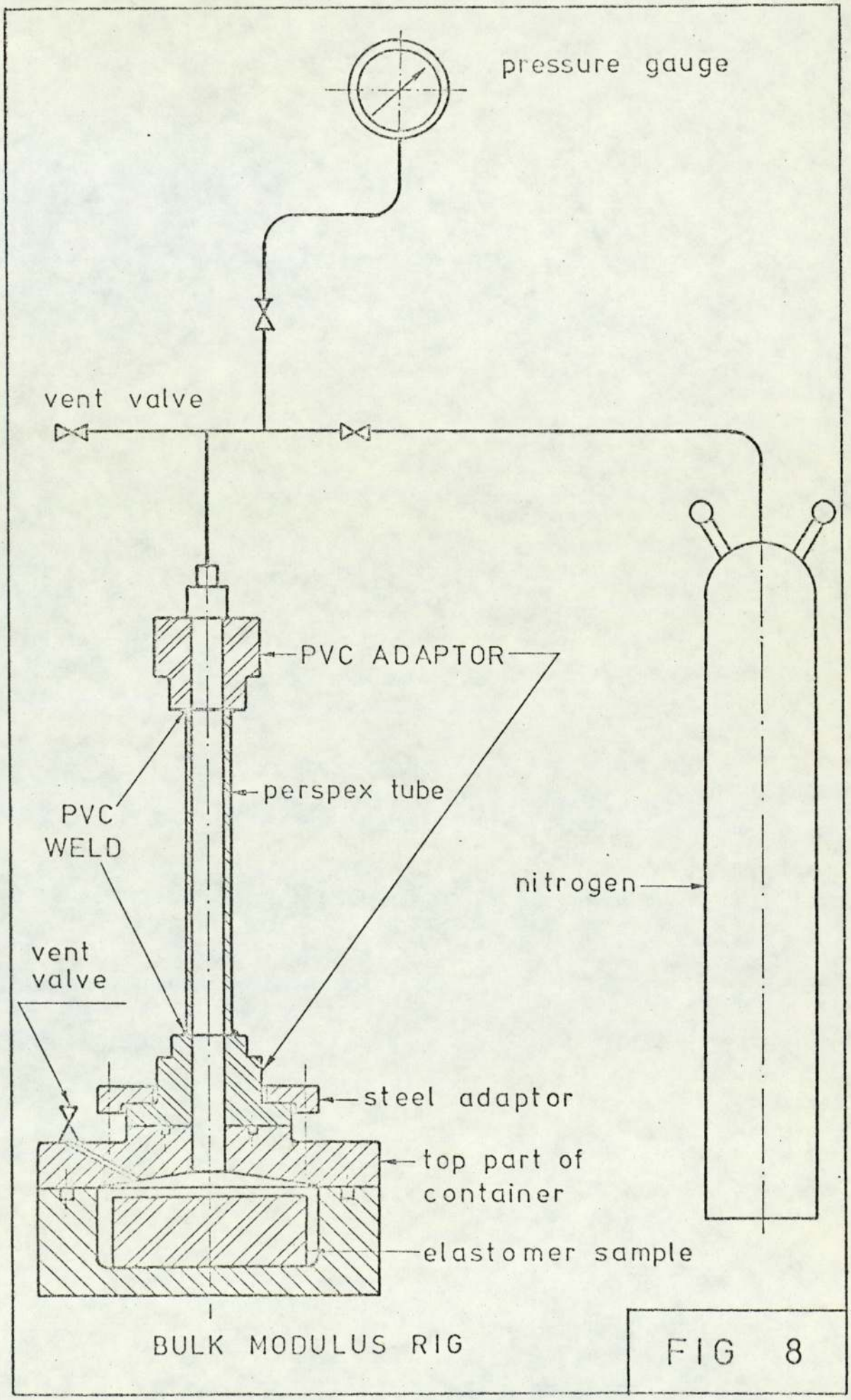

BULK MODULUS RIG

FIG 8

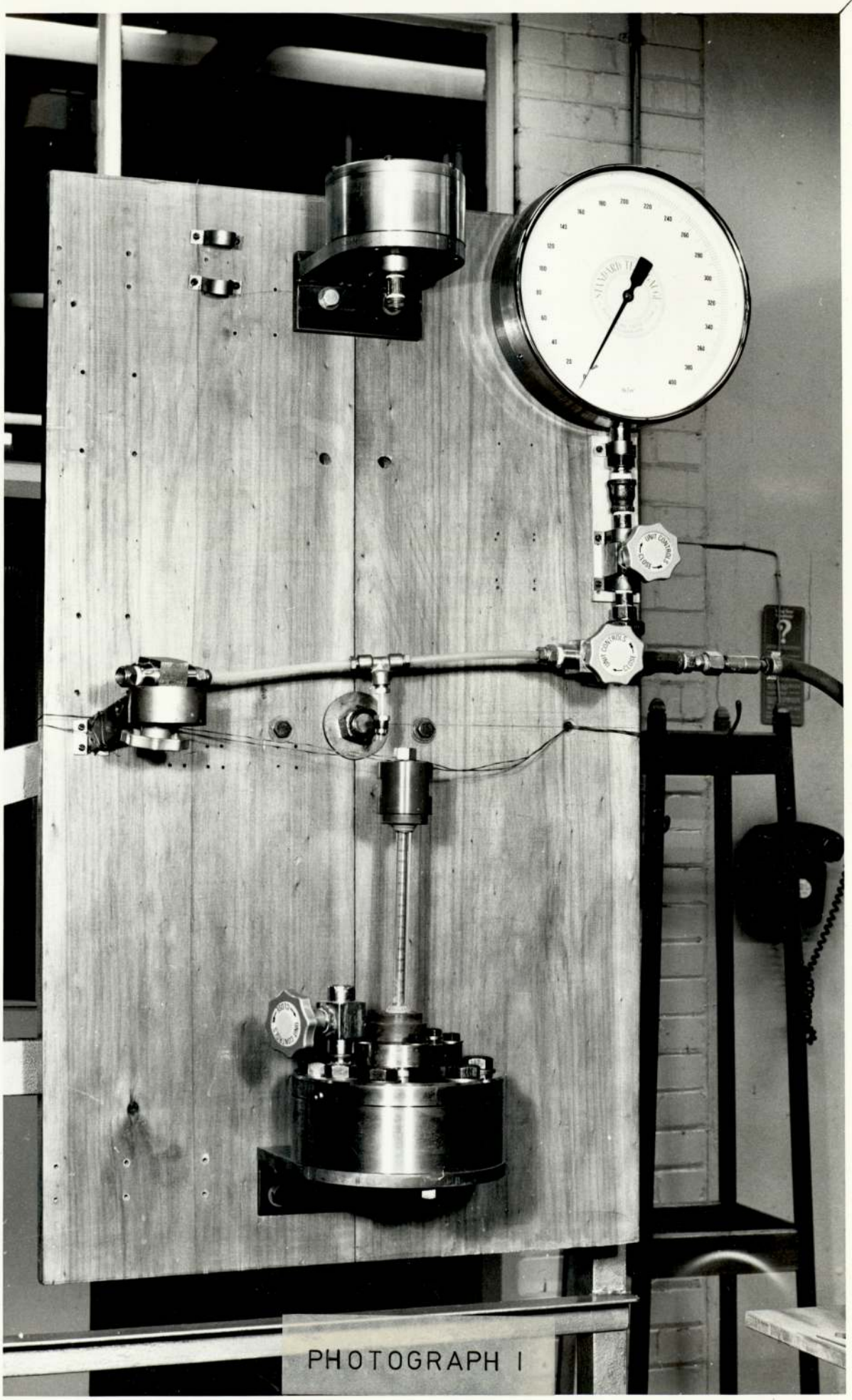

PHOTOGRAPH I

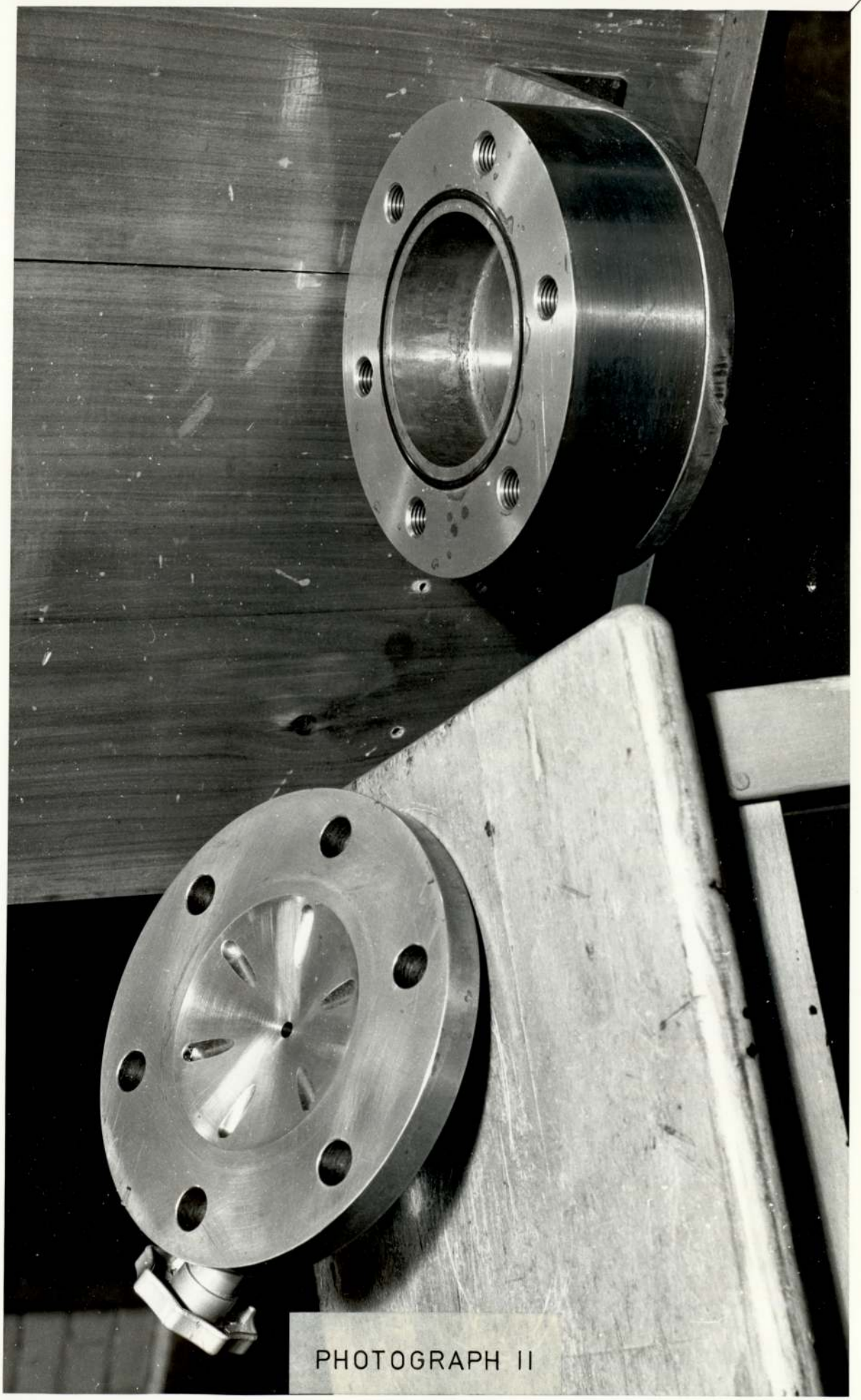

PHOTOGRAPH II

Once filled, the perspex tube is pressurized by nitrogen up to 27.5 bar through the upper PVC adaptor. Differences of the water levels are read on the graduation scale of perspex tube. As the whole bulk modulus rig expands under pressure and as water slightly compresses, it is necessary to calibrate the rig using a disc made of a material of known elastic properties, say a steel disc. Fig. 9 shows the arrangement, and photograph III shows two discs and also the mould used for producing the rubber disc.

The mould was made in the University workshops and discs of natural rubber were moulded. The Chemistry department at the University was consulted and the following formula of the rubber contents was used:

Natural rubber	1000 g	
Zinc oxide	50 g	mixed together and added to natural rubber first in BUNBURY mix
Stearic acid	30 g	
CBS*	10 g	
PBN**	10 g	
HAF***black	150 g	
Sulphur	25 g	

The mould was kept for 1½ hours at 140°C in the press at 50 tons/in^2. Dummy steel discs were made with the same dimensions as the rubber samples.

The inner diameter of the perspex tube "d_p" was measured on a projector in the metrology laboratory at Aston University. Magnification factor of the projector is ten, and the average

---

* CBS - Cyclo-hexyl benzthiazyl sylphenamide
** PBN - Phenyl-β-naphthylamine
*** HAF - High abrasion furnace

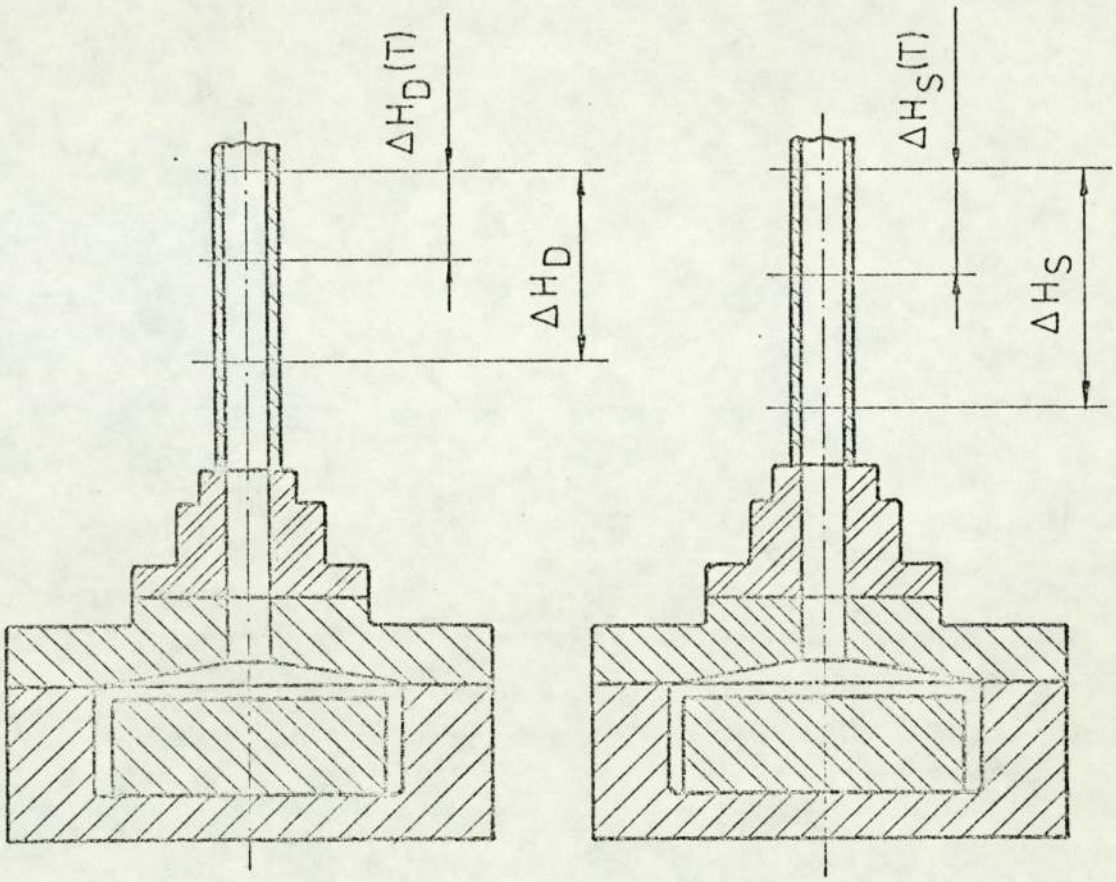

ΔH_S – REAL DISPLACEMENT OF WATER LEVEL UNDER GIVEN PRESSURE WITH ELASTOMER IN RIG

ΔH_D – REAL DISPLACEMENT OF WATER LEVEL UNDER GIVEN PRESSURE WITH DUMMY STEEL DISK IN RIG

$\Delta H_S(T), \Delta H_D(T)$ – corresponding theoretical displacements of water level as if there is neither expansion of rig nor compression of water

CALIBRATION OF BULK MODULUS RIG

FIG 9

PHOTOGRAPH III

result of eight readings:

$$d_p = 6.449 \text{ mm}$$

The corresponding cross sectional area

$$A_p = \pi \times 6.449^2/4 = 32.661864\text{mm}^2$$

For a given pressure, expansion of the container and compression of the water do not vary, no matter whether an elastomer sample or the dummy disc is in the container.

Therefore, referring to fig. 9

$$A_p \times \Delta H_S - A_p \times \Delta H_S(T) = A_p \times \Delta H_D - A_p \times \Delta H_D(T)$$

or

$$A_p \times \Delta H_S - \Delta V_S = A_p \times \Delta H_D - \Delta V_D$$

where ΔV_S and ΔV_D are volume changes of sample and dummy disc due to pressurization from the nitrogen bottle. Therefore volume change of the sample

$$\Delta V_S = \Delta V_D + A_p \times (\Delta H_S - \Delta H_D) \qquad (7)$$

Here ΔH_S and ΔH_D are the measured differences of liquid levels between the ambient pressure and the given pressure for the sample and dummy disc respectively.

Dividing by the volume of the rubber disc (which is equal to the volume of the dummy steel disc) V equation (7) becomes:

$$\frac{\Delta V_S}{V} = \frac{\Delta V_D}{V} + \frac{A_p}{V} (\Delta H_S - \Delta H_D) \qquad (8)$$

The complete procedure for evaluating the bulk modulus is shown for natural rubber made at Aston University. The rubber disc when moulded had the following dimensions - 87.376mm dia x 31.496mm thick. The steel dummy disc had the same dimensions. Experimental results for these two are given below:

DUMMY STEEL DISC		NATURAL RUBBER DISC	
gauge pressure [bar]	water level at perspex tube [mm]	gauge pressure [bar]	water level at perspex tube [mm]
0	311	0	312
5.998	305.5	5.585	306.5
9.791	301	8.412	301
12.169	298	11.052	298
14.548	295.5	12.962	295.5
16.685	294	15.444	293
19.029	292	17.133	291
21.374	289.5	18.823	289.3
23.373	288	21.236	287
25.855	286	23.408	284.5
27.096	285	25.510	282.3
		26.924	281

Thé rig with a rubber disc inside was "cycled" a few times from ambient to maximum pressure so that rubber can settle. This is a common practice when testing rubber components. The first cycle is not 'typical' and if stress against strain curves are plotted for each cycle, the differences between the first few cycles can be large. Then the subsequent

cycles are almost identical.

Maximum pressure for the perspex tube is recommended not to exceed 40 bar, but 27.5 bar is chosen for safety. After this cycling, results for the steel and rubber discs were taken.

Existence of similar conditions when the steel disc is in the rig is thus achieved. Pressure was read up to 400 lbf /in^2 on a Budenberg gauge and the results were then converted to bars.

Fig. 10 shows the results. A polynomial of the first order is obviously the best fit. A regression analysis programme based on the least squares method is available on the departmental Hewlett Packard Computer. This programme was used to fit straight lines to the two sets of points as shown in Fig. 10 . Results in steps of 5 bars are shown in the following table:

	DUMMY DISC		RUBBER DISC	
	gauge pressure [bar]	water level [mm]	gauge pressure [bar]	water level [mm]
1)	0	310.14	0	311.07
2)	5	305.40	5	305.37
3)	10	300.65	10	299.67
4)	15	295.91	15	293.96
5)	20	291.17	20	288.26
6)	25	286.42	25	282.56

These results were used for calculating differences of water levels based upon ambient conditions.

From the value of bulk modulus for steel [307]

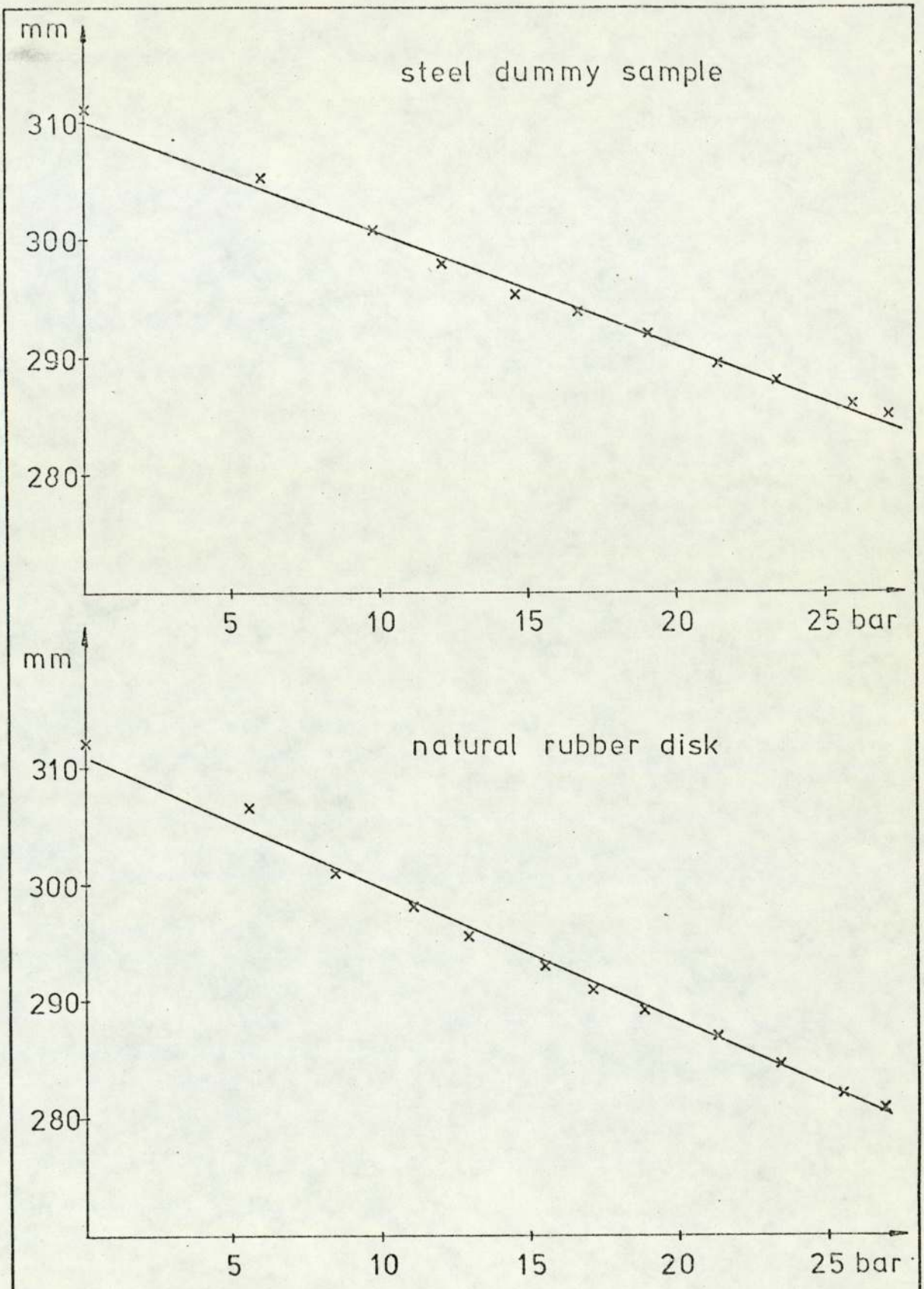

GAUGE PRESSURE AGAINST WATER LEVEL IN PERSPEX TUBE

FIG 10

$K = 1.76 \times 10^6$ bar, the volumetric strain $\Delta V/V$ for the steel disc can be calculated under various pressures.

The volume of rubber i.e. steel disc under ambient conditions for this case is:

$$V = \pi \times 87.376^2 \times 31.496/_4 = 188855.484 mm^3$$

Using equation (8) relative volume changes $\Delta V_S/V$ of rubber for various pressures are calculated as follows:

	ΔH_D	ΔH_S	$\Delta H_S - \Delta H_D$	$\frac{\Delta V_D}{V} \times 10^6$	$\frac{A_p}{V}(\Delta H_S - \Delta H_D) \times 10^6$	$\frac{\Delta V_S}{V} \times 10^3$
[bar]	[mm]	[mm]	[mm]	[-]	[-]	[-]
5	4.74	5.70	0.96	2.84	166.03	0.169
10	9.49	11.40	1.91	5.68	330.38	0.336
15	14.23	17.14	2.91	8.52	503.27	0.512
20	18.97	22.81	3.84	11.36	664.11	0.675
25	23.72	28.51	4.79	14.20	828.41	0.843

These results show that the contribution of compressibility of steel $\Delta V_D/V$ are small compared to the other term on the right hand side of equation (8). The expansion of rig $\frac{A_p}{V}(\Delta H_S - \Delta H_D)$ is the dominant term. As H_S and H_D were related linearly with pressure see fig. 10 , one would expect also that $\frac{\Delta V_S}{V}$ is linear, because the dominant term in the expression for $\Delta V_S/V$ consists of water-level differences multiplied by a constant A_p/V. Fig. 11 is the plot of relative rubber volume change against pressure and confirms that the relationship is linear.

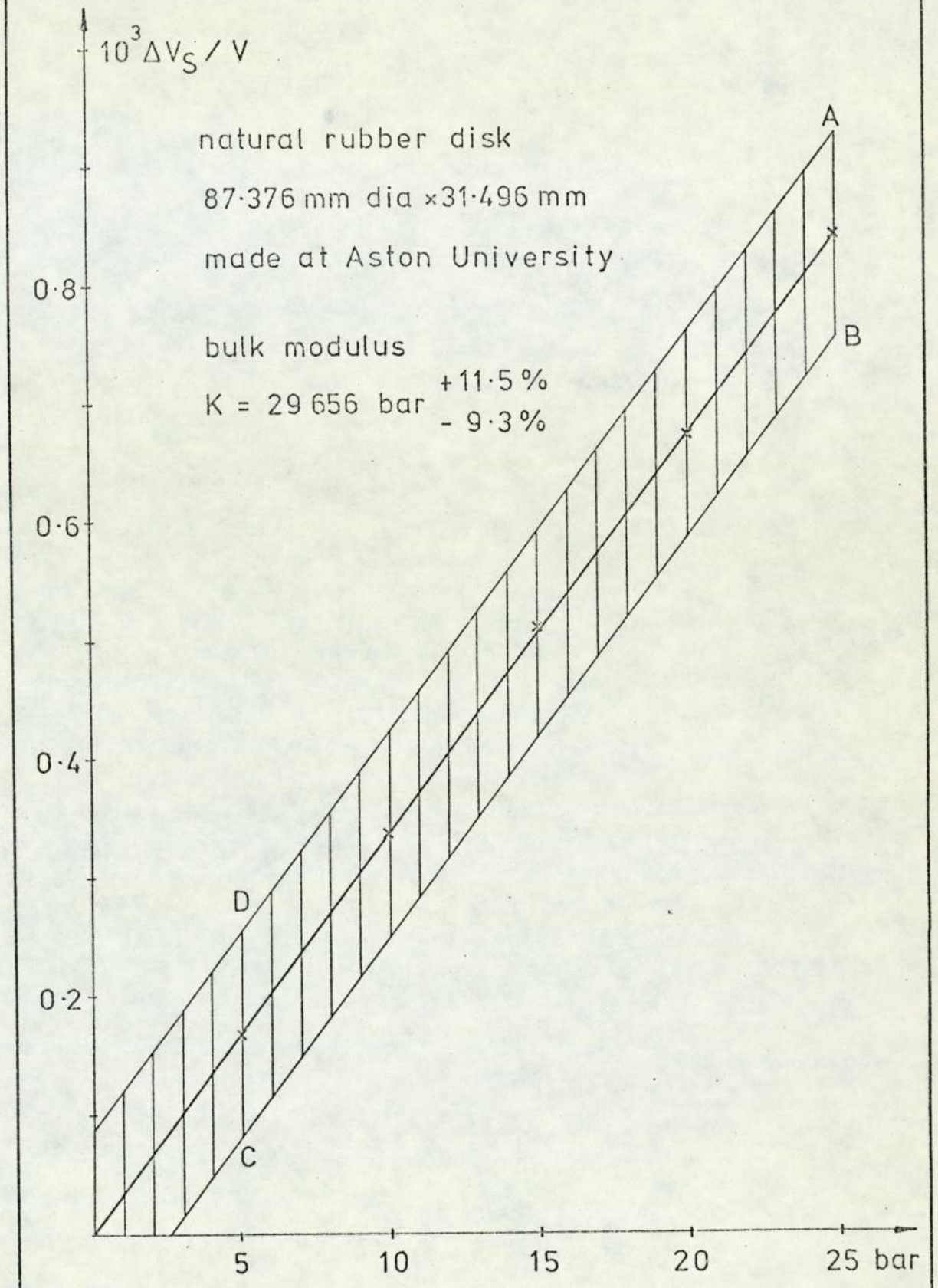

VOLUMETRIC STRAIN AGAINST GAUGE PRESSURE

FIG 11

Pressure is read on the 400 lbf/in^2 pressure gauge. This pressure gauge had been calibrated with a dead weight tester and it shows almost 1 lbf/in^2 higher readings.

The graduation scale on the perspex tube is given in millimetres. It is estimated that the tolerance on a reading on this scale is ±0.25mm. As differences are involved this tolerance becomes ±0.5mm.

Take a value of pressure, say 25 bar and impose ±0.5mm tolerance on water level readings. This results in the following volumetric strain $\Delta V_S/V$:

$\Delta H_S - \Delta H_D$ [mm]	$\frac{\Delta V_D}{V} \times 10^6$	$\frac{A_p}{V}(\Delta H_S - \Delta H_D) \times 10^6$	$\frac{\Delta V_S}{V} \times 10^3$	K [bar]
4.79	14.20	828.41	0.843	29656
5.29	14.20	914.88	0.929 *	26911
4.29	14.20	741.94	0.756 **	33069

Errors in calculating bulk modulus are

$$\text{error}_{min} = \frac{26911 - 29656}{29656} \times 100 = -9.3\%$$

$$\text{error}_{max} = \frac{33069 - 29656}{29656} \times 100 = 11.5\%$$

Errors in calculating bulk modulus due to errors in pressure reading is:

$$\text{Error} = \frac{29738 - 29656}{29656} \times 100 = 0.28\%$$

Errors in bulk modulus due to pressure readings are much smaller than errors due to water level readings. Errors

* Point A in Fig. 11 ** Point B in Fig. 11

due to pressure can therefore be neglected and the main sources of errors are inaccuracies of water level readings.

If calculation of errors is repeated for 5 bar nominal pressure then points C and D in Fig. 11 are obtained and

$$error_{min} = -33.7\%$$

$$error_{max} = 106.1\%$$

and error due to pressure is equal to 1.37%.

From Fig. 11 it is seen that AD and BC are lines parallel to the nominal strain-pressure curve and the whole area represent a band of errors. It is obviously advantageous to calculate bulk modulus at higher pressures because errors are then smaller. The pressure of 25 bar is chosen to calculate bulk moduli for other compliant materials. The procedure is exactly the same as for this natural rubber just described and the results of volumetric strain against pressure are given in figures 12 – 16 . In each figure the value of bulk modulus is noted, together with a tolerance for 25 bar pressure. Photograph IV shows some elastomer discs and dummy steel discs used in the bulk modulus rig.

For some compliant bearing materials (for example, certain plastics) which were used in the experiments, additional discs for bulk modulus testing could not be obtained. An attempt has been made to relate elastomer hardness to bulk modulus of the elastomers in figures 11 – 16 with a view to using this relationship for other elastomers. A linear relationship is shown in figure 17 . Using the six experimental points, this relationship has been obtained by the least squares method. Hardness was measured according to the

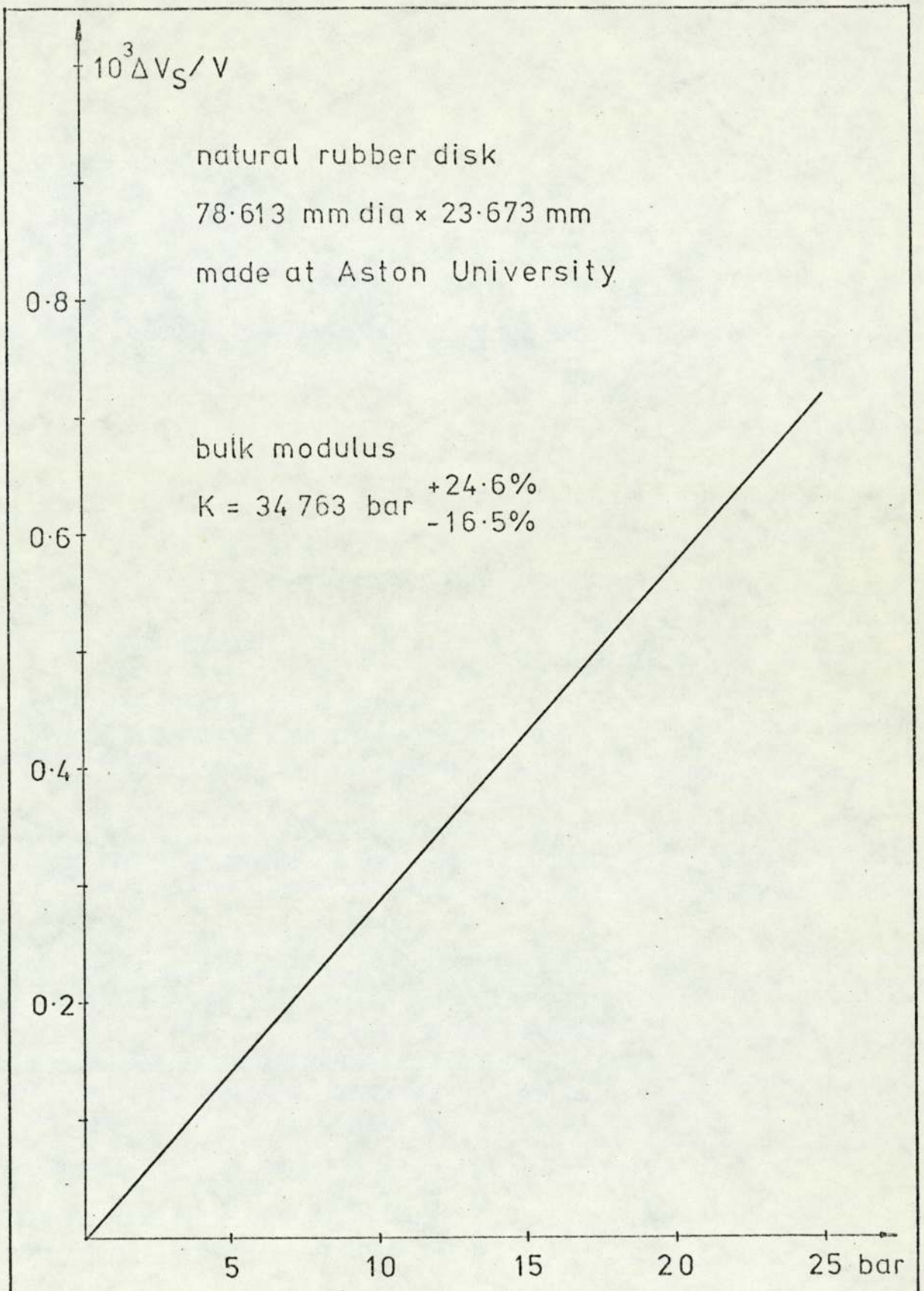

VOLUMETRIC STRAIN AGAINST GAUGE PRESSURE

FIG 12

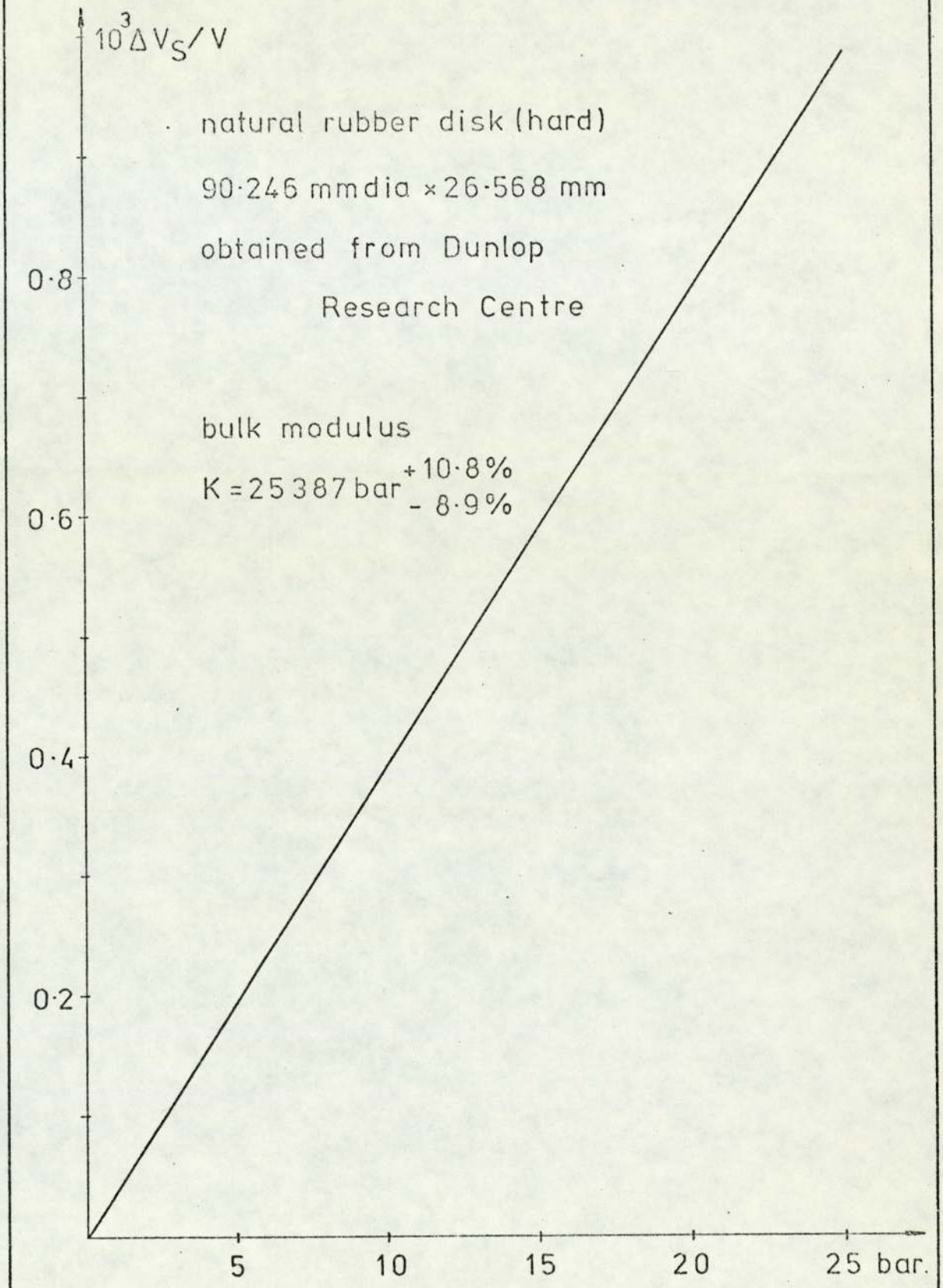

VOLUMETRIC STRAIN AGAINST GAUGE PRESSURE

FIG 13

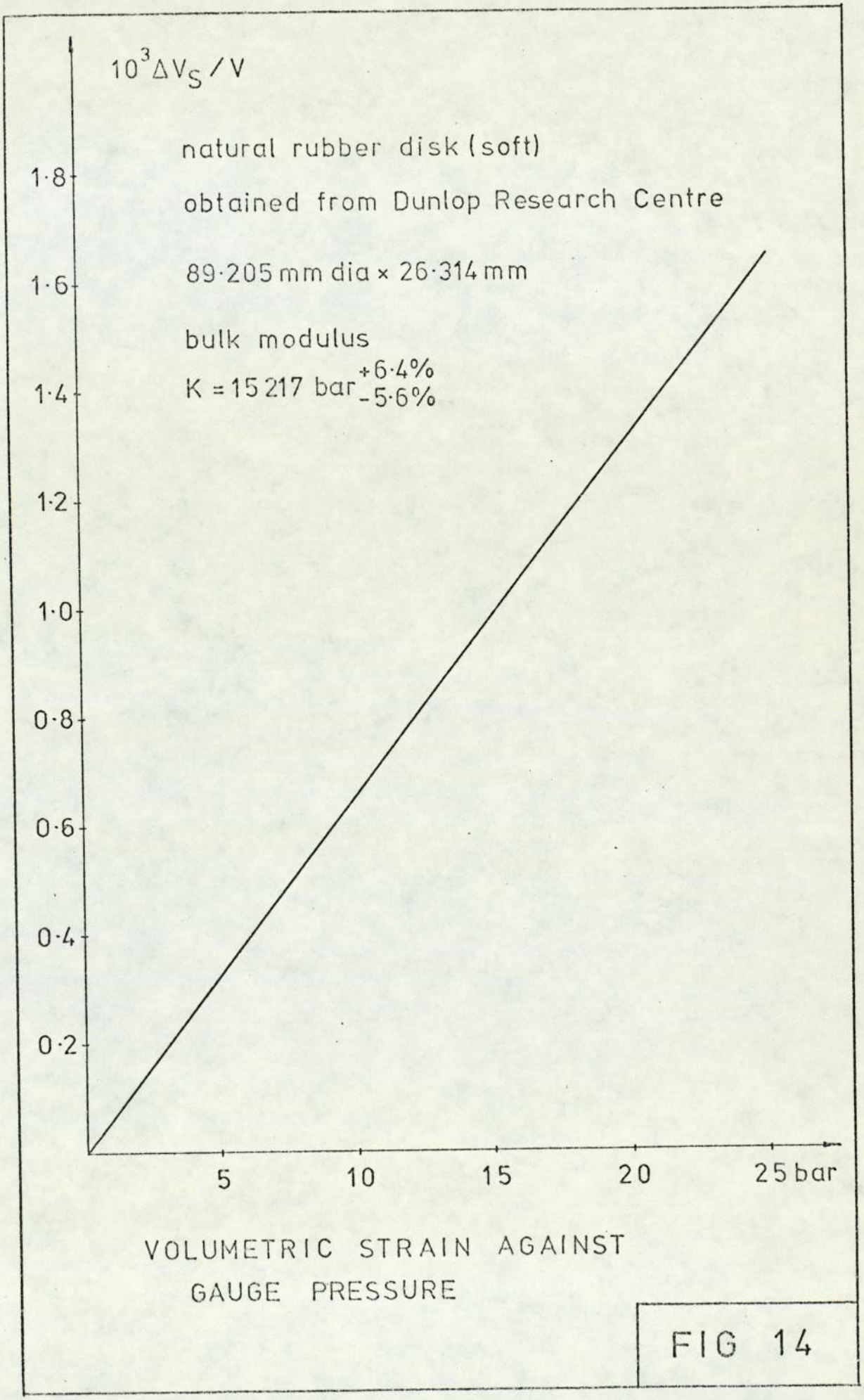

VOLUMETRIC STRAIN AGAINST GAUGE PRESSURE

FIG 14

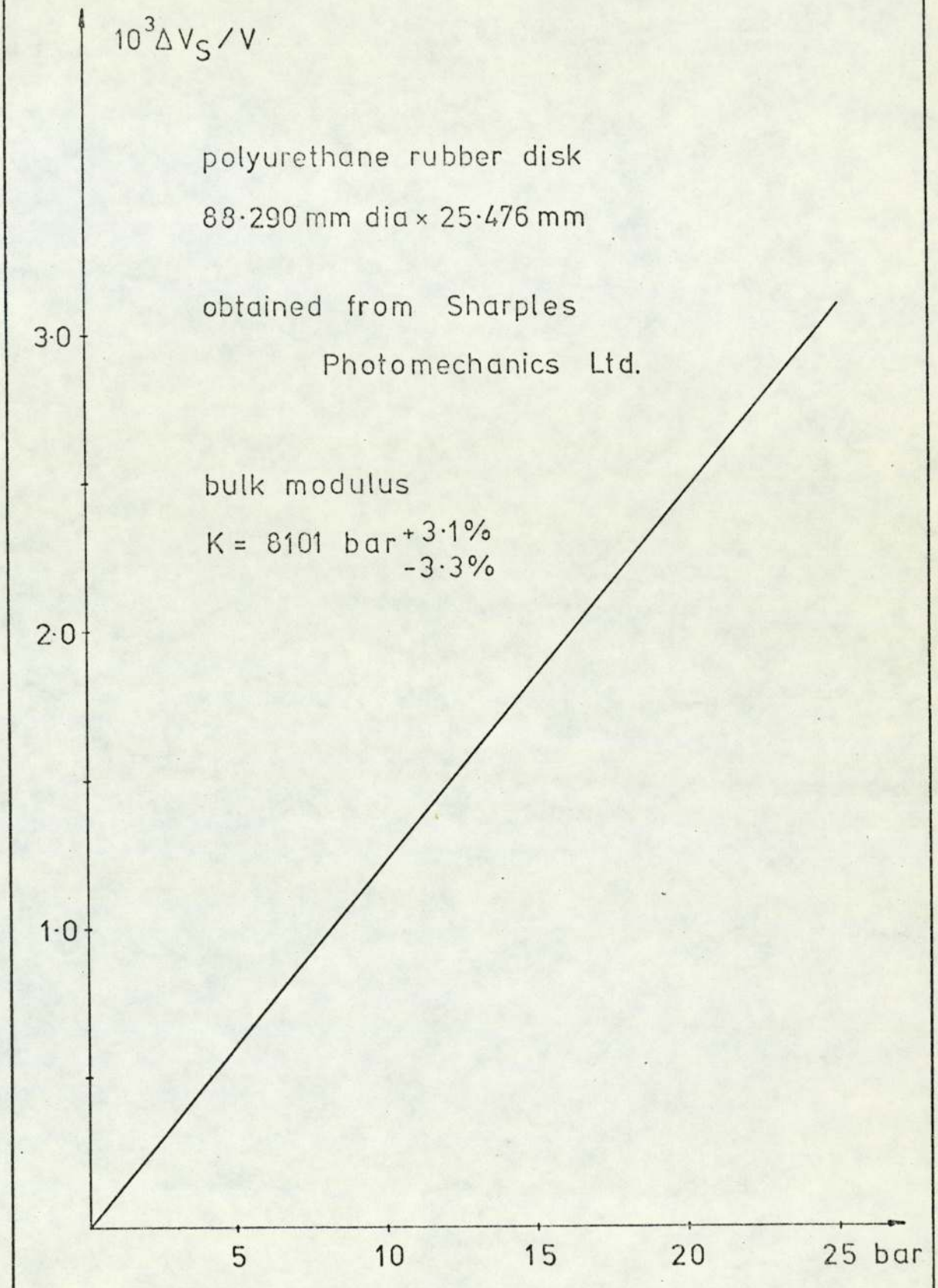

VOLUMETRIC STRAIN AGAINST GAUGE PRESSURE

FIG 15

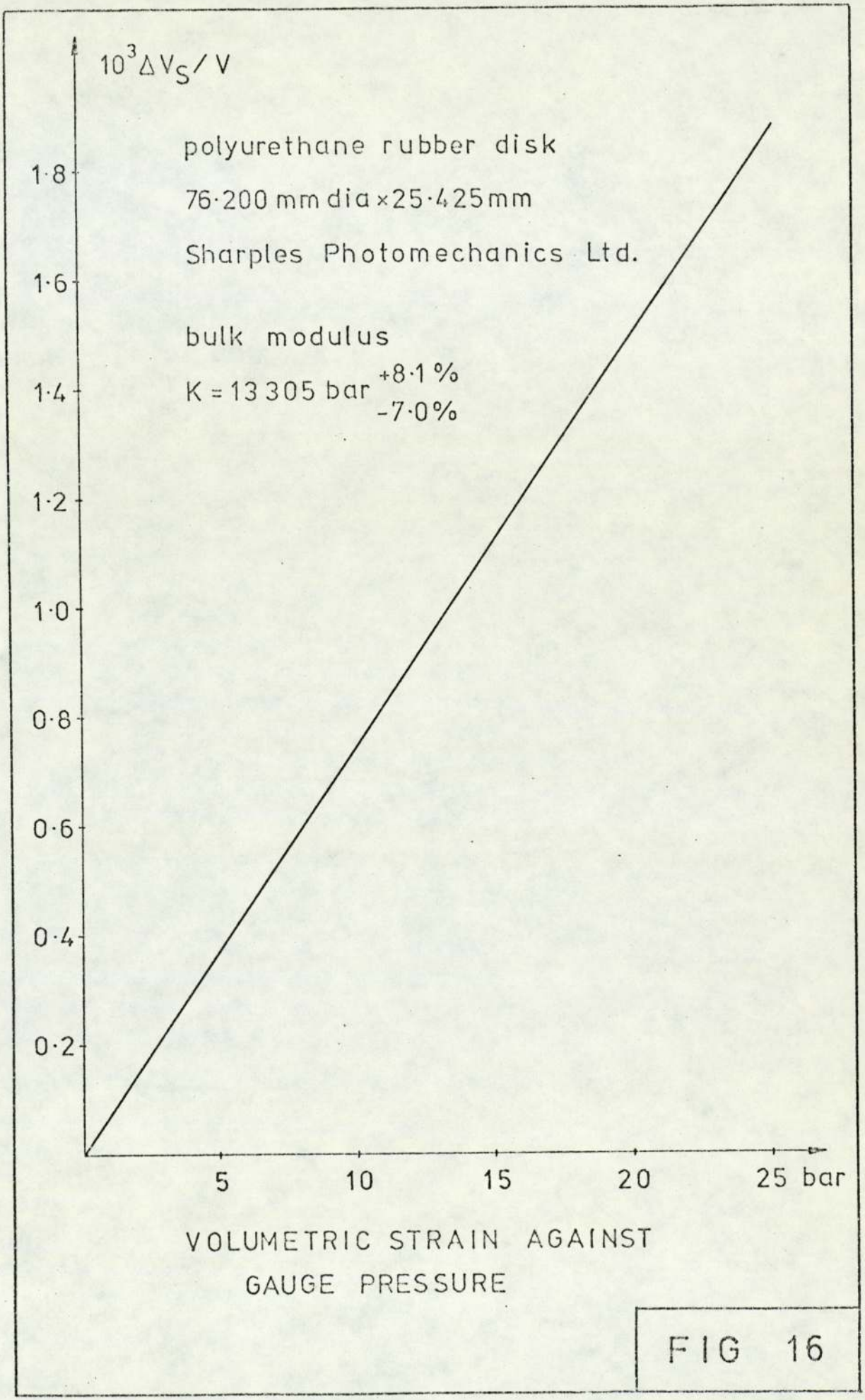

VOLUMETRIC STRAIN AGAINST GAUGE PRESSURE

FIG 16

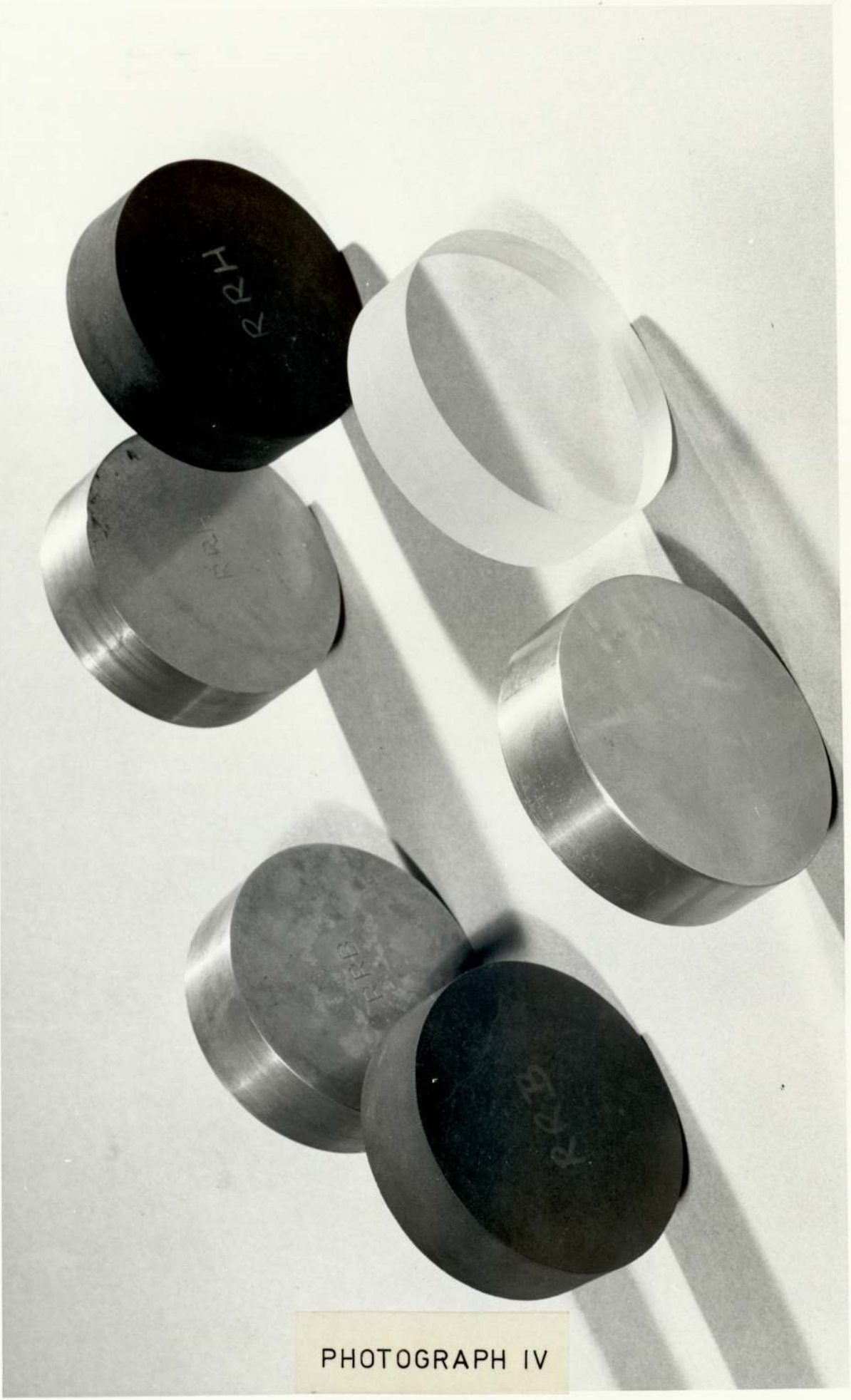

PHOTOGRAPH IV

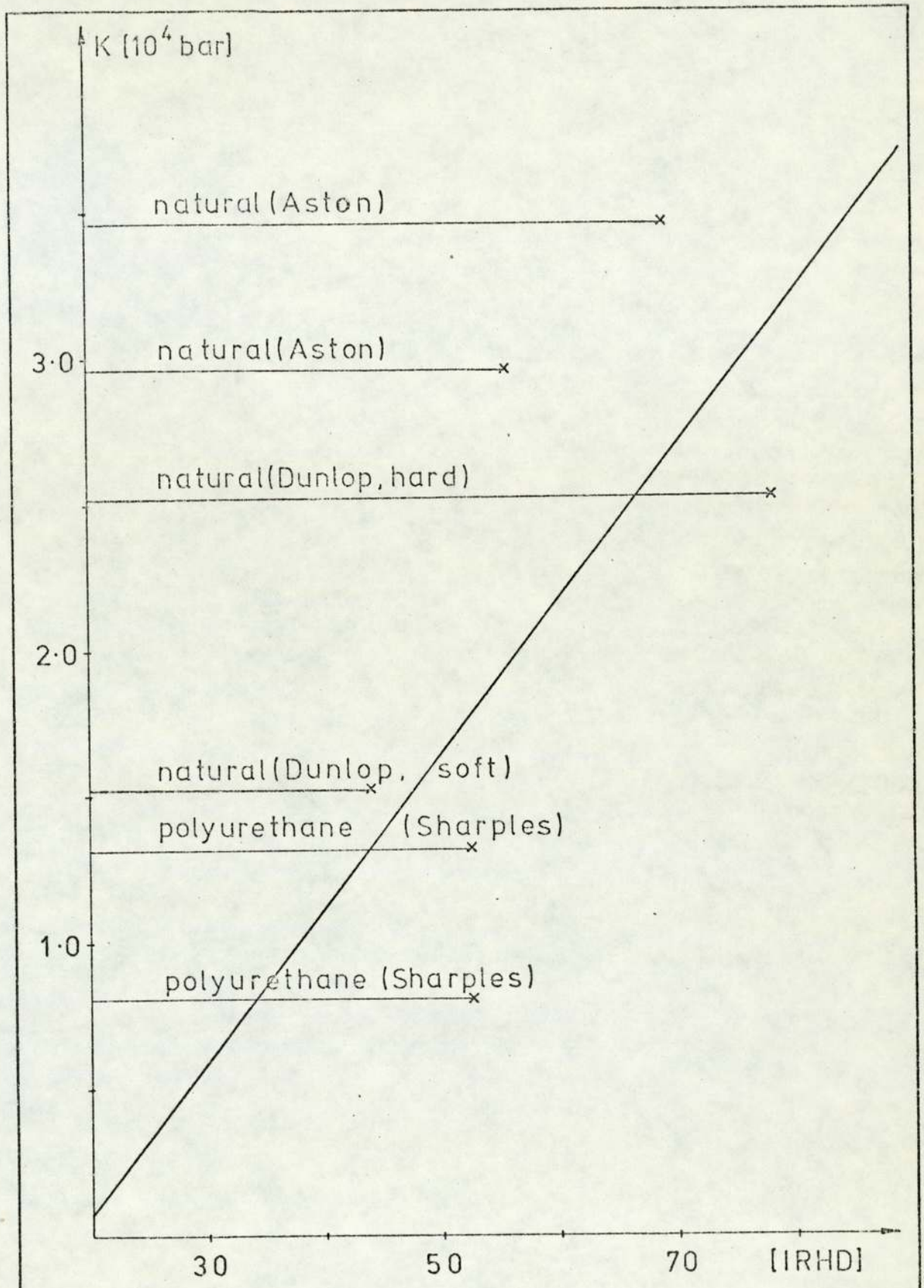

BULK MODULUS AGAINST RUBBER HARDNESS

FIG 17

specification of the rubber hardness tester manufactured by H.W. Wallace & Co. Ltd. and showed in photograph V . Hardness is obtained in units of International Rubber Hardness Degrees which closely correspond to values of shore "A" Durometer hardness and British Standard hardness degrees.

The International Hardness Test is based on measurements of the penetration of a rigid ball into the rubber specimen under specified conditions. The measured penetration is converted into IRHD, the scale of degrees being so chosen that zero represents a material having an elastic modulus of zero and hundred represents a material of infinite elastic modulus [310], standard D1415-68.

4.3 Elastic Modulus Evaluation

Elastic modulus of various rubbers was first determined using a Hounsfield "E type" tensile testing machine. Dumb bell test pieces were cut with a "D" cutter, the speed of testing being 20 in/min [309, part A2].

This Hounsfield tester is designed to give Young's Moduli at 100%, 200% and 300% strains. Since strains in compliant bearings are at least two orders of magnitude smaller, the resulting graphs of forces against elongations need to be read very near to the origin. Difficulty of reading force magnitude for such small elongations is increased because the mechanism for rotating the graph paper does not respond instantly to loading. It was concluded that these tests are not accurate enough for evaluation of elastic moduli.

PHOTOGRAPH V

It is possible to determine the elastic modulus under compression by measuring the elastomer deflection during bearing tests. The elastomer disc is then subjected to compression from the bearing load and from the reaction of the lower bearing surface, see sketch below:

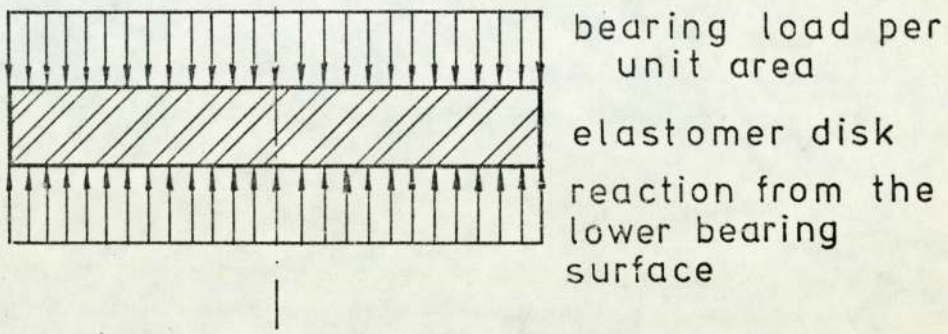

During the bearing operation, the elastomer disc is subjected to compression from the bearing load and from the pressure distribution in the film, as shown in the following sketch:

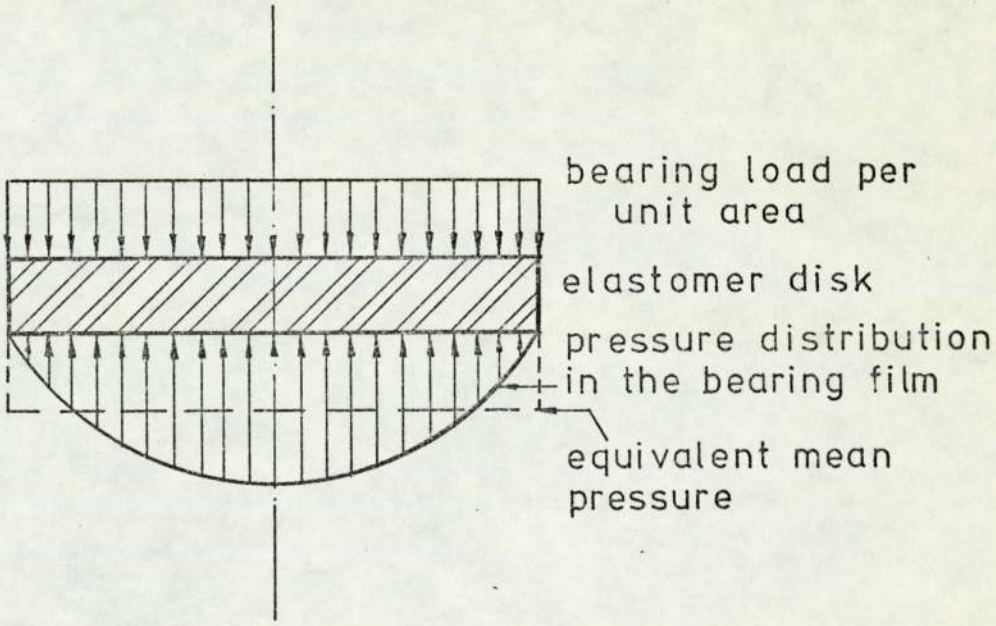

If the pressure distribution in the bearing film is substituted by the equivalent mean pressure (load divided by bearing area) the loading conditions when evaluating elastic modulus are the same as the elastomer loading conditions during bearing operations.

During the real bearing operation the loading conditions are predominantly compressive. Elastic modulus is also

calculated under compression and this is an additional advantage over the methods of evaluating the elastic modulus in tension, such as the Hounsfield tester.

The test bearing with a compliant material is screwed onto a slave journal bearing and the whole unit is placed on the lower thrust bearing surface. Deflection of the elastomer is measured by three mitronic comparators spaced uniformly around the circumference of the top part of the journal bearing, see photograph VI . Results of a typical load test are shown in fig.18 . Material is natural rubber made in the Chemistry department of the University. The hardness of this rubber is measured as 54.5 IRHD and dimensions of the elastomer are 133.82mm dia x 12.28mm. The upper surface of the elastomer is bonded to a steel backing plate and together with it, it forms a test bearing pad. The lower surface of the rubber (128.27mm dia, the same as the lower test bearing rigid surface), forms the effective bearing surface.

The deflection under the inherent load of 92.67N acting on the elastomer is not known because it is not possible to measure this deflection by mitronic comparators.

Once experimental values of load are plotted against elastomer deflection, see fig. 18 , it is seen that the relationship is linear, and a first degree polynomial is fitted through these points by means of a least squares fit. In order to correct for the deflection under inherent load, a line is drawn parallel to the fitted line and passing through the origin. In this way it is observed that the deflection under the inherent load is 5.5 μm. Now, the

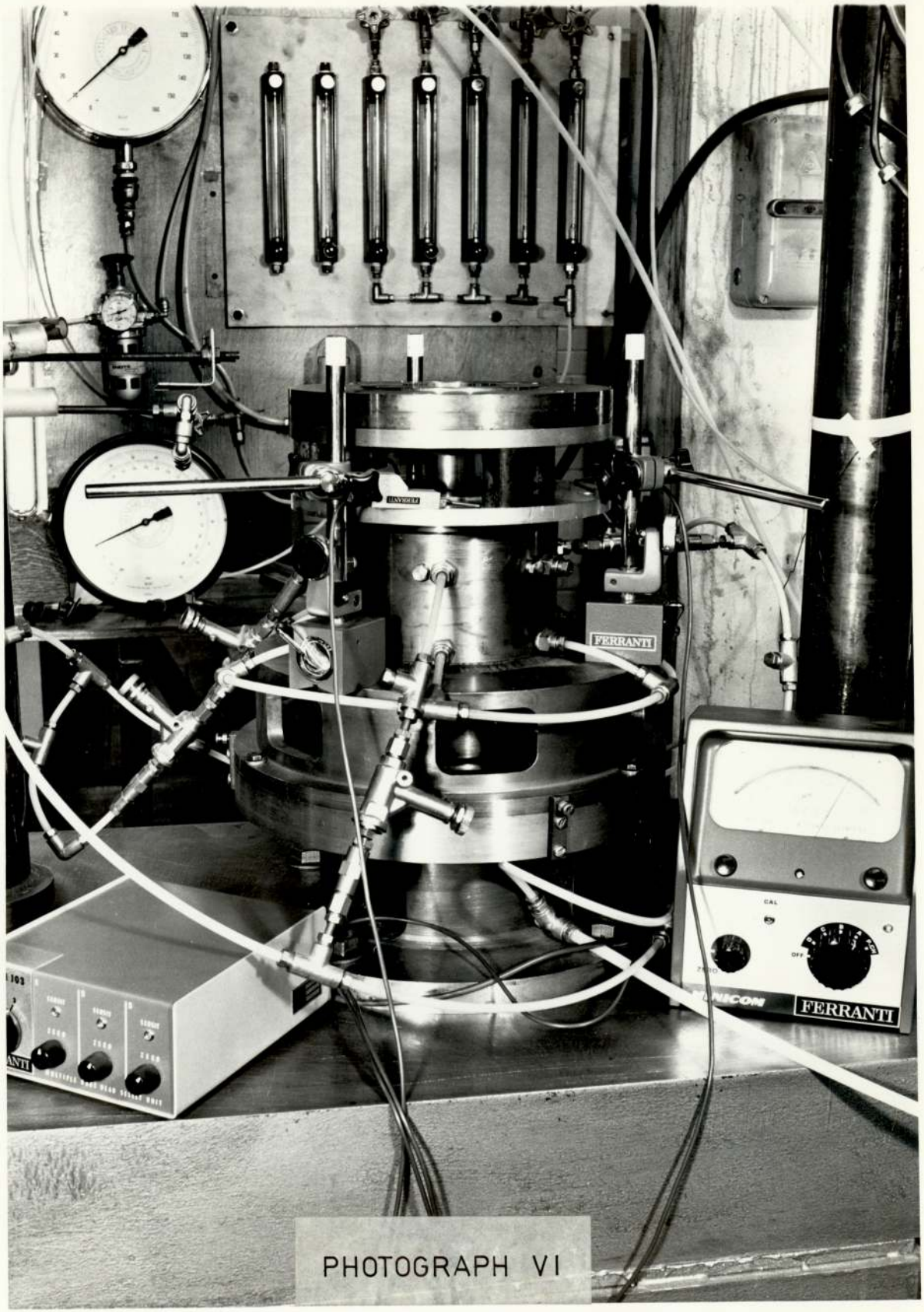

PHOTOGRAPH VI

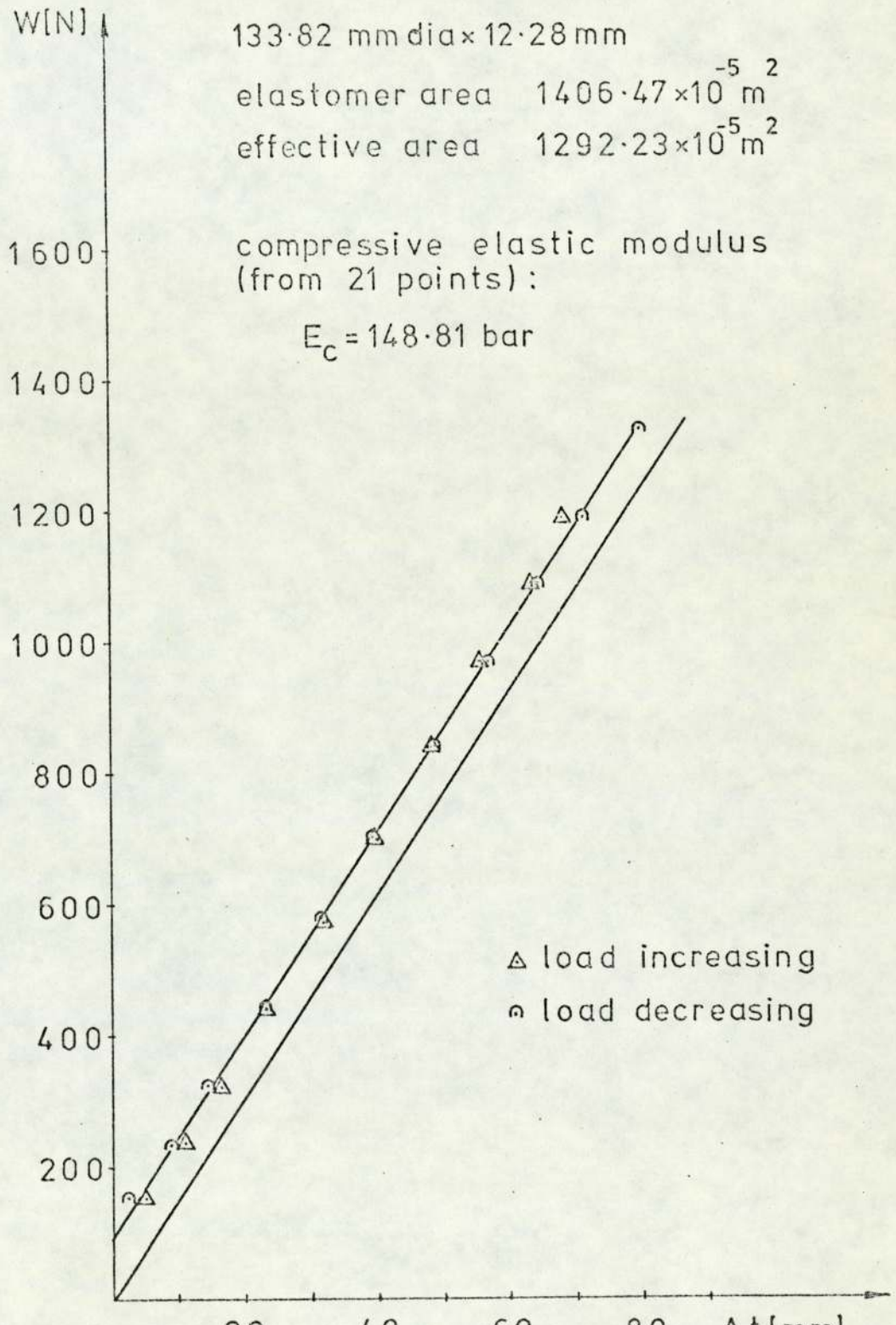

LOAD AGAINST ELASTOMER DEFLECTION

FIG 18

compressive elastic modulus based upon the effective bearing area and initial rubber thickness can be calculated. It is equal to E_c = 148.81 bar. Dimensions of the elastomer were obtained by a vertical travelling microscope taking the average of a few readings. The accuracy of readings is ±10μm. Fig. 19 shows the relationship between elastomer load per unit area and axial strain from which the compressive elastic modulus is calculated. This is an apparent value of elastic modulus and it has to be corrected following the procedure given by Lindley [307]. True elastic modulus of small strains [307] is given by:

$$E = \frac{E_c}{1+2kS_e^2} \qquad (9)$$

for rubber bonded between two rigid flat plates.

In the above relationship k is a factor used in the calculation of compression characteristics of elastomers and it is given in fig. 20 . For hardness of 54.5 IRHD, k = 0.64.

The elastomer shape factor S_e is defined as loaded area divided by force-free areas, i.e. approximately:

$$S_e = \frac{\pi D^2}{4 \times \pi Dt} = \frac{D}{4t}$$

where D is the effective bearing diameter. Then:

$$E = \frac{148.81}{1+2 \times 0.64 \times 2.611^2} = 15.3 \text{ bar}$$

In developing relationship (9), it is assumed that the rubber disc is bonded to two rigid flat plates or it adheres to them.

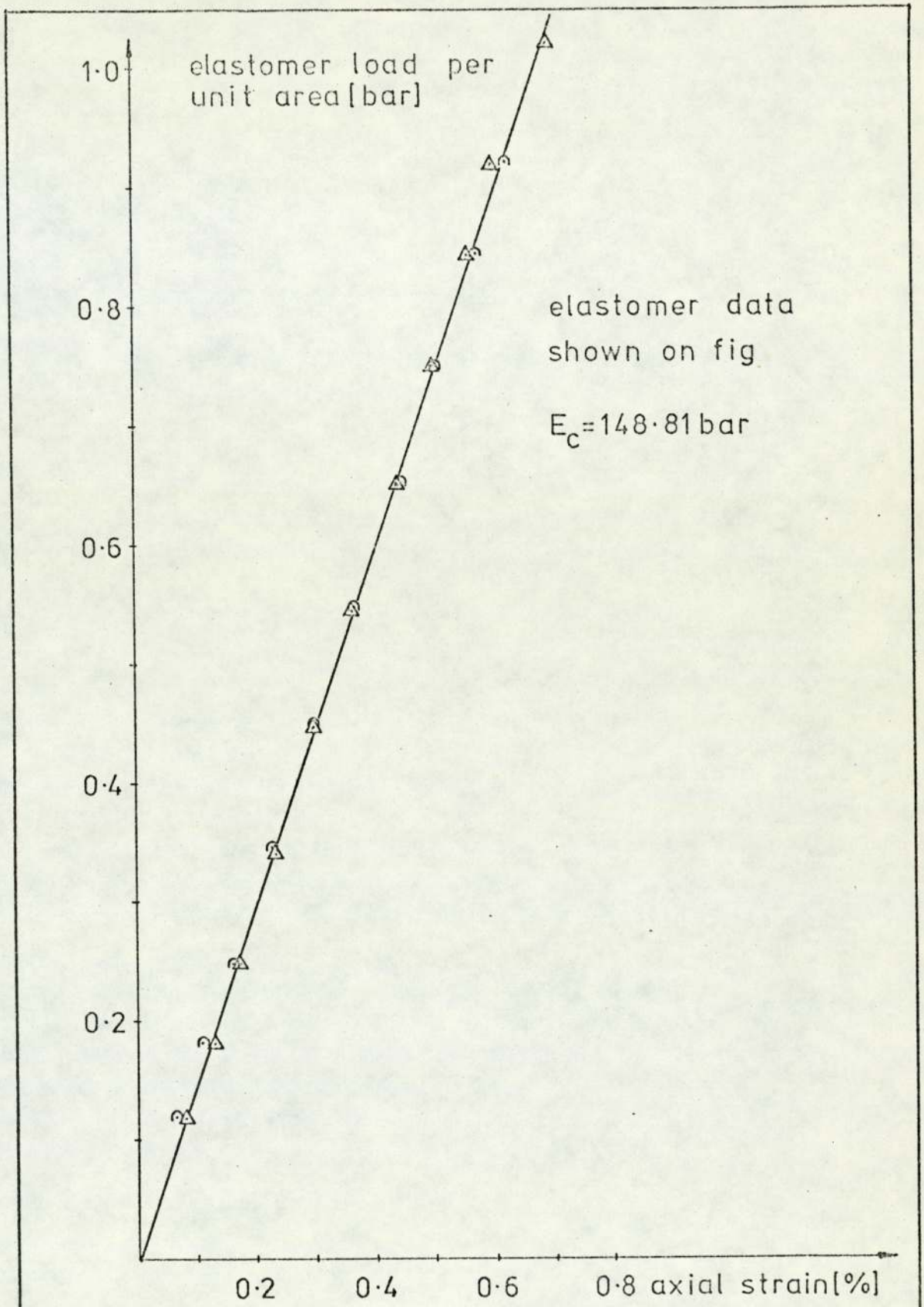

ELASTOMER LOAD PER UNIT AREA AGAINST AXIAL STRAIN

FIG 19

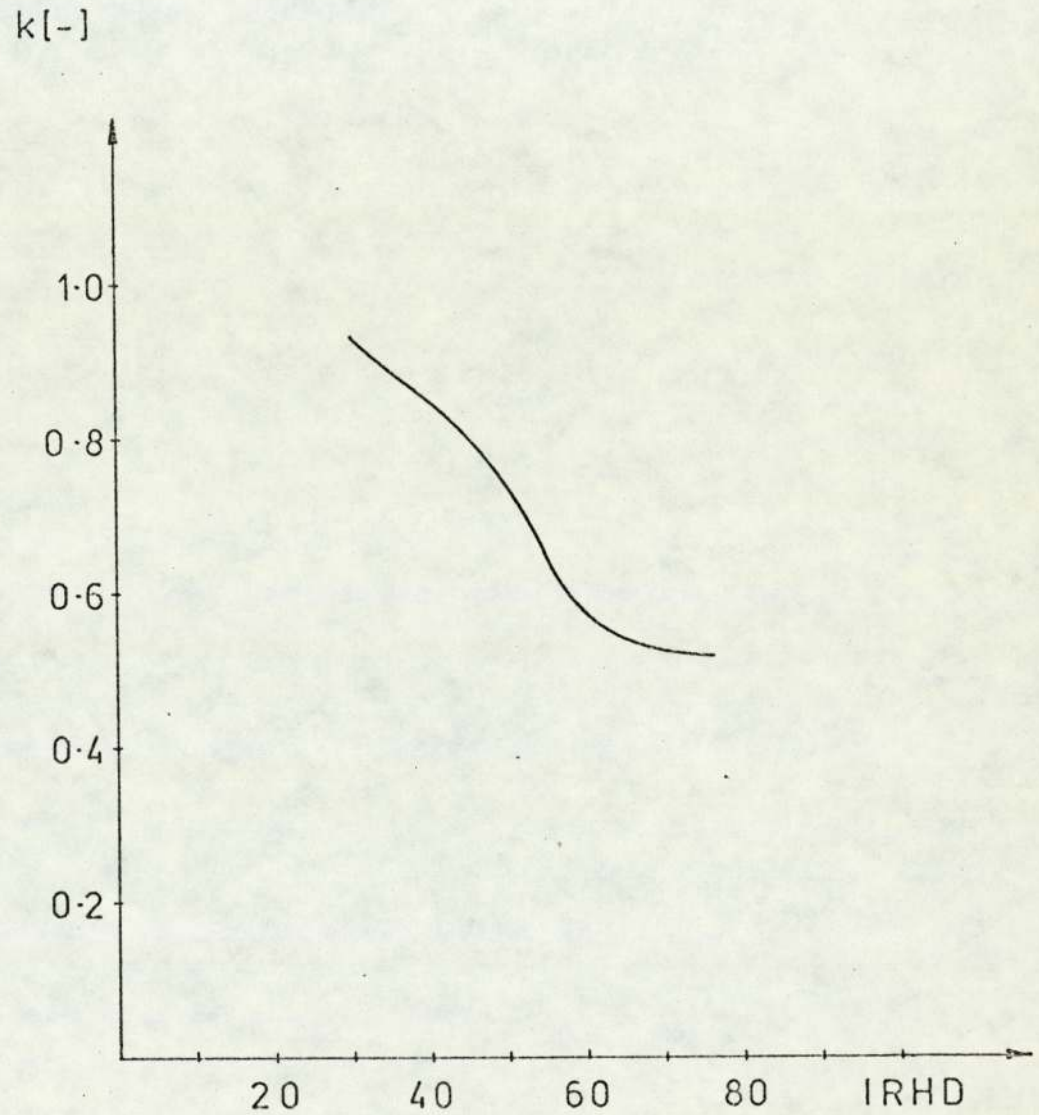

RUBBER HARDNESS AGAINST A FACTOR 'k' USED IN CALCULATING COMPRESSION CHARACTERISTICS OF ELASTOMERS

FIG 20

Experimental results of compressive characteristics of other elastomers are shown in fig. 21 and summarised in table IV-1 . It is seen that the ratio of elastic modulus to bulk modulus is in each case smaller than 0.001 and Poisson's ratio to four decimal places is at least 0.4999.

From equation (6) compressibility is given as

$$\frac{\Delta V}{V} = \frac{p}{K} = \frac{p \times 3(1-2\nu)}{E} \qquad (10)$$

Based upon the mean pressure (load divided by the effective bearing area), the compressibility is calculated in the last column of table IV-1 for a typical bearing load of 322.5N.

When compared to steel, it is seen that on average these elastomers compress about 50 times more than steel, which is more than one order of magnitude. However, absolute values of compressibility of elastomers are of the order of 10^{-5} which is very small indeed.

4.4 Estimated Errors and Comparison with Rightmire's Results

Errors in calculating elastic moduli of the elastomers can be divided into:

1) errors of compressive characteristics
2) errors due to correction from compressive modulus to true elastic modulus at small strains.

In evaluating the compressive characteristics, loads,

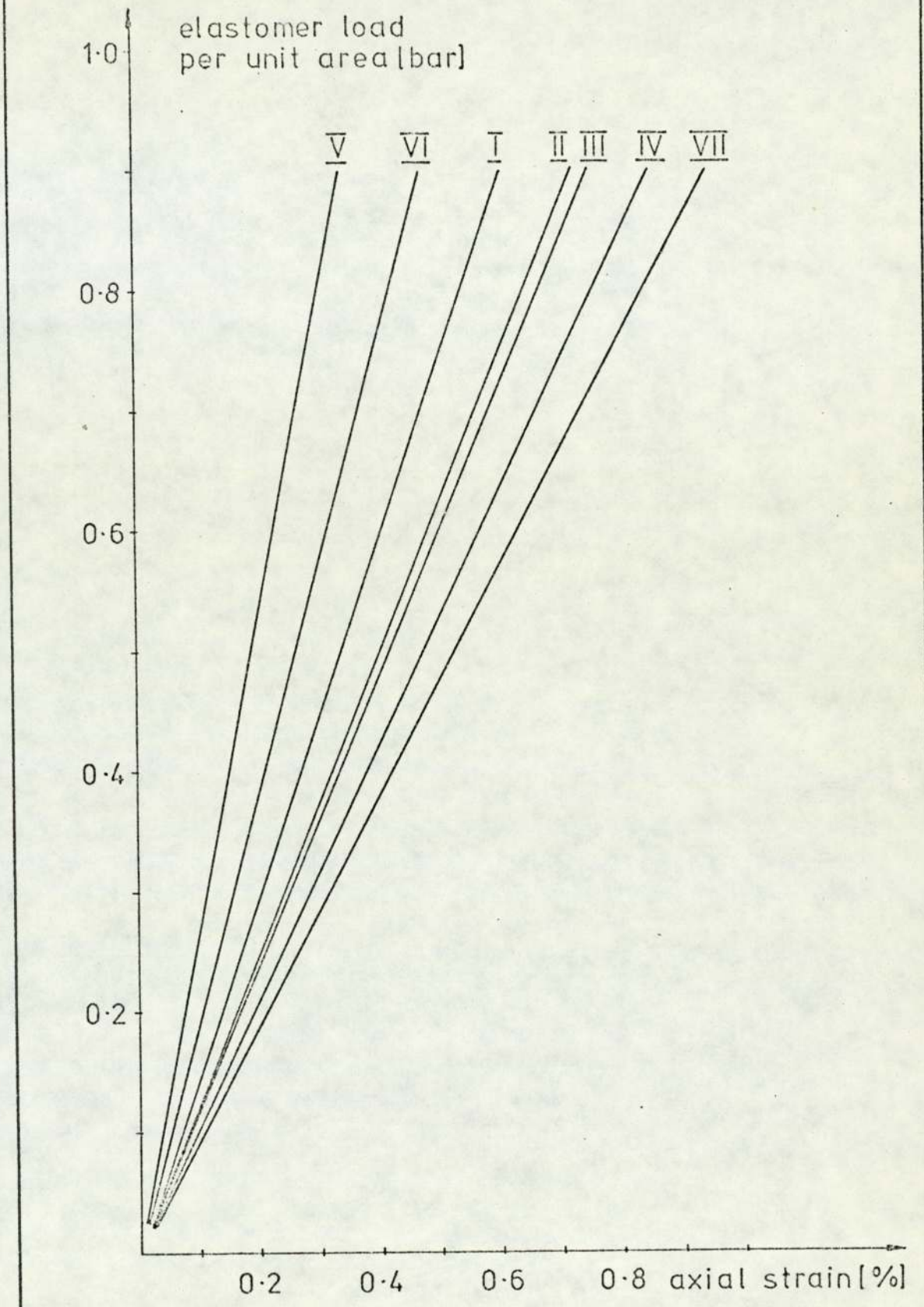

ELASTOMER LOAD PER UNIT AREA AGAINST AXIAL STRAIN FOR VARIOUS ELASTOMERS

FIG 21

	Elastomer	Made or obtained from	Dimensions [mm]	E_c [bar]	E [bar]	IRHD	$E/_K \times 10^3$	Poisson's ratio ν	$\frac{\Delta V}{V} \times 10^3$ Compressibility for typical bearing load of 322.5N
I	Natural	Aston	133.82 dia x 12.28	148.81	15.30	54.5	0.475	0.499921	0.008
II	Natural	Aston	126.90 dia x 12.46	124.9	13.17	54.4	0.409	0.499932	0.008
III	Natural	Aston	102.00 dia x 12.37	122.9	19.09	56.3	0.593	0.499901	0.012
IV	Natural	Aston	77.13 dia x 12.42	105.8	25.91	56.1	0.084	0.499866	0.021
V	Polyurethane	Sharples	134.00 dia x 3.12	254.0	2.15	60.5	0.201	0.499967	0.023
VI	Viton(hard)	Du Pont	131.20 dia x 2.19	190.5	0.89	88.6	0.024	0.499996	0.007
VII	Viton(soft)	Du Pont	132.16 dia x 3.20	95.9	0.74	55	0.039	0.499994	0.013

TABLE IV-1 TO SUMMARIZE ELASTOMERS OF FIG. 21

deflections and elastomer dimensions are measured. Errors due to wrong load readings are negligible because load can be read within ± 0.05N and the minimum loads on elastomers are more than 90N. Mitronic comparators have been calibrated against high quality slip gauges and it is known that these comparators show correct readings. Elastomer dimensions are measured by a vertical traversing microscope, the accuracy of which is ±10μm. This is not important for elastomer diameters, but when measuring small thicknesses of about 2-3mm, the errors in compressive modulus are of the order of 0.5%.

In order to estimate errors arising from the correction of compressive elastomer characteristics to true elastic moduli, it should be remembered that in developing relationship (9) it has been assumed that the elastomer is bonded between the two rigid flat plates.

In this experimental setup either the upper elastomer surface is bonded to its metal backing or neither of the surfaces is bonded. Results in table IV-I refer to the case when the upper elastomer surface is bonded to its backing plate.

In all cases the other elastomer surface touches the lower test bearing surface. The elastomer surface and the lower rigid test bearing surface can be cleaned with "inhibisol", a cleaning solvent. In that case, it is considered that there should not be much sliding of these surfaces.

Measurement of any sliding has not been attempted and it is considered to be negligible, if test bearing surfaces (elastomer and steel) are cleaned with inhibisol. Then relationship (9) completely applies to

the situation. However, possible values of coefficient of friction have been measured.

If there is perfect sliding between both elastomer surfaces and the flat plates, the modulus obtained under compression test would be the true elastic modulus of the elastomer. However, even if the elastomer is not bonded to either of the surfaces and both elastomer surfaces are lubricated, there will always be some friction between the elastomer disc and flat plates.

A natural rubber disc made at Aston and of dimensions 128.27mm dia x 12.82mm has been tested in compression under two conditions:

1) Not bonded to either surface, cleaned with inhibisol; compression modulus E_c=63.55 bar obtained.
2) Not bonded, both surfaces lubricated by silicon oil, compression modulus E_c=34.50 bar obtained.

In the first case the value is about a half of the corresponding value of E_c for a bearing which has one of the surfaces bonded to a metal backing (see table IV-1).

In the second case the value of E_c approaches the true value of elastic modulus E for natural rubber (see table IV-1), although it does not quite reach there and it is roughly about twice as large as this modulus.

In order to estimate coefficient of friction in both cases, it was assumed that sliding friction of this rubber disc on the inclined plane is a fair representation of the situation. A 203.2mm dia (8in dia) optical inclinable (and

rotary) table, manufactured by Optical Measuring Tools Ltd., was used and coefficients of friction based upon tangents of angles of inclination were obtained.

In the first case when both elastomer and metal surface are cleaned with inhibisol μ=0.271 and in the second case when the surfaces are lubricated by silicone oil, μ=0.010. Both results represent average values of more than ten readings in each case, and the repeatability of readings is good.

These results confirm that compressive characteristics of unbonded rubber, cleaned with inhibisol will not be the same as characteristics of a rubber bonded with one surface. True elastic modulus E of rubbers, and natural rubbers I, II, III and IV in particular, should lie between values of E obtained for these rubbers and the value of 34.5 bar obtained under compression when using a good lubricant. It is not possible to say where true values of E are, but the errors can be large.

At the beginning of this chapter it has been shown that even relatively large errors in bulk and elastic moduli bring small errors to values of Poisson's ratio, i.e. to compressibility characteristics of elastomers. Lowe [210] has used results of Rightmire [305] and has shown that a linear relationship exists between Poisson's ratio ν and shear modulus G of various elastomers. Results of Rightmire converted to elastic modulus E are shown in Fig. 22 . The straight line on this figure is a least squares fit of his experimental points.

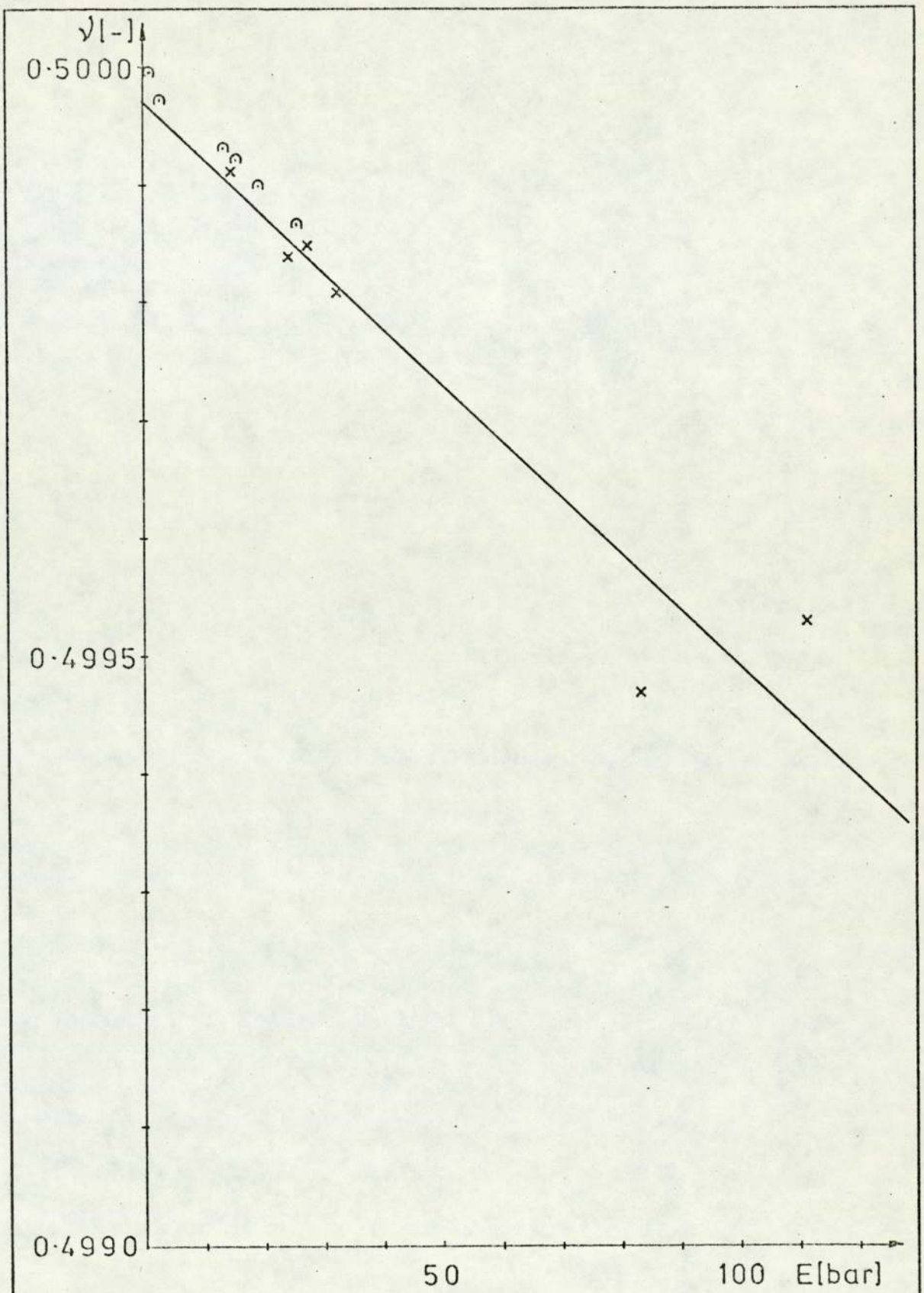

COMPARISON OF RIGHTMIRE'S WORK(×)
WITH AUTHOR'S EXPERIMENTS(○) FOR
VARIOUS ELASTOMERS

FIG 22

Even though there is some uncertainty about true elastic moduli, the author's results compare favourably with those of Rightmire and they give some more data in the region close to $\nu=0.5$.

V DESIGN AND DESCRIPTION OF THE MAIN EXPERIMENTAL APPARATUS

In order to assist in the design of the main experimental facility for compliant bearing tests, the available theories of compliant lubrication are examined, Dowson's and Taylor's theory [201] and Castelli's et al theory [202] to [205].

Dowson's and Taylor's theory concerns compliant lubrication with an incompressible fluid and pressure distribution is given in analytic form. This theory has therefore been modified as follows for compressible lubrication in order to obtain design information for the rig. Because of its simplicity, the theory was preferred to the theory of Castelli et al in the initial stages of the project.

5.1 Modification of Dowson's and Taylor's Theory for Compressible Lubrication

Reynolds Equation for gas lubrication assuming isothermal conditions and steady-state operations (given by equation (I.4), Appendix I) states:

$$\frac{d}{dr}\left[h^3 r \frac{d}{dr}(p^2)\right] = 0 \qquad (1)$$

From Dowson's and Taylor's theory [201] elastic compression of the bearing liner is given by:

$$\delta = \frac{(p-p_a)t}{E^1} \qquad (2)$$

where t is the elastomer thickness in the unstressed state and

$$E^1 = \frac{E}{1-2\nu^2/(1-\nu)} \tag{3}$$

Film thickness is defined as:

$$h = h_o + \delta = h_o + \frac{(p-p_a)t}{E^1} \tag{4}$$

where h_o is the film thickness without elastomer deformation.

Dimensionless film thickness is defined as:

$$\bar{H} = \frac{h}{h_o} = 1 + \frac{(p-p_a)t}{E^1 h_o} =$$

$$= 1 + L(P-1) \tag{5}$$

where bearing parameter

$$L = \frac{p_a t}{E^1 h_o} \tag{6}$$

With reference to Dowson's and Taylor's theory [201], it will be assumed that the elastic deflection δ can be approximately calculated from the equation for pressure distribution in rigid bearings with isoviscous compressible fluids. From equation (I-8), Appendix I;

$$P^2 = 1 + \frac{P_p^{\,2} - 1}{\ell n R_p} \ell n R \tag{7}$$

From equation (5), film thickness can now be expressed as

$$\bar{H} = 1 + L\left[\left(1 + \frac{P_p^{\,2} - 1}{\ell n R_p} \ell n R\right)^{\frac{1}{2}} - 1\right] \tag{8}$$

From (1), Reynolds Equation in dimensionless form can be written as:

$$\frac{d}{dR}\left[\bar{H}^3 R \frac{d}{dR}(P^2)\right] = 0 \tag{9}$$

which can be integrated once to give

$$\frac{d}{dR}(P^2) = \frac{A}{H^3 R}$$

$$= \frac{A}{R}(1+L(P-1))^{-3} \tag{10}$$

through equation (5). Here A is a constant of integration. Expanding binominally

$$\frac{d}{dR}(P^2) = \frac{A}{R}(1 - 3L(P-1) + 6L^2(P-1)^2 - \cdots) \tag{11}$$

Powers higher than unity can be neglected if the convergence of successive terms exists. In that case

$$\frac{d}{dR}(P^2) = \frac{A}{R}(1 - 3L(P-1))$$

$$= \frac{A}{R}\left\{1 + 3L - 3L\left[(1+\frac{P_p^2 - 1}{\ell n R_p}\ell n R)^{\frac{1}{2}}\right]\right\}$$

$$= \frac{A(1+3L)}{R} - \frac{A \times 3L}{R}\left[1 + \frac{P_p^2 - 1}{\ell n R_p}\ell n R\right]^{\frac{1}{2}} \tag{12}$$

which can be directly integrated to give

$$P^2 = A(1+3L)\ell n R - AL\frac{2\ell n R_p}{(P_p^2 - 1)}\left[1 + \frac{P_p^2 - 1}{\ell n R_p}\ell n R\right]^{3/2} + B \tag{13}$$

where B is another constant of integration.

Constants A and B are calculated from boundary conditions shown in Fig. I-1, Appendix I and they are

$$B = 1 + \frac{2AL \ln R_p}{P_p^2 - 1}$$

$$A = \frac{P_p^2 - 1}{\ln R_p + L\left[3\ln R_p - \frac{2\ln R_p}{(P_p^2-1)}(P_p^3-1)\right]}$$

When L = 0, these constants reduce to

$$B = 1$$

$$A = \frac{P_p^2 - 1}{\ln R_p}$$

so that equation (13) reduces to equation (7), the rigid bearing pressure distribution. The bearing parameter L=0 when elastomer thickness t=0, i.e. when there is no elastomer in the bearing.

When $L \neq 0$, equation (13) becomes

$$p^2 = 1 + \frac{(P_p^2-1)\{\ln R + L \times f(R)\}}{\ln R_p + L \times f(R_p)} \qquad (15)$$

where

$$\left.\begin{aligned} f(R) &= 3\ln R - \frac{2\ln R_p}{P_p^2-1}\left[\left(1 + \frac{P_p^2-1}{\ln R_p}\ln R\right)^{3/2} - 1\right] \\ f(R_p) &= 3\ln R_p - \frac{2\ln R_p}{P_p^2-1}(P_p^3-1) \end{aligned}\right\} \qquad (16)$$

It has been shown in chapter IV that a typical elastomer used in these bearings has the following properties

$$E = 20 \text{ bar}$$

$$\nu = 0,4999$$

so that

$$E^1 = \frac{E}{1-2\nu^2/(1-\nu)} = \frac{20}{0{,}0006} = 33342 \text{ bar}$$

Also take

$$h_o = 15 \ \mu m$$

$$t = 12500 \ \mu m$$

$$p_a = 1{,}0039 \quad \text{bar}$$

so that the bearing parameter becomes

$$L = \frac{1{,}0039}{33342} \times \frac{12500}{15} = 0{,}025$$

From equation (11) comparison of the term in the binomial expression of power two with the term of power unity for P=4, gives

$$\frac{6L^2(P-1)^2}{3L(P-1)} = 2L(P-1) = 0{,}15 << 1$$

and this means that neglecting the terms with powers higher than unity is justified.

Consider three typical port pressures given in an example in Appendix I, fig. I-2. For this example the corresponding three dimensionless port pressures become

$$\text{I} \quad P_p = p_p/p_a = 1{,}628644$$

$$\text{II} \quad " \quad = 2{,}370590$$

$$\text{III} \quad " \quad = 3{,}371632$$

and the dimensionless pressure distribution against dimensionless radius, equation (7), is drawn on fig. 23 for the case of rigid bearings.

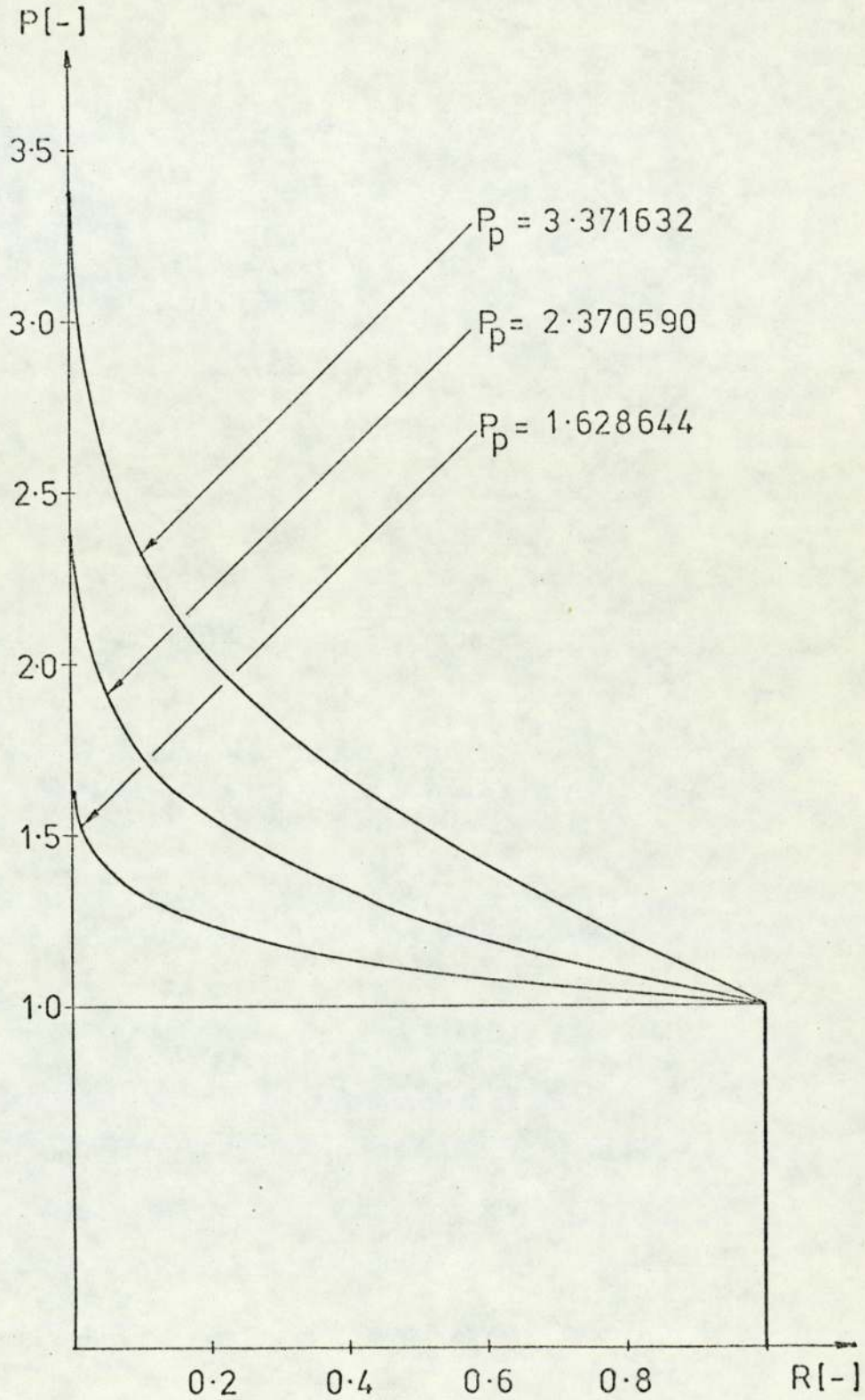

RIGID RADIAL PRESSURE DISTRIBUTION

FIG 23

Equation (15) is then used to draw the compliant radial pressure distribution with the value of bearing parameter L=0.025. For this small value of the bearing parameter compliant pressure distribution almost coincides with the rigid pressure distribution i.e. the maximum deviation from the rigid pressure distribution is only 1.88%, so that the pressure cannot be shown with the scale used to draw fig. 23. This is understandable when one considers that Dowson's and Taylor's theory concerns axial displacements only and radial displacements are assumed to be zero. As there are no radial displacements for an almost incompressible elastomer axial displacements are so small that the compliant pressure distribution reduces to the rigid bearing pressure distribution. The main experimental apparatus was then designed assuming this rigid pressure distribution existed in the compliant bearing.

§ .2 Initial Main Rig Design

In order to obtain information about bearing performance, it is preferred to measure bearing supply pressure, bearing film pressure at various bearing radial positions, bearing flow rate, bearing film thickness at various radial positions and distance between the bearing rigid surface and the non-deformed elastomer.

The compliant thrust bearing essentially consists of a rigid member in which pressure transducers and displacement probes are situated and through which air is admitted to the bearing film and of a compliant member. It is convenient that this rigid member has a diameter of 127 mm in order to accommodate the necessary transducers. It is also convenient that this rigid member is the lower (stationary) bearing member

so that transducers are stationary and that they are not disturbed during bearing tests.

A ratio of port to outer radius is chosen to be

$$R_p = \frac{r_p}{r_o} = \frac{6,35}{63,5} = 0,1 \qquad (17)$$

which is probably smaller than for a conventional design for bearings operating with oil [101]. The reason for this choice is to reduce the volume of the pocket (port), so that pneumatic hammer instability is avoided [109]. Presence of the port implies orifice or capillary rather than inherent compensation, because the port curtain area $2\pi r_p h$ is larger than the orifice cross sectional area. Orifice compensation is chosen because of smaller dimensions than the long capillary restrictor. Although this does not matter very much when one bearing is designed for research purposes, it may matter in practical applications where size is a dominant factor in a restricted environment.

Because of choking the operational range of port to supply pressure is preferred to be,

$$0,528 < P_p/P_s < 1 \qquad (18)$$

Fig. 24 follows from the computer programme described in Appendix I and it represents dimensionless load against port pressure for the case of port to outer radius ratio $R_p = 0.1$.

For supply pressure $p_s = 5,5$ bar, orifice diameter d= 0,330 mm and discharge coefficient $C_D = 0,8$ [107], and with reference to section A1,5b of Appendix I, figures 25,26 and 27 are obtained. It is seen that maximum stiffness at these

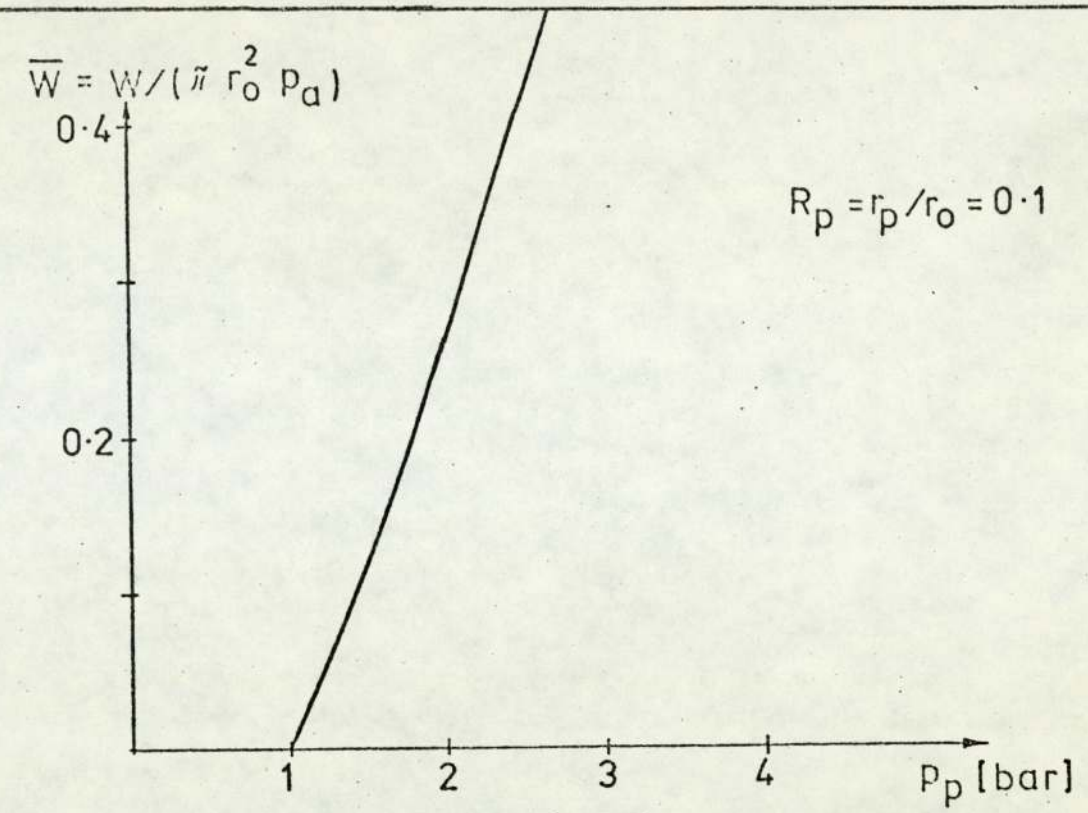

DIMENSIONLESS LOAD V. PORT PRESSURE IN INITIAL BEARING DESIGN

FIG 24

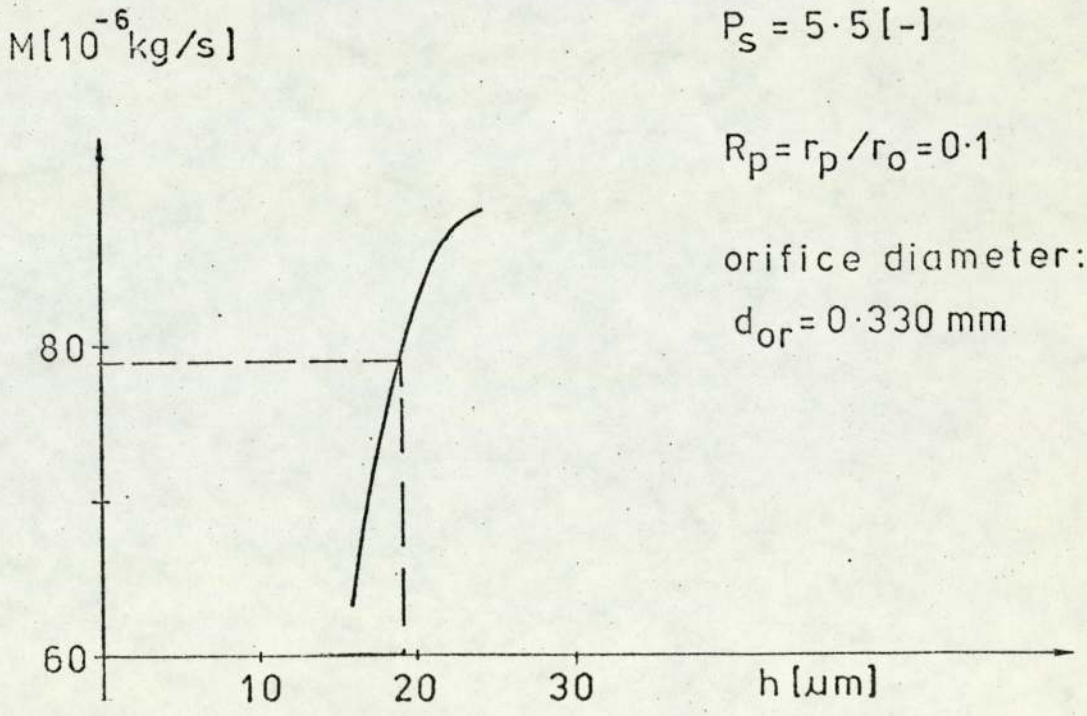

FLOW V. FILM THICKNESS IN INITIAL BEARING DESIGN

FIG 25

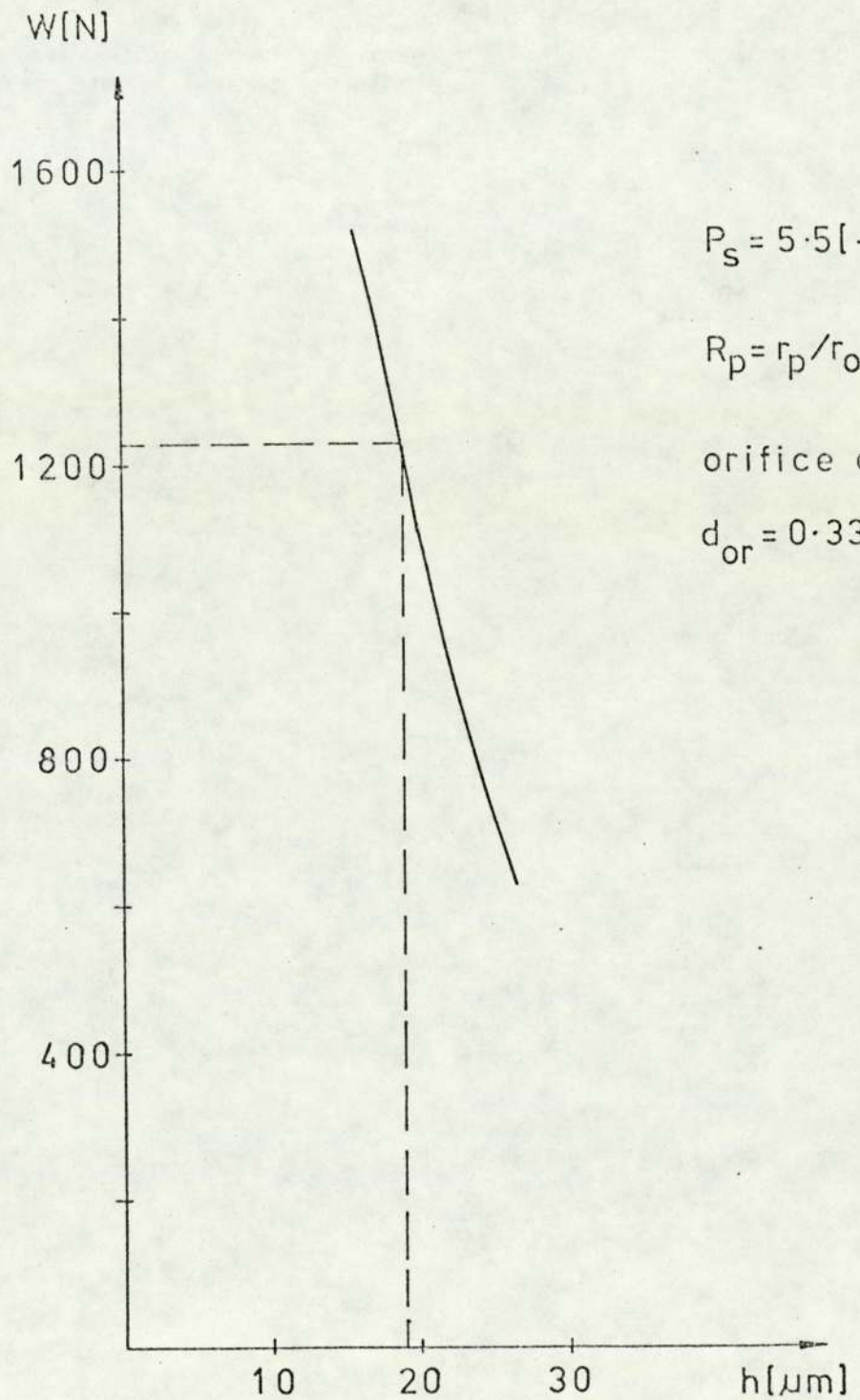

LOAD V. FILM THICKNESS IN INITIAL BEARING DESIGN

FIG 26

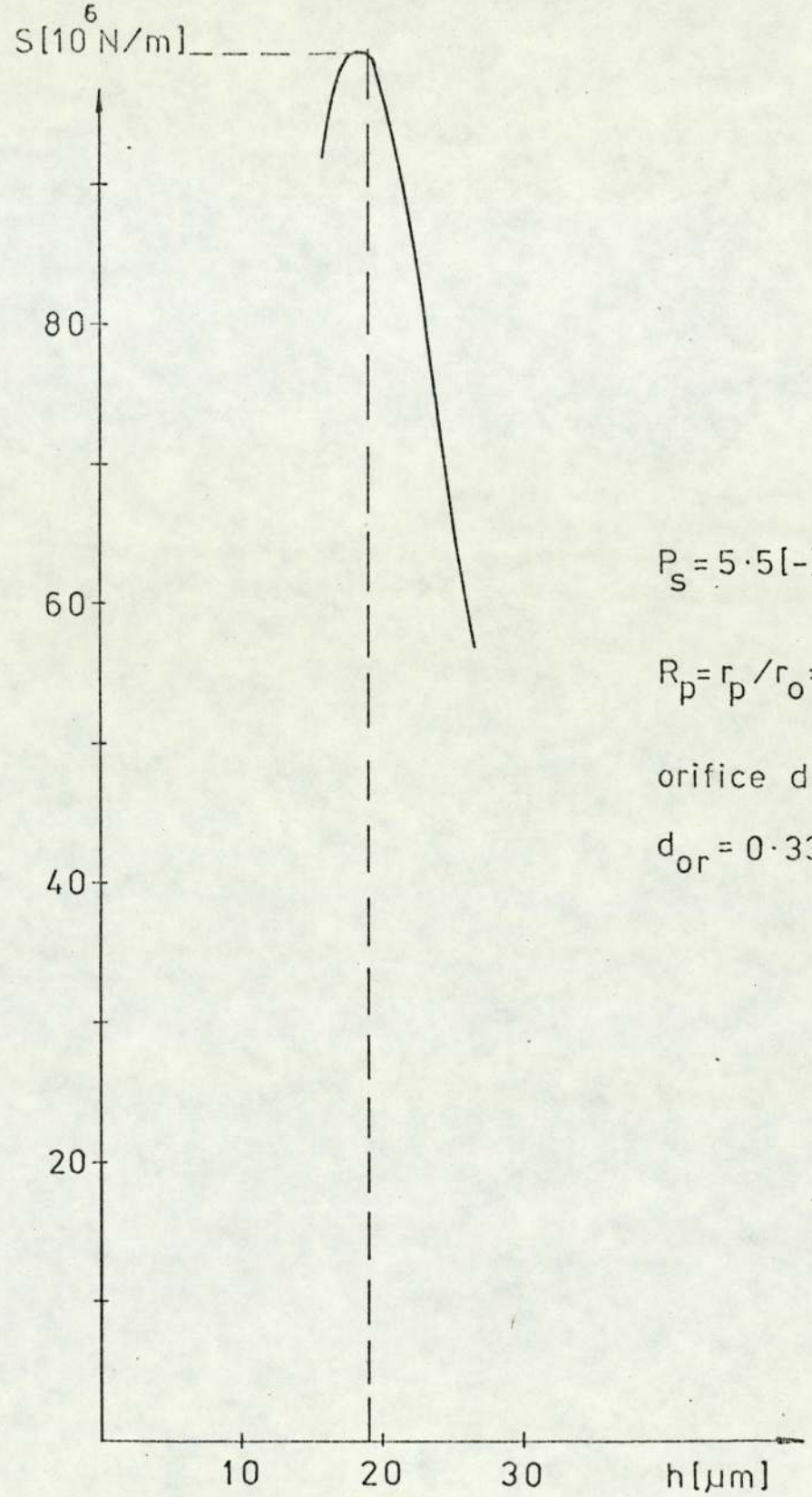

STIFFNESS V. FILM THICKNESS IN INITIAL BEARING DESIGN

FIG 27

conditions occur at h = 19 μm. At this film thickness

$$\left.\begin{aligned} M &= 79 \times 10^{-6}\ \frac{kg}{s} \\ W &= 1230\ N \\ S &= 99{,}7 \times 10^{6}\ \frac{N}{m} \end{aligned}\right\} \qquad (19)$$

It was the aim in the design that maximum stiffness occurs at about 20 μm, because at this film thickness the air flow is not excessive. It has been estimated that the laboratory air supply system is capable of achieving $25 \times 10^{-3}\ \frac{kg}{s}$ for continuous running. Figure for the mass flow given by equation (19) is almost three orders of magnitude smaller. If the design value of film thickness for maximum stiffness is much smaller than 20μm, the surface roughness of both bearing surfaces may appreciably influence the behaviour of the gas film and the bearing performance would not then be easily predictable.

Schematic diagram of main apparatus design is shown in fig 28. A slave journal bearing was incorporated in order to control the alignment of the test bearing. Air is fed to the journal housing at two admission planes. There are six equispaced holes in each plane but to every second hole in the upper plane air is admitted through a finely adjustable needle valve.

Fig.29 shows a cross section of the bearing pad and the layout of pressure transducers and displacement probes. Provision has been made, if the need arises, to change the adaptor containing the orifice restrictor at entry to the bearing film. This adaptor is sealed from the back by an 'O'

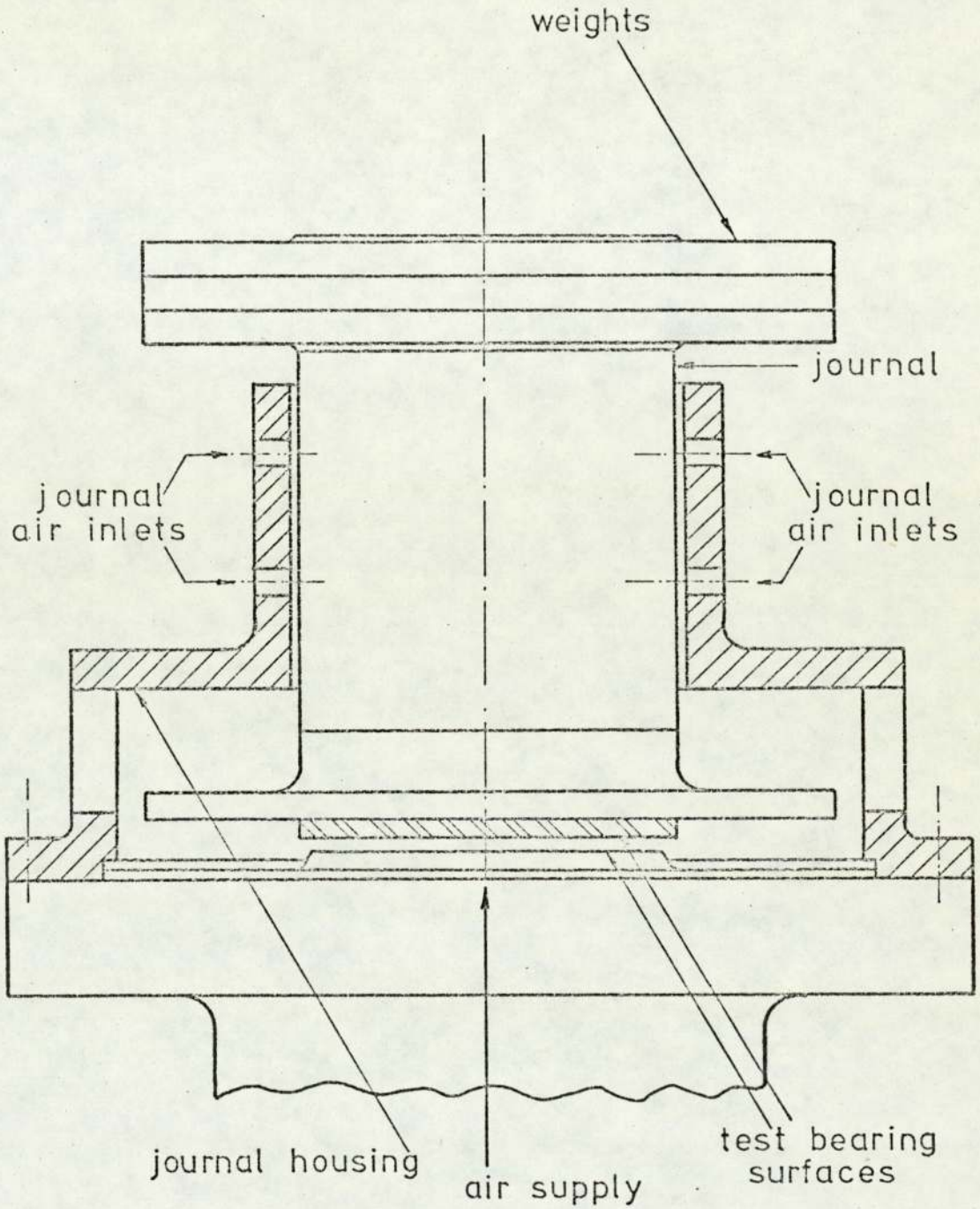

MAIN TEST APPARATUS

INITIAL DESIGN

FIG 28

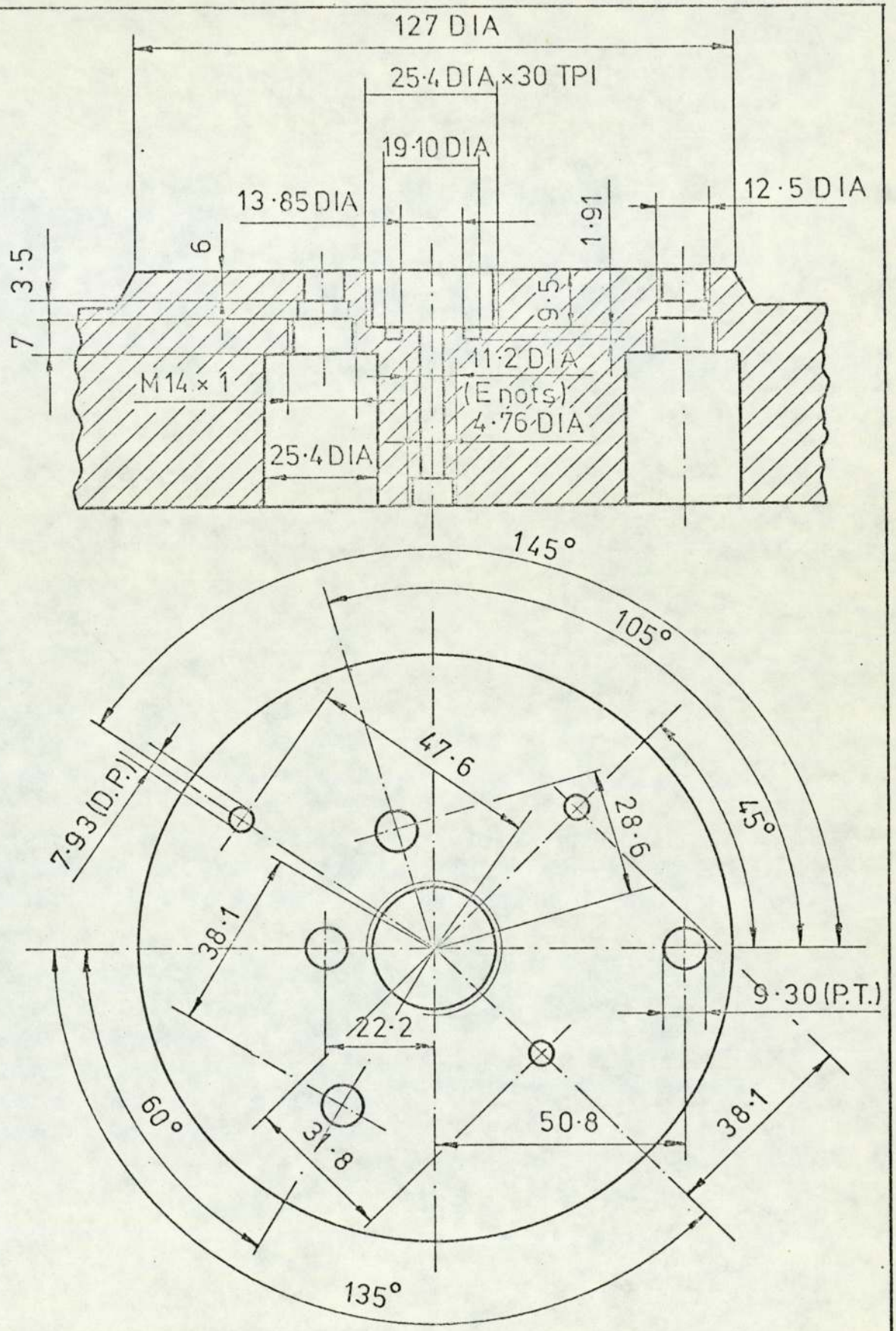

LAYOUT OF PRESSURE TRANSDUCERS (P.T.) AND DISPLACEMENT PROBES (D.P.)

FIG 29

ring so that there are no leaks via its threads.

Resistive type pressure transducers are selected because of their versatility: they are suitable for operating both at steady state and dynamic conditions. This means that the same transducers could be used to investigate, at a later date, the dynamic performance of compliant bearings. Through the four bridge amplifiers pressure signals can be read on an ultra violet recorder.

Displacements in the thrust bearing were to be measured by three capacitance probes and a distance meter. Position of the adaptors of these probes, which were to be screwed from underneath are shown on fig. 29. There were also three other probes outside the thrust bearing area to be used for alignment purposes.

The air pressurizing system with the instruments and controls for measuring pressure and flow rate is shown in fig. 30. Pressurized air is obtained from the compressor tank. After a pressure regulator and two filters, one line branches off to the slave journal bearing and the main line continues through another pressure regulator and through flowmeters to the test bearing. Just before the test bearing is reached there is a branch off for the supply pressure gauge and manometer. If the supply pressures are small they can be read on a mercury manometer more accurately than on the supply pressure gauge so either (or both) can be used.

5.3 Modifications to the Main Rig

Restrictor Change

The bearing of $R_p = 0.1$ was made but the initial

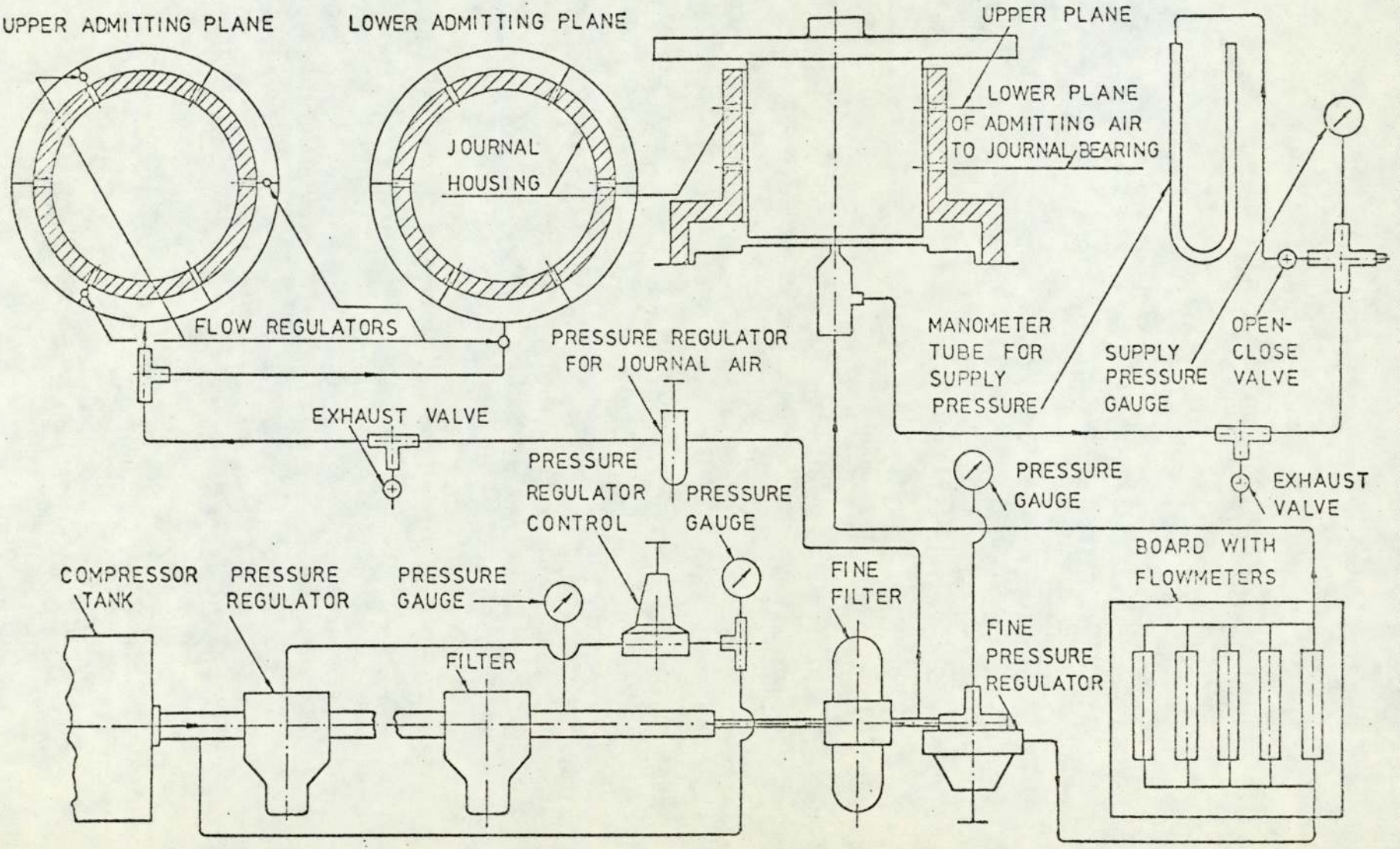

SCHEMATIC LAYOUT OF AIR SUPPLY SYSTEM

FIG 30

tests showed that it was highly unstable, even though care was taken that port volume was kept to a minimum. After these initial tests, the method of test-bearing compensation was changed from orifice to inherent in order that the bearing became more stable [109]. To achieve this, another adaptor was made and screwed onto the lower bearing plate. Bearing in mind that load and stiffness of inherently compensated bearings are lower than for orifice compensated bearings, the diameter of the hole in the middle of this adaptor was made 0.5715, so that the "port" radius was now equal to:

$$r_p = 0.28575\text{mm} \qquad (20)$$

This last dimension was measured on a ten times magnifying projector in the metrology laboratory. With the outer bearing radius measured to be:

$$r_o = 64.135\text{mm}$$

the ratio of these is:

$$R_p = \frac{0.28575}{64.135} = 0.004455 \qquad (21)$$

as mentioned in Appendix I.

Modifications due to Difficulties in Assembling the Rig

The journal was initially made of aluminium but subsequently sleeved with steel to avoid assembly damage.

Assembly was facilitated by reducing the test bearing upper plate in diameter to enable it to be passed through the slave journal housing.

However, three displacement probes now located beyond the test bearing perimeter could not be used any more, but mitronic comparators were readily introduced instead. These

transducers work on a differential transformer principle. They have magnetic bases and can conveniently be placed on the journal housing and be locked in position by a magnetic field. The sensing heads were placed on the top part of the journal as shown on photograph VII. They check bearing alignment, measure film thickness during rigid bearing tests and measure displacement between the bearing rigid surface and the non-deformed elastomer during compliant bearing tests.

On one of the reduced test bearings it was then possible to incorporate a pressure tapping in the middle, as shown below, in order to take readings of inlet bearing pressure during tests.

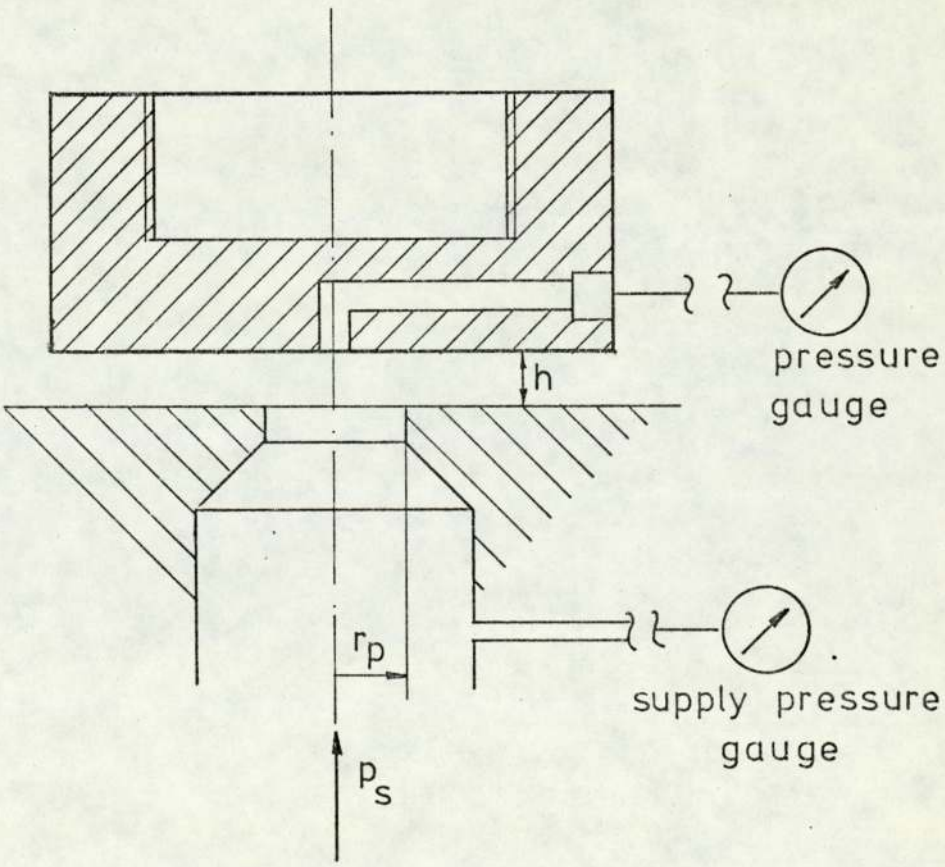

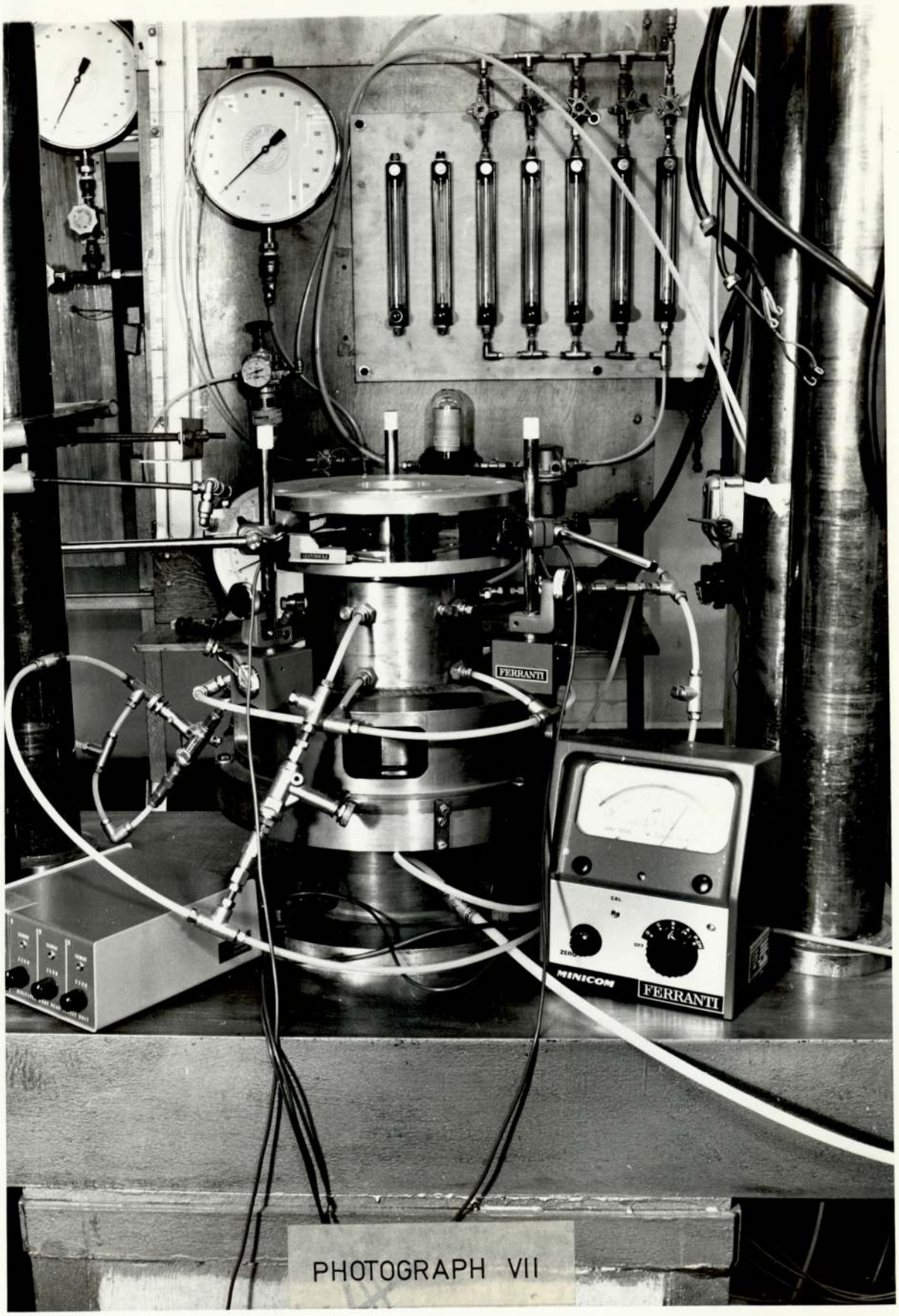

PHOTOGRAPH VII

Modifications in order to make the test bearing leakproof

In the thrust bearing area on the upper surface of the lower bearing plate, there are four holes for the pressure transducers, three holes for capacitance probes' adaptors and one hole for the air supply adaptor. It is imperative to ensure that there are no leaks before the air reaches the outer bearing edge where r_o = 64.135mm.

Threads in the capacitance probes' adaptors were prone to leaks even though they were sealed from the back by a solution of silicone rubber. New adaptors were made to seal against the lower bearing plate with "O" rings. These adaptors had to be larger than the previous adaptors in order to make the holes in the lower bearing plate free of previous threads. Capacitance probes were sealed against the adaptors by perspex sleeves with a tight fit.

Pressure transducers were sealed by fibre washers and the air supply adaptor by an "O" ring.

There should be no leaks anywhere in the supply line after the flowmeters see fig. 30.

Leaks in the thrust bearing area were tested by introducing a soap solution or a lighter flame to places of suspected leaks. These simple methods can be used also in other places of the supply line.

Another method of testing for leaks in the air pressurizing system is by a chamber designed to calibrate the pressure transducers, see photograph VIII. This method was used before a test was started with the rig dismantled.

PHOTOGRAPH VIII

With the pressure chamber in position bolted to the lower bearing plate and with the chamber vent valve closed, there should be no flow through the flowmeters. If the spherical float of the most sensitive flowmeter is resting on its seat, i.e. if it is in the lowest possible position, this is an indication that there are neither leaks in the supply line after the flowmeters nor in the thrust bearing area.

This pressure chamber was designed for calibr ating pressure trasnducers in position. Previously it was attempted to calibrate each transducer in an adaptor outside the main rig by bringing a known air pressure to it. However it was noticed that galvanometer deflections shown on the ultra violet recorder depend upon the tightness of the transducers in their adaptors. The pressure chamber itself is sealed with an "O" ring against the bearing lower plate outside the test bearing area.

Similarly to pressure transducers, capacitance probes are best calibrated in their respective positions. This can be achieved with shims or feeler gauges of known thickness. Also a "bridge" of slip gauges as shown in sketch below was used.

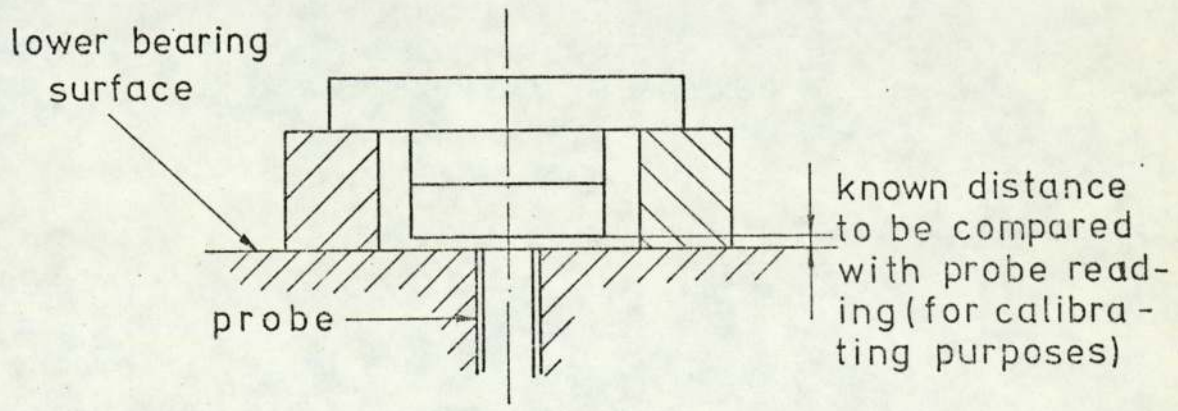

The possibility of unknown leaks is reduced if the instrumentation in the test bearing area is not frequently disturbed. Performing calibration of this instrumentation in position prevents their unnecessary disturbance.

General Examination of the Main Rig

Because of the small size of the clearances in the thrust bearing during experiments, it is essential that all dimensions are as near as possible to those specified. It is also necessary to have test bearing surfaces as flat as possible so that measured performance can be correlated to a theoretical prediction.

For example, it is important that the journal housing is placed vertically on the bottom plate, so that when the journal is parallel to the journal housing, the surfaces of the thrust bearing are also parallel to each other. Therefore it was made sure that the centrelines of the journal housing and of the journal are as near to each other as possible. After rectifying the rig in the University workshops, these two centrelines were measured to be 0.038mm apart. This measurement is done with the journal and the lower plate bolted together and placed in a lathe chuck, i.e. the centrelines were in a horizontal position. In this position of the journal and the lower plate, the centrelines would tend naturally to the maximum distance between them and during bearing tests this distance can be smaller.

The journal housing was checked for ovality in three positions along its bore, and it was found that in the worst case it was 0.0032mm out. This measurement was done in the Metrology Laboratory. The journal housing is seen on

photograph IX. The journal with a compliant bearing screwed on is shown on the same photograph upside down from its normal position during bearing tests.

Displacement probes should be as level as possible with the lower thrust bearing surface, in order to measure true displacements. Pressure transducers can be a few micrometres below this surface, so that they are not damaged during any operation to make this surface flat.

With the instrumentation and the air supply adaptor in position, the lower test bearing surface was surface ground. This has been done after consulting the manufacturer of the displacement probes for approval. Because of the size of the lower bearing plate, the surface grinding had to be done outside the University workshops, where a surface grinder large enough for this operation could be found.

By checking the probes after grinding with an AVO multimeter, it was found that they were shorting . This was rectified by cleaning carefully the probes' guard rings of any steel particles embedded in them after the grinding operation. The cleaning was done by means of a sharp sewing needle under a ten times magnifying projector.

After this, the bearing lower plate was checked for flatness by Talylin instrument, see photograph X.

Talylin uses a stylus to trace the surface irregularities. The traversing speed of the stylus is determined by the horizontal magnification factor used on the tracing paper. For the minimum horizontal factor of two, the speed is smallest. The movement of the stylus is converted by means of an electro-

PHOTOGRAPH IX

PHOTOGRAPH X

magnetic transducer into electric signals.

As stated earlier, bearing lift-off is measured by mitronic comparators. The pneumatic film thickness in the case of rigid bearings is larger than this lift-off for an equivalent surface roughness. This surface roughness can be estimated from a Talylin instrument trace.

The checking of the lower test bearing surface on the Talylin was done in five or six directions and across all adaptors and probes as shown on photograph X. The average flatness of this bearing surface is estimated to be 3.2 μm. The average flatness of the rigid top bearing surface is estimated to be 1.5 μm as shown below:

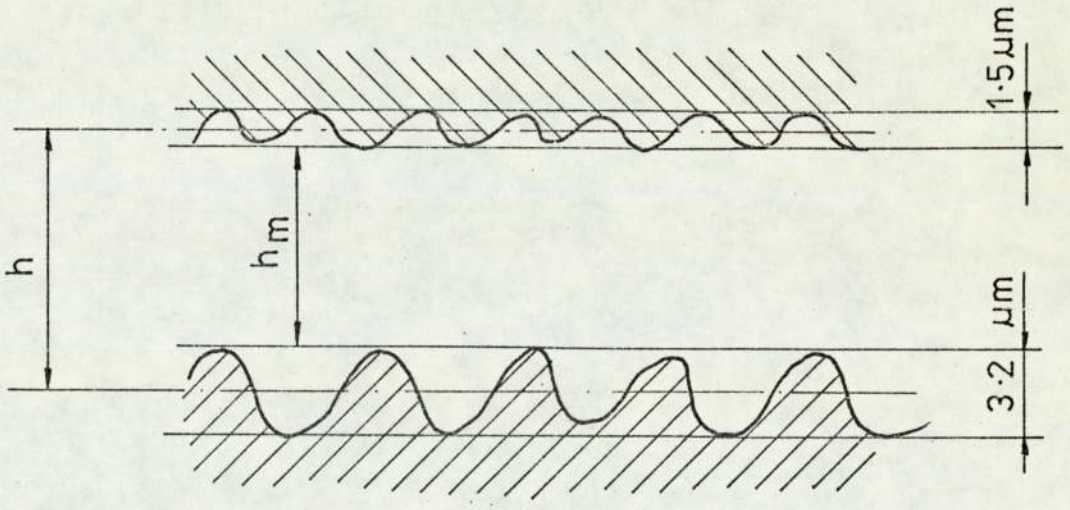

The pneumatic film thickness h could then approximately be equal to

$$h = h_m + \frac{3.2}{2} + \frac{1.5}{2} = h_m + 2.35\ \mu m \qquad (21)$$

Flow measurements will show that the film thickness derived from the measured flow rate is larger than the measured film. For the rigid bearing experiments this discrepancy is about 2.5 μm.

In the case of an elastic bearing, the top bearing surface has to be sprayed by some conductive paint if the film profile is to be measured by conductive probes, because elastomers are generally non-conductive.

Elastomers need grinding, with the help of chalk dust before spraying. After spraying with a type of silver paint, grinding or lapping is necessary for two reasons:

a) to achieve uniform thickness of the silver paint

b) to achieve flatness comparable to the elastomer before spraying.

Generally, flatness of rubbers is of the order of 2–4 μm.

Fig. 31 shows two traverses of the Talylin across the lower thrust bearing surface. Sharp peaks should be ignored because of the inertia of the stylus even at its lowest speed when some probes or adaptors are traversed. Horizontal magnification is two, and on the vertical scale one division represents 2.5 μm. Flatness of 3.2 μm was estimated after averaging several traverses along the lower thrust bearing surface. Flatness of 1.5 μm was similarly obtained for the top rigid thrust bearing surface.

After these modifications, positions of the displacement probes and pressure transducers were measured in the Production Engineering Department and they are shown in Fig.32. Photograph XI represents the top view of the lower bearing surface.

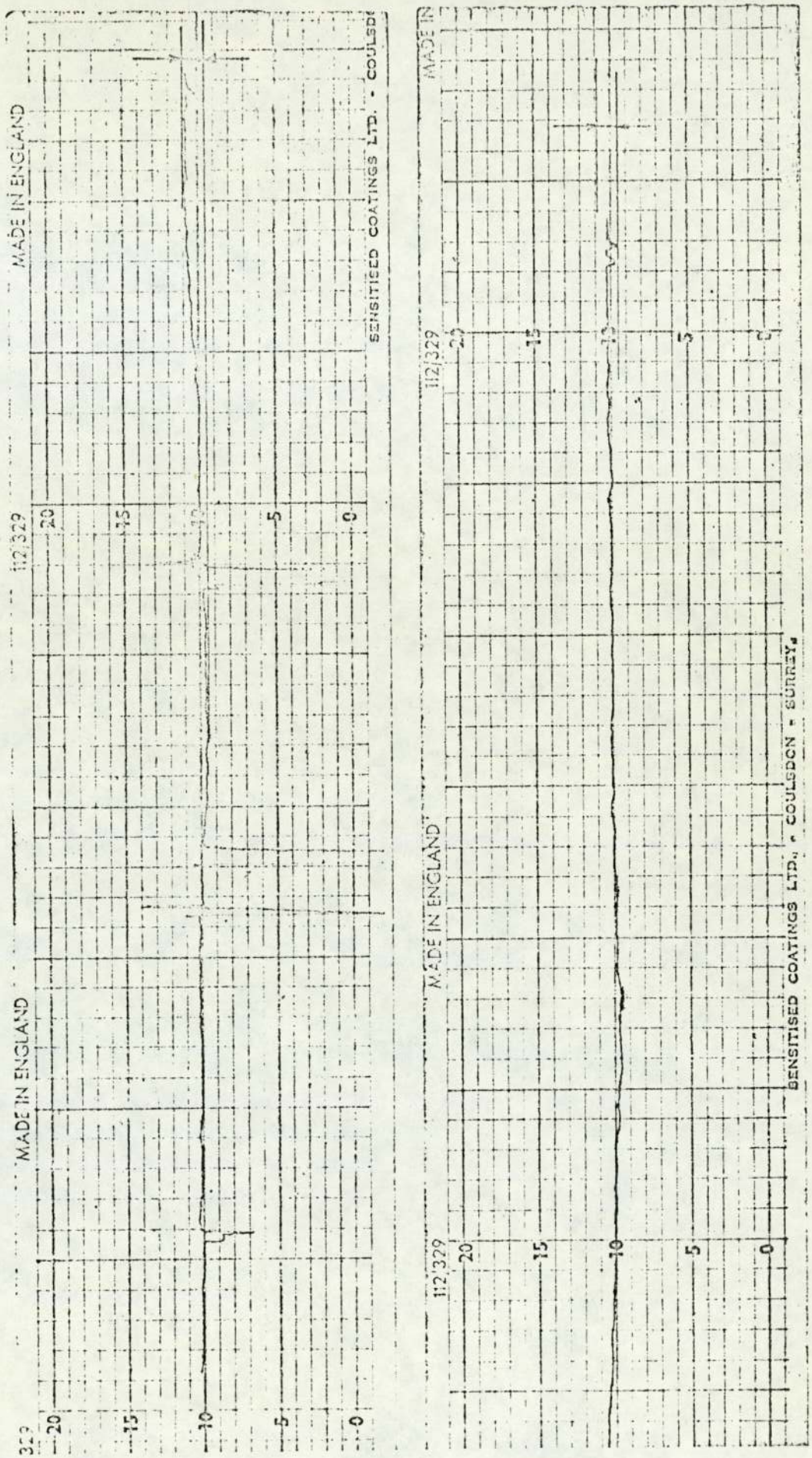

TALYLIN TRACES ACROSS THE LOWER TEST BEARING SURFACE

FIG 31

A, B, C DISPLACEMENT PROBES

1, 2, 3, 4 PRESSURE TRANSDUCERS

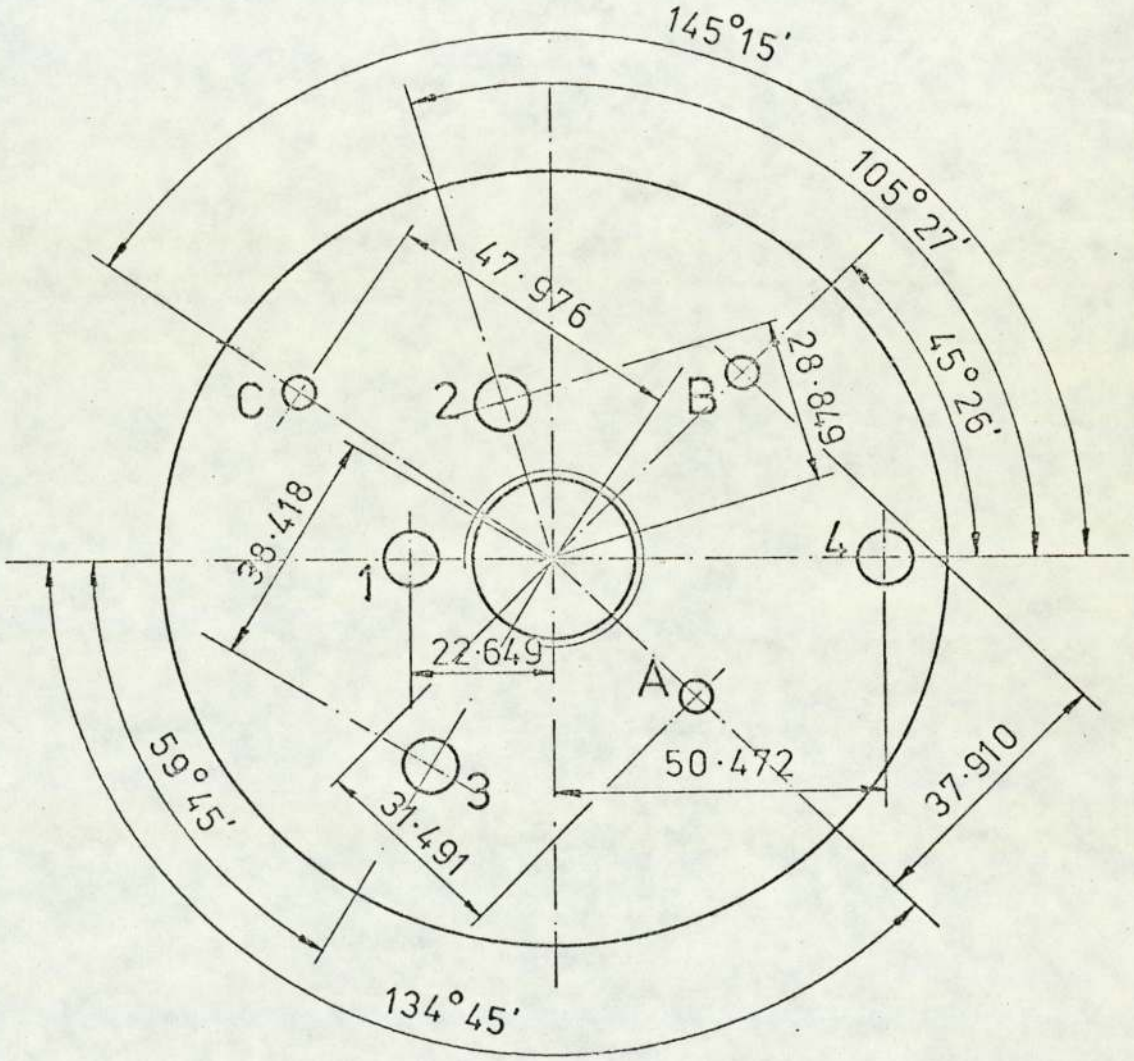

RADIAL POSITIONS OF PRESSURE TRANSDUCERS AND DISPLACEMENT PROBES

FIG 32

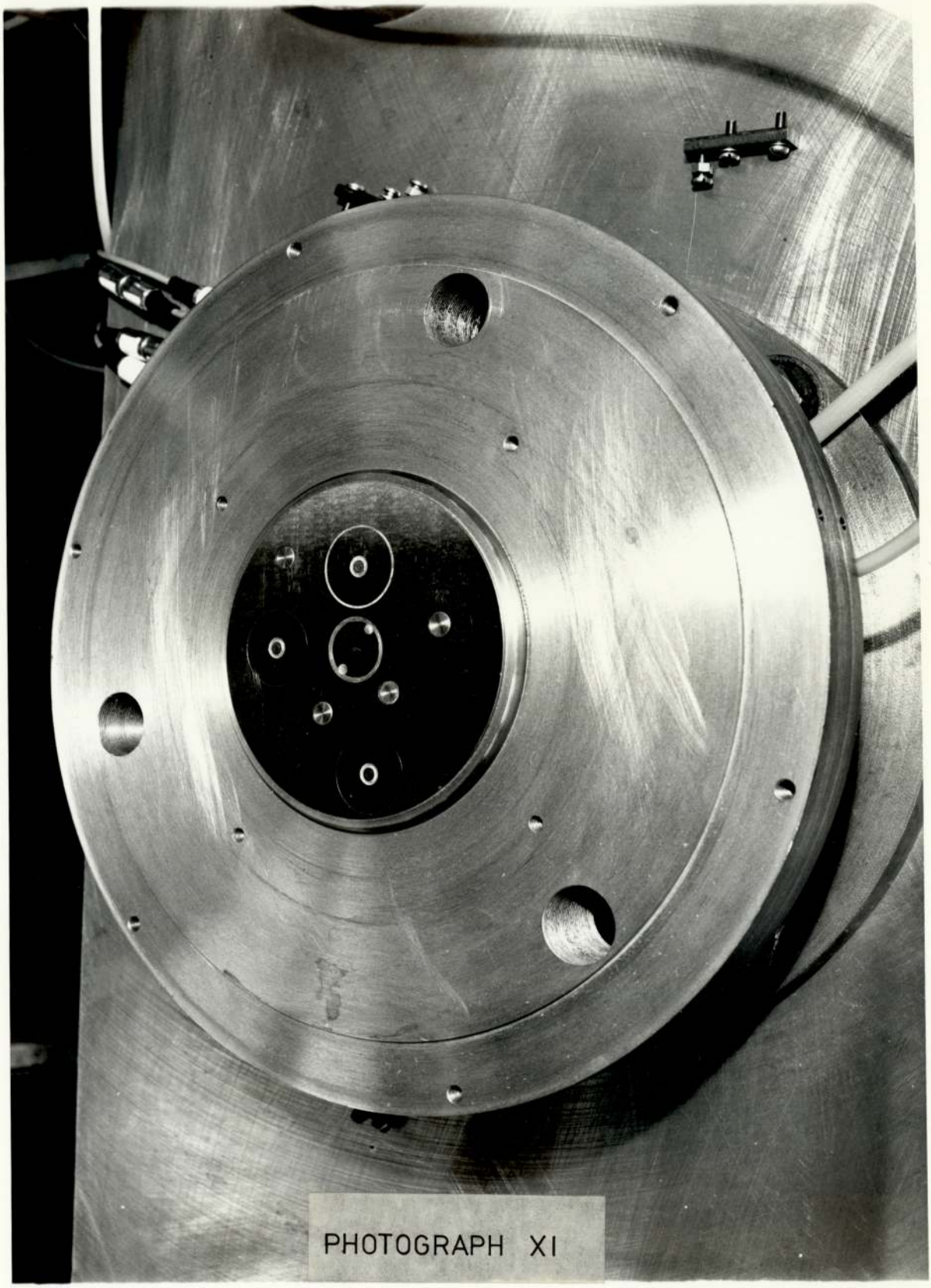

PHOTOGRAPH XI

VI RIGID BEARING EXPERIMENTS

Bearing load, mass flow and stiffness were initially predicted for design purposes in Chapter V. The bearing performance will not be the same as the predicted performance primarily due to modifications of the rig such as the restrictor change, but also because of the following.

1) In the initial design, bearing surfaces were represented by two geometric planes. In this chapter it is shown that this simple representation is not adequate if the two surfaces are as near to each other as the two thrust bearing surfaces in the test bearing.

2) The value of discharge coefficient used in predicting performance is only approximate.

This chapter gives the rigid bearing performance after taking into account the complex effects of the geometric texture of bearing surfaces. Values of experimentally determined discharge coefficient are also presented.

Either bearing load or supply pressure or film thickness can be kept constant in turn during rigid bearing tests whilst the other two quantities are varied. All three types of experiments were performed for rigid bearings.

For rigid bearings, keeping the bearing load constant

means that pressure at the entrance to the bearing film is kept constant. Coefficients of discharge were determined experimentally from these tests. Film pressures were measured and flow versus film thickness relationship was also deduced from these tests. However relationships of load versus film thickness and hence stiffness versus film thickness could not be established by this type of tests.

Experiments where supply pressure is kept constant and where load is varied are useful in determining bearing performance. Here, relationships for mass flow, load and stiffness versus film thickness can be established both in dimensional and dimensionless form.

Experiments where film thickness is kept constant and where both load and supply pressure are varied, serve as a useful check for the bearing performance determined by the first two types of tests.

6.1 Discrepancies between measured film thicknesses and film thicknesses derived from flow measurements

Talylin measurements of the bearing surfaces have revealed that the average flatness of the lower bearing surface is about 3.2 μm and the average flatness of the top bearing surface is about 1.5 μm.

The Talylin instrument gives a picture of the surface texture in two dimensions, i.e. it gives a profile of the surface. The whole group of instruments which mechanically analyse surfaces by traversing styluses over them are sometimes called profilometers . These instruments usually trace a small representative sample of the surface. Some of these

instruments are based upon a very small sample which may not be representative of the whole area studied. The Talylin instrument does not suffer from this defect. It is capable of traversing 100 mm. of the total of about 130 mm i.e. about 80% of the bearing diameter. At the same time this instrument achieves a high magnification in the vertical direction thus giving an outstanding capacity for studying the surface geometry of these bearings.

The average flatness of seven measurements in various directions over the lower bearing surface gives a value of 3.2 μm. The flatness is here defined as the difference between the highest peak and the lowest valley on a given Talylin trace.

The average flatness of eight measurements for a particular top bearing surface is obtained as 1.45 μm.

If a simple model for the pneumatic film is assumed such that the pneumatic film h is equal to the measured film plus a half of both flatnesses, then

$$h = h_m + \frac{3.2 + 1.45}{2} =$$

$$= h_m + 2.325 \text{ m}$$

so that the surface roughness effects defined in this way are equal to

$$SF = 2.325 \ \mu m \qquad (1)$$

The value of the surface roughness effects from this simple model is now compared with the values from flow measurements.

Equation (I-13) of Appendix I shows that for a given load (i.e. given film entry pressure), mass flow is proportional to the cube of film thickness, i.e. film thickness:

$$h \propto M^{1/3} \tag{2}$$

Fig. 33 shows a plot of measured films versus films derived from flow measurements, keeping the bearing load constant. Experiments with three different loads were performed. A least squares fit through the points of all three loads gives a line parallel to a 45^{o} line drawn from the origin as shown in Fig. 33 . The two lines are 2.5 μm apart. Similar graphs for porous aerostatic thrust bearings were obtained by Taylor and Lewis[142]. Measured flow versus measured films during experiments is shown in Fig. 34 . It is seen that for a given load and a given film, measured flow rate is higher than the theoretical flow rate. If 2.5 μm is added to every measured film, Fig. 35 is obtained. Here the experimental points agree much better with the theory lines.

The difference between measured and derived film thicknesses was found to be consistent throughout the rigid bearing tests and it is equal to:

$$SF = 2.5 \pm 0.5 \ \mu m \tag{3}$$

The value of 2.5 μm with its given tolerance represents the equivalent surface roughness effects of the rigid bearings. This means that all measured films in the rigid bearing experiments should be corrected by 2.5 μm, i.e. the real film thickness

$$h = h_m + SF \tag{4}$$

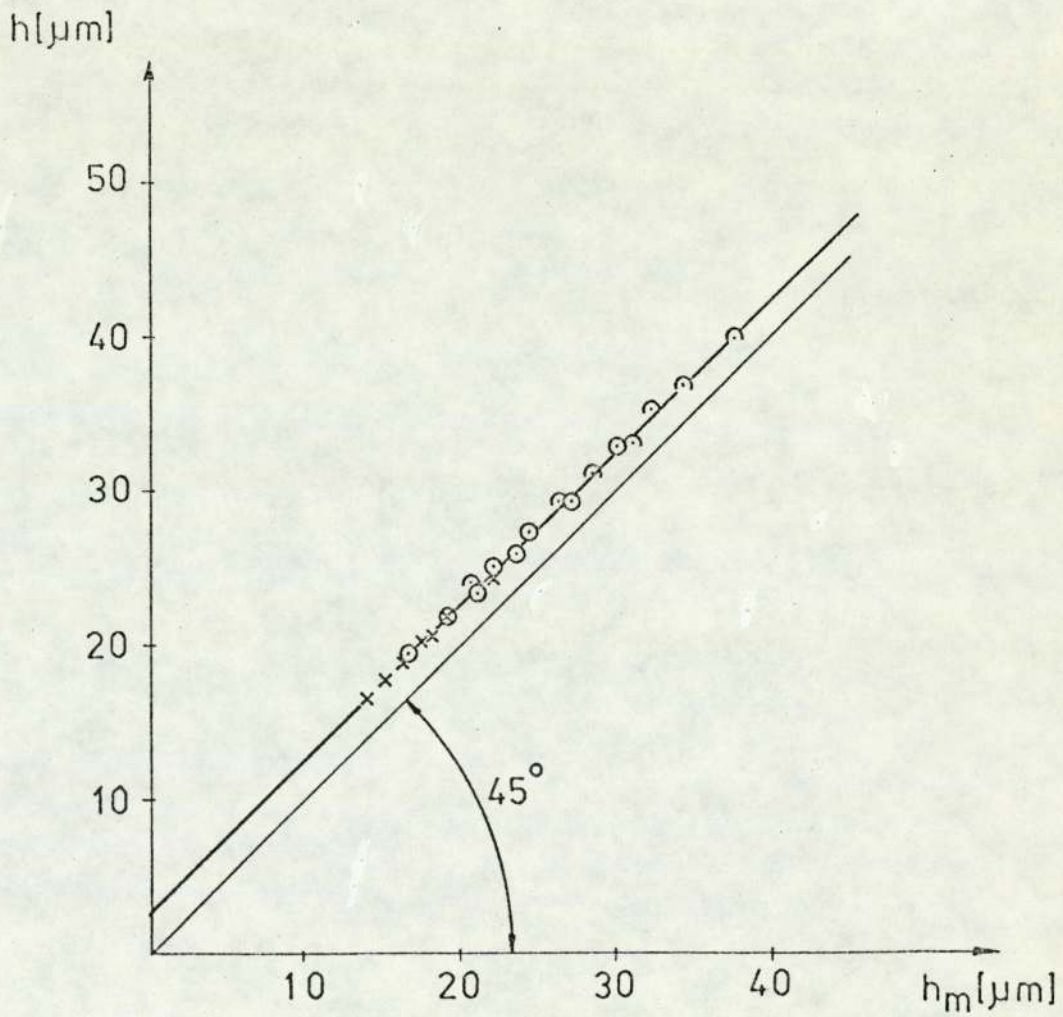

MEASURED FILM V. FILM DERIVED FROM FLOW MEASUREMENTS

CONSTANT LOAD TESTS

FIG 33

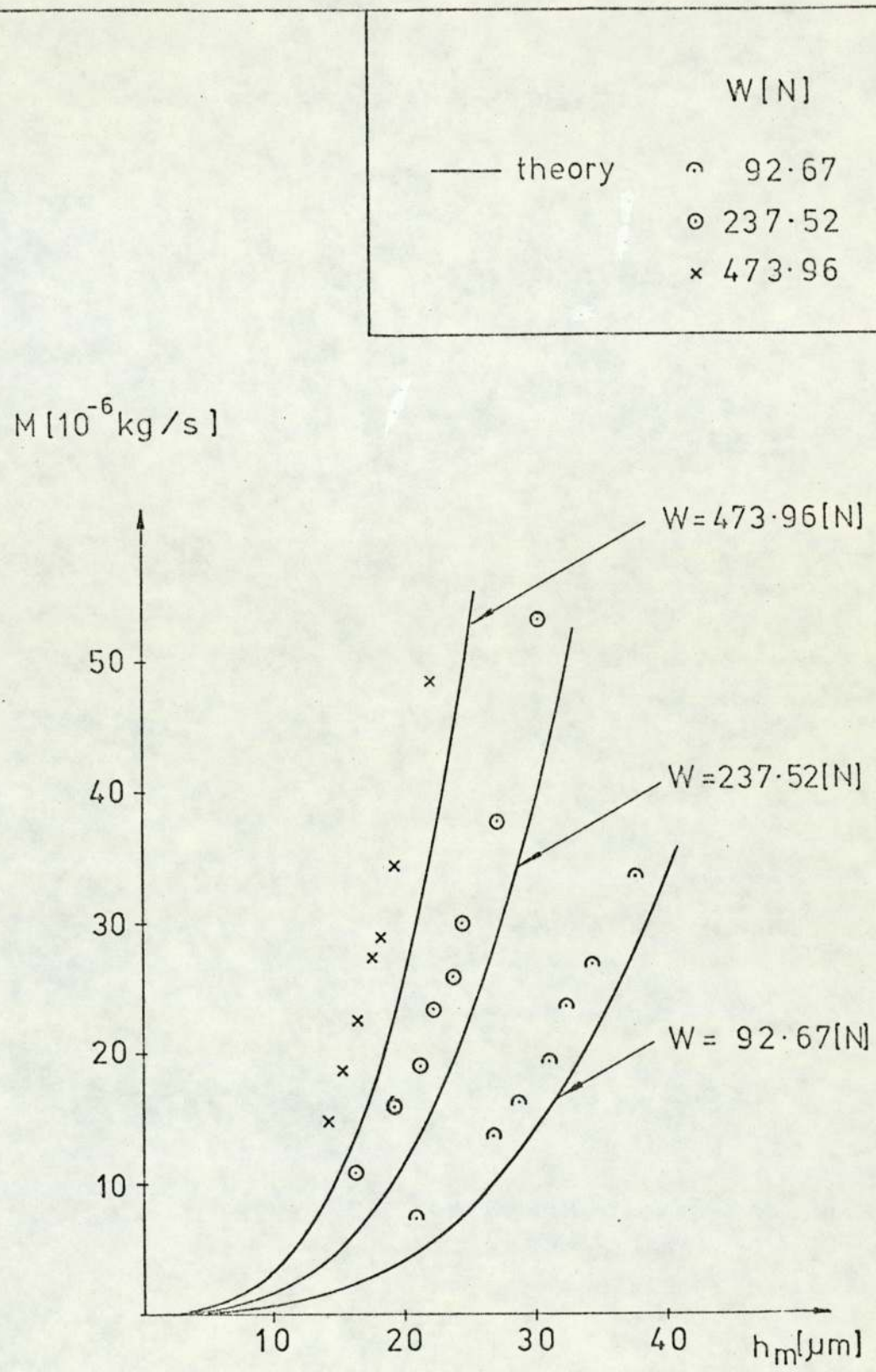

MEASURED FILM V.

MEASURED MASS FLOW

CONSTANT LOAD TESTS

FIG 34

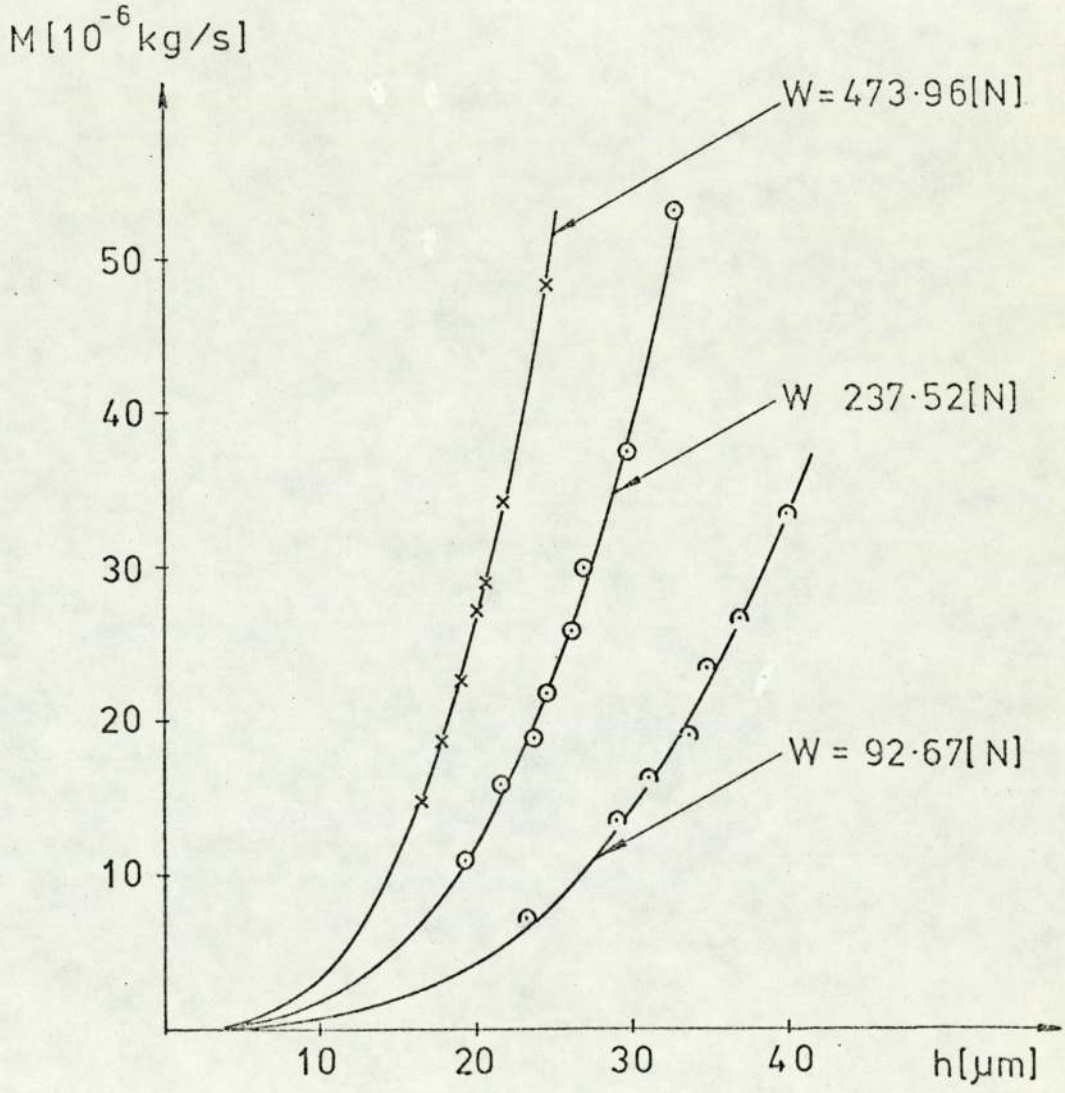

MEASURED FILM CORRECTED FOR

2·5[μm] V. MEASURED MASS FLOW

CONSTANT LOAD TESTS

FIG 35

Measured film h_m [μm]	20.9	26.7	28.6	31.2	32.4	34.5	37.7
Measured absolute supply pressure p_s [bar]	1.91925	2.08025	2.17800	2.36200	2.47700	2.71275	3.16126
Measured mass flow rate M $[\frac{kg}{s} x10^{-6}]$	7.33	13.52	16.18	19.32	23.58	26.67	33.52
Film derived from measured flow h_d [μm]	24.06	29.51	31.33	33.24	35.52	37.01	39.94
Mass flow rate calculated from measured film $[\frac{kg}{s} x10^{-6}]$	4.804	10.015	12.309	15.981	17.896	21.607	28.194
Corrected film $h=h_m+2.5$ [μm]	23.4	29.2	31.1	33.7	34.9	37.0	40.2
Mass flow calculated from corrected film $[\frac{kg}{s} x10^{-6}]$	6.742	13.100	15.827	20.138	22.367	26.652	34.183
Port/supply pressure ratio P_p/P_s [-]	0.86096	0.79433	0.75868	0.69958	0.66710	0.60912	0.52270
Discharge coefficient C_D[-] calculated from corrected film h	0.617	0.637	0.654	0.663	0.661	0.659	0.648

TABLE VI-1 RIGID EXPERIMENTS KEEPING LOAD CONSTANT

W = 92.67 [N] (MINIMUM POSSIBLE LOAD), P_p = 1.62864[-]
$\bar{W}$ = 0.07144[-]

TABLE VI-2 (FOLLOWING PAGE)

RIGID EXPERIMENTS KEEPING

LOAD CONSTANT

$W = 237.52 [N]$

$P_p = 2.37053 \quad [-]$

$\bar{W} = 0.18309 \quad [-]$

Measured film h_m [µm]	16.8	19.2	21.2	22.2	23.6	24.5	27.2	30.3
Measured absolute supply pressure p_s [bar]	2.85650	3.04625	3.23600	3.45450	3.68450	3.90875	4.61600	5.45550
Measured mass flow rate M $[\frac{kg}{s} \times 10^{-6}]$	10.89	15.81	18.99	23.32	25.79	29.99	37.65	53.39
Film derived from measured flow $h_d [\frac{kg}{s} \times 10^{-6}]$	19.49	22.07	23.46	25.12	25.98	27.32	29.47	33.11
Mass flow rate calculated from measured film $[\frac{kg}{s} \times 10^{-6}]$	6.974	10.411	14.015	16.093	19.334	21.631	29.600	40.917
Corrected film $h=h_m+2.5$ [µm]	19.3	21.7	23.7	24.7	26.1	27.0	29.7	32.8
Mass flow calculated from corrected film $[\frac{kg}{s} \times 10^{-6}]$	10.574	15.030	19.581	22.165	26.152	28.951	38.534	51.904
Port/supply pressure ratio P_p/P_s [-]	0.84012	0.78779	0.74160	0.69469	0.65133	0.61396	0.51989	0.43989
Discharge coefficient C_D [-] calculated from measured film h_m	0.466	0.513	0.552	0.540	0.555	0.554	0.568	0.597
Discharge coefficient C_D [-] calculated from corrected film h	0.615	0.656	0.690	0.669	0.679	0.673	0.678	0.699

Measured film h_m [µm]	14.1	15.3	16.5	17.5	18.3	19.2	22.2
Measured absolute supply pressure P_s [bar]	4.06400	4.31700	4.60450	4.89775	5.19100	5.58200	6.90450
Measured mass flow rate M $[\frac{kg}{s} \times 10^{-6}]$	14.86	18.56	22.54	27.33	28.94	34.49	48.49
Film derived from measured flow h_d [µm]	16.51	17.78	18.97	20.23	20.62	21.86	24.49
Mass flow rate calculated from measurement film $[\frac{kg}{s} \times 10^{-6}$	9.254	11.824	14.830	17.693	20.232	23.366	36.120
Corrected film $h=h_m+2.5$ [µm]	16.6	17.8	19.0	20.0	20.8	21.7	24.7
Mass flow calculated from corrected film $[\frac{kg}{s} \times 10^{-6}]$	15.101	18.618	22.644	26.410	29.708	33.734	49.748
Port/supply pressure ratio P_p/P_s [-]	0.83868	0.78953	0.74023	0.69591	0.65659	0.61060	0.49365
Discharge coefficient C_D [-] calculated from measured film h_m	0.514	0.515	0.524	0.529	0.531	0.531	0.565
Discharge coefficient C_D [-] calculated from corrected film h	0.712	0.697	0.694	0.692	0.686	0.678	0.700

TABLE VI-3 RIGID EXPERIMENTS KEEPING LOAD CONSTANT

$W = 473.96[N]$, $P_p = 3.37163[-]$, $\bar{W} = 0.36536[-]$

where the surface roughness effects SF are given by equation (3).

It is seen that the simple model proposed gives values for surface roughness somewhat lower than that obtained by flow measurements. This is attributed not only to the stylus diameter, but also to the complex, tri-dimensional nature of the bearing surfaces and to difficulties in predicting the behaviour of real surfaces from profilometry measurements.

Data to plot figures 33, 34 and 35 is given in tables VI-1, VI-2 and VI-3.

6.2 Experiments to determine the discharge coefficient of the bearing restrictor

For the bearing performance to be predicted accurately, it was necessary to know how the equivalent discharge coefficient of the inherently compensated bearings varies with the supply conditions.

Generally, coefficients of discharge for orifices are dependent upon the Reynolds number [17]. The Reynolds number is determined by the flow rate and hence the pressure drop across the orifice. If the bearing load is kept constant, i.e. the entrance pressure to the bearing film is kept constant, coefficients of discharge are then determined by the supply conditions. Similar reasoning was followed to obtain the equivalent discharge coefficient for inherent compensation as, for a constant load, the entrance pressure to the bearing film was kept constant.

Thus the equivalent discharge coefficient is best

determined experimentally, by varying the supply pressure. The same three loads used previously for investigating surface roughness effects, section 6.1 , are chosen

The equivalent discharge coefficient is proportional to the square of film thickness and is inversely proportional to a function of the ratio of film entry pressure to supply pressure as shown by equation (I-64), Appendix I, i.e.

$$C_D \propto \frac{h^2}{f(P_p/P_s)} \qquad (5)$$

Discharge coefficients can be calculated from measured film thicknesses, measured supply pressures and measured loads. Then they can be plotted against film entry/supply pressure ratios for different loads. Fig. 36 is such a plot for three different loads.

It is clear from fig. 36 that the discharge coefficients of the constant load experiments vary little with the film entry/supply pressure ratio. The average value of these discharge coefficients is about 0.54.

However, the real or pneumatic film thickness is larger than the measured film by SF, the surface roughness. From flow measurements it has been found that SF is about 2.5 [μm].

When the corrected value of film thickness is used in equation (5), then larger discharge coefficients are obtained, see fig. 37 .

The discharge coefficient C_D was determined experimentally for the whole range of rigid bearing experiments, for various

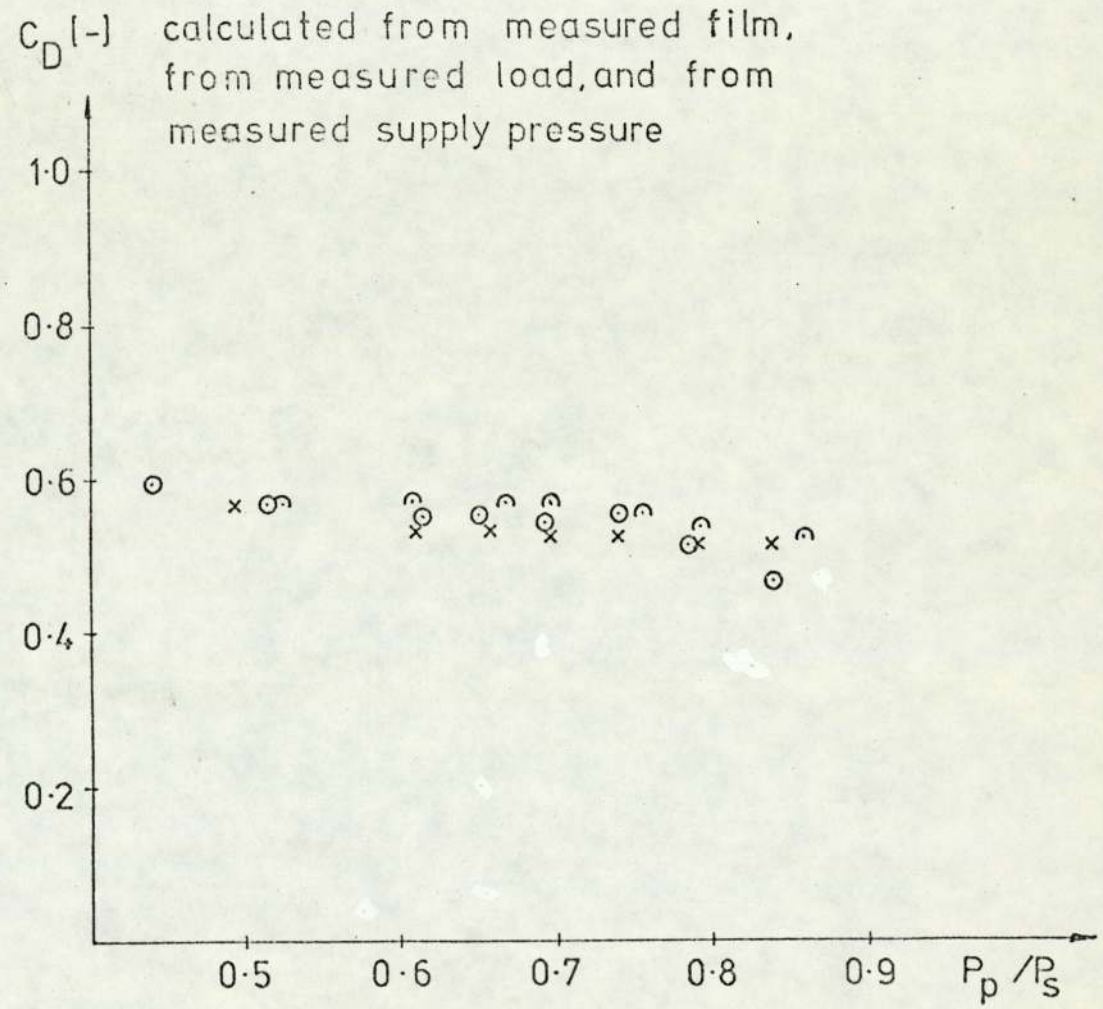

COEFFICIENT OF DISCHARGE V. FILM ENTRY/SUPPLY PRESSURE RATIO

CONSTANT LOAD TESTS

FIG 36

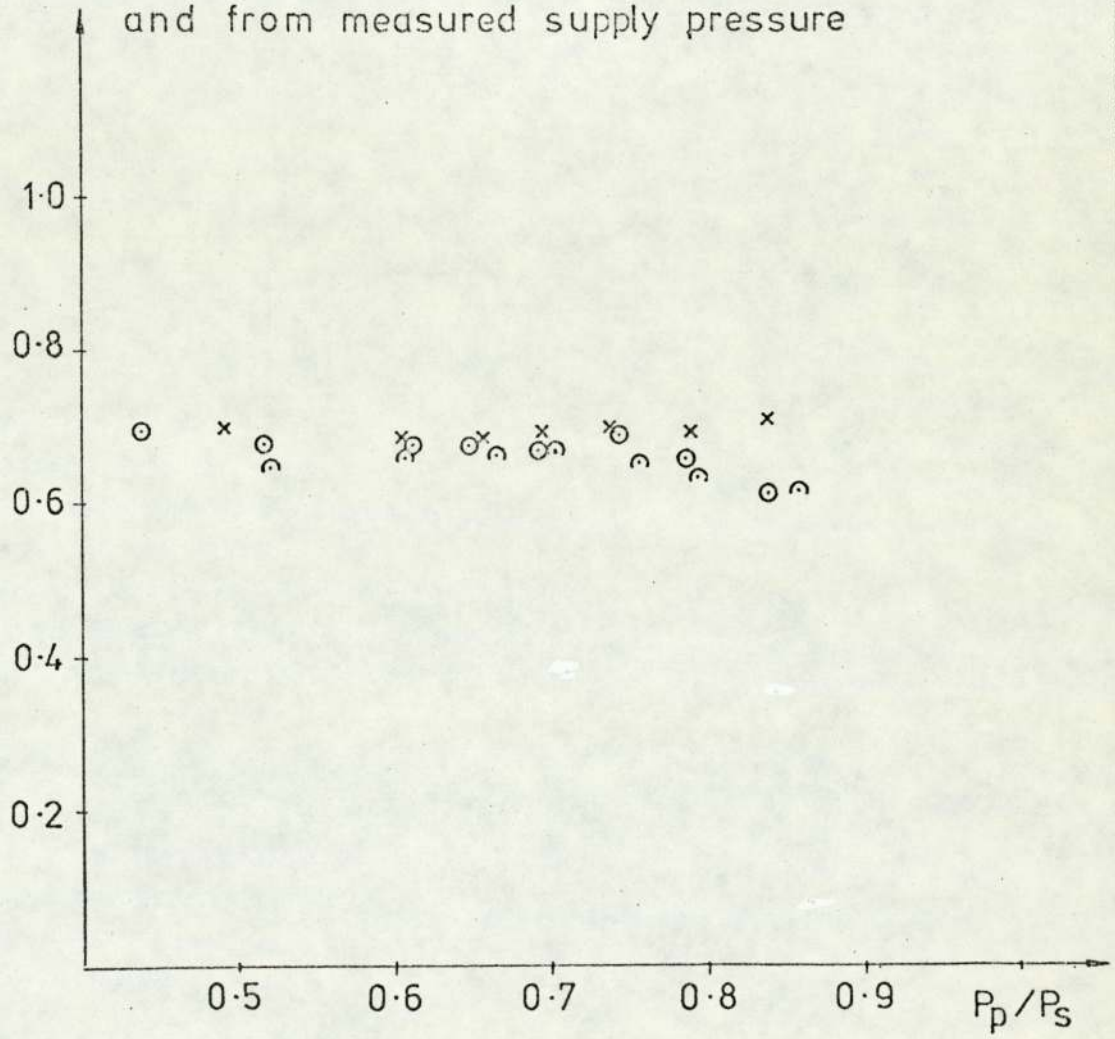

COEFFICIENT OF DISCHARGE V. FILM ENTRY/SUPPLY PRESSURE RATIO

CONSTANT LOAD TESTS

FIG 37

loads and various supply pressures. It was found that C_D is almost constant for varying film entry/supply pressure ratio as shown in fig. I-5 , Appendix I and fig. 37. The average value for C_D for the many rigid bearing experiments is obtained as:

$$C_D = 0.68 \qquad (6)$$

During the rigid experiments C_D varied between 0.65 and 0.71.

It is necessary to use this empirical average value of the coefficient of discharge for inherent compensation so that theoretical load-film thickness and stiffness film thickness curves can be obtained and compared with the experimental data.

6.3 Film Pressure Measurements

There are four pressure transducers spaced at different radial positions in the bearing area. Their function is to check experimentally film pressures predicted by the theory. They are sensitive to bearing tilt and are an additional means of ensuring that the thrust bearing surfaces are parallel.

One of the tests for pressure measurements was done with five different loads and for each load the supply pressure was varied. At every different supply pressure film pressures were monitored in order to confirm that their values are independent of the supply pressure in the case of rigid bearings. The results of this experiment are given in table VI-4. From this table it follows that errors based upon both minimum and maximum absolute pressures in the bearing film at a given radial position (for different supply pressures) are less than 1.5% .

MEASURED FILM PRESSURES (bars)

R	0.353	0.450	0.599	0.787
		W=92.67N		
1	1.1519	1.1189	1.0819	1.0369
av.	1.1519	1.1189	1.0819	1.0369
		W=152.49		
1	1.2419	1.1919	1.1369	1.0589
2	1.2459	1.1969	1.1389	1.0629
3.	1.2449	1.1969	1.1389	1.0619
4	1.2469	1.2009	1.1419	1.0629
5	1.2479	1.2009	1.1419	1.0639
av.	1.2455	1.1975	1.1397	1.0621
		W=237.52N		
1	1.3719	1.2919	1.2099	1.0999
2	1.3789	1.2999	1.2119	1.0919
3	1.3839	1.3079	1.2119	1.0919
4	1.3839	1.3099	1.2139	1.0949
av.	1.3796	1.3024	1.2119	1.0946
		W=337.05N		
1	1.5189	1.4149	1.3019	1.1389
2	1.5299	1.4219	1.3019	1.1349
3	1.5339	1.4319	1.3049	1.1319
av.	1.5276	1.4229	1.3029	1.1352
		W=473.66N		
1	1.7339	1.5739	1.4269	1.2099
2	1.73339	1.5989	1.4299	1.1939
3	1.7339	1.5869	1.4319	1.1919
4	1.7419	1.6039	1.4269	1.1939
av.	1.7359	1.5909	1.4289	1.1974

TABLE VI-4

Within experimental scatter it seems reasonable to accept the theoretical prediction that film pressure does not depend upon supply pressure in the case of rigid bearing experiments with constant loads. Therefore average values of film pressures at different radial positions and for various supply pressures were compared with the theoretical pressures in fig. 38 . A good agreement is obtained.

From Appendix I mass flow through the bearing film can be expressed as:

$$M = -\frac{\pi h^3}{6\eta R_a T_a} pr \frac{dp}{dr} =$$

$$= -\frac{\pi h^3}{6\eta R_a T_a} pR \frac{dp}{dR} \qquad (7)$$

It is now possible to fit polynomials of various powers to the experimental pressure points and obtain values of $(pR\frac{dp}{dR})$ experimentally. Table VI-5 gives results for powers 2, 3 and 4 and compares them with theory. Errors for each power are also presented. It is seen that the errors are smallest for the power n = 2.

Equation (7) is valid not only for rigid bearings but also for the compliant case and it establishes the pattern of analysing compliant bearings. If values of $(pR\frac{dp}{dR})$ and M are obtained experimentally then film thickness h can be calculated at various radial positions.

6.4 Experiments keeping the measured Film Thickness Constant

The purpose of these experiments is to see if viscous flow predominates throughout the range of film thicknesses investigated, so that the viscous flow theory developed in

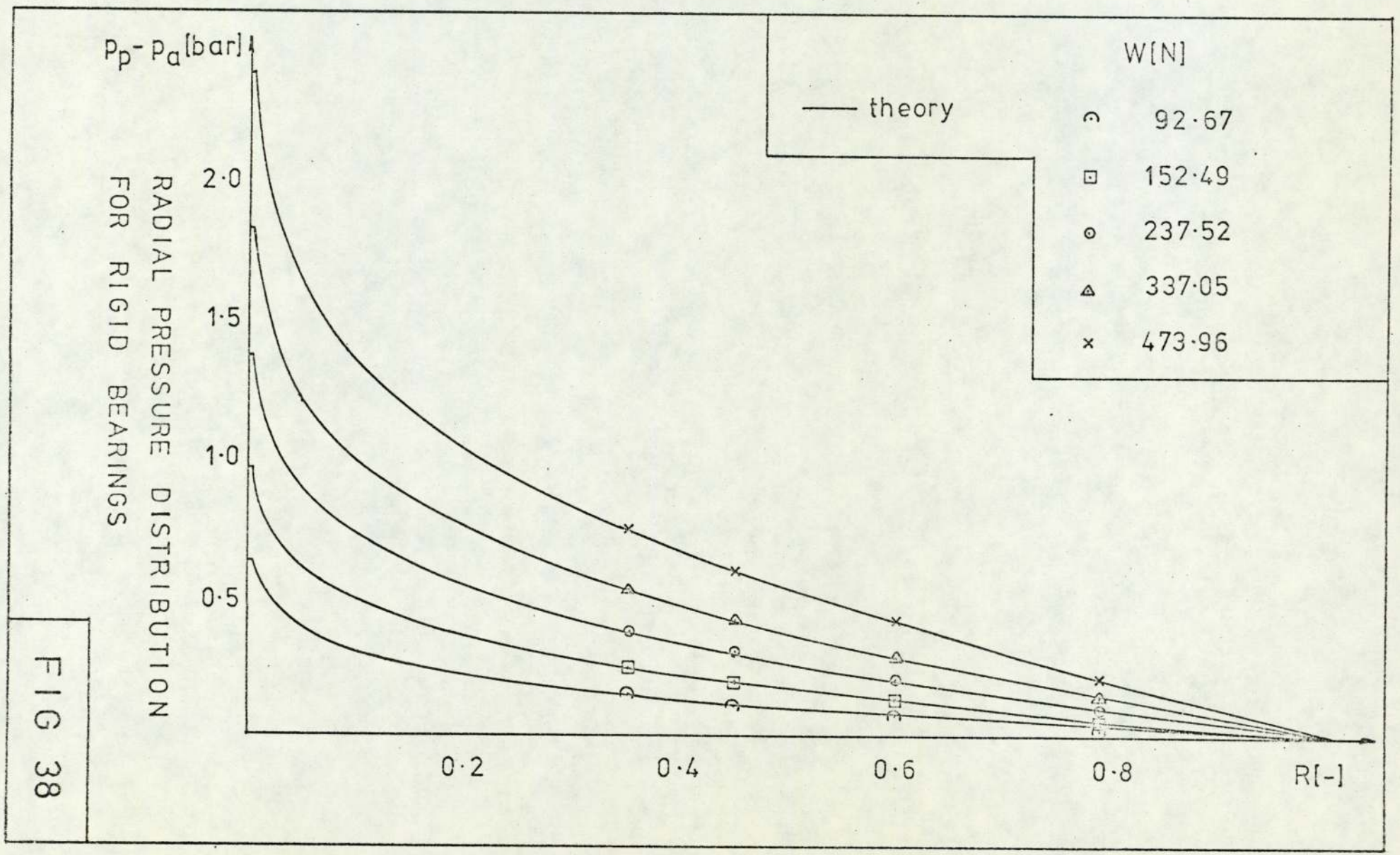

RADIAL PRESSURE DISTRIBUTION FOR RIGID BEARINGS

FIG 38

p_p [bar]	$(pR\frac{dp}{dR})_{ther}$ [bar²]	$(pR\frac{dp}{dR})_{exp}$ [bar²] n = 2	$\frac{\text{theor-exp}}{\text{ther}} \times 100$ [%] n = 2	$(pR\frac{dp}{dR})_{exp}$ [bar²] n = 3	$\frac{\text{theor-exp}}{\text{theor}} \times 100$ [%] n = 3	$(pR\frac{dp}{dR})_{exp}$ [bar²] n = 4	$\frac{\text{theor-exp}}{\text{theor}} \times 100$ [%] n = 4
1.630	0.15268	0.14881	2.53	0.14662	3.97	0.13584	11.03
1.965	0.26391	0.25673	2.72	0.24710	6.37	0.22355	15.29
2.375	0.42771	0.41822	2.22	0.41043	4.04	0.37718	11.81
2.825	0.64437	0.61985	3.81	0.60264	6.48	0.53335	17.23
3.385	0.96556	0.93311	3.36	0.91985	4.73	0.85042	11.93

TABLE VI-5

Appendix I can be used. In order to discuss this point it is necessary to introduce Reynolds number to the argument.

Reynolds number is usually defined as:

$$R_e = \frac{\rho \, v_{mean} \, \ell}{\eta}$$

where v_{mean} is the mean flow velocity and ℓ is a length that characterises the flow. It is customary to take film thickness h as this characteristic length in thrust bearing analysis [103]. Substituting the mean velocity by (volumetric flow Q divided by the flow area A = 2πrh), the Reynolds number becomes:

$$Re = \frac{\rho Q h}{A \eta} = \frac{M \, h}{A \, \eta}$$

$$= \frac{M}{2\pi r \eta} \qquad (8)$$

These experiments were performed at three measured film thicknesses 10, 20 and 30 μm as shown in table VI-6 . Load and supply pressures were varied during these tests.

The Reynolds numbers defined by equation (8) are also included in table VI-6 . These Reynolds numbers were calculated for $r(=r_p)$ = 0.28575mm because the Reynolds numbers are highest at the smallest radius of the film.

In reference [143] it is stated that flow where inertia forces are predominant in radial thrust bearings occurs at a Reynolds number based on film thickness Re > 1900, and Re=1000 is usually used for design purposes. Comolet [103] recommends this design value to be 500. It may therefore be expected that a local inertial flow may occur near the entry to the test bearing for large loads, i.e. for large mass flow rates.

Measured film h_m [μm]	load W[N]	mass flow $M[10^{-6}\frac{kg}{s}]$	derived film h [μm]	Reynolds number (at $r=r_p$) Re[-]
10	337.05	4.172	12.37	128.3
10	473.96	6.237	12.36	191.8
20	152.49	10.448	22.62	321.2
20	237.52	17.477	22.85	537.4
20	337.05	26.091	22.79	802.2
20	473.96	39.457	22.86	1213.2
30	152.49	30.961	32.49	951.9
30	237.52	49.319	32.29	1516.4
30	337.05	76.226	32.58	2343.7

TABLE VI-6

- ambient conditions $p_a = 1.0019$ |bar|

  $T_a = 294.2$ |°K|

- Reynolds number Re calculated for radius $r_p = 0.286$mm, i.e. at entry to the bearing film.

However the Reynolds number drops rapidly as the radius increases. For example, at r=1mm the last Reynolds number in Table VI-6 at maximum mass flow becomes Re=669.7.

These tests show that the viscous flow theory developed in Appendix I is adequate for the normal working range for rigid bearing analysis.

Films derived from mass flow measurements are about 2.5 μm greater than the measured films, which is in line with the constant load tests and constant supply pressure tests. Therefore, apart from showing that the viscous flow theory is adequate, these tests are a useful check of other types of bearing tests.

6.5 Experiments keeping the supply pressure constant and varying the load

Ambient conditions for these rigid bearing experiments were

$$p_a = 1.0056 \text{[bar]}$$
$$T_a = 293.2 \ [^{o}K] \qquad (9)$$

Surface roughness effects were very similar to those established when the load and film thickness were kept constant. Measured films versus films derived from flow measurements are shown on fig. 39. On average the difference is 2.5 [μm].

Dimensionless mass flow versus dimensionless film thickness for four different supply pressures is shown in fig. 40 . The four supply pressures were chosen so as to cover the range of supply pressures encountered in the rigid bearing experiments.

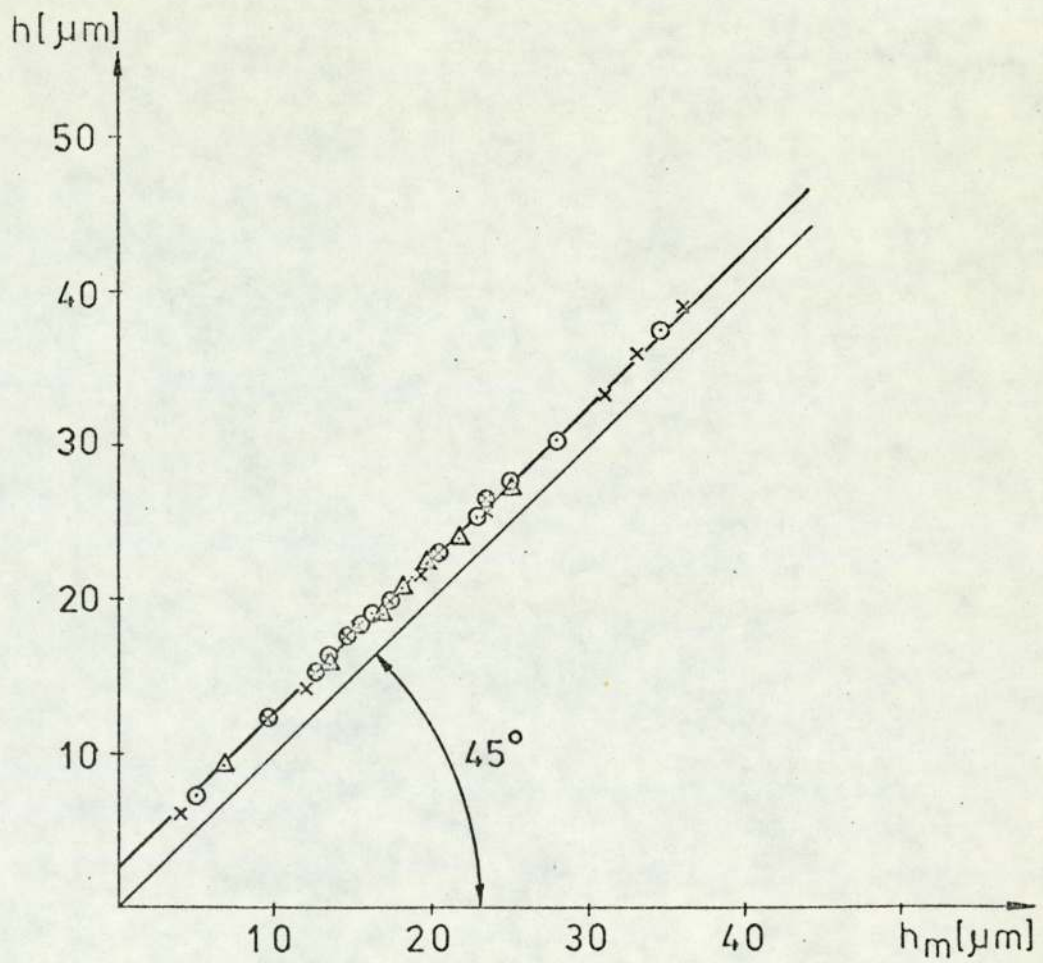

MEASURED FILM V. FILM DERIVED FROM FLOW MEASUREMENTS

CONSTANT SUPPLY PRESSURE TESTS

FIG 39

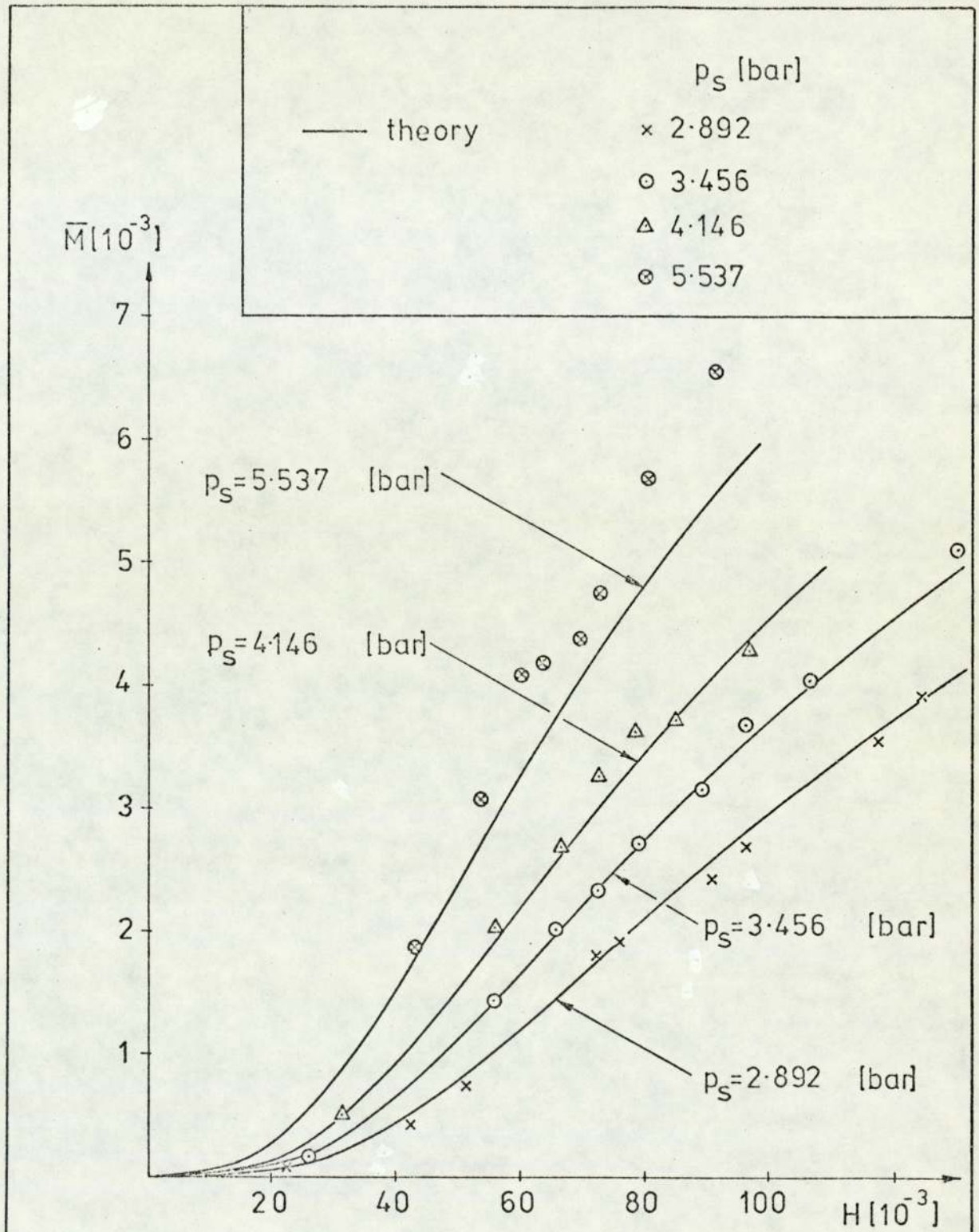

DIMENSIONLESS FLOW V.
DIMENSIONLESS FILM THICKNESS

CONSTANT SUPPLY PRESSURE TESTS

FIG 40

Theoretical lines in fig. 40 have taken into account the experimentally obtained value of discharge coefficient C_D=0.68. By equating the mass flow through the orifice and through the bearing, equation I-64 , Appendix I, and taking C_D=0.68 a theoretical film can be obtained for a given film entry pressure (i.e. given load) and a given supply pressure. With this theoretical film, theoretical mass flow through the bearing is obtained from equation I-13 , Appendix I, and this is how the theory lines on fig. 40 are established.

Both dimensionless load and dimensionless stiffness versus dimensionless film thickness are shown in figures 41 and 42 respectively. Theory lines on these figures similarly as for the flow rates have taken into account the experimentally obtained value of discharge coefficient C_D=0.68.

Bearing performance in dimensional form gives more feeling about the orders of magnitude in question, hence figures 43 , 44 and 45 are presented for flow, load and stiffness versus film thickness with dimensions of SI units.

From figures 42 and 45 it is seen that at low values of film thickness the agreement between theory and experiment is not good. When film thickness is low the ratio of film entry pressure to supply pressure approaches unity. Fig. 45 shows that a departure of coefficient of discharge from its mean value C_D=0.68 is most pronounced in this region. It is because of C_D that experiments and theory do not agree well at low values of film thickness, figures 42 and 45 .

Better agreement could have been obtained by taking into account the variation of C_D with film entry pressure and calculating theoretical stiffness from equation I-69 , Appendix I,

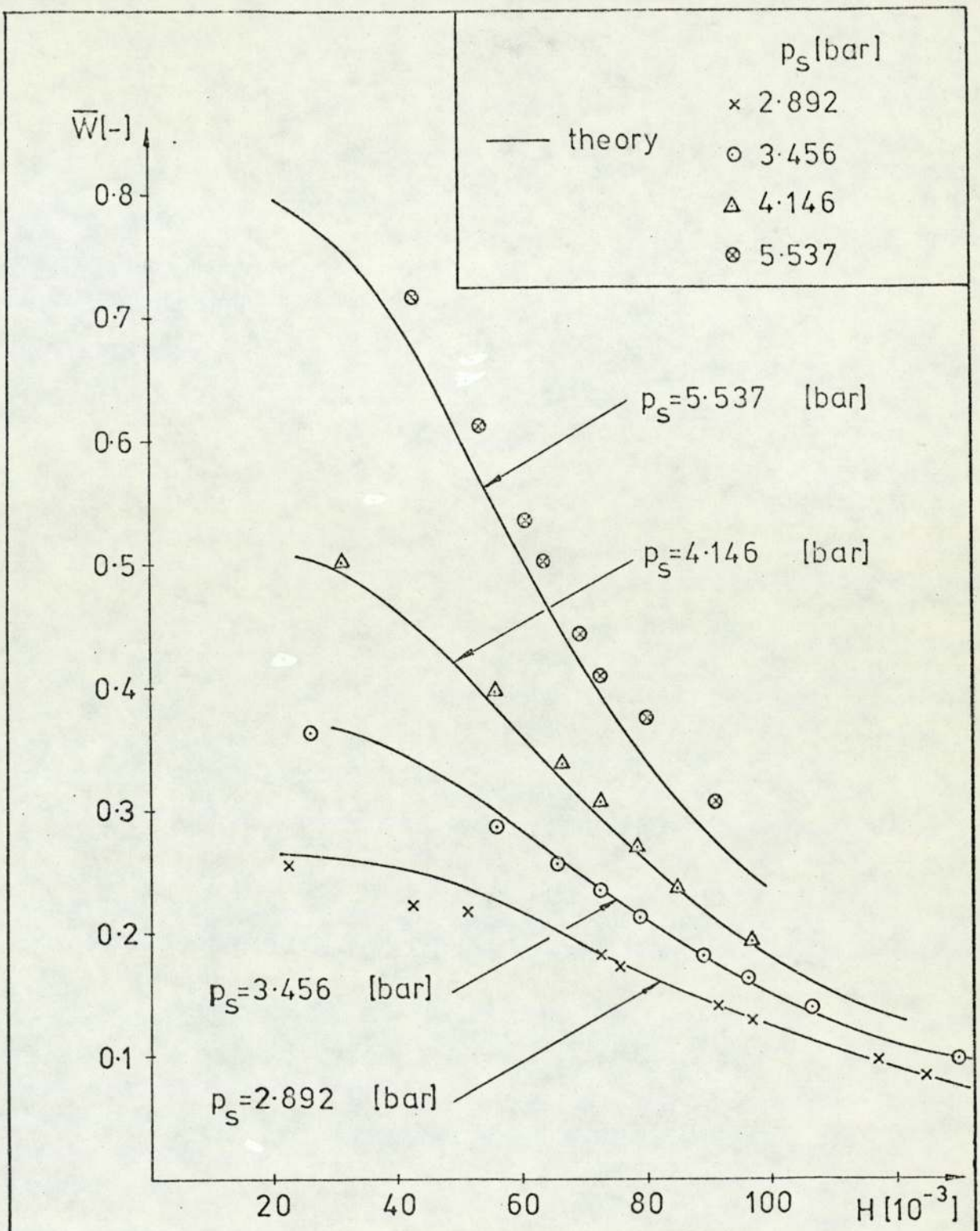

DIMENSIONLESS LOAD V.
DIMENSIONLESS FILM THICKNESS

CONSTANT SUPPLY PRESSURE TESTS

FIG 41

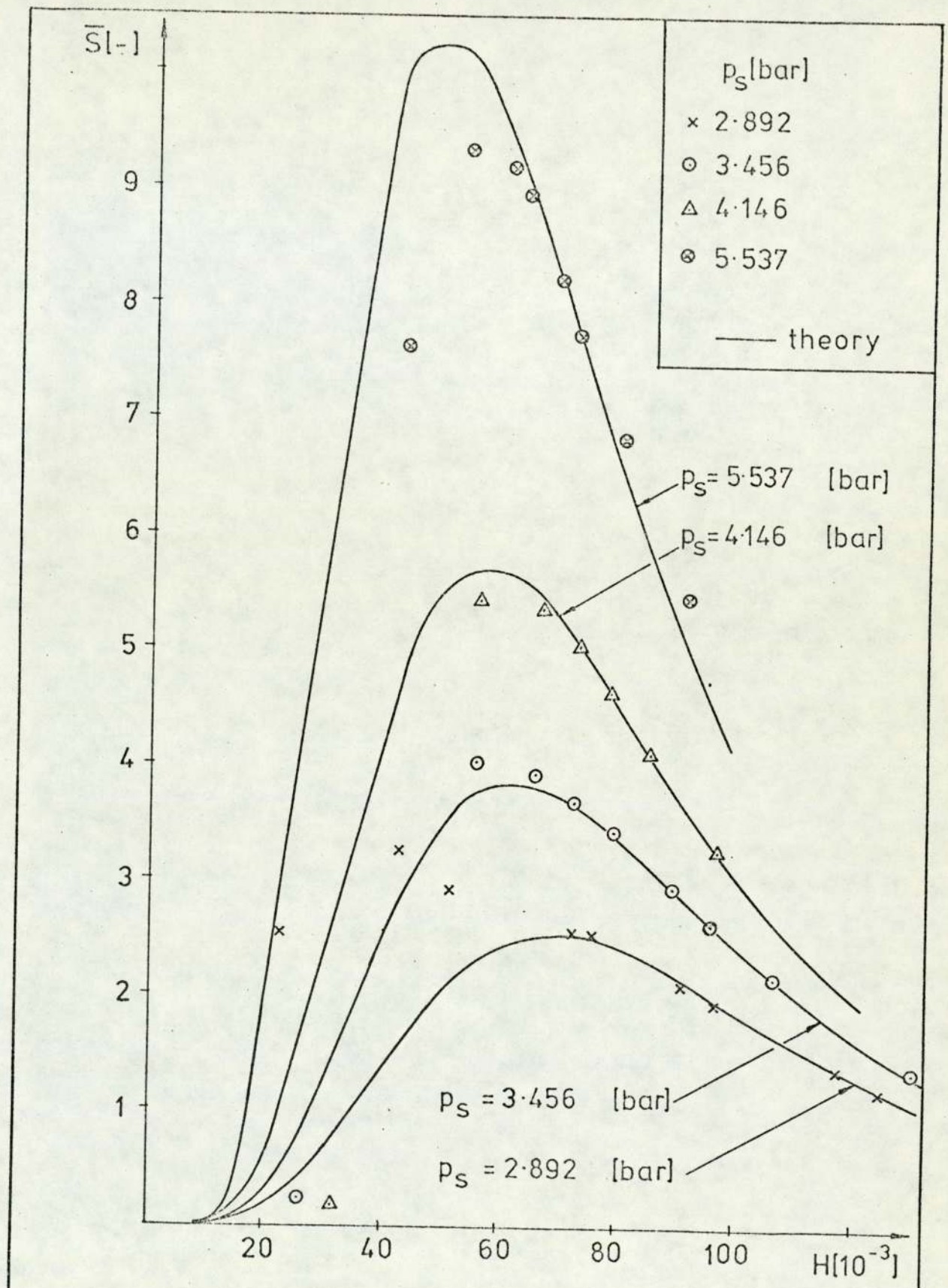

DIMENSIONLESS STIFFNESS V.
DIMENSIONLESS FILM THICKNESS

CONSTANT SUPPLY PRESSURE TESTS

FIG 42

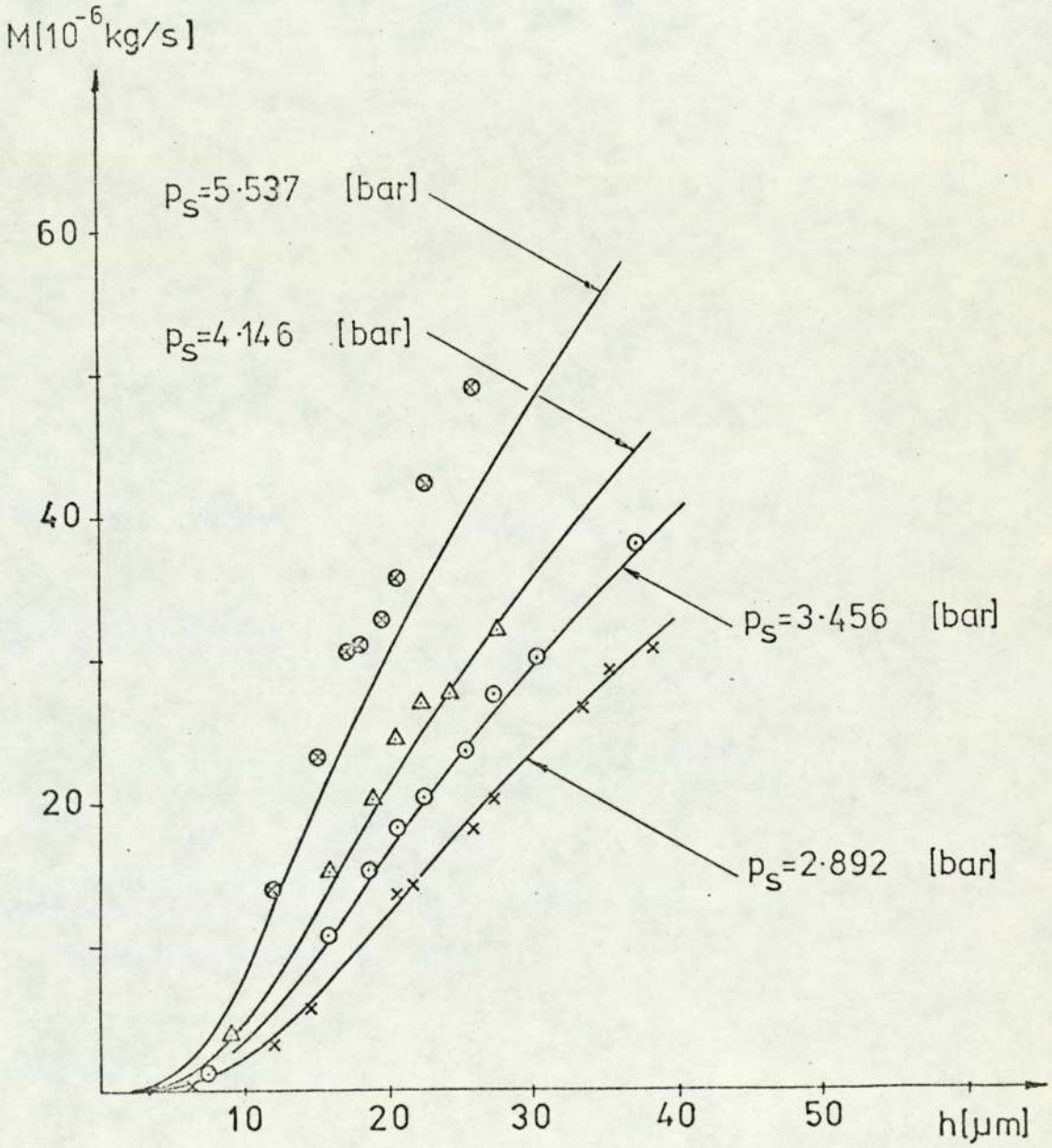

FLOW V. FILM THICKNESS

CONSTANT SUPPLY PRESSURE TESTS

FIG 43

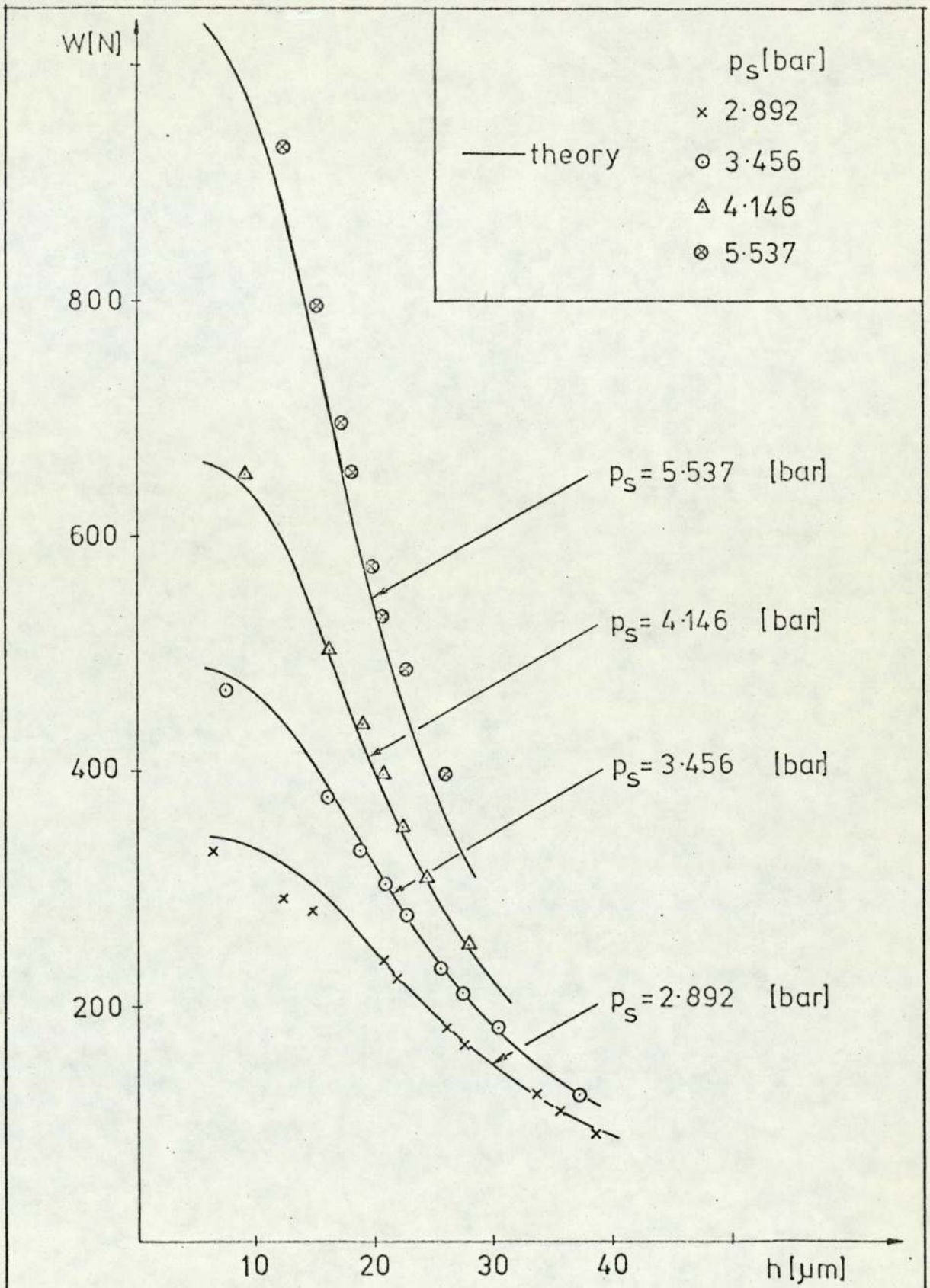

LOAD V. FILM THICKNESS

CONSTANT SUPPLY PRESSURE TESTS

FIG 44

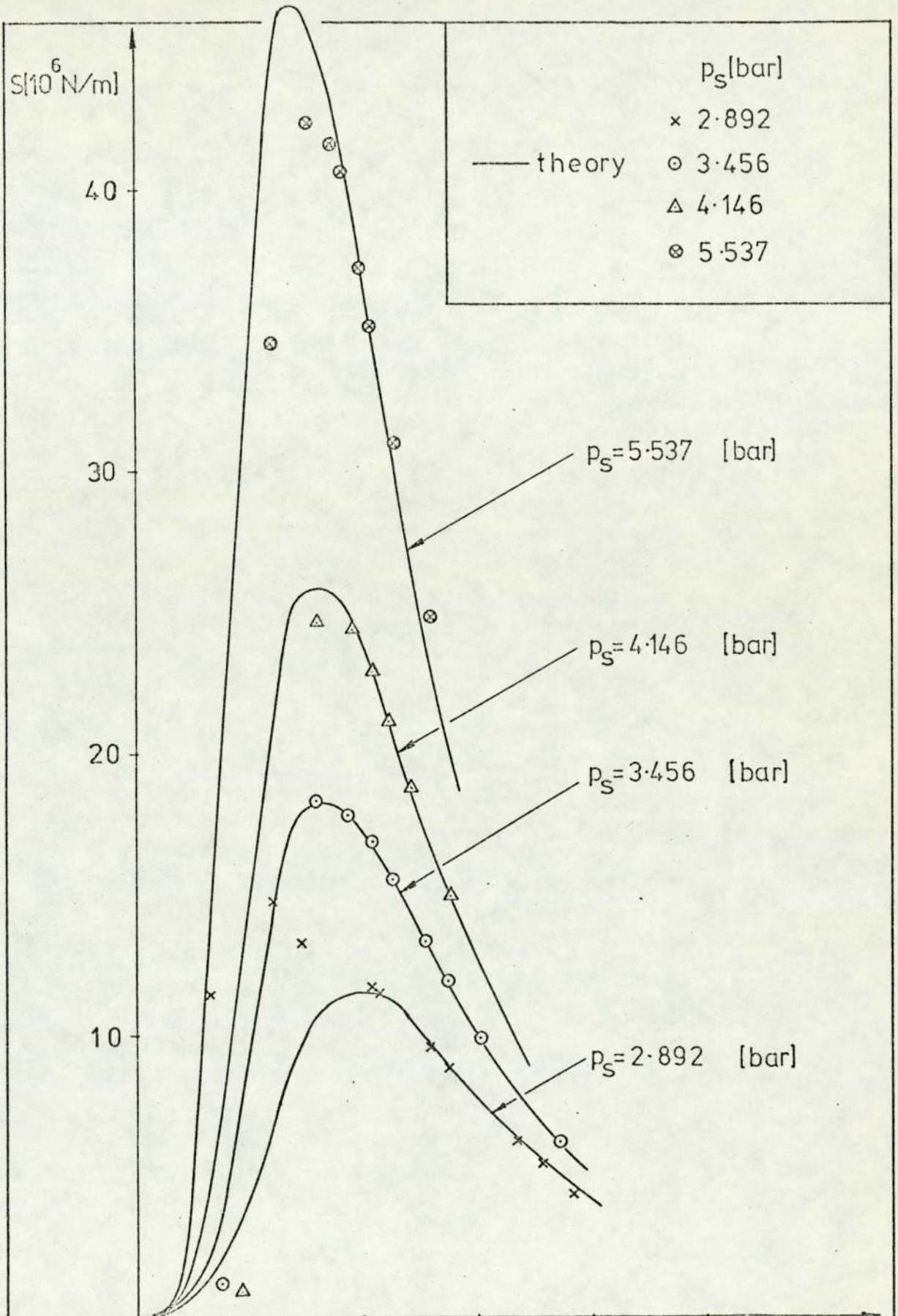

STIFFNESS V. FILM

CONSTANT SUPPLY PRESSURE TESTS

FIG 45

Measured film h_m [μm]	36.0	33.0	31.0	25.0	23.5	19,2	18.1	12.1	9.6	3.9
Measured load **W** [N]	92.67	110.03	124.74	167.01	181.72	224.18	238.89	281.35	290.18	332.84
Measured mass flow rate $M[10^{-6}\frac{kg}{s}]$	30.70	29.22	26.53	20.13	18.21	14.23	13.50	5.52	3.05	0.45
Corrected film $h=h_m+2.5$ [μm]	38.5	35.5	33.5	27.5	26.0	21.7	20.6	14.6	12.1	6.4
Film derived from measured flow h_d [μm]	38.71	35.82	33.16	27.21	25.51	21.73	20.85	14.54	11.79	5.93
Dimensionless port pressure P_p [-]	1.62695	1.72564	1.80663	2.02724	2.10091	2.30531	2.37388	2.56614	2.60521	2.79023
Port/supply pressure ratio P_p/P_s [-]	0.56553	0.59984	0.62799	0.70467	0.73028	0.80133	0.82516	0.89199	0.90558	0.96989
Dimensionless stiffness $\bar{S}$[-]	0.96369	1.19128	1.37725	1.95063	2.11729	2.52645	2.57957	2.92534	3.25286	2.51625
Stiffness $S[10^6\frac{N}{m}]$	4.382	5.417	6.263	8.870	9.628	11.489	11.731	13.303	14.792	11.443
Dimensionless load $\bar{W}$ [-]	0.07132	0.08468	0.09600	0.12852	0.13984	0.17252	0.18384	0.21652	0.22331	0.25614
Dimensionless flow $\bar{M}[10^{-3}]$	4.09	3.90	3.54	2.69	2.43	1.90	1.80	0.74	0.41	0.06
Dimensionless film $H[10^{-3}]$	134.7	124.2	117.2	96.2	91.0	75.9	72.1	51.1	42.3	22.4

TABLE VI-7 RIGID EXPERIMENTS KEEPING SUPPLY PRESSURE CONSTANT

$P_s = 2.87686$ [-]

Measured film h_m [μm]	5	13.5	16.3	18.2	20.1	23	25	28	34.8
Measured load W [N]	469.44	375.30	332.84	303.42	275.66	233.20	211.33	181.91	124.74
Measured mass flow rate $M[10^{-6}\ \frac{kg}{s}]$	1.29	10.82	15.24	18.47	20.45	23.73	27.52	30.38	38.31
Corrected film $h = h_m + 2.5$ [μm]	7.5	16.0	18.8	20.7	22.6	25.5	27.5	30.5	37.3
Film derived from measured flow h_d[μm]	7.33	16.27	19.12	21.13	22.68	25.39	27.68	30.24	37.48
Dimensionless port pressure P_p [-]	3.34891	2.96872	2.79023	2.66325	2.54071	2.34735	2.24441	2.10184	1.80663
Port/supply pressure ratio P_p/P_s [-]	0.97430	0.86369	0.81177	0.77483	0.73918	0.68292	0.65297	0.61149	0.52561
Dimensionless stiffness $\bar{S}$ [-]	0.24162	4.02871	3.91500	3.70181	3.42035	2.92867	2.60928	2.17401	1.36210
Stiffness S $[10^6 \frac{N}{m}]$	1.099	18.320	17.803	16.834	15.554	13.318	11.866	9.886	6.194
Dimensionless load $\bar{W}$ [-]	0.36126	0.28882	0.25614	0.23350	0.21214	0.17946	0.16263	0.13999	0.09600
Dimensionless flow $\bar{M}[10^{-3}]$	0.17	1.44	2.03	2.32	2.73	3.16	3.67	4.05	5.11
Dimensionless film $H[10^{-3}]$	26.2	56.0	65.8	72.4	79.1	89.2	96.2	106.7	130.5

TABLE VI-8 RIGID EXPERIMENTS KEEPING SUPPLY PRESSURE CONSTANT

$P_s = 3.43723$ [-]

Measured film h_m [μm]	25.2	21.8	1919	18.3	16.5	13.5	6.6
Measured load W [N]	252.33	309.50	351.96	397.76	440.22	516.17	652.73
Measured mass flow rate M $\left[10^{-6}\frac{kg}{s}\right]$	32.18	27.91	27.23	24.63	20.22	15.27	3.91
Corrected film $h = h_m + 2.5$ [μm]	27.7	24.3	22.4	20.8	19.0	16.0	9.1
Film derived from measured flow h_d[μm]	27.28	24.06	22.71	20.92	18.81	16.06	9.25
Dimensionless port pressure P_p[-]	2.43545	2.68982	2.87121	3.06120	3.23288	3.53100	4.04538
Port/supply pressure ratio P_p/P_s [-]	0.59064	0.65233	0.69632	0.74240	0.78403	0.85633	0.38108
Dimensionless stiffness $\bar{S}$ [-]	3.29437	4.14174	4.65880	5.04723	5.37277	5.44693	0.19308
Stiffness S $\left[10^6 \frac{N}{m}\right]$	14.981	18.834	21.186	22.952	24.433	24.770	0.878
Dimensionless load $\bar{W}$ [-]	0.19418	0.23818	0.27085	0.30610	0.33878	0.39718	0.50231
Dimensionless flow $\bar{M}$ $\left[10^{-3}\right]$	4.29	3.72	3.64	3.28	2.70	2.04	0.52
Dimensionless film H$\left[10^{-3}\right]$	96.9	85.0	78.4	72.8	66.5	56.0	31.8

TABLE VI-9 RIGID EXPERIMENTS KEEPING SUPPLY PRESSURE CONSTANT

$P_s = 4.12340$ [-]

Measured film h_m [μm]	9.8	12.8	14.9	15.7	17.4	18.3	20.4	73.6
Measured load W [N]	930.95	795.52	696.17	653.71	574.38	530.15	485.82	397.56
Measured mass flow rate M $\left[10^{-6} \frac{kg}{s}\right]$	13.93	23.20	30.58	31.38	32.70	35.63	42.52	49.02
Corrected film $h = h_m + 2.5$[μm]	12.3	15.3	17.4	18.2	19.9	20.8	22.9	26.1
Film derived from measured flow h_d[μm]	12.12	15.39	17.87	18.51	19.81	21.07	23.16	26.32
Dimensionless port pressure P_p [-]	5.03385	4.56065	4.20421	4.04895	3.7345	3.58513	3.41324	3.06038
Port/supply pressure ratio P_p/P_s [-]	0.91405	0.82813	0.76341	0.73521	0.68156	0.65099	0.61378	0.55571
Dimensionless stiffness $\bar{S}$ [-]	7.60674	9.32088	9.17246	8.95016	8.21686	7.74090	6.83817	5.46070
Stiffness S $\left[10^6 \frac{N}{m}\right]$	34.591	42.386	41.712	40.701	37.366	35.202	31.096	24.832
Dimensionless load $\bar{W}$ [-]	0.71642	0.61220	0.53574	0.50307	0.44202	0.40798	0.37387	0.30595
Dimensionless flow $\bar{M}$ $\left[10^{-3}\right]$	1.86	3.09	4.08	4.18	4.36	4.75	5.67	6.54
Dimensionless film H $\left[10^{-3}\right]$	43.0	53.5	60.9	63.7	69.6	72.8	80.1	91.3

TABLE VI-10 RIGID EXPERIMENTS KEEPING SUPPLY PRESSURE CONSTANT

$P_s = 5.50717$ [-]

with the term $\frac{dC_D}{dP_p} \neq 0$. However this has not been carried out because the normal operating region of these bearings is on the right of maximum stiffness where the agreement between theory and experiment is good.

Data for figures 40 - 45 is shown in tables VI-7 to VI-10.

6.6 Comparison with the Designed Performance

It is now possible to compare the bearing performance with the performance envisaged in the initial rig design for maximum stiffness as follows:

	initial design i	P bearing performance	ratio P/i
Film h [μm]	19	19	1
Mass flow M[10^{-6} $\frac{kg}{s}$]	79	31	0.39
Load W [N]	1230	530	0.43
Stiffness S[10^6 $\frac{N}{m}$]	99.7	36.4	0.37

It is seen that primarily because of the change of the bearing restrictor, the three important bearing parameters: mass flow, load and stiffness are smaller than designed (for the same film thickness).

The experiments so far have established a reasonable agreement with theory and one is now more confident about the rig performance with compliant bearings.

VII COMPLIANT BEARING EXPERIMENTS

7.1 Apparent Film Thickness

Consider three situations of a compliant bearing in order of increasing load as shown in fig. 46. It is taken that h_o is a uniform film thickness without elastomer deformation and that h_1 and h_2 are mean film thicknesses.

If the unloaded elastomer thickness with no deformation is marked as "t_o" (case (a)), then mean elastomer thicknesses in (b) and (c) are:

$$t_1 = t_o - (\Delta t)_1$$

$$t_2 = t_o - [(\Delta t)_1 + (\Delta t)_2]$$

where $(\Delta t)_1$ and $(\Delta t)_2$ are mean elastomer compressions due to load increments.

Distances A_o, A_1 and A_2 take into account both mean film thickness and mean elastomer thickness. These overall distances are equal to :

$$A_o = t_o + h_o \qquad \text{hence} \quad A_o - t_o = h_o$$

$$A_1 = t_1 + h_1 \qquad \text{hence} \quad A_1 - t_o = h_1 - (\Delta t)_1$$

$$A_2 = t_2 + h_2 \qquad \text{hence} \quad A_2 - t_o = h_2 - [(\Delta t)_1 + (\Delta t)_2]$$

or in general the apparent value of bearing film thickness

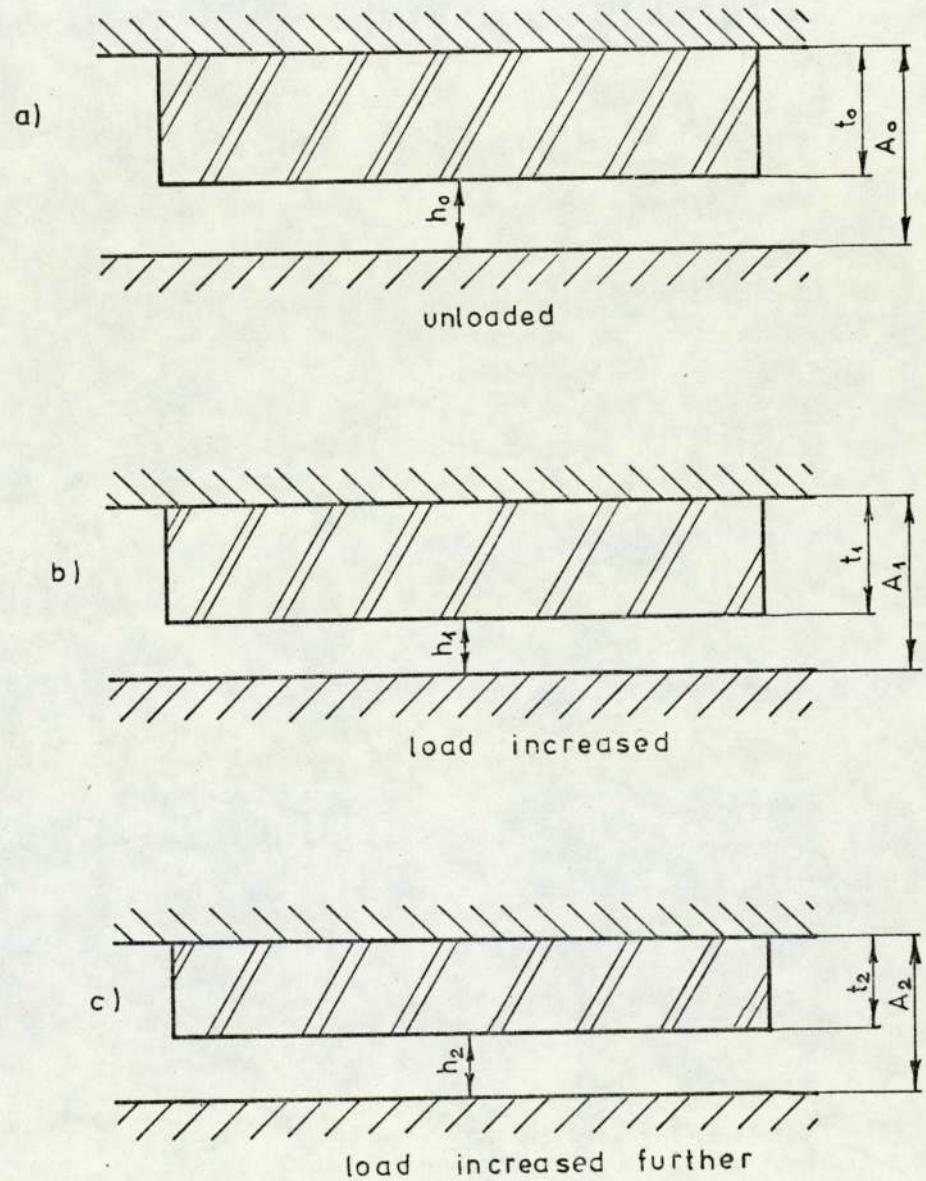

COMPLIANT BEARING

($t_0 > t_1 > t_2$,
$h_0 > h_1 > h_2$)

FIG 46

$$h_a = A_n - t_o = h_n - \sum_1^n \Delta t \qquad (1)$$

This apparent value of film thickness is by definition related to the initial elastomer thickness with no deformation t_o. It consists of the mean bearing film and of elastomer total compression due to load increments. They were both measured during the compliant bearing tests by means of mitronic comparators.

This apparent value of film thickness is important for bearing parameters such as load and stiffness. How much a bearing will "give" under a certain load is described by the change of distance A (between two surfaces in a compliant bearing which are rigid). Referring to the cases b) and a) of fig. 46, this distance change is equal to (A_1-A_o). If a constant value t_o is subtracted from both A_1 and from A_o this distance change is still equal to

$$A_1 - A_o = h_o - h_1 + \Delta t \qquad (2)$$

Therefore for compliant bearings the relative change in axial distance under an increment of load is described not only by the change of the bearing film but also by the elastomer compression.

For parameters like volumetric and mass flow rate, bearing film is more important than the apparent film, although if desired they can be plotted against the apparent film similarly to bearing load.

7.2 Types of Tests Performed

Constant Load Tests

These tests were performed in order to estimate film entry pressure at zero film thickness i.e. when the film entry pressure is equal to the supply pressure.

It was not possible to measure the film entry pressure experimentally in compliant tests. Graphs of supply pressure against film thickness were drawn from which supply pressures at zero film thickness (i.e. film entry pressures at zero film thickness) were extrapolated.

Whilst with rigid experiments film entry pressures are uniquely determined by the bearing load, this is not the case with the compliant experiments. Here different film entry pressures correspond to different film thicknesses, i.e. to different supply pressures.

Film Pressure Measurements

These measurements were performed during the constant load tests in order to see how the film pressure is influenced by the varying supply pressure.

Whilst with rigid bearings supply pressure practically has no influence on the film pressure distribution, i.e. for one load there is only one film pressure distribution, with the compliant bearing this pressure distribution changes with the supply pressure so that for the same load there exist different pressure distributions in the bearing film depending upon values of supply pressures.

Polynomials of various degrees were fitted to these experimentally determined pressure distributions. Then the load capacity was checked from equation (I-17), Appendix I which states

$$\bar{W} = R_p^2 P_p + 2 \int_{R_p}^{1} PRdR - 1 \qquad (3)$$

In each case the calculated load capacity varied with the supply pressure. The pressure was measured (for bearings of largest diameter) in the region of $0.353 < R < 0.787$. The curve uniting the measured pressure points did not show a pronounced change of shape when compared to rigid bearings except that it was only slightly convex upwards, whilst the rigid pressure distribution is slightly concave upwards, see fig. 38 chapter VI. Therefore a second order polynomial was fitted to the compliant pressure points because this polynomial showed the best agreement with rigid theory see table VI-5, chapter VI.

The absolute dimensionless film pressure for compliant lubrication was therefore determined as:

$$P = 1 + B_o + B_1 R + B_2 R^2 \qquad (4)$$

Here B_o, B_1 and B_2 are the second order polynomial coefficients determined by the least squares method.

Local Film Thickness Measurements

It was hoped to obtain local film thickness measurements by means of three displacement probes spaced radially in the lower bearing surface. However, the displacement probes

were shorting after being in contact with the elastomers sprayed with silver paint due to paint transfer to them. As soon as this had been discovered, a compliant test had to be stopped in order to clean the probes by means of a sewing needle under the microscope. In this way the test apparatus was disturbed during a bearing test and thus the results obtained were not reliable. Further development remains to be done.

By differentiating the pressure polynomial with respect to radius, the product (film pressure x radius x film pressure derivative with respect to radius) can be obtained at any radial position covered by the range of experiments. By knowing the mass flow, the local film thickness can thus be calculated, see equation (7), chapter VI.

Constant Supply Pressure Tests

These tests enabled the relationships of load and flow with apparent film thickness (and with film thickness) to be determined experimentally. They are the most important type of tests to determine the bearing performance. Rigid theory lines are plotted on the graphs of compliant experiments so that a comparison of rigid and compliant bearing performance can be made.

7.3 Constant Load Tests and Film Pressure Measurements

As an example of these types of tests one typical test will be described. The load, excluding the elastomer weight of 2.95 N was W = 92.67 N. The elastomer was natural rubber made at Aston University (referring to table VII-2, section 7.4

of this chapter this elastomer's number is I_b). Supply pressures were varied between 1.372 [bar] and 5.758 [bar] under the following ambient conditions

$$p_a = 1.006 \text{ bar}$$

$$T_a = 295^{\circ}K$$

Under the load of 92.67 N, the elastomer compression was determined to be 7μm. If the apparent film thickness is desired, it can be obtained by subtracting 7μm from the measured film thickness (neglecting surface roughness effects). However, for this test it is not important because the load was kept constant.

Apart from film pressures also supply pressures, film thicknesses and flow rates were monitored.

The results are shown in table VII-1. Fig. 47 shows a plot of supply pressure v. film thickness. The continuation of the curve below the minimum film thickness measured gives an estimate of the value of the film entry pressure at zero film thickness.

A second order polynomial is fitted to measured pressure points as given by equation (4). The term $(1+B_o)$ represents the film entry pressure estimated from the condition that the bearing radius is approximately R=0 at film entry. Fig. 48 shows a plot of film entry pressure determined in such a way against the supply pressure. It is seen that there is a variation of film entry pressure with supply pressure i.e. with film thickness. The point estimated from fig. 47 for zero film thickness is also shown in fig. 48 (for $p_p = p_s =$ 1.006 bar).

Gauge film pressures [bar]					absolute supply pressure [bar]	measured film thickness [μm]	measured mass flow $[10^{-6}kg/s]$	estimated film entry pressure [bar]	load calculated from fitted polynomial [N]
test	R=0.353	0.450	0.599	0.787					
1	0.100	0.082	0.097	0.040	1.1722	20.5	5.22	1.0089	67.0
2	0.115	0.095	0.095	0.040	1.4918	33	11.23	1.0761	76.1
3	0.120	0.105	0.093	0.040	1.848	43	29.70	1.0966	78.5
4	0.122	0.108	0.096	0.040	2.308	49	45.78	1.0875	78.3
5	0.130	0.110	0.095	0.042	2.883	54	66.56	1.1351	86.5
6	0.128	0.112	0.095	0.043	3.458	58	82.19	1.1241	85.9
7	0.131	0.114	0.095	0.043	4.033	61	102.76	1.1365	87.7
8	0.135	0.114	0.095	0.045	4.608	64	122.93	1.1616	93.0
9	0.135	0.118	0.096	0.047	5.183	69	148.90	1.1554	94.5
10	0.135	0.120	0.093	0.050	5.758	72	172.32	1.1742	99.1

TABLE VII-1, W = 92.67[N]

p_p ⇒ determined by fitting a second order polynomial through the experimental pressure points and taking R=0

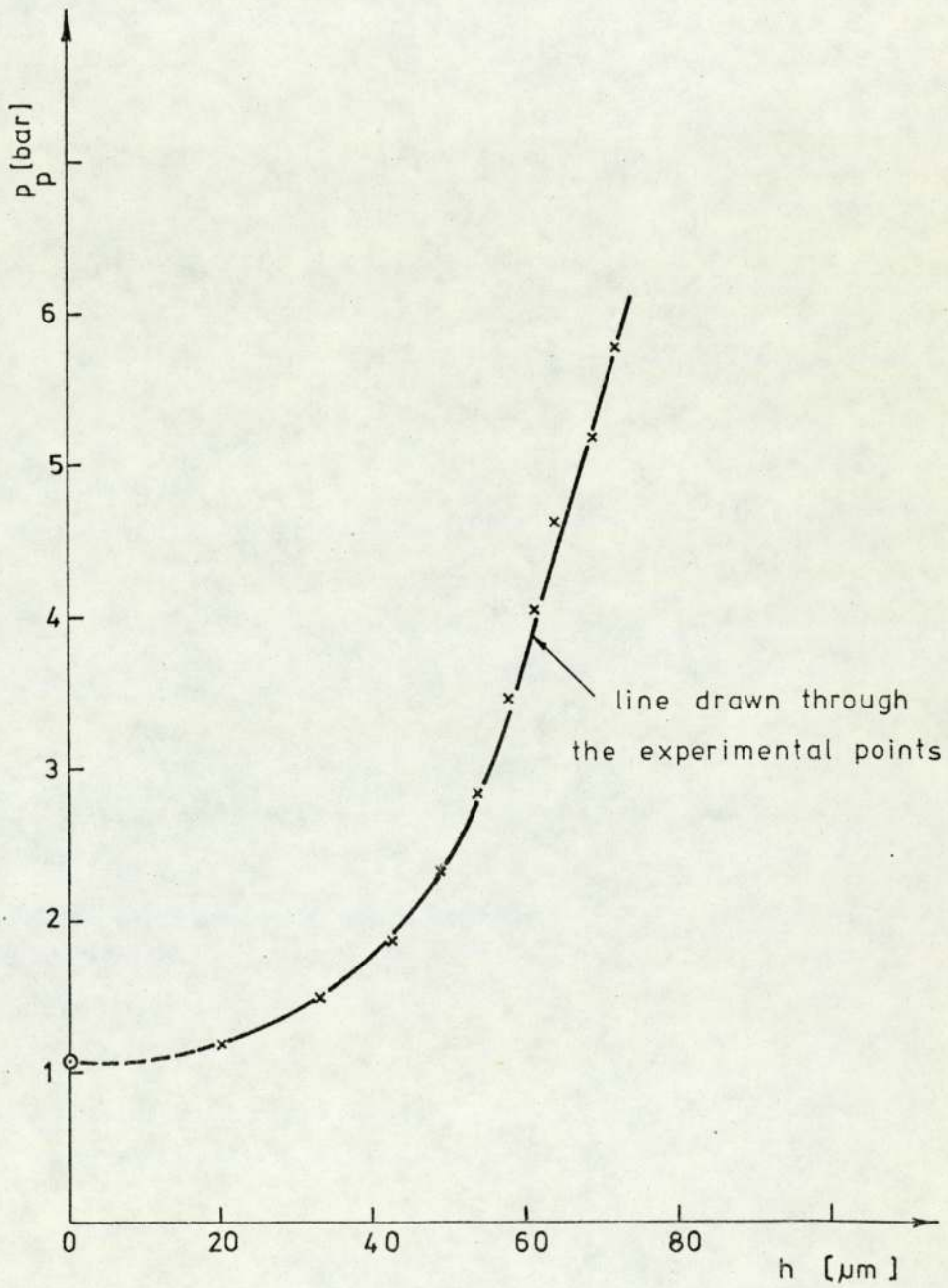

SUPPLY PRESSURE

v

FILM THICKNESS

FIG 47

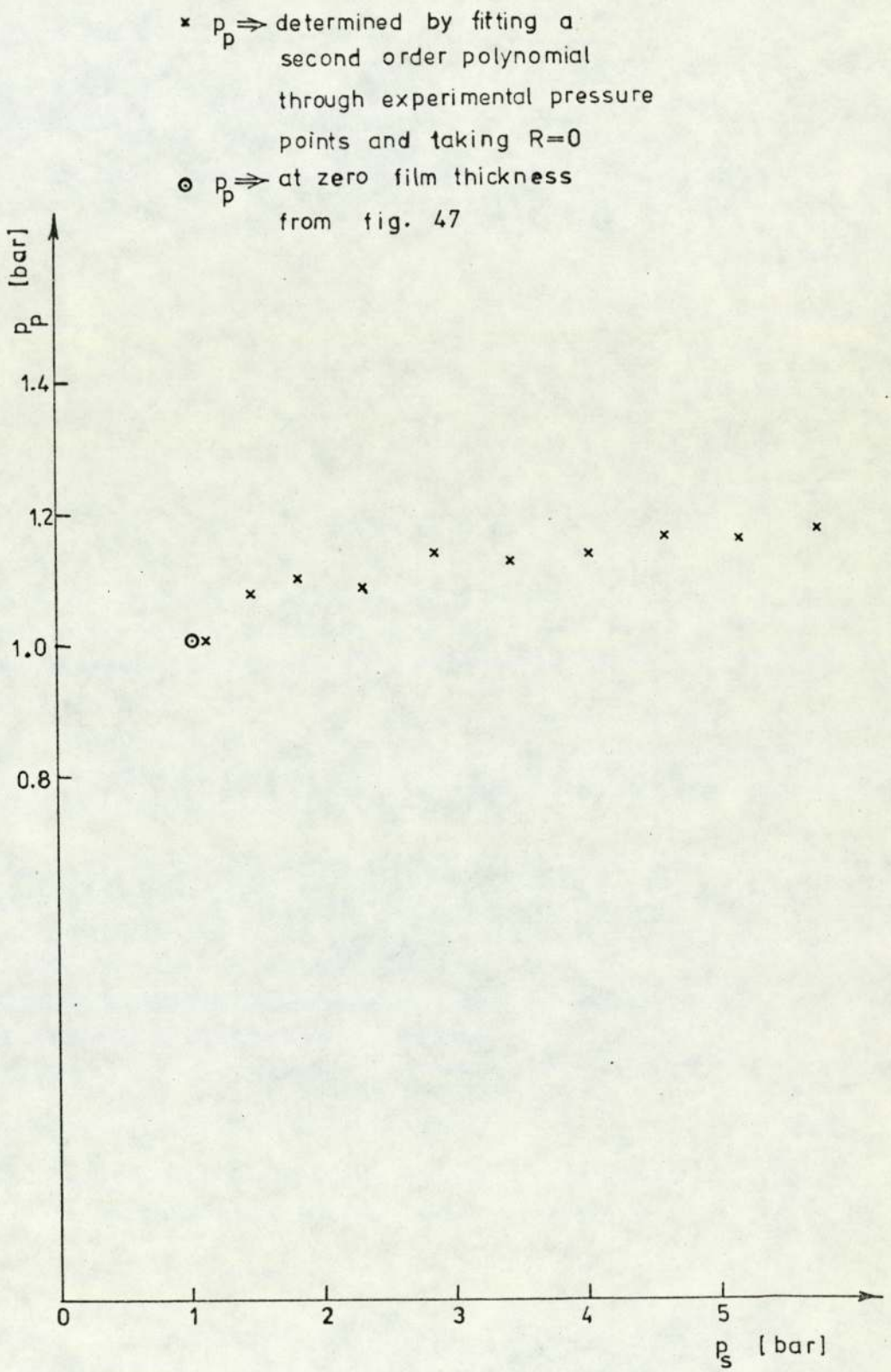

FILM ENTRY PRESSURE
v
SUPPLY PRESSURE

FIG 48

Using equations (4) and (3) the load capacity can now be calculated and it is shown in fig. 49. Similarly as film entry pressure, the load capacity, determined by fitting a polynomial through pressure points, also increases.

Referring to table VII-1, other calculations concerning test 8 are shown in table VII-2.

R [-]	fitted gauge pressure p_g [bar]	p [bar]	$\frac{dp}{dR}$ [bar]	$pR\frac{dp}{dR}$ [bar^2]	h [μm]
0.353	0.13437	1.14095	-0.17030	-0.06859	80.82
0.450	0.11730	1.12388	-0.18165	-0.09187	73.32
0.599	0.08894	1.09552	-0.19908	-0.13064	65.20
0.787	0.04944	1.05602	-0.22108	-018374	58.19
1.000	-0.00030	1.00628	-0.24600	-0.24754	52.69

TABLE VII-1b

These calculations were performed using equation (7) of chapter VI. Film thickness profile is thus estimated and it is shown in fig. 50 (Equation (7) of chapter VI cannot be used to estimate film thickness profiles at R→0). Measured mean film thickness h = 64 μm is also shown.

Flow rates versus film thickness are plotted on fig. 51. Neither elastomer compression nor surface roughness have been taken into account. Comparison with rigid bearing theory shows that for constant loads flow consumption at a given film thickness is smaller than for rigid bearings. This has been

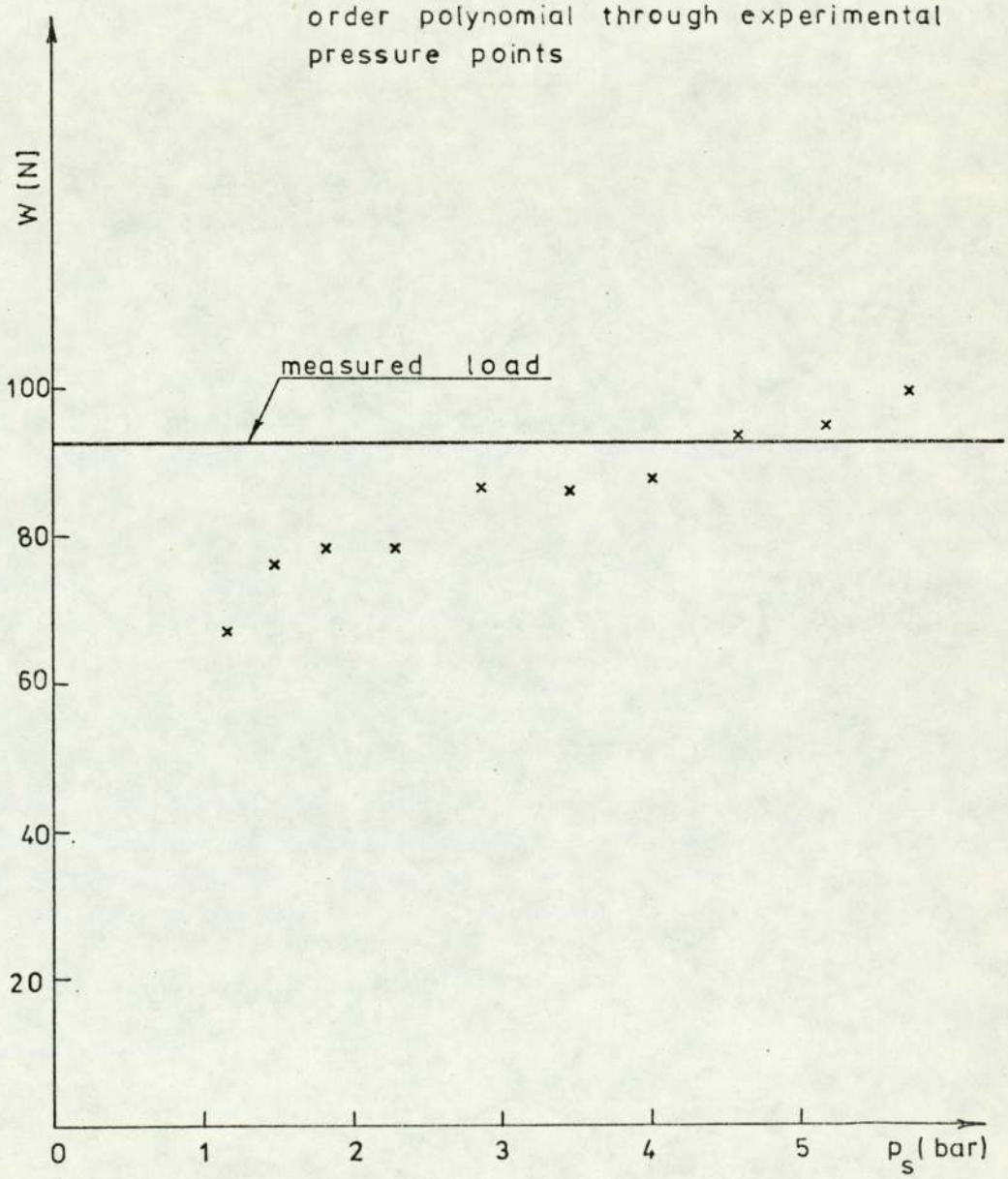

LOAD v SUPPLY PRESSURE

FIG 49

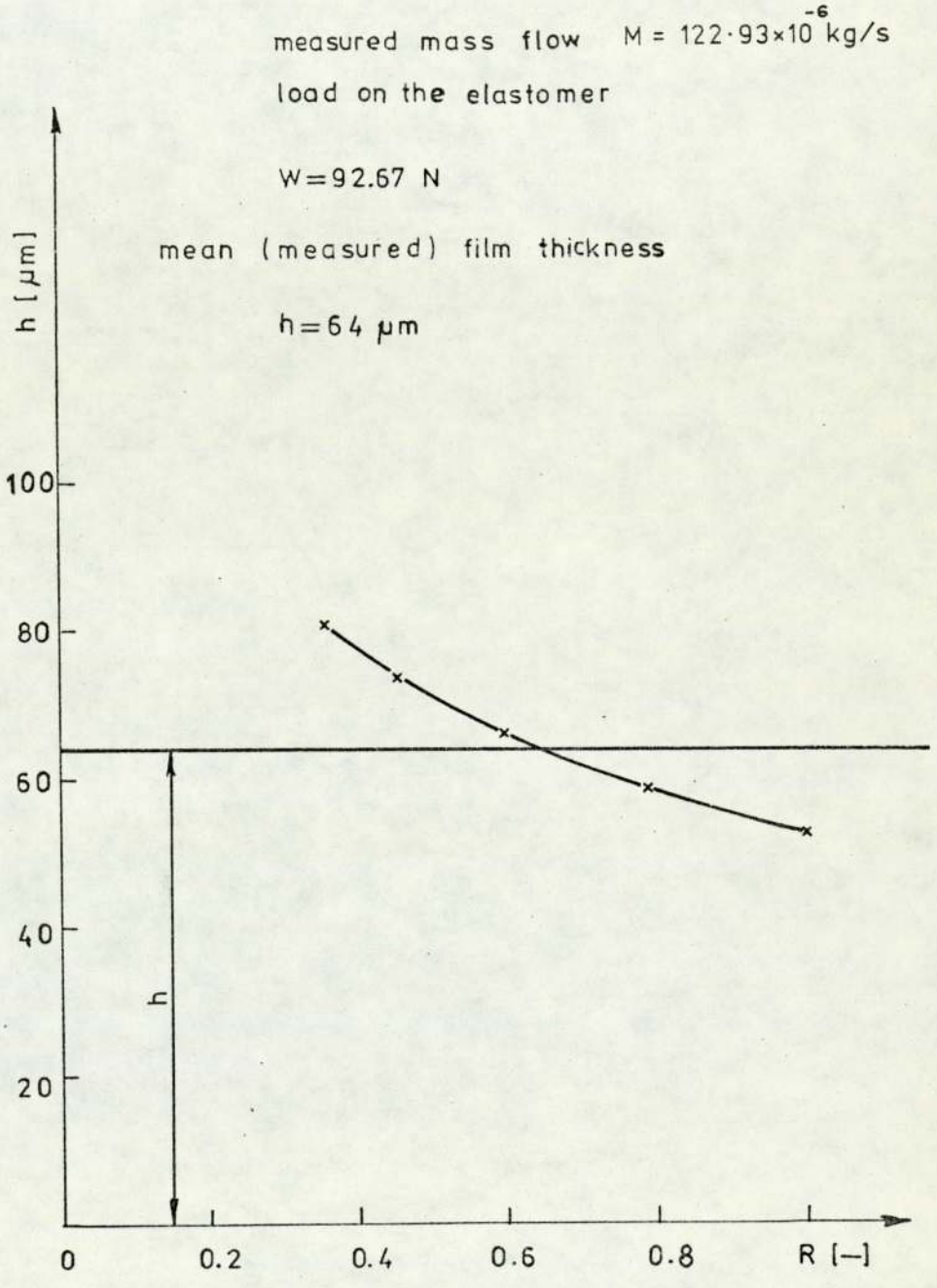

FILM THICKNESS PROFILE

FIG 50

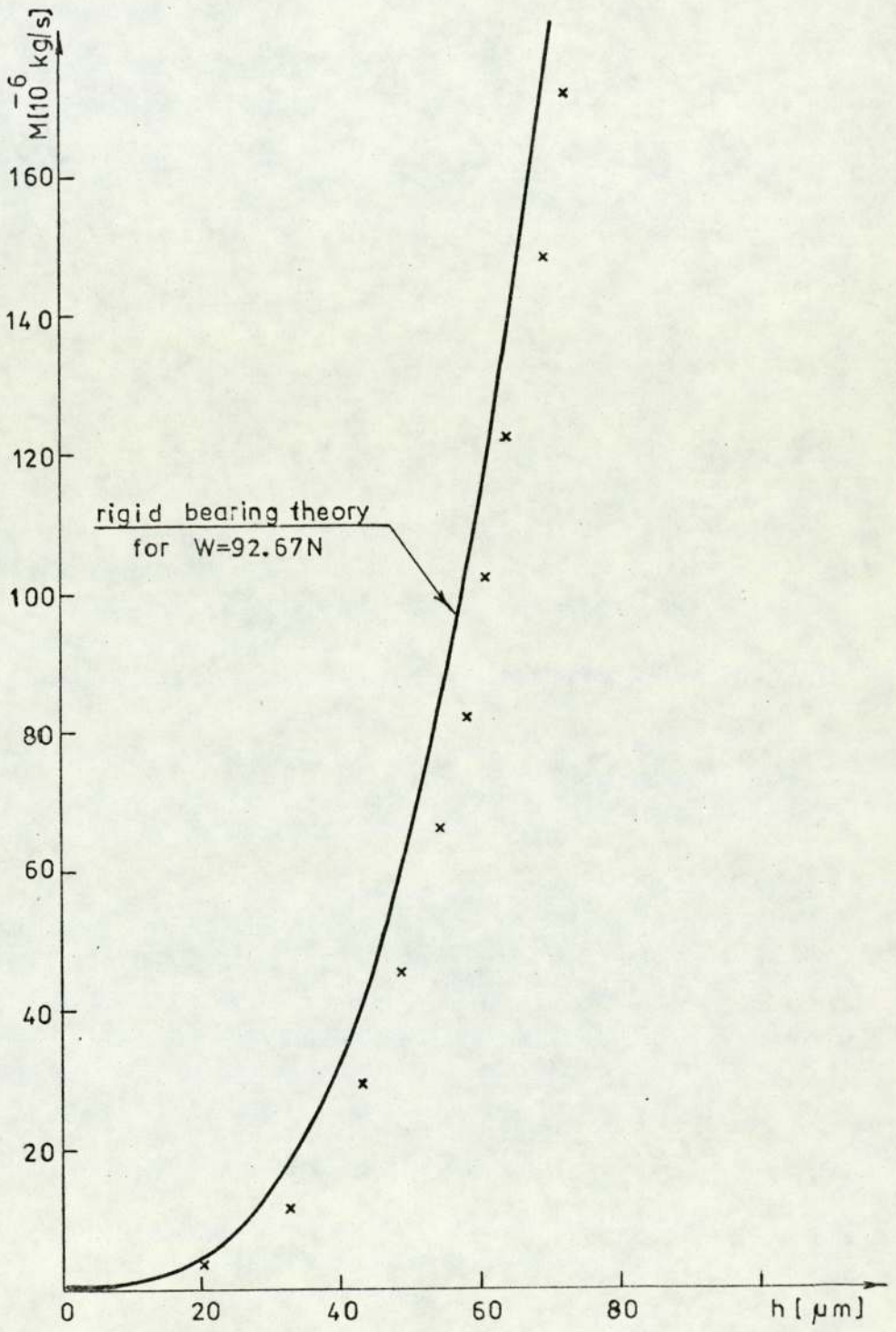

MASS FLOW
v
FILM THICKNESS

FIG 51

initially predicted in chapter I.

Referring to fig. 49 the reason for the load calculated from a polynomial to increase with supply pressure is thought to be as follows:

- As film thicknesses are larger than with rigid bearings it is possible that some inertial flow exists. Although for constant load tests (at a given film thickness) mass flows are smaller than the corresponding rigid theory, the absolute values of the operating flow rates are much larger. Looking at the equation (8), chapter VI the corresponding Reynold s numbers are larger and it is estimated that the local inertial flow is extended radially outwards further than with the rigid case.

It is to be noted with these tests that the estimated film entry pressures are smaller than with rigid bearings. The comparison of a rigid and compliant pressure distribution for a constant load would give general shapes of film pressures as follows:

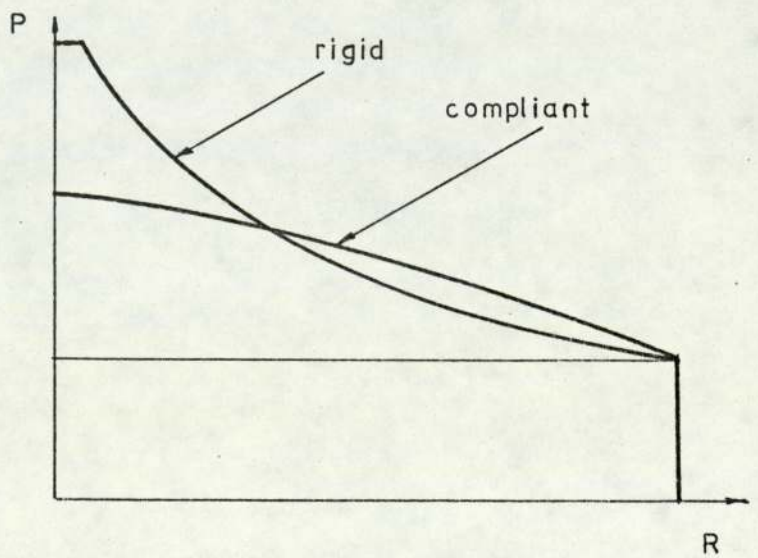

It has been noted that for harder and thinner specimens film entry pressure is greater than for the thicker and softer ones, see fig. 52.

Determination of film entry pressures is one of the main obstacles in this experimental work. They could not be measured experimentally and it has been tried to fit polynomials to measured pressure distributions and thus extrapolate for film entry pressures.

The author has attempted to make a comparison between one of his own compliant experiments and the theory of Pirvics and Castelli [206]. Data for the experiment were:

$$\left.\begin{aligned} \bar{W} &= 0.071 \quad [-] \\ \nu &= 0.4999 \quad [-] \\ c^1 &= \frac{h_a\, G}{t\, p_a} = 0.033 \quad [-] \end{aligned}\right\} \text{measured}$$

$P_p = 1.15$ [-] - estimated from measured pressures through polynomials

$$\left.\begin{aligned} R_p &= 0.0045 \\ \frac{t}{R_o} &= 0.196 \end{aligned}\right\} \text{measured}$$

The theory [206] is valid for the following conditions

$$R_p = \frac{r_p}{r_o} = 0.0625$$

$$\frac{t}{R_o} = 0.1875$$

$$\nu = 0.5$$

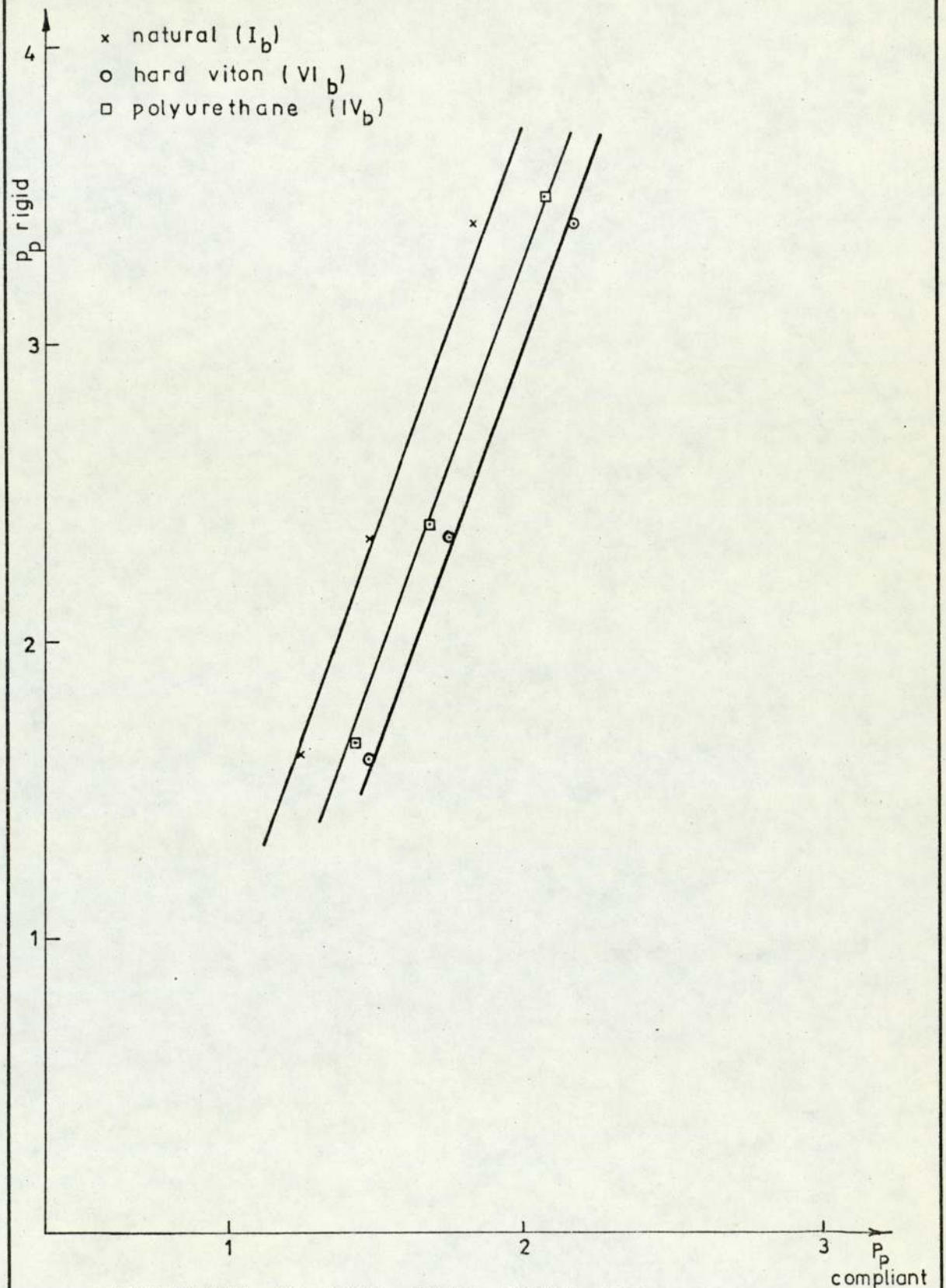

COMPARISON OF RIGID FILM ENTRY PRESSURE AND COMPLIANT FILM ENTRY PRESSURE FOR ZERO FILM THICKNESS

FIG 52

—— theory of Pirvics and Castelli
($R_p = 0{\cdot}0625$, $t/R_o = 0{\cdot}1875$, $\gamma = 0{\cdot}5$)

⊙ author's experiment for film entry pressure P_p 1·15 [-]
(Bearing I_b)

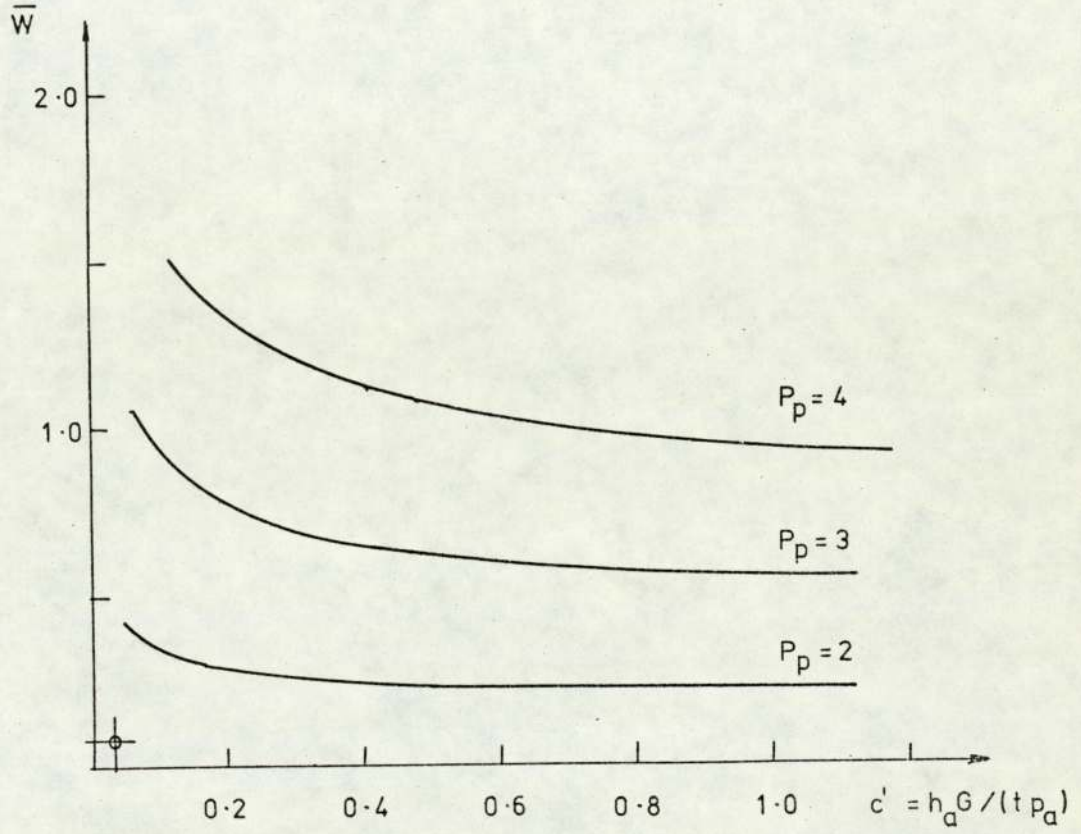

DIMENSIONLESS LOAD v
DIMENSIONLESS APPARENT CLEARANCE

FIG 53

It can be seen that the aspect ratio t/R_o and Poisson's ratio ν of the experiments are only slightly different than those for the theory. For the ratio of the radii, however, the difference is one order of magnitude. This is considered not to matter very much because theory [206] postulates that film entry pressure P_p is equal to the supply pressure P_s, i.e. bearing restrictor is not taken into account. Also for a small ratio of inner to outer radius the contribution of the term $P_p R_p^2$ to the load capacity, (equation (3)), is small.

The difficulty of comparing experiments with theory is not only because of approximations in obtaining film entry pressures and the differences in radii ratio, but also because of the following:

1) Small size of the diagram in reference [206] which is reproduced in fig. 53.
2) Theory is available only for certain values of film entry pressures and it is not available for the value estimated in the experiment.

7.4 Constant Supply Pressure Tests

It has been shown that for compliant bearings it is possible to sustain the same loads as for rigid bearings with smaller flow rates, i.e. smaller supply pressures. Therefore the range of supply pressures for compliant bearings will not be the same as for rigid bearings. In order to cover the range of supply pressures investigated it was found convenient

to choose the following four nominal values of absolute supply pressures [bars] : 1.80, 2.30, 2.90 and 3.50.

Table VII-2 shows elastomers (various rubbers and plastics) that have been investigated. Generally two and sometimes three diameters of the same material had been tested in unbonded (a) and bonded (b) state. (Elastomers whose numbers end with (b) are bonded). The range of hardness investigated is 40-90 [IRHD]. Elastomers for the investigations were either obtained from various suppliers or made at Aston University. Photograph XII shows a mould in which elastomers I_a-III_a and I_b-III_b were made. Photograph XIII shows some elastomers bonded to steel backing plates. The bonding adhesive is also shown. Photograph XIV shows some unbonded elastomers used during the investigations. A typical test of the bearing IV_b is presented in table VII-3 and figures 54 and 55. It is seen that for an elastomer of medium hardness, load capacity is improved compared to corresponding rigid loads for a given supply pressure. Measured flow rates when plotted against apparent film thickness show an increased flow consumption for compliant bearings (at a given film thickness).

The performance of the unbonded bearing IV_a is shown in figures 56 and 57. Figure 56 shows that the stiffness is smaller than with the bonded bearing IV_b. Load is still better than the rigid case except for the lowest supply pressure. The characteristics of nearly constant stiffness with film thickness, typical for bonded bearings, is retained.

PHOTOGRAPH XII

PHOTOGRAPH XIII

PHOTOGRAPH XIV

Number	Elastomer	Made at or obtained from	Dia x t Dimensions [mm]	t/R_o	IRHD	E_c [bar]
I_a	natural	Aston	126.90x12.82	0.202	54.4	67.03
II_a	"	"	102.00x12.69	0.249	56.3	59.81
III_a	"	"	77.13x12.77	0.331	56.1	51.21
I_b	natural	Aston	126.90x12.46	0.196	54.4	123.62
II_b	"	"	102.00x12.37	0.243	56.3	123.68
III_b	"	"	77.13x12.42	0.322	56.1	106.81
IV_a	Polyurethane	Sharples	128.10x3.35	0.052	60.5	209.95
V_a	"	"	77.02x3.37	0.088	61.2	148.32
IV_b	Polyurethane	Sharples	128.10x3.12	0.049	60.5	262.44
V_b	"	"	77.02x3.14	0.082	61.2	196.87
VI_a	Hard Viton	Du Pont	127.32x2.38	0.037	90.0	169.70
VII_a	"	"	76.80x2.29	0.060	89.0	121.17
VI_b	Hard Viton	Du Pont	127.32x2.19	0.034	90.0	189.53
VII_b	"	"	76.80x2.19	0.057	89.0	142.31
$VIII_a$	Medium Viton	Du Pont	127.83x2.34	0.037	81.0	102.57
IX_a	"	"	76.45x2.39	0.063	81.0	81.33
$VIII_b$	Medium Viton	Du Pont	127.83x2.13	0.033	81.0	111.75
IX_b	"	"	76.45x2.15	0.056	81.0	89.37
X_a	Soft Viton	Du Pont	128.20x3.20	0.050	56	90.96
XI_a	"	"	77.05x3.23	0.084	56.5	70.47
X_b	Soft Viton	Du Pont	128.20x3.05	0.048	58.2	107.01
XI_b	"	"	77.05x3.07	0.080	57.8	82.90
XII_a	Natural RRH	Dunlop	126.90x4.05	0.064	78.2	132.41
$XIII_a$	"	"	77.20x4.02	0.104	79.0	112.38
XII_b	Natural RRH	Dunlop	126.90x3.95	0.062	79.5	162.40
$XIII_b$	"	"	77.20x3.97	0.103	80.0	131.06
XIV_a	Natural RRB	Dunlop	127.30x4.11	0.065	39.2	65.40
XV_a	"	"	78.00x3.96	0.102	38.7	49.31
XIV_b	Natural RRB	Dunlop	127.30x3.91	0.061	40.6	81.30
XV_b	"	"	78.00x3.93	0.101	40.1	60.52

TABLE VII-2

W [N]	h[μm]	$h_a = h - \Sigma\Delta t$ [μm]	M[10^{-6}kg/s]	$\bar{W}$[-]	c^1[-]
		p_s = 1.838 [bar]			
92.67	30.1	29.2	29.3	0.072	0.066
152.49	17.0	15.5	16.0	0.118	0.035
194.96	11.0	9.1	7.9	0.184	0.013
237.42	8.2	5.9	3.2	0.184	0.013
		p_s = 2.299 [bar]			
455.13	8.7	4.3	10.7	0.353	0.010
410.90	10.7	6.8	17.5	0.319	0.015
322.54	16.1	13.0	24.3	0.184	0.045
237.42	22.3	20.0	32.0	0.184	0.045
152.49	30.1	28.6	39.2	0.118	0.064
		p_s = 2.874 [bar]			
322.54	24.5	21.4	45.3	0.250	0.048
455.62	19.7	15.3	41.0	0.353	0.034
592.22	14.8	9.1	35.7	0.460	0.020
720.98	10.0	3.1	28.2	0.559	0.007
825.11	5.5	-0.6	20.3	0.640	-0.001
1025.05	2.1	-10.0	6.1	0.795	-0.022
		p_s = 3.449 [bar]			
1190.45	3.3	-11.8	12.5	0.924	-0.026
1097.95	8.1	-2.4	28.6	0.852	-0.005
985.47	11.6	2.1	39.6	0.764	0.005
856.44	14.5	6.2		0.665	0.014
720.98	17.6	10.7		0.559	0.024
592.22	20.3	14.6		0.460	0.033

TABLE VII-3

BEARING IV_b

BEARING IV_b

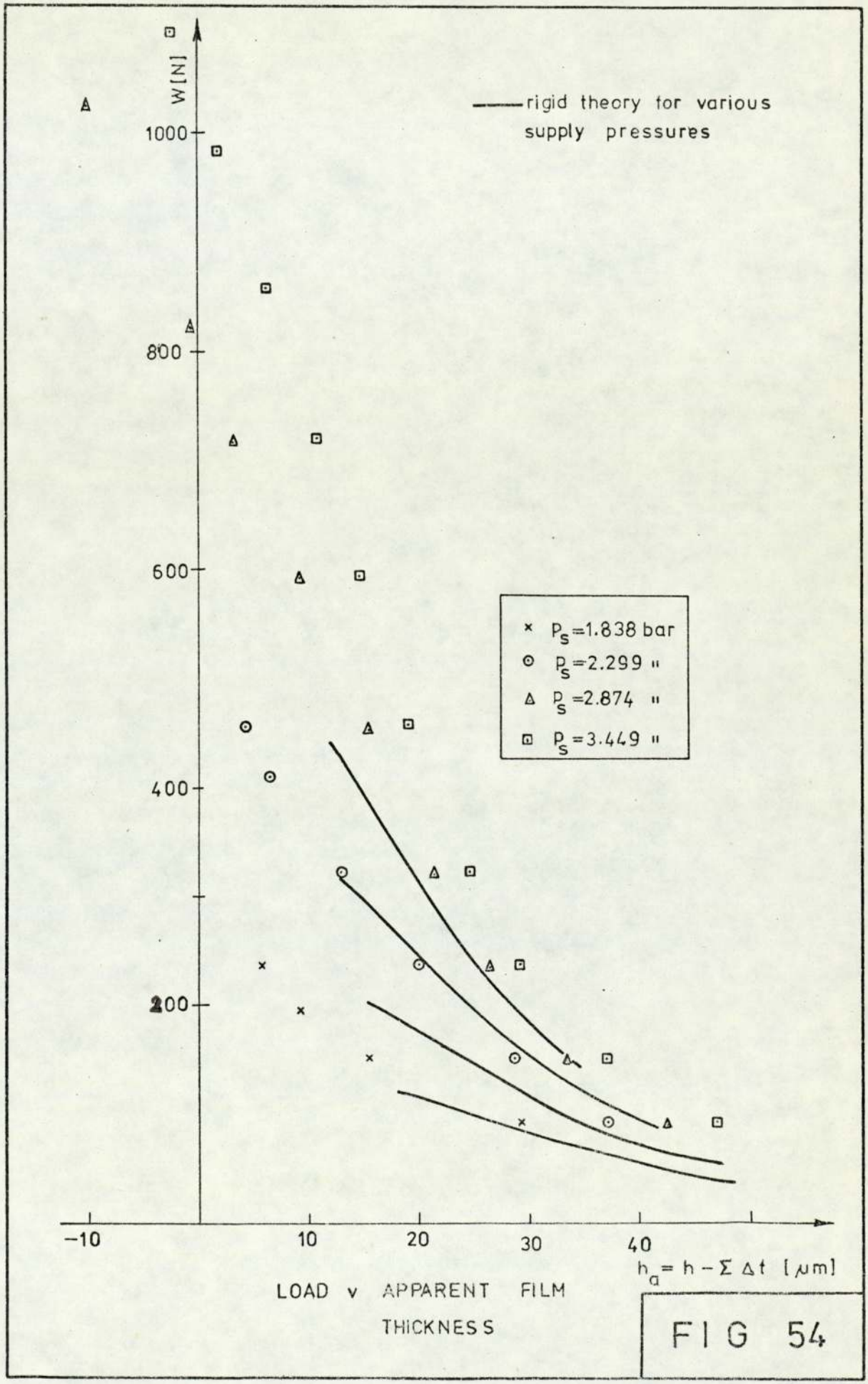

LOAD v APPARENT FILM THICKNESS

FIG 54

BEARING IV_b

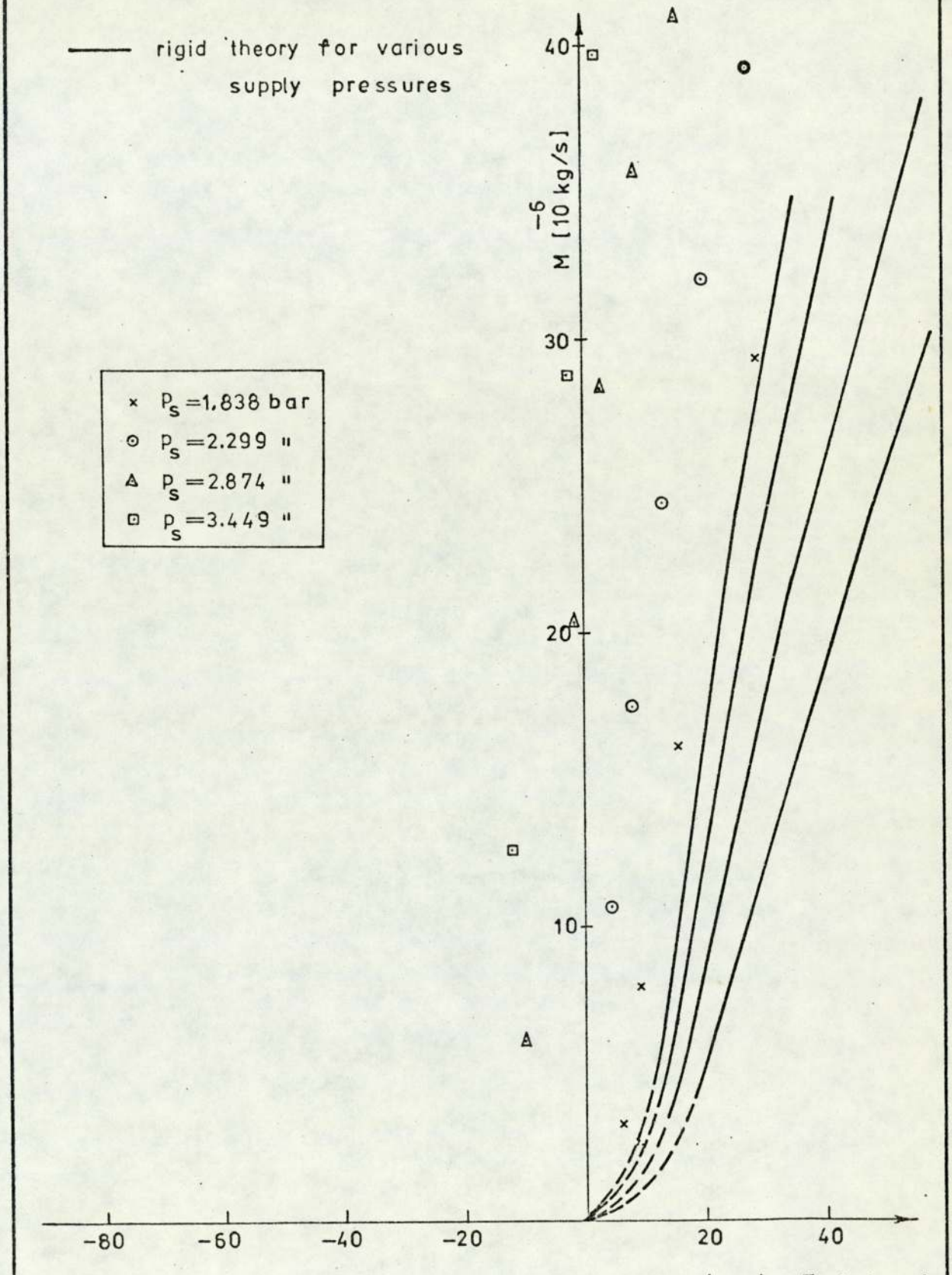

FLOW v APPARENT FILM THICKNESS

FIG 55

BEARING IV_a

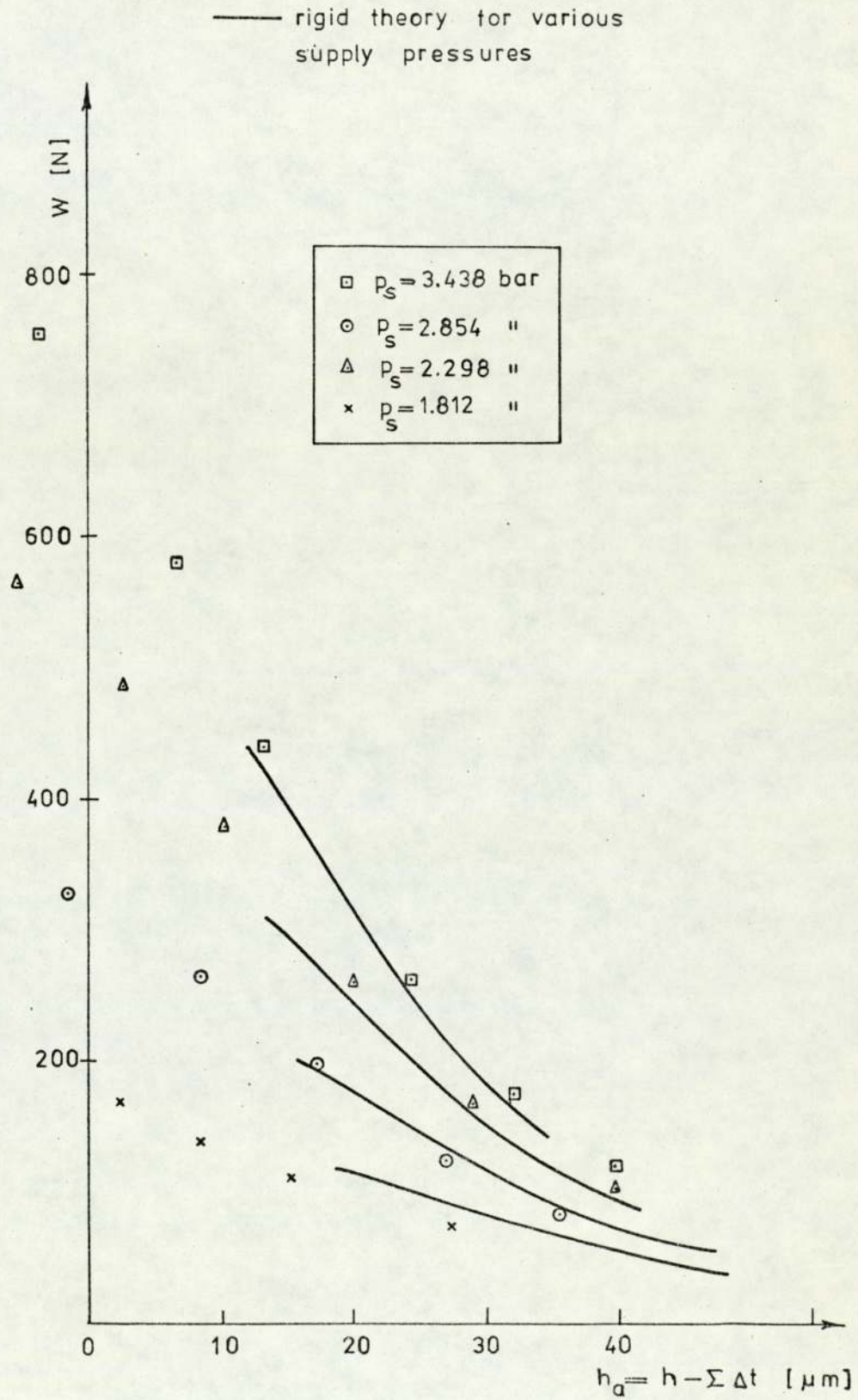

LOAD v APPARENT FILM THICKNESS

FIG 56

BEARING IV_a

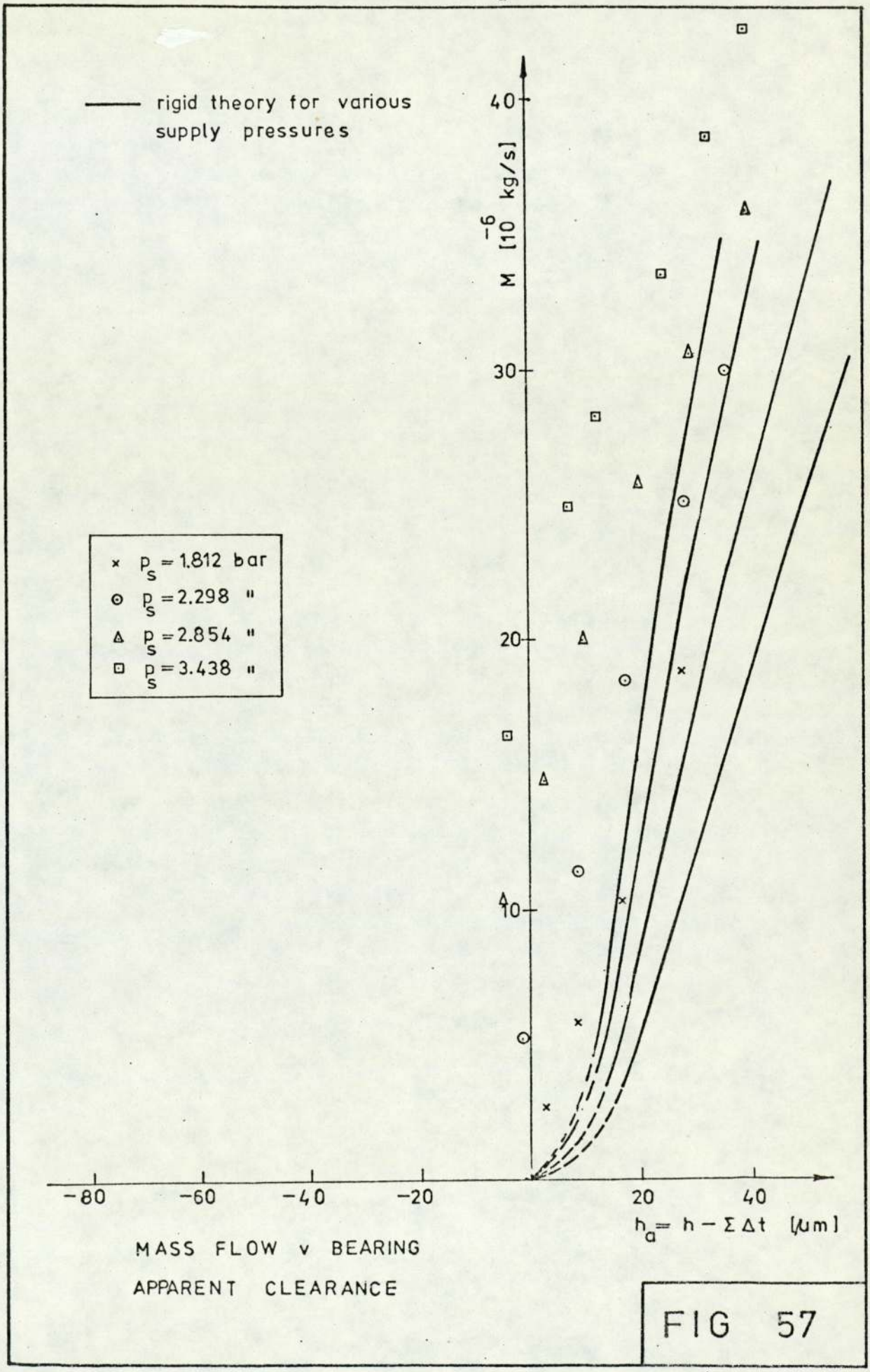

MASS FLOW v BEARING APPARENT CLEARANCE

FIG 57

BEARING I_a

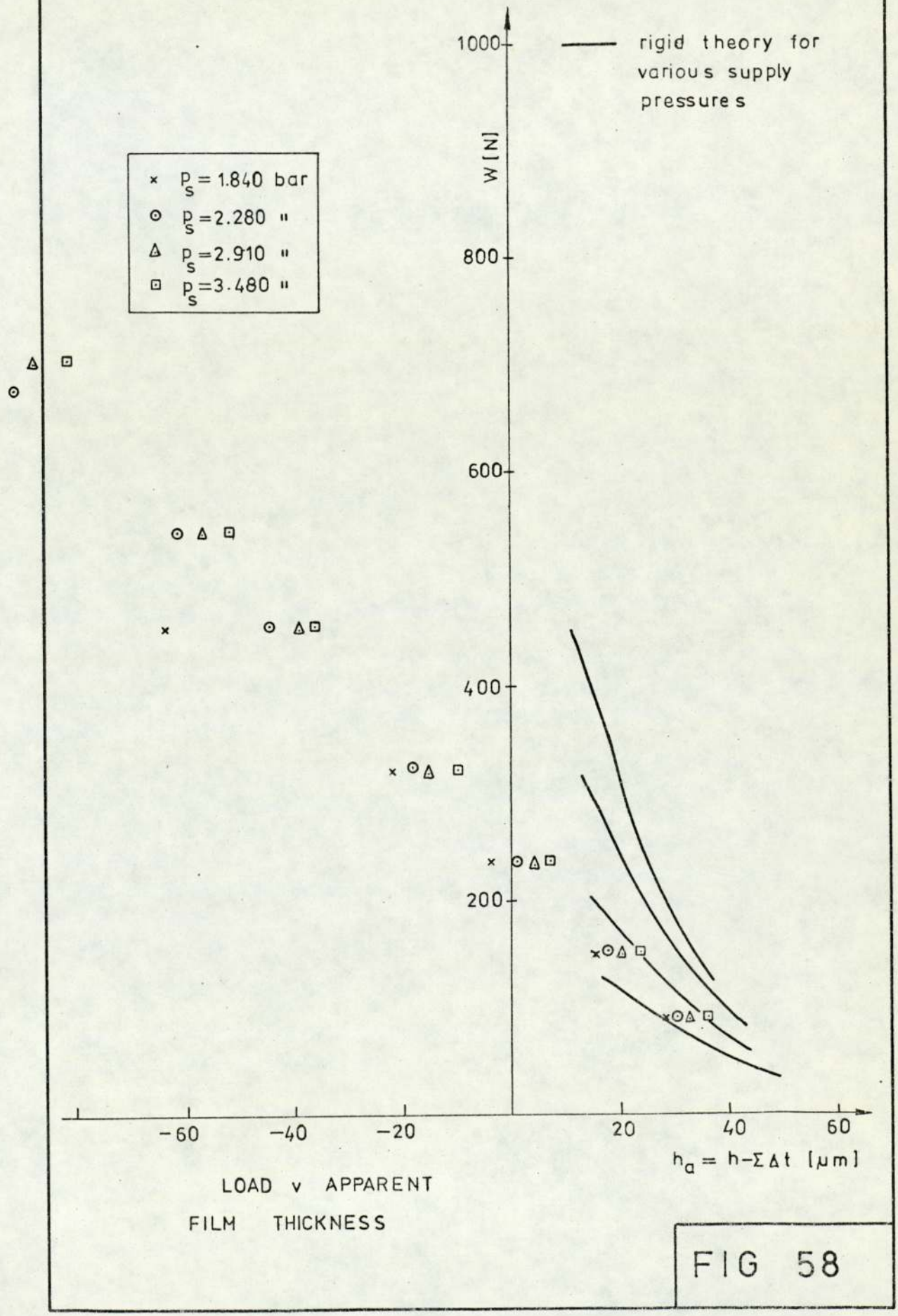

LOAD v APPARENT FILM THICKNESS

FIG 58

BEARING I_a

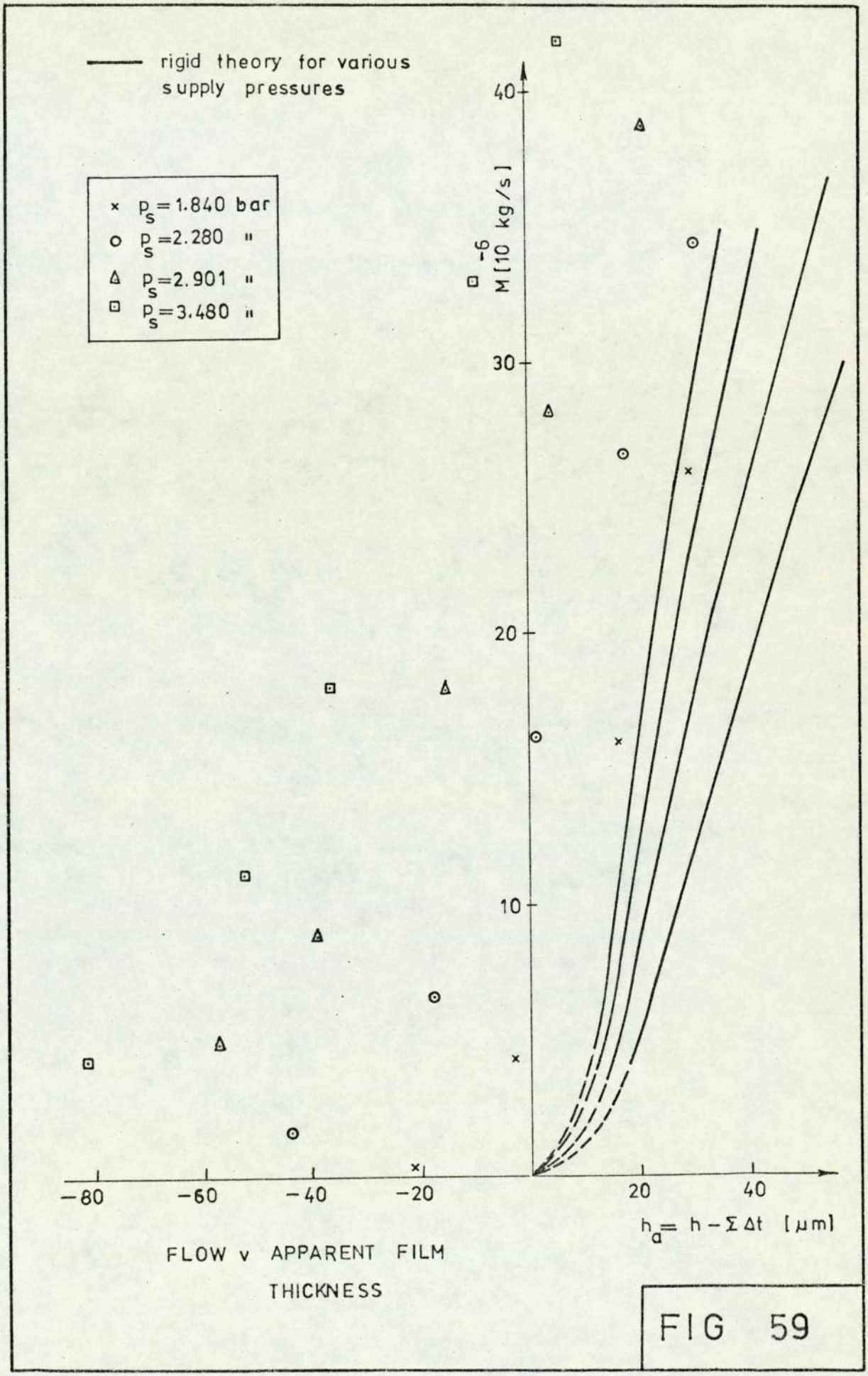

FLOW v APPARENT FILM THICKNESS

FIG 59

BEARING II_a

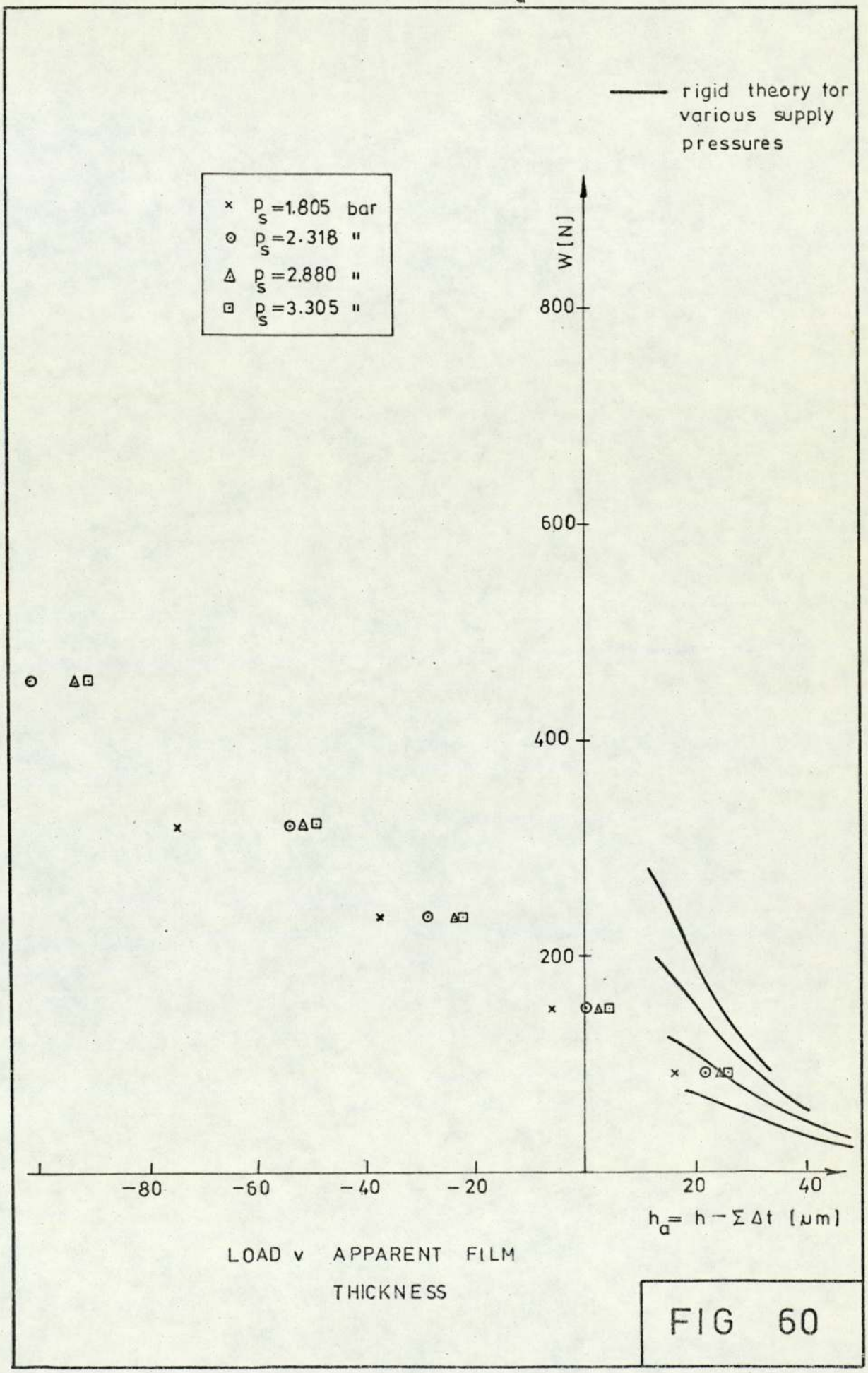

LOAD v APPARENT FILM THICKNESS

FIG 60

BEARING II_a

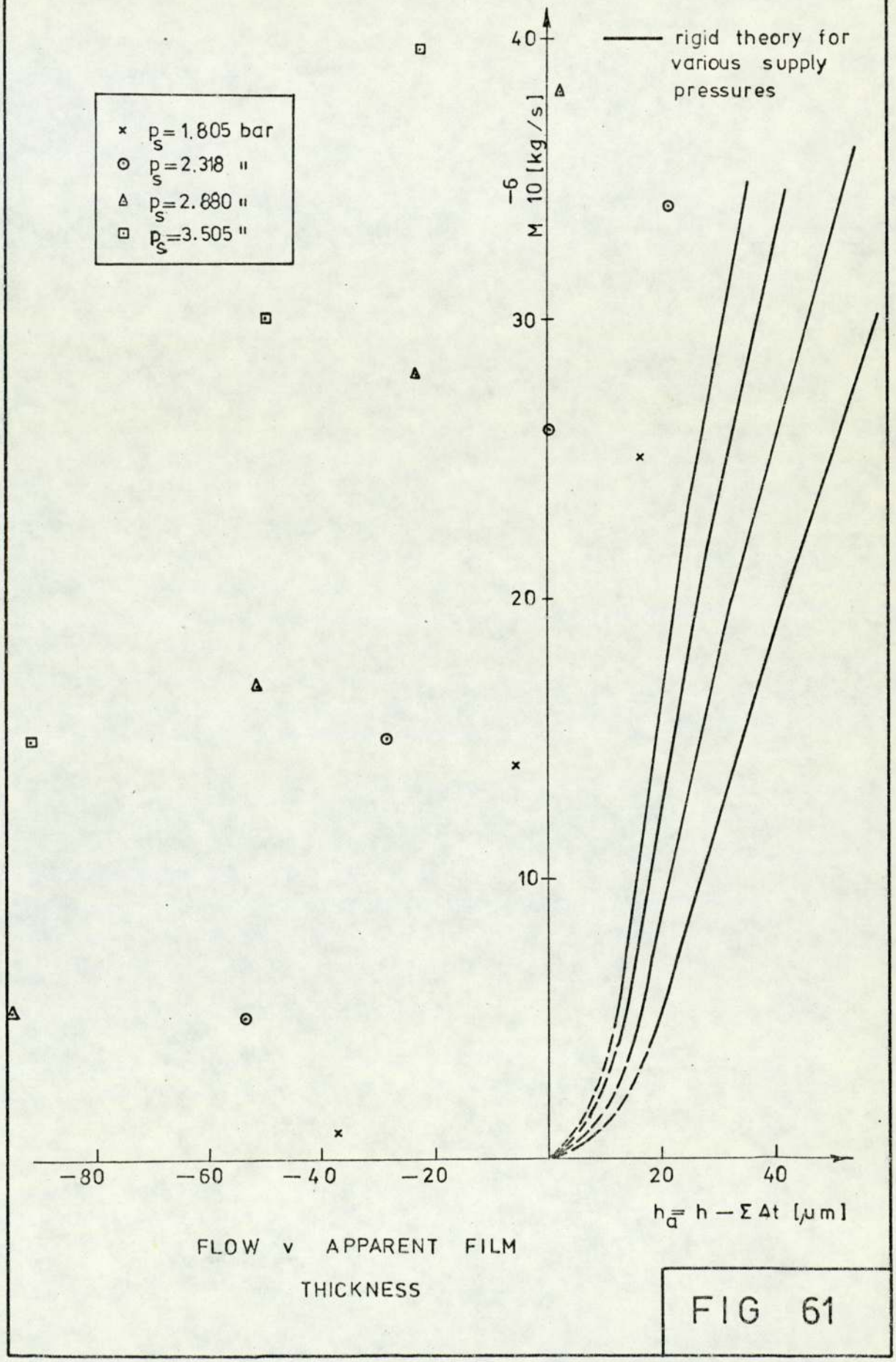

FLOW v APPARENT FILM THICKNESS

FIG 61

BEARING III_a

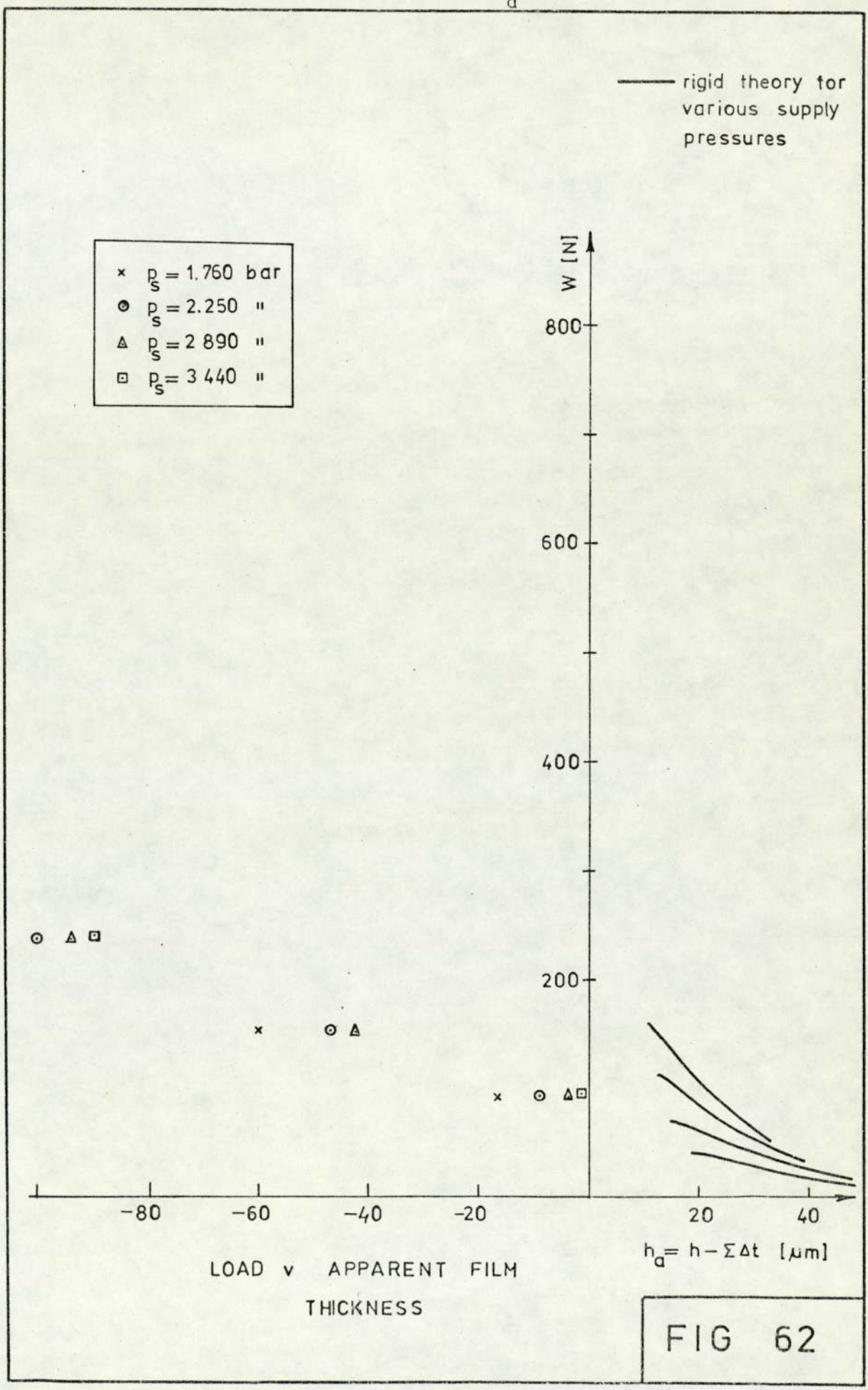

LOAD v APPARENT FILM THICKNESS

FIG 62

BEARING III_a

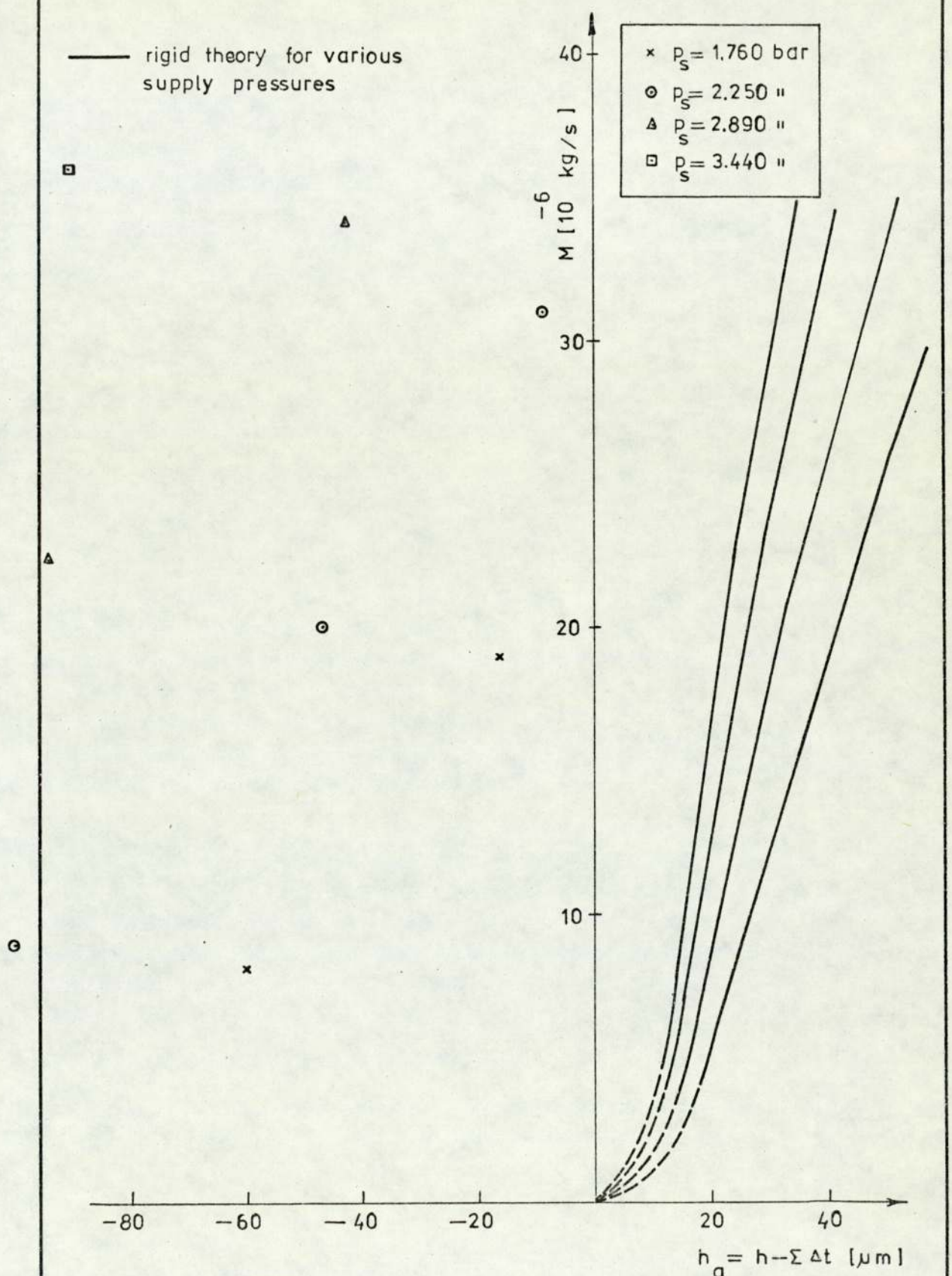

FLOW v APPARENT FILM THICKNESS

FIG 63

BEARING I_b

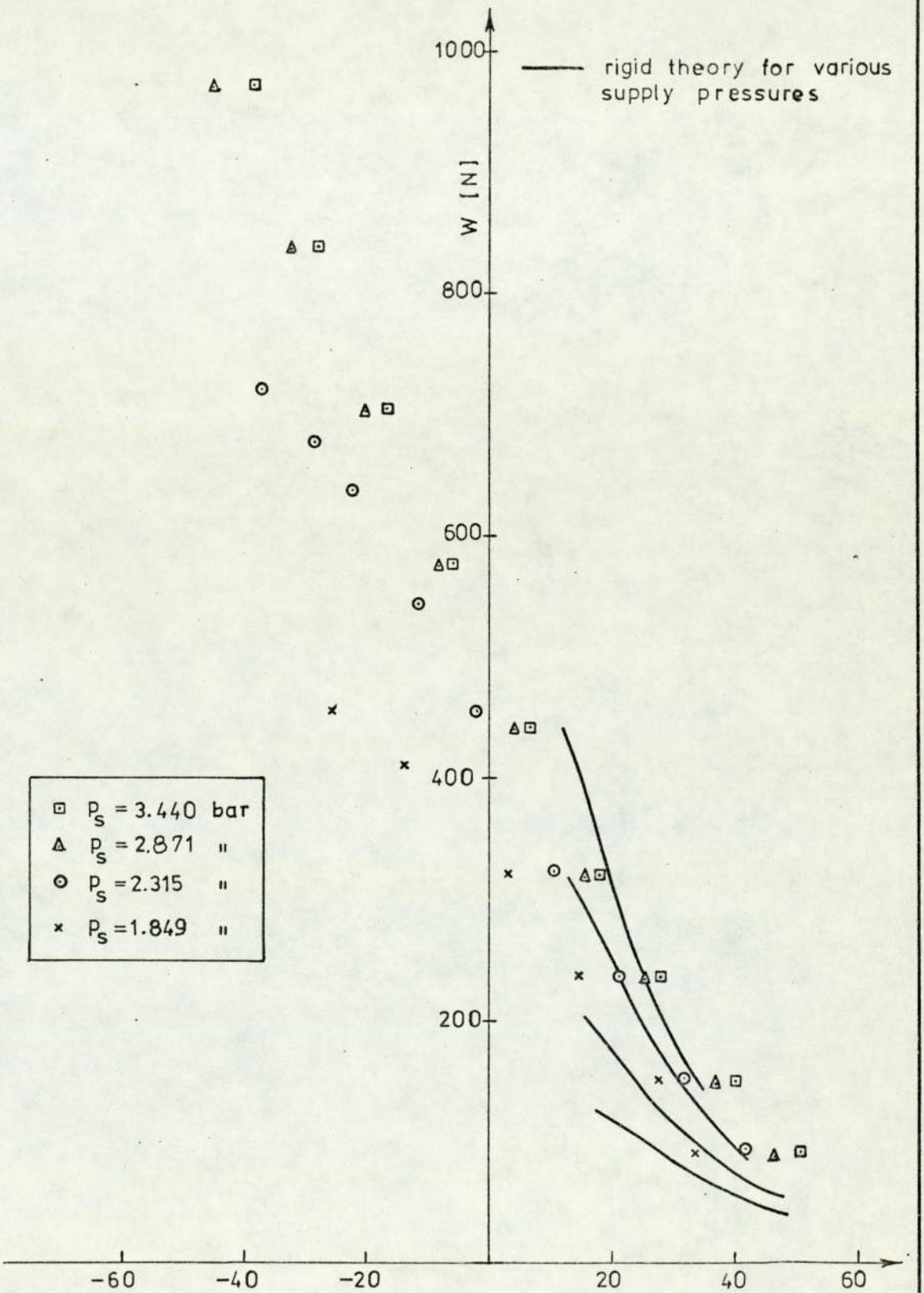

LOAD v APPARENT FILM THICKNESS

FIG 64

BEARING Ib

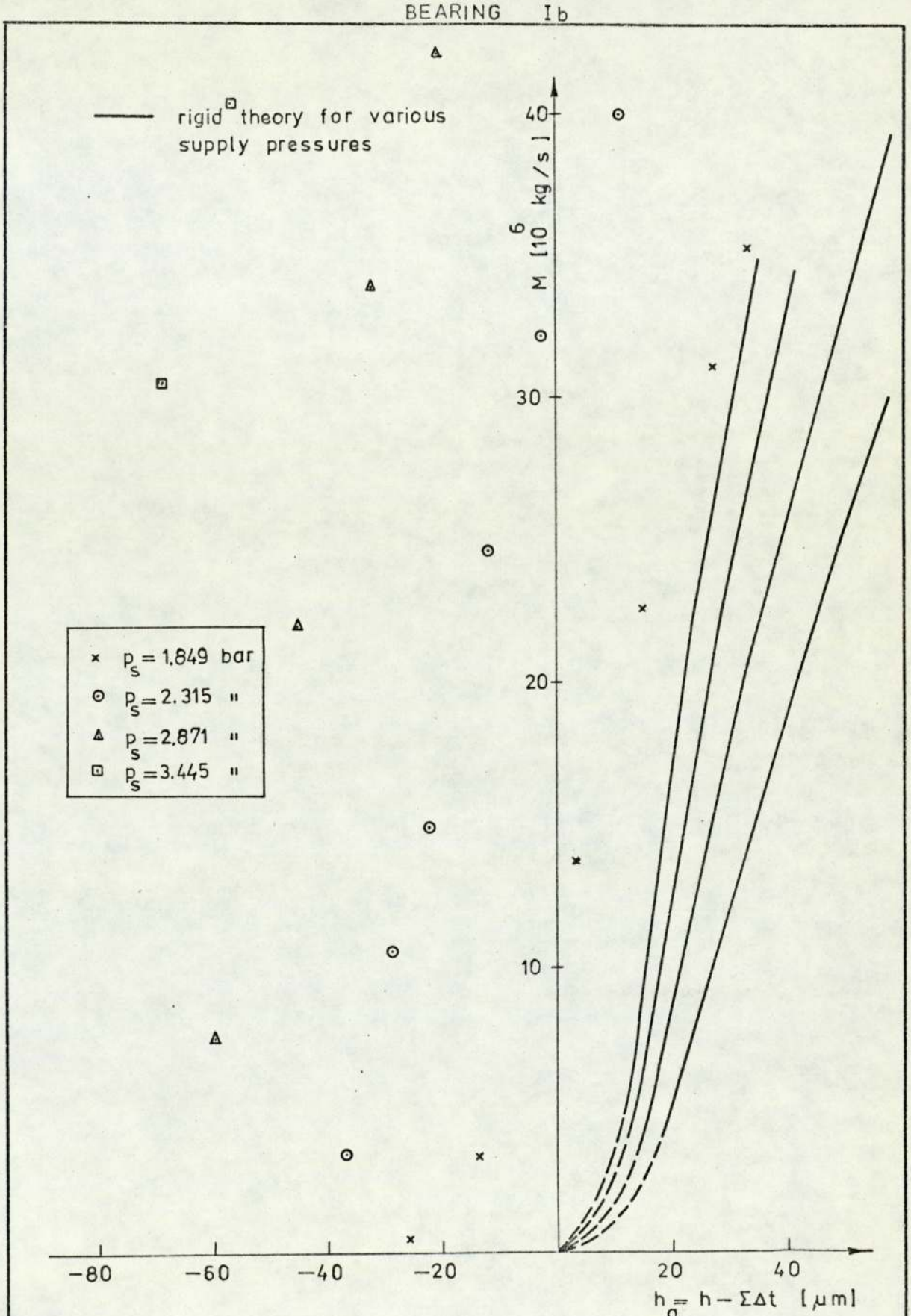

FLOW v APPARENT FILM THICKNESS

FIG 65

BEARING II_b

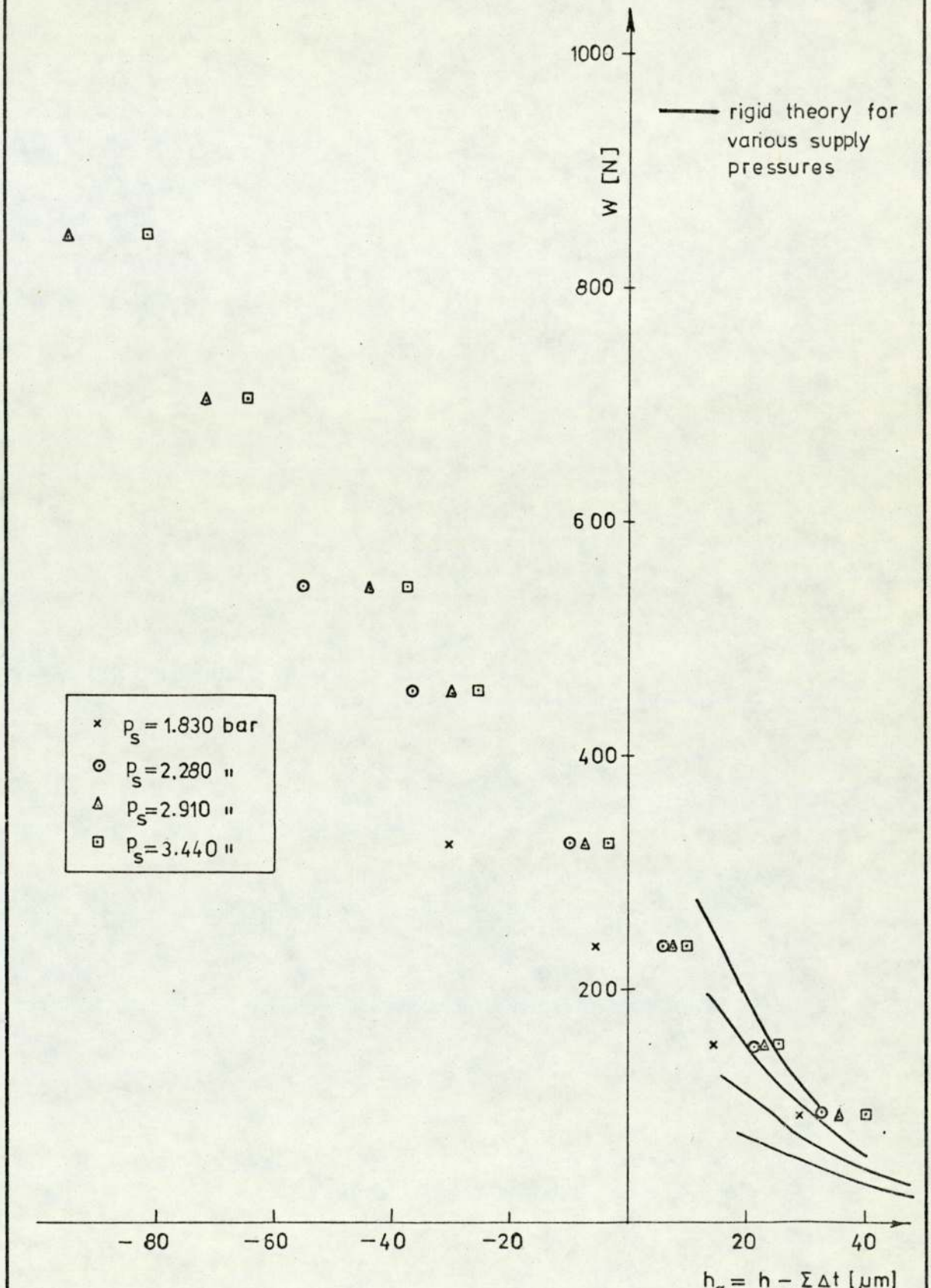

LOAD v APPARENT FILM THICKNESS

FIG 66

BEARING II_b

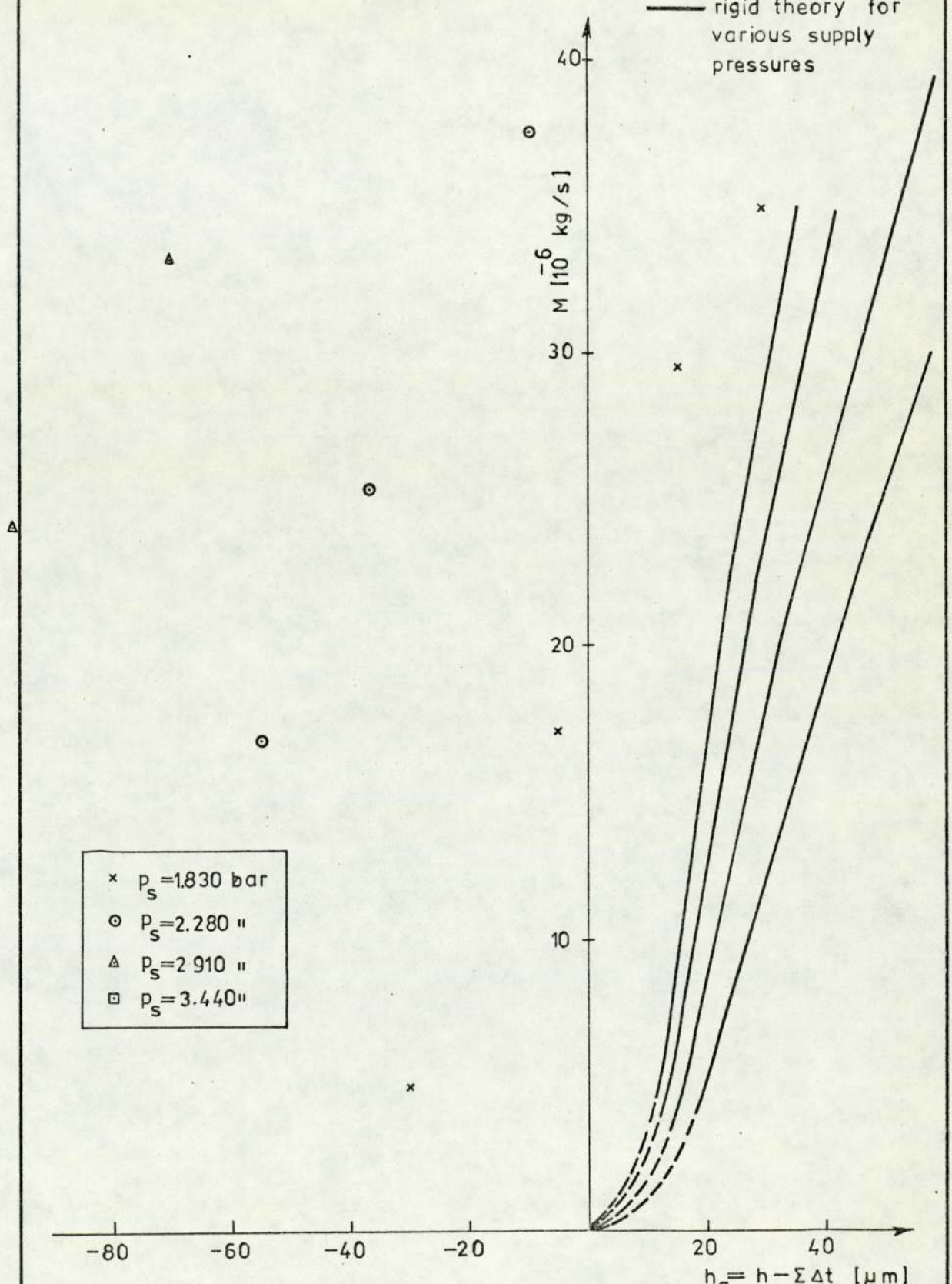

FLOW v APPARENT FILM THICKNESS

FIG 67

BEARING III_b

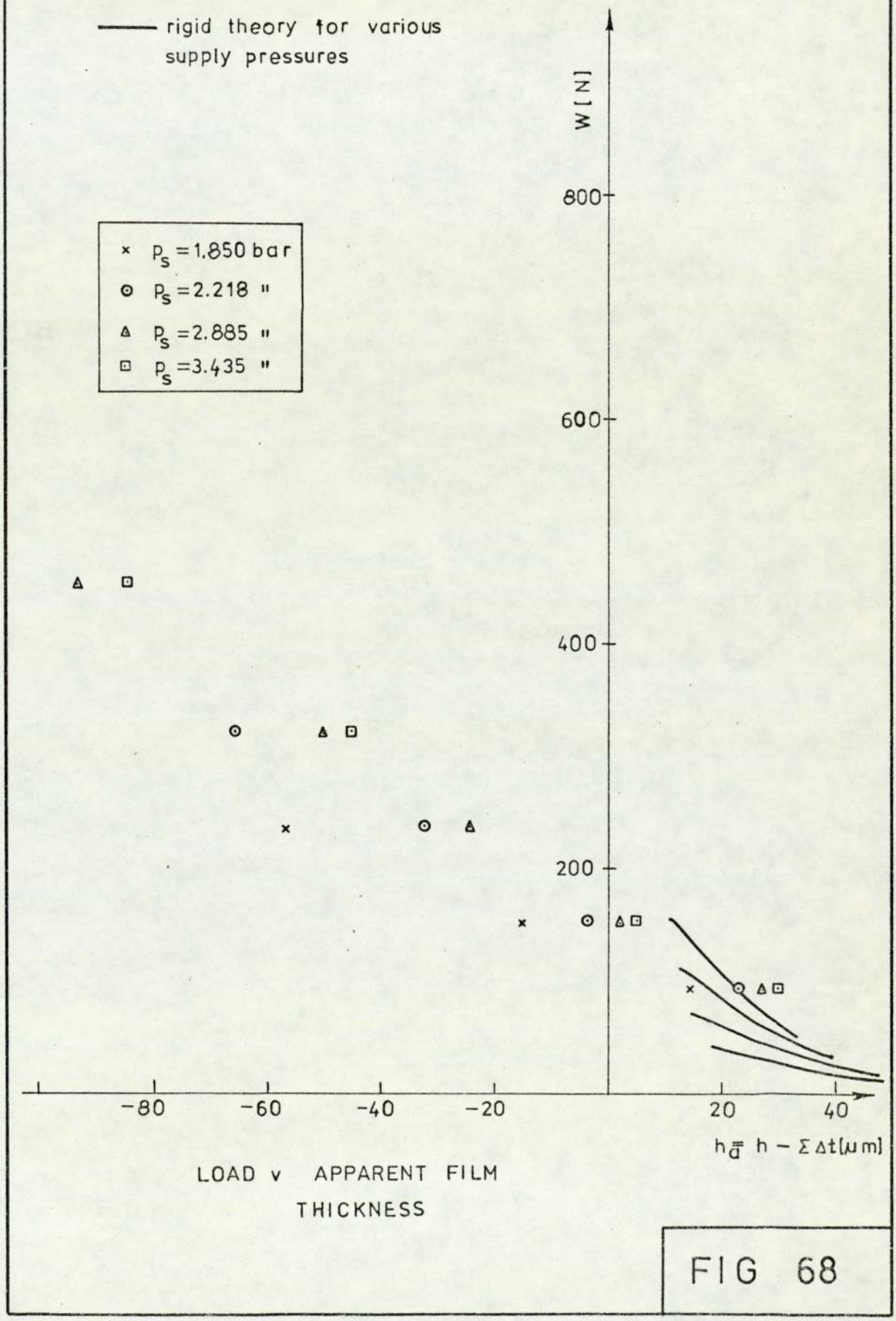

LOAD v APPARENT FILM THICKNESS

FIG 68

BEARING III_b

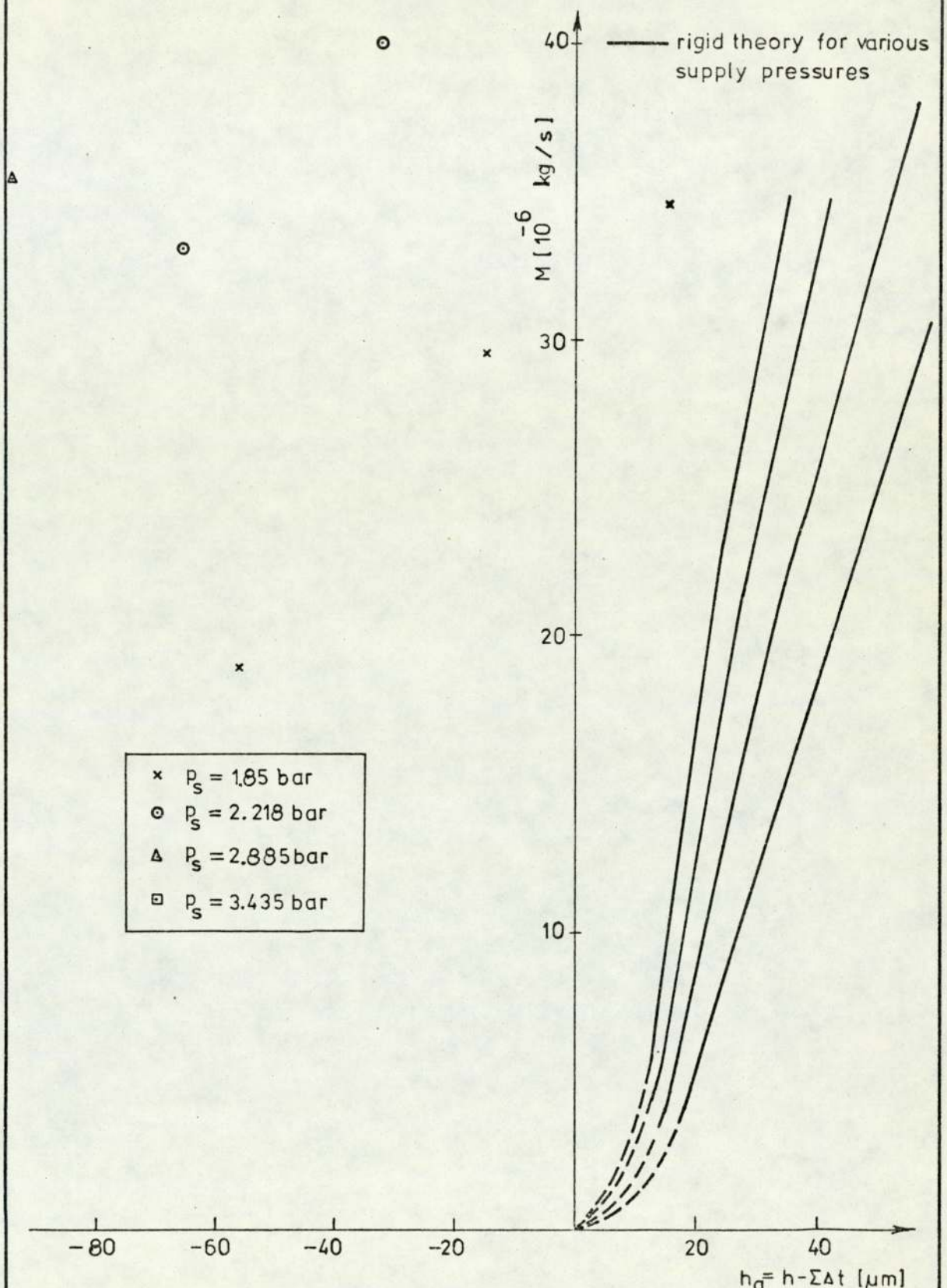

ELOW v APPARENT FILM THICKNESS

FIG 69

BEARING VIII$_b$

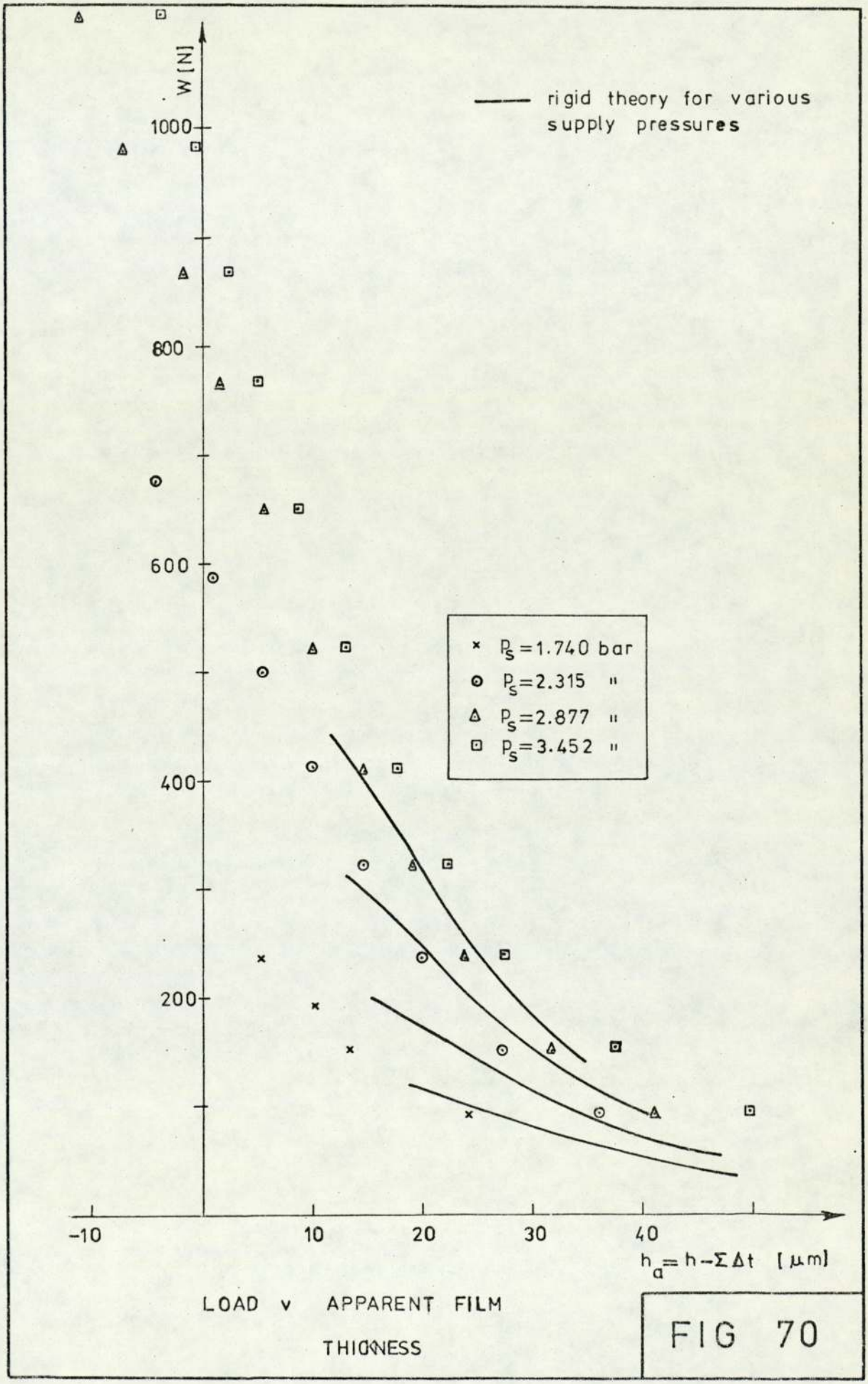

LOAD v APPARENT FILM THICKNESS

FIG 70

BEARING VIII$_b$

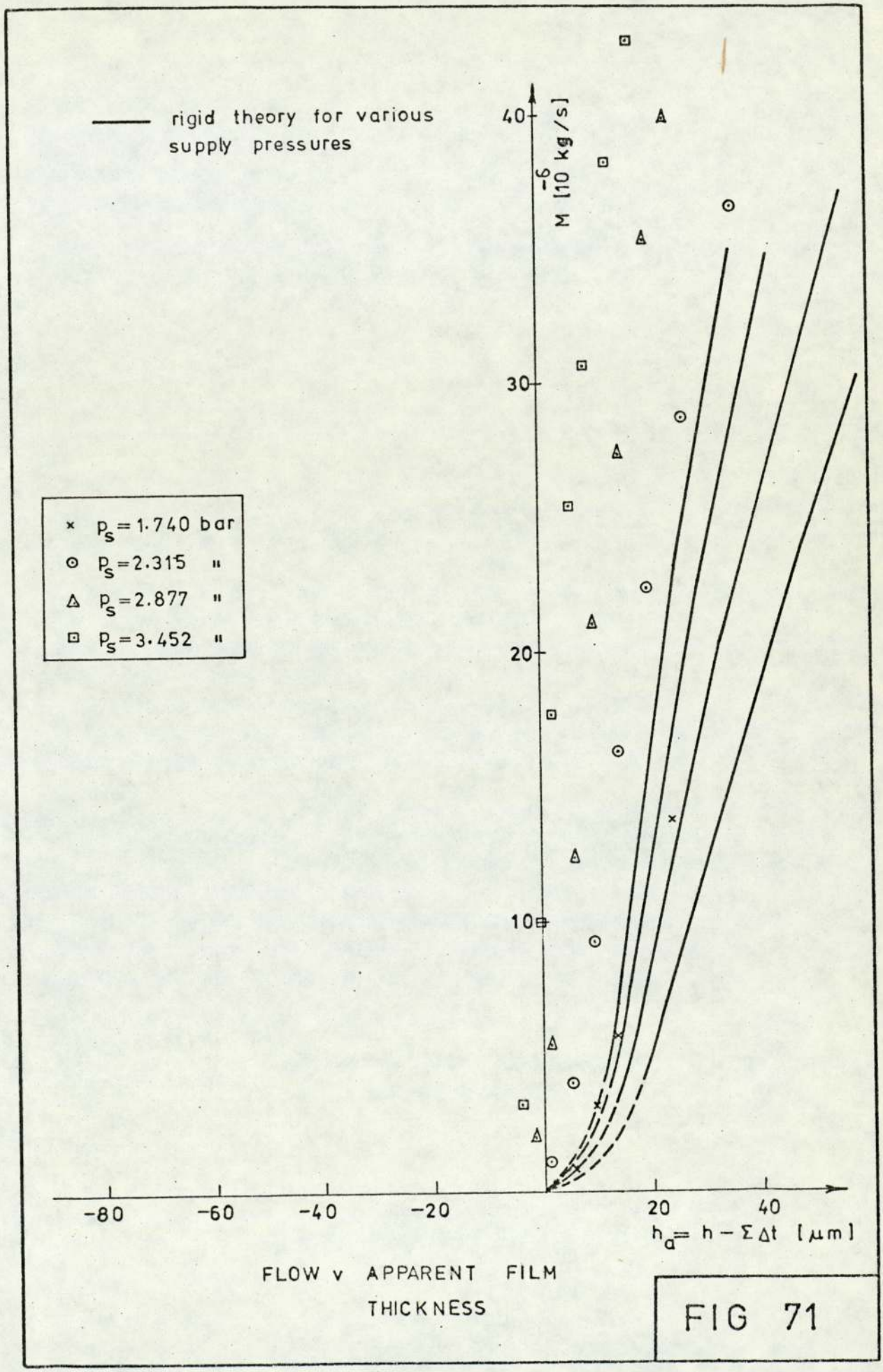

FLOW v APPARENT FILM THICKNESS

FIG 71

With reference to Table VII-2, an investigation programme has now been set up in order to determine the performance of other elastomers. Usually the same elastomer sample has been tested as an unbonded specimen and as the bonded one. First, unbonded elastomers are tested, then they are bonded and surface ground so that the elastomer surface is similarly flat as the rigid bearing surface. From table VII-2 it can be noted that the aspect ratio of the bonded elastomers is always somewhat smaller than for the corresponding unbonded ones. This is so, because elastomer thickness of a bonded elastomer is reduced by the grinding process. Unbonded elastomers were not ground and they were tested as obtained (or as made in moulds). Their flatness on a talylin trace is of the same order of magnitude as flatness of bonded bearings.

There follow figs. 58-71 of load and flow rates against the apparent film thickness of some elastomers in table VII-2.

7.5 Discussion of Compliant Bearing Results

In order to predict the bearing performance, it is important to find out how bearing parameters such as hardness, thickness and diameter influence the load carrying capacity and mass flow rate. Both bonded and unbonded elastomers are discussed.

Hardness and Thickness (Elastomer Diameter is approximately constant

Referring to the table VII-2, bearings chosen to discuss the influence of hardness and thickness upon bearing performance are VIII, IV and XIV ("a" and "b"). Medium viton (VIII) is

the thinnest and the hardest elastomer, i.e. its compliance is the smallest. The compliance of polyurethane (IV) is increased, and the compliance of soft natural rubber (XIV) is increased further. Comparisons are made at a nominal absolute supply pressure p_s = 2.90 [bar].

Fig. 72 is a plot of load against apparent film thickness for bonded elastomers. Rigid theory line is also shown. It is seen that the load of all three bearings is superior to rigid bearings. A beneficial effect of compliance upon bearing load carrying capacity is detected.

This compliance effect is seen better if dimensionless load is plotted against dimensionless apparent film thickness, fig. 73.

This is because dimensionless apparent film thickness c^1 depends both upon elastomer thickness and upon a characteristic of the material which is related to hardness. Thus this variable truly describes the compliance of a bearing liner.

Flow rates are shown in fig. 74. Air flow consumption of all three materials is greater than the rigid bearing flow consumption for a given apparent clearance. The more a bearing is compliant, the flow consumption is greater.

The performance of the unbonded bearings (VIII, IV and XIV) is shown in figures 75 and 76. The load capacity is reduced compared to bonded bearings, but it is still superior to rigid bearings, particularly at low values of apparent clearance. Gradients of lines connecting experimental flow points are smaller than for the bonded bearings. This means that flow rates of unbonded bearings increase slower with

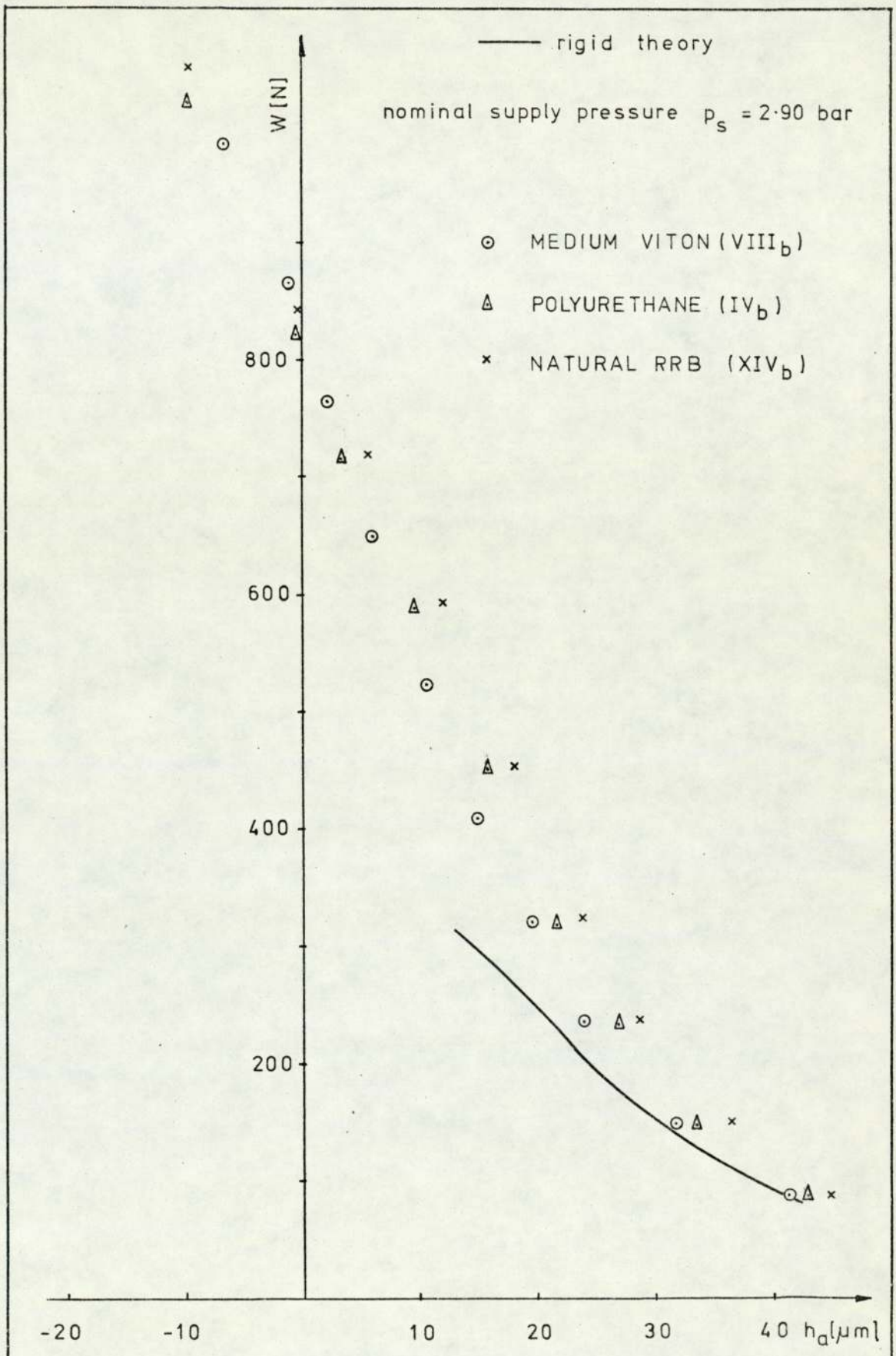

LOAD v APPARENT FILM THICKNESS
- BONDED ELASTOMERS

FIG 72

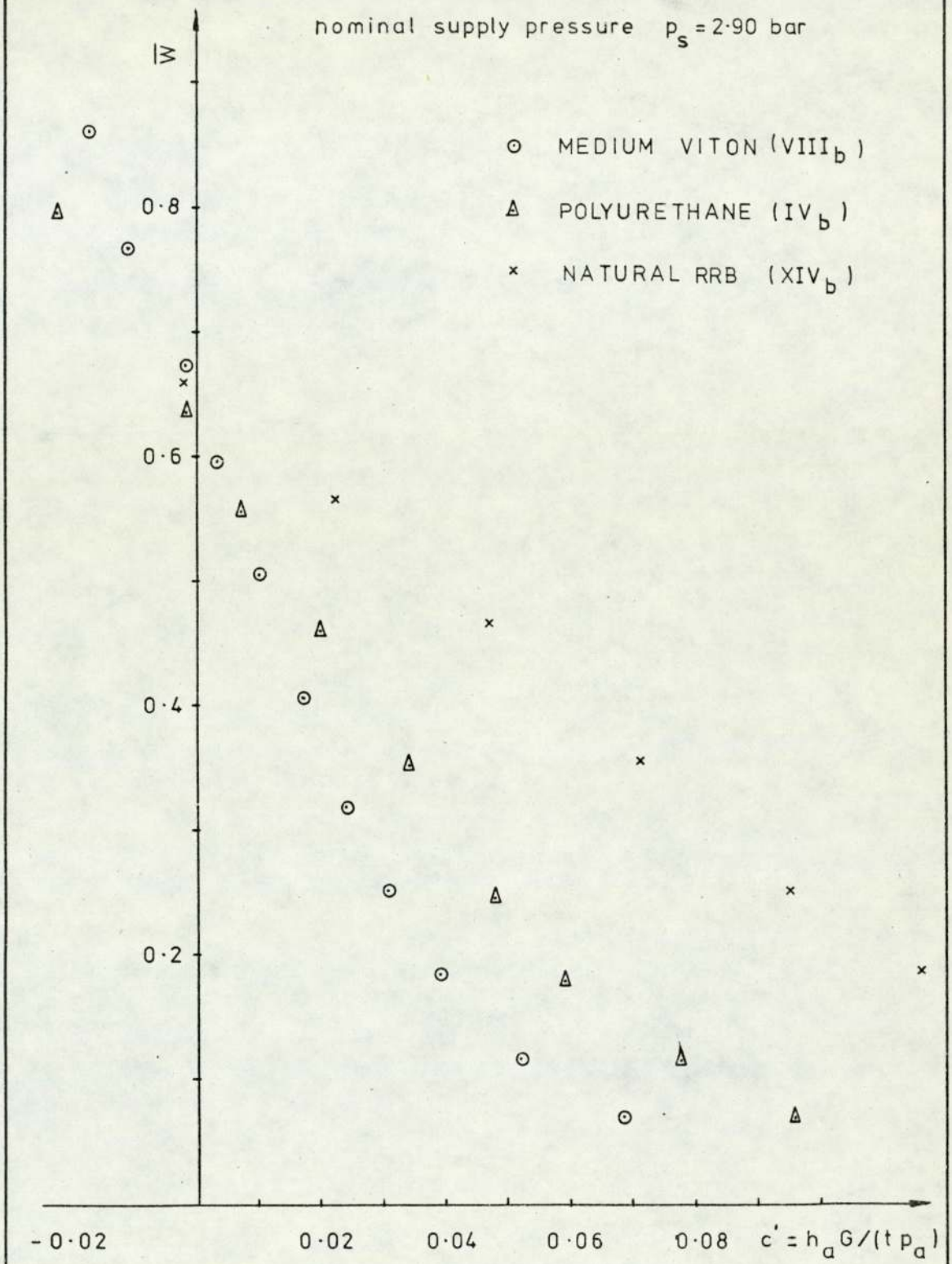

DIMENSIONLESS LOAD v DIMENSIONLESS APPARENT CLEARANCE

FIG 73

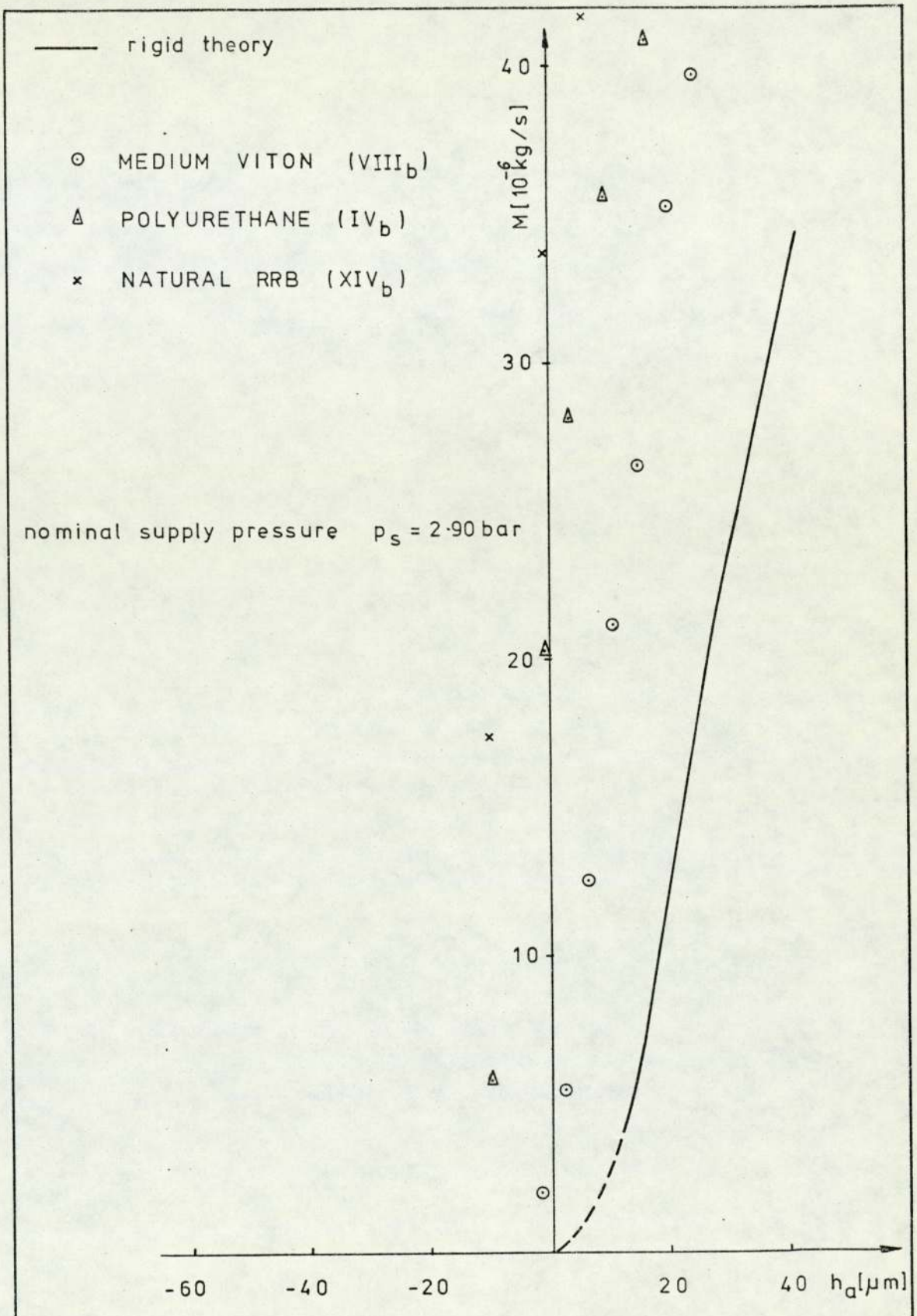

FLOW v APPARENT FILM THICKNESS
- BONDED ELASTOMERS

FIG 74

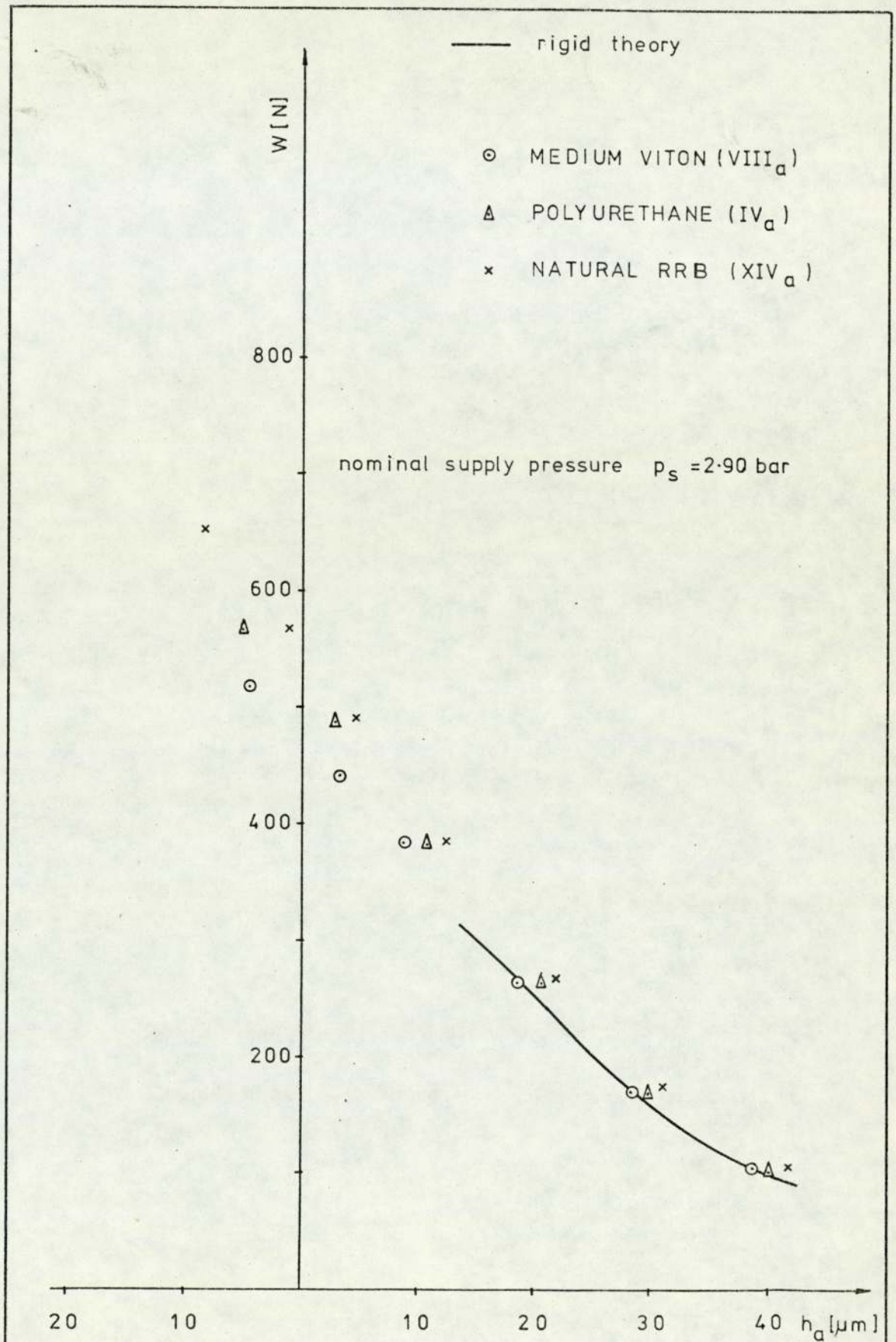

LOAD v APPARENT FILM THICKNESS
- UNBONDED ELASTOMERS

FIG 75

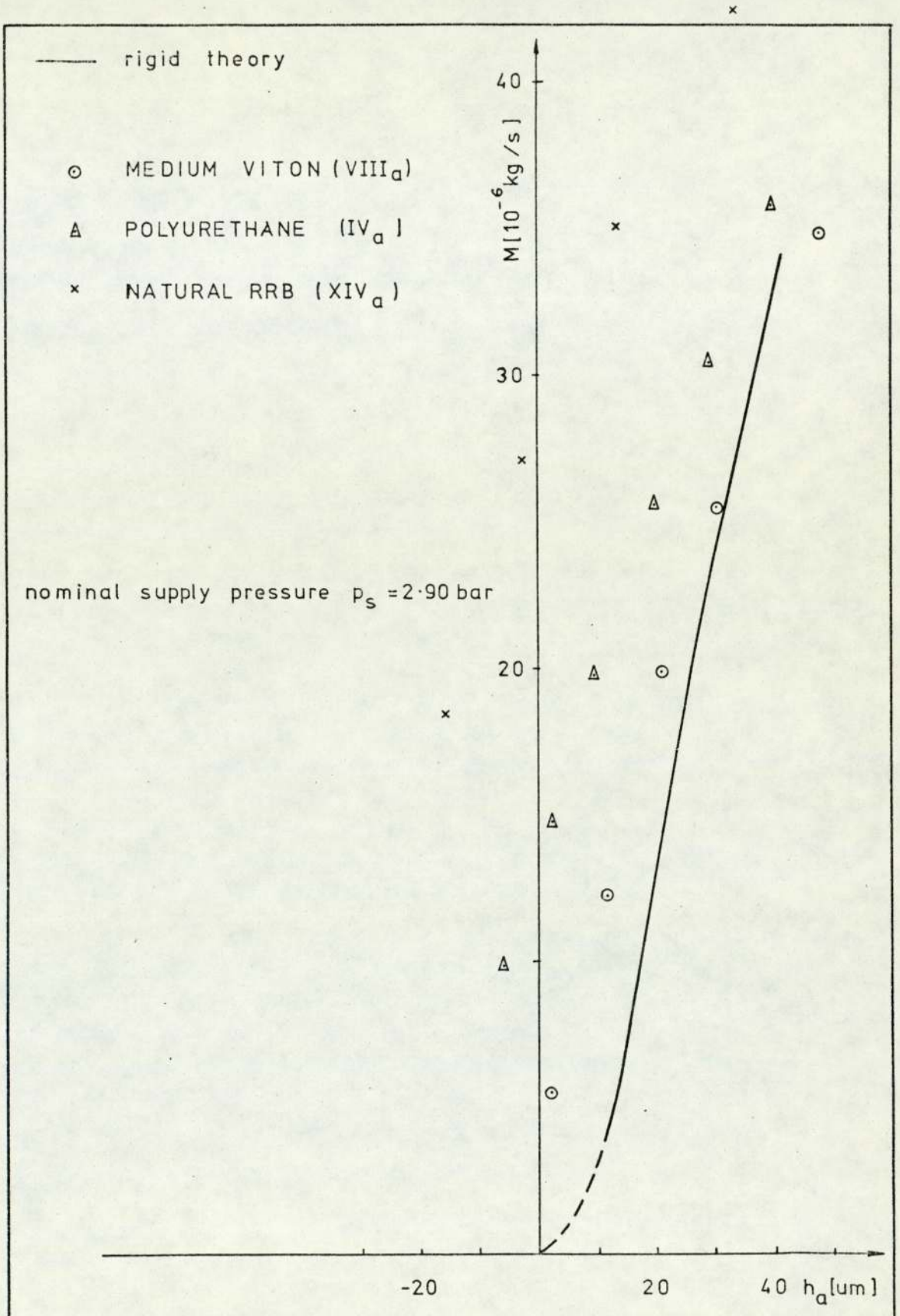

FLOW v APPARENT FILM THICKNESS
- UNBONDED ELASTOMERS

FIG 76

film thickness than flow rates of bonded bearings.

Similar deductions can be drawn for other nominal supply pressures investigated except that at the lowest pressure of 1.80 bar, rigid bearings are superior to unbonded compliant bearings.

Referring again to table VII-2 it has been discovered that elastomer thickness is a major variable to influence compressive characteristics of elastomers, particularly the ratio of compressive modulus of unbonded elastomers to compressive modulus ot bonded elastomers. A plot of this ratio with elastomer thickness is shown in fig. 77. It is seen that E_c (not bonded) $/E_c$(bonded) approaches unity for thin elastomers but it is 0.54 for elastomers 12.5mm thick. This is of importance when a bearing designer intends to use thick unbonded elastomers as bearing compliant materials.

Elastomer Diameter (Hardness and Thickness are approximately constant

In order to discuss this parameter, bearings I, II and III ("a" and "b") are chosen. They are natural rubber bearings made at Aston University.

Fig. 78 shows load against apparent clearance for bonded and unbonded compliant bearings of three diameters. The corresponding rigid theory lines are also shown.

Bonded bearings are superior than rigid theory, whilst the load of unbonded bearings is smaller than rigid load for a given film thickness.

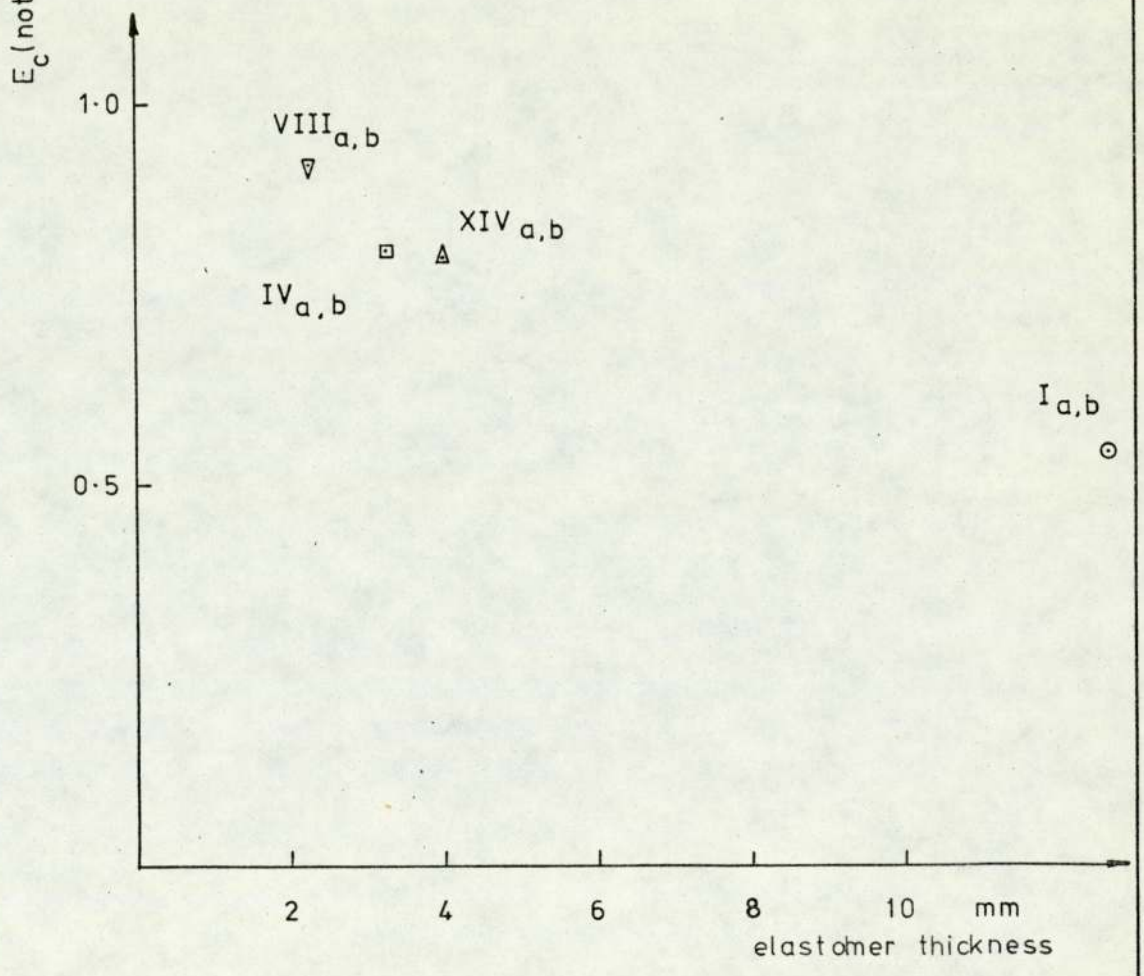

RATIO OF COMPRESSIVE ELASTIC MODULI v
ELASTOMER THICKNESS

FIG 77

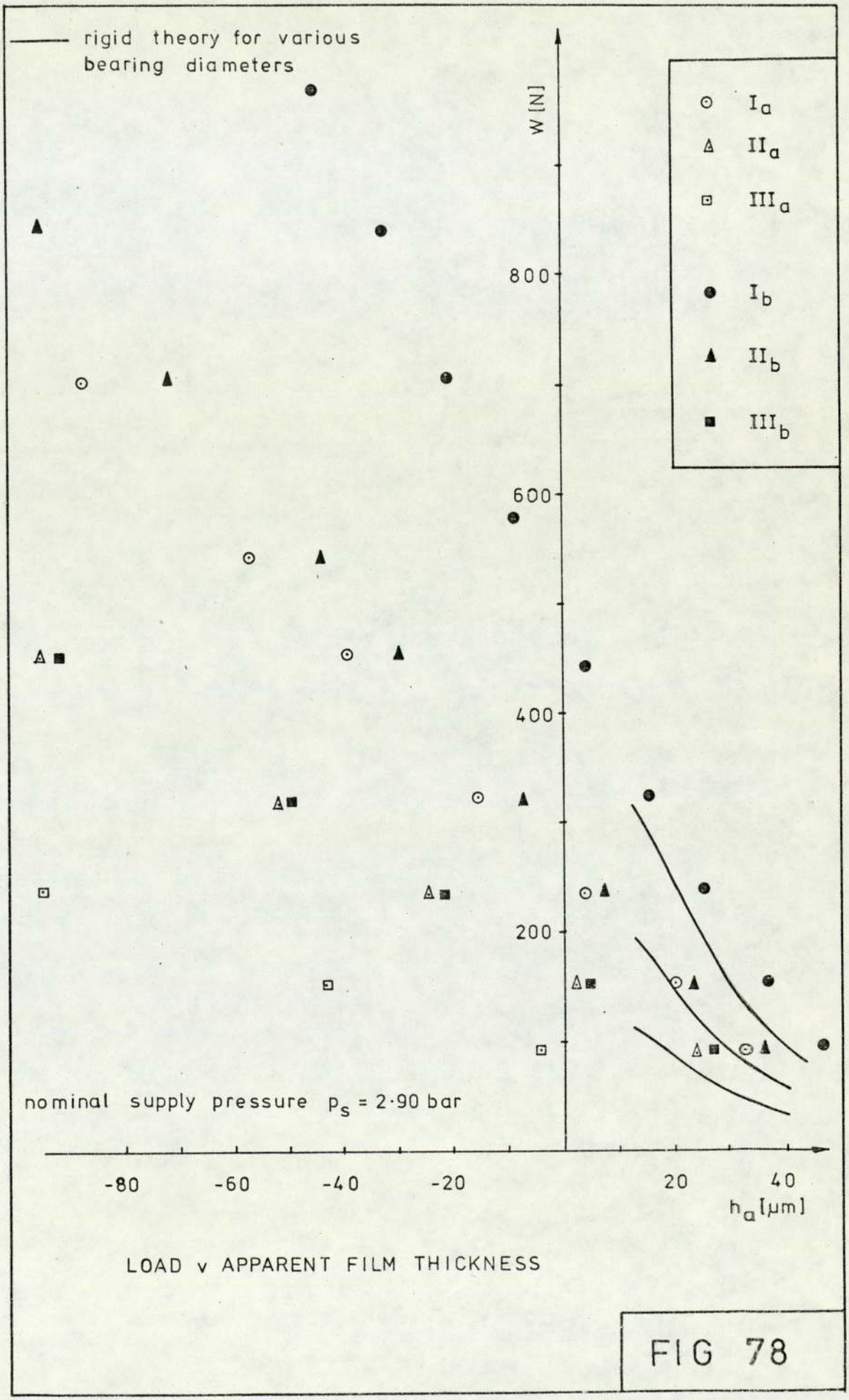

LOAD v APPARENT FILM THICKNESS

FIG 78

It is to be noted that elastomer thickness of bearings I, II and III is larger than with any other bearings investigated. Unbonded bearings of these large thicknesses are inferior because they "give" more under a given load, i.e. $\Sigma\Delta t$ is larger so that apparent film thickness becomes smaller. Referring also to fig. 77 it is concluded that the use of unbonded elastomers of large thicknesses is not justified because of their inferior performance.

Fig. 79 is a plot of flow rates v. apparent clearance of bonded and unbonded elastomers. Rigid theory (one line for all three diameters) is also presented. For a given clearance, flow rates are larger than predicted by rigid theory. Similarly as with bearings VIII, IV and XIV discussed previously gradients of lines drawn through the experimental flow points are less steep for unbonded bearings, i.e. flow rates of these bearings increase less rapidly with film thickness.

Fig. 80 shows the influence of the elastomer diameter upon the compressive elastic modulus. For bonded elastomers of larger diameters compressive moduli are larger than these moduli of unbonded elastomers of smaller diameters.

Temperature Effects

The temperature of the laboratory where experiments were performed was 21 ± 1°C. These small variations of temperature have an insignificant influence to elastomer properties.

However, certain elastomers were sometimes exposed to a temperature change when they were taken out of the laboratory for machining purposes or for profilometry measurements.

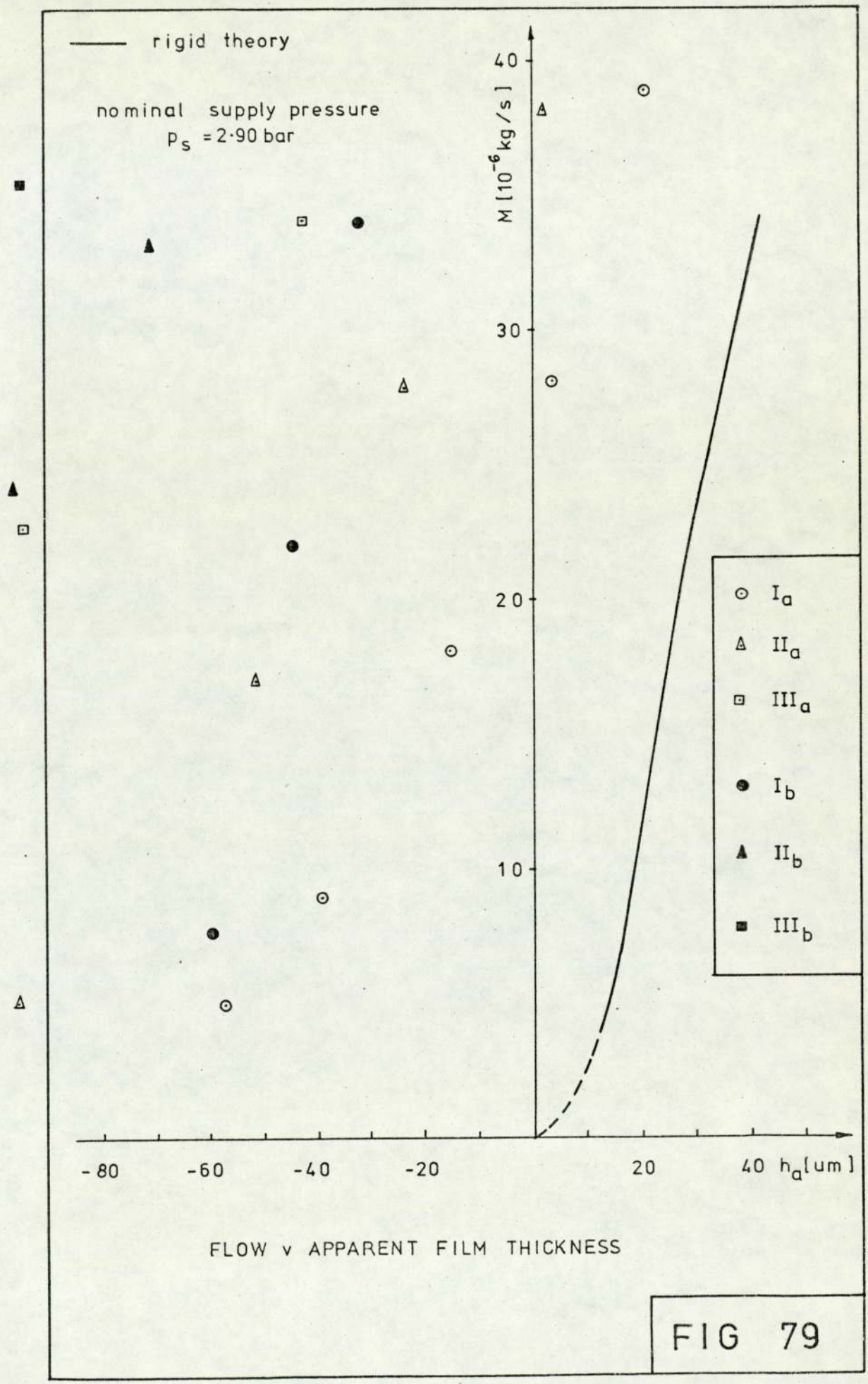

FLOW v APPARENT FILM THICKNESS

FIG 79

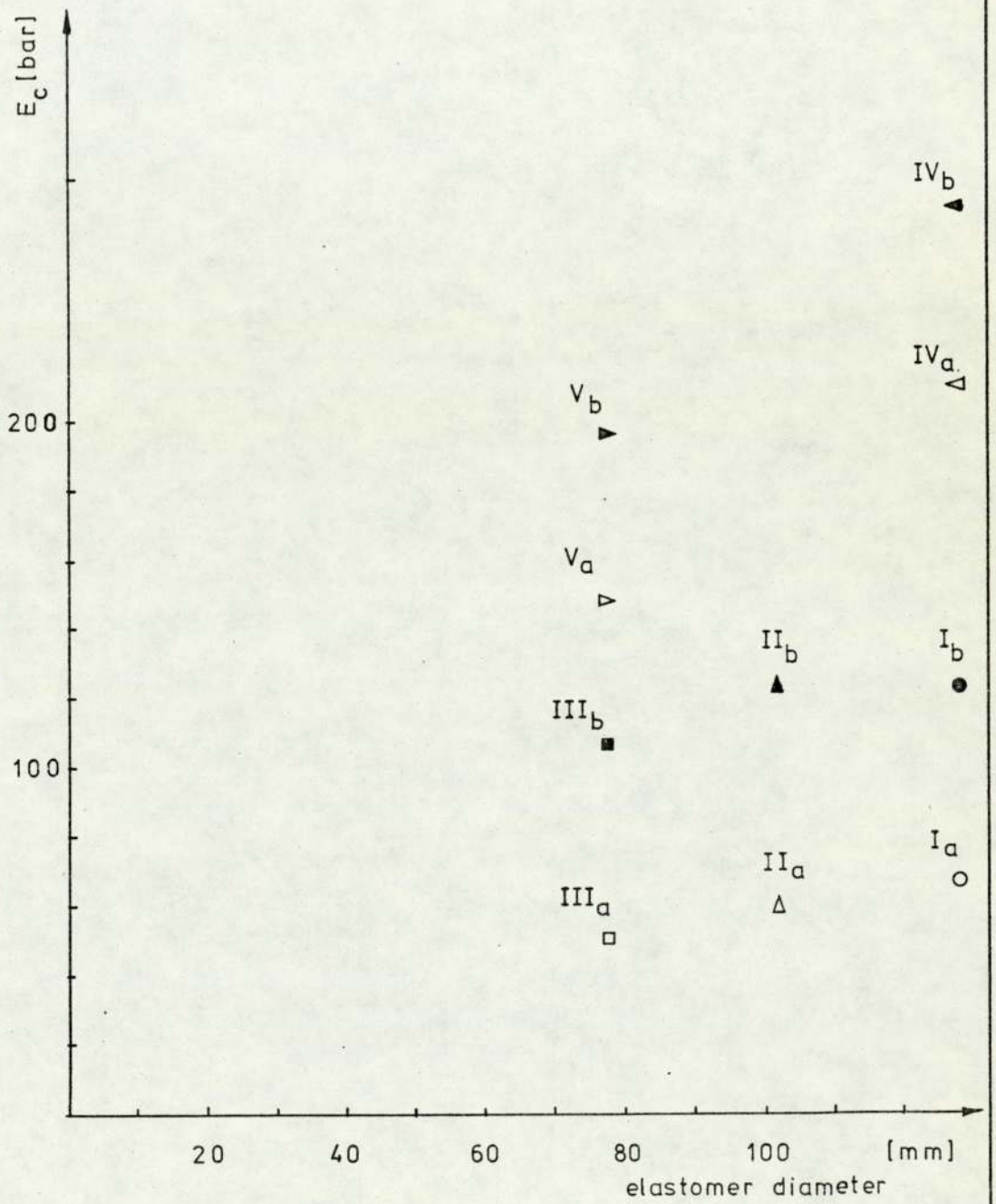

COMPRESSIVE MODULUS v
ELASTOMER DIAMETER

FIG 80

These changes in temperature induced stresses to elastomers and they made the bonded elastomers become concave with their unbonded free surface outwards. For example, for bearing I_b the difference between the elastomer thickness at the periphery and at the centre was once noticed to be 5-6 μm. Elastomers were then ground once more and care was taken that they were exposed to as small temperature changes as possible.

VIII CONCLUSIONS AND FUTURE WORK

Pioneering work of Dowson and Taylor [201], theoretical work of the Columbia group [202] to [206], experimental work of Lowe [210], work of Smith and Gupta [214] and [219] and work of other researchers have made significant contributions to the available knowledge of steady state compliant lubrication. However, there are still some areas within the steady state compliant lubrication that need to be investigated. Compliant lubrication under dynamic conditions still remains to be performed.

8.1 Steady Performance

The effect of compensation on the performance of rigid bearings has been reported [122] and [123]. Gas rigid bearings are investigated with inherent, orifice and slot (or capillary) compensation, see for example [13], section 10. Investigation of the effect of compensation on compliant bearings remains to be performed. From a practical point of view, inherent or capillary compensated bearings are better than the orifice compensated bearings with a port. The port brings instabilities to the bearing performance and should be avoided.

Work on bearing stiffness is closely connected to studies of various compensating elements. This property, for rigid bearings, was studied in [121] and [124] and some static stability criteria was given according to the type of compensating element used. The author of this thesis has experienced

very little, if any, instabilities of compliant bearings with an inherent restrictor. However, Lowe [211] has reported some instabilities and possibilities to extend this work to other restrictors and to derive a static stability criteria for various restrictors should be investigated.

Surface roughness effects have been extensively studied [130] to [136] for bearings with rigid surfaces. It is shown in this thesis that surface roughness effects should be taken into account in order to obtain agreement with rigid bearing theory. Lewis and Taylor [139] have investigated the performance of an elastic porous thrust bearing and they have taken roughness of the porous surface into account. Lau and Harman [212] have investigated a smooth compliant pad operating on a rough moving surface. It may be possible to extend these studies to the combined roughness effects of the rigid member and the compliant member. It is thought that the compliant flatness depends upon local film pressure. A simple model of estimating flatness from profilometry measurements, proposed for rigid bearings, cannot thus be used here.

If ambient temperature where tests are performed is kept constant temperature effects upon the elastomer properties need not be taken into account. It is envisaged that possible applications of compliant bearings will be in an environment with varying temperature. Lowe [210] reported thermal expansion coefficients of natural rubbers of various hardnesses. It seems worthwhile to extend this work to other elastomers. In connection with thermal effects, a study of ageing of various compliant materials should be performed.

Regarding the theoretical work, finite difference scheme presented in chapter III should be developed further. Finite elements methods are another possibility. A programme has been developed in the solid mechanics section of the Mechanical Engineering Department at Aston University under the supervision of Mr. T.H. Richards. This programme analyses axisymmetric solids of revolution and some encouraging results have been reported. A different formulation of this programme would enable almost incompressible and completely incompressible materials to be analysed.

8.2 Dynamic Performance

Dynamic operation of compliant air bearings is an obvious extension beyond steady state working and it is envisaged to consist of bearing tests under dynamic conditions and of testing elastomer properties under dynamic conditions. A possible schematic diagram for dynamic bearing tests is shown in fig. 81. As a first step, harmonic motion should be imposed on a bearing in order to find out how these applied sinusoidal movements affect the bearing performance. At a later date random vibrations, more likely to be encountered in practical applications could also be investigated.

The author had hoped at the beginning of this research project to do some dynamic tests but it was soon discovered that that aim was too ambitious. However, some work to test elastomer properties under dynamic conditions has been carried out.

That work has been carried out by using the existing departmental setup for testing properties of solid propellents

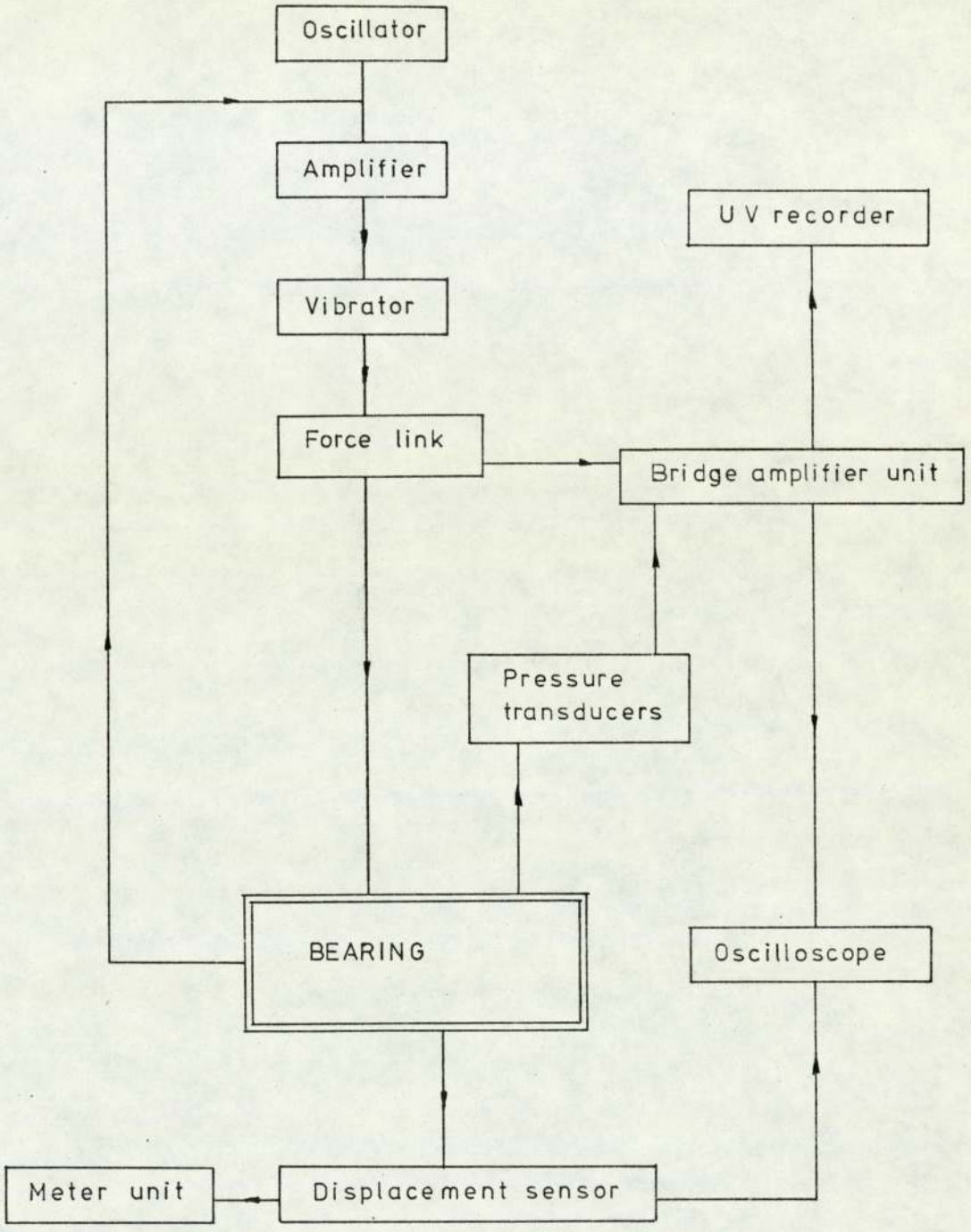

BEARING TESTS UNDER DYNAMIC CONDITIONS

FIG 81

under dynamic conditions, which is shown in fig. 82.

A mathematical model of longitudinal vibrations with end masses was used as a basis for these investigations [316]. The analysis is equally valid for forced vibrations of a viscoelastic rod except that elastic modulus E is replaced by a complex modulus E*. Measurements are performed by keeping the force constant whilst the acceleration and phase are varied with frequency. The set of results of one measurement is given in table VIII-1. Figures 83 and 84 give plots of elastomer acceleration and phase (between force and acceleration) with frequency.

A computer programme developed by the author of reference [316] is then used to analyse these data. Results are given as components of the complex modulus (E_1 - real modulus, E_2 - loss modulus) in fig. 85. The material tested was natural rubber made at Aston University and the mould for this rubber is shown in photograph XV. The mould was made at the University workshops.

Figures 83 and 85 show that the first resonant frequency is around 160 [Hz] and this region should be avoided in practical applications of compliant bearings lined with elastomers whose dynamic properties are similar to the natural rubber investigated. Also for elastomers of this type as a first approximation it can be taken that the real modulus is independent of frequency. This may considerably simplify the theoretical analysis of compliant surface aerostatic thrust bearings under dynamic conditions.

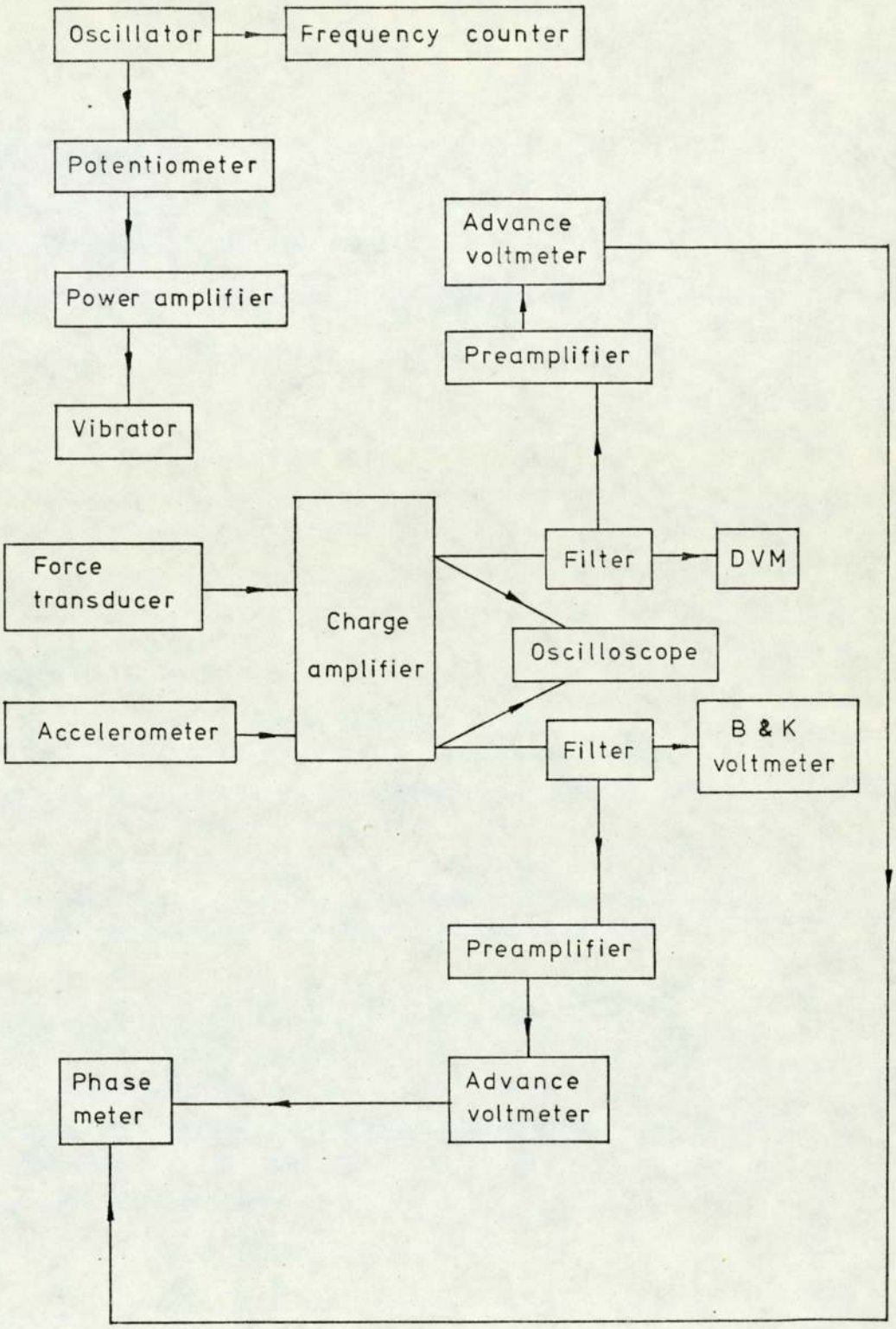

MEASUREMENT OF DYNAMIC MODULUS OF ELASTOMERS

FIG 82

TEST OF ELASTOMER PROPERTIES UNDER DYNAMIC CONDITIONS -

The force (volts) is kept constant and equal to 0.4 V

Frequency	acc^n		phase	
	volts	g	o	radians
1000	0.82	1.04	25	-16.14
980	0.92	1.17	1	-15.73
960	1.03	1.31	344	-15.43
940	1.21	1.53	321	-15.03
920	1.39	1.76	299	-14.61
900	1.60	2.03	277	-14.26
880	1.79	2.27	257	-13.91
860	1.88	2.38	236	-13.54
840	1.99	2.52	215	-13.18
820	2.02	2.56	199	-12.90
800	2.22	2.81	180	-12.57
780	2.49	3.16	166	-12.32
760	2.82	3.57	145	-11.96
740	3.30	4.18	126	-11.62
720	3.85	4.88	101	-11.19
700	4.10	5.20	71	-10.66
680	4.05	5.13	51	-10.31
660	3.82	4.84	37	-10.07
640	3.65	4.63	20	-9.77
620	3.80	4.82	10	-9.60
600	4.20	5.32	355	-9.34
580	5.00	6.34	345	-9.16

Frequency	acc^n		phase	
	volts	g	^{o}	radians
560	6.30	7.98	329	-8.88
540	7.70	9.76	309	-8.53
520	8.90	11.28	268	-7.82
500	7.90	10.01	238	-7.30
480	6.25	7.92	217	-6.93
460	5.50	6.97	206	-6.74
440	5.38	6.82	195	-6.54
420	5.53	7.01	185	-6.37
400	6.02	7.63	178	-6.25
380	7.46	9.46	170	-6.11
360	11.00	13.94	157	-5.88
350	14.90	18.88	145	-5.67
340	20.00	25.35	108	-5.03
330	20.00	25.35	88	-4.68
320	15.60	19.77	56	-4.12
300	9.40	11.91	30	-3.67
280	6.75	8.56	20	-3.49
260	5.50	6.97	16	-3.42
240	5.82	7.38	18	-3.46
220	6.40	8.11	8	-3.28
200	8.15	10.33	3	-3.19
180	12.30	15.59	355	-3.05
170	21.40	27.12	351	-2.98
160	45.20	57.29	297	-2.04
155	36.8	46.66	244	-1.12

Frequency	acc^{n}			phase	
	volts		g	o	radians
150	23.00		29.15	221	-0.72
140	10.75		13.62	203	-0.40
120	5.60		7.10	197	-0.30
110	4.40		5.58	193	-0.23

TABLE VIII-1

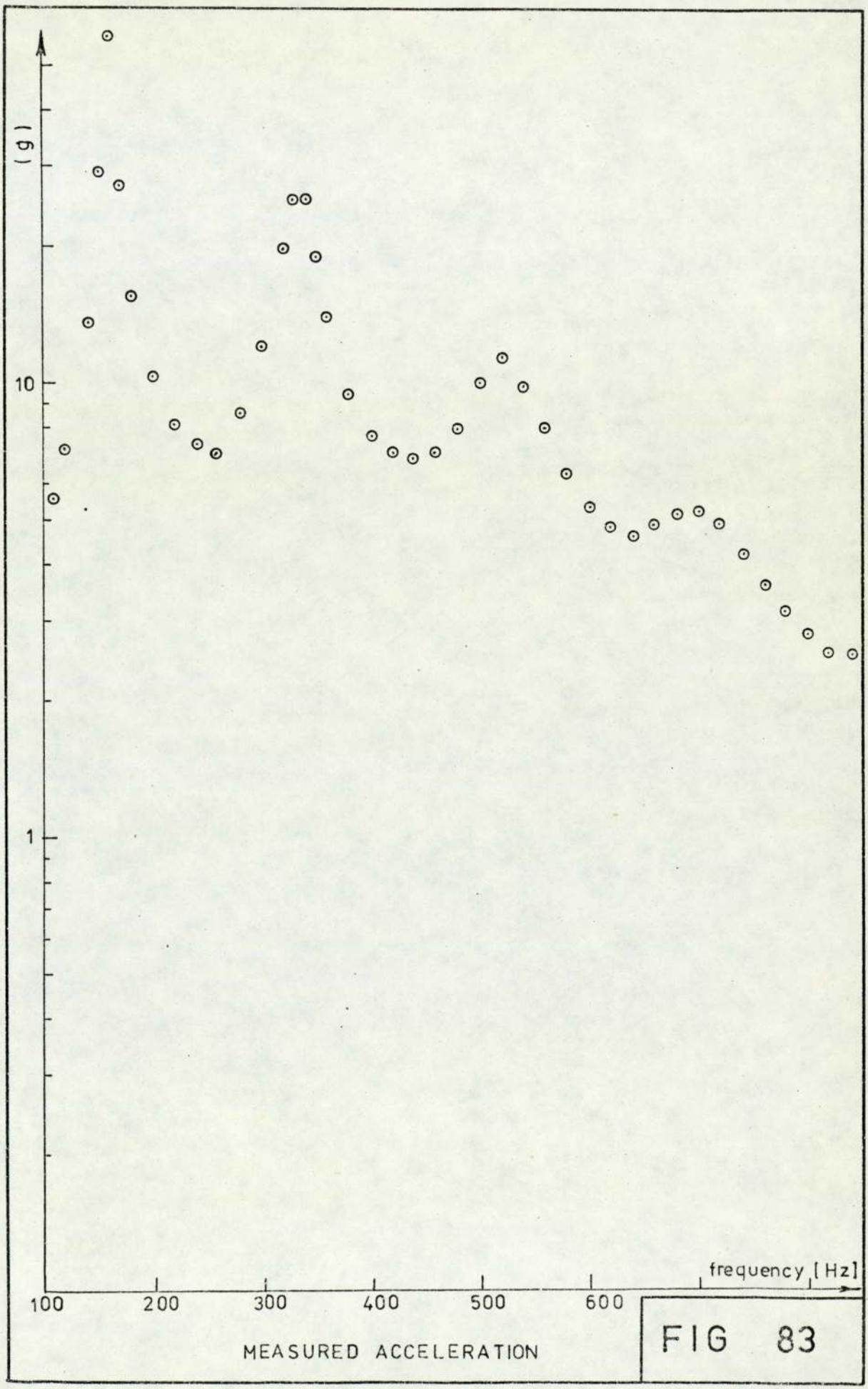

MEASURED ACCELERATION

FIG 83

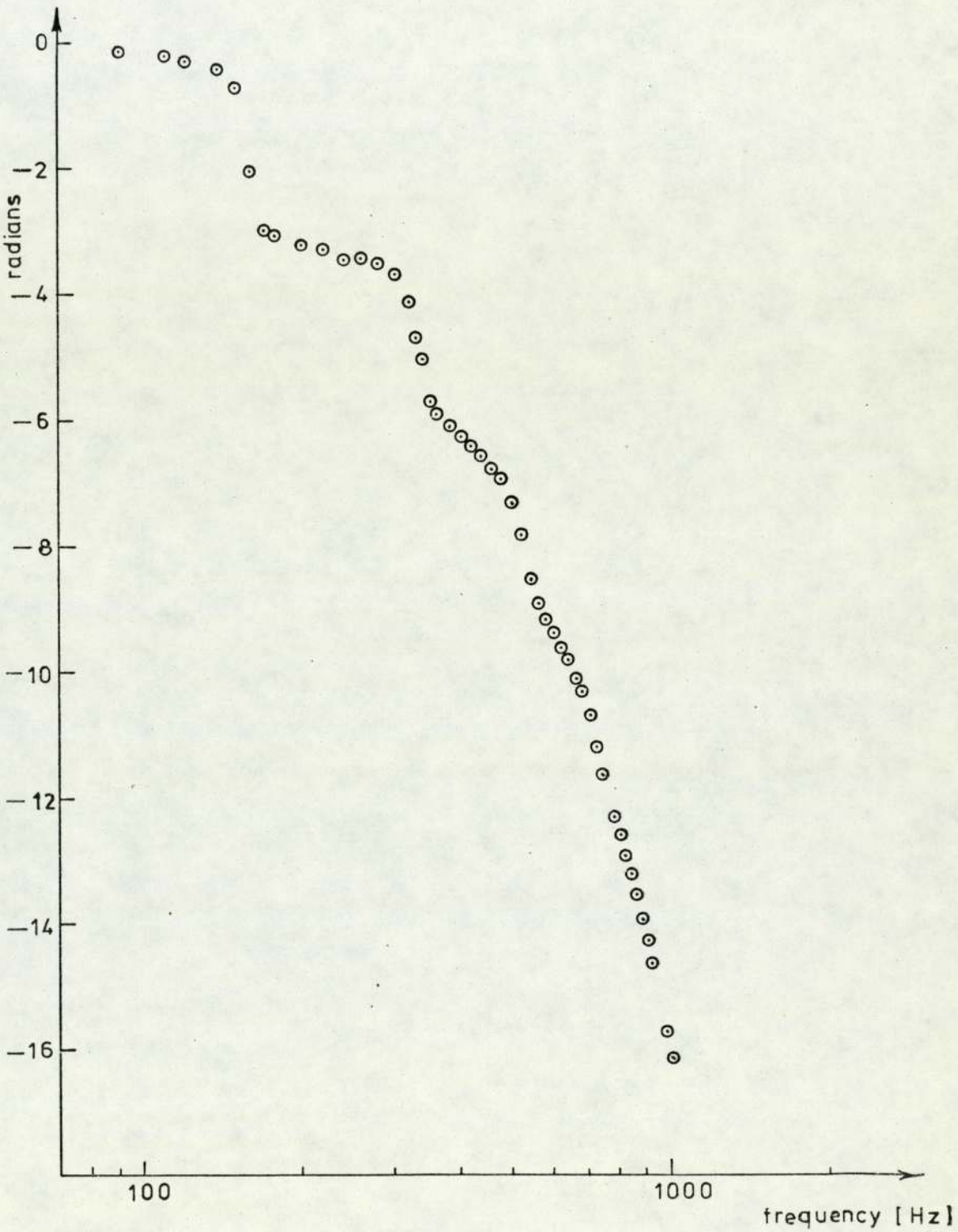

MEASURED PHASE

FIG 84

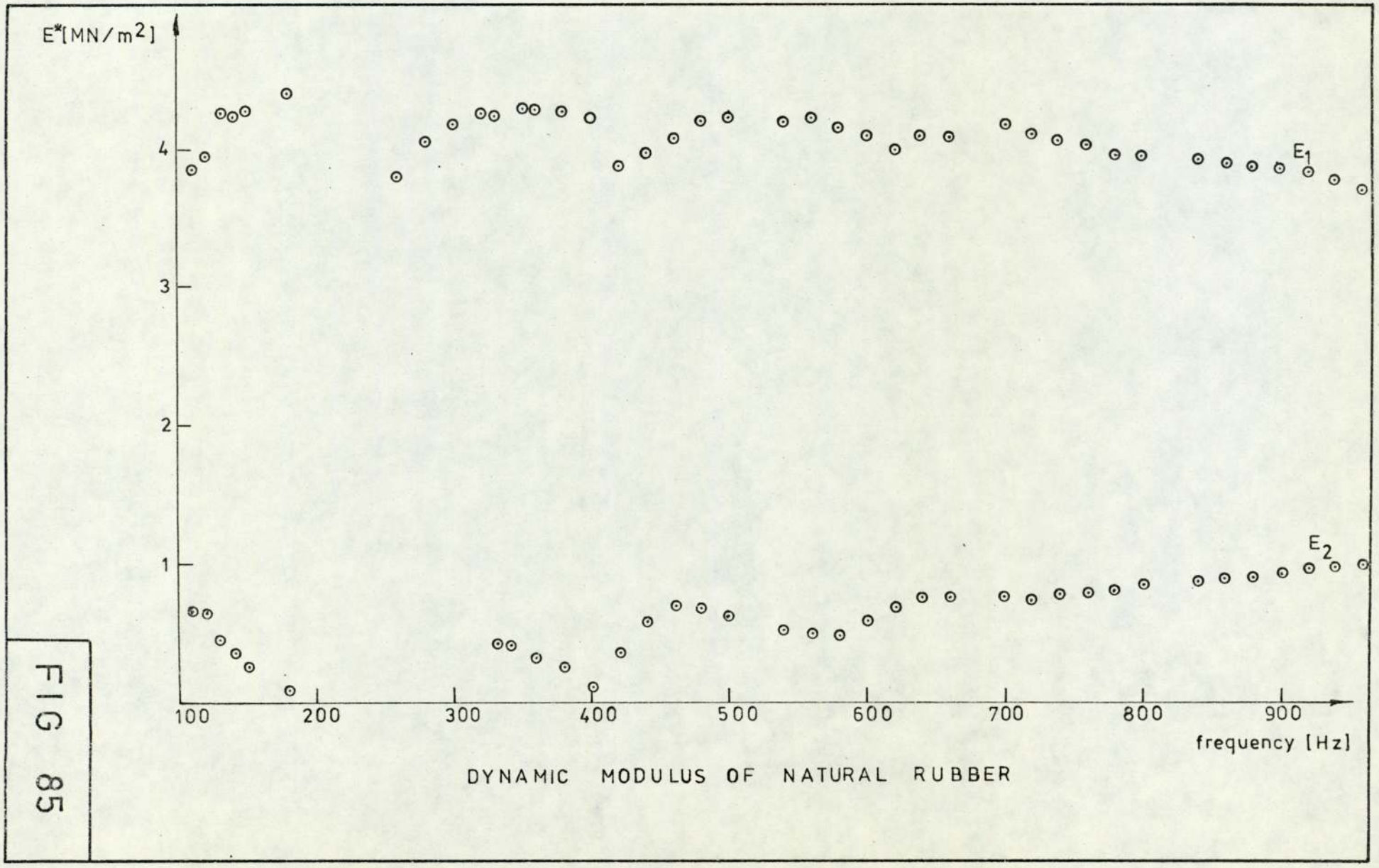

DYNAMIC MODULUS OF NATURAL RUBBER

FIG 85

PHOTOGRAPH XV

APPENDIX I

RIGID BEARING THEORY

AI.1 Assumptions

The assumptions on which the following analysis rests can be stated:

(a) Shear stress in the lubricant is directly proportional to the rate of shear, i.e. the lubricant is a Newtonian fluid.

(b) Inertia and body force terms in the equations of motion are negligible compared to the pressure and viscous terms.

(c) The variation of pressure across the lubricant film (in z or axial direction) is negligible. Furthermore, since axial symmetry is assumed, film pressure is a function of radius only.

(d) Velocity derivatives across the film thickness (in z direction) are large compared to all other velocity gradients.

(e) Air temperature varies very little during the operation of these bearings, and air can be taken to be isoviscous.

(f) Air is taken to be a perfect gas.

(g) There is no slip at the boundaries of the air film.

(h) Because of almost isothermal conditions, air pressure is proportional to air density.

AI.2 Volumetric and Mass Flow Rates

Equations of motion (Navier-Stokes equations) in general state:

Inertia = body force + pressure force + viscous resistance.

Referring to assumptions AI.1:

$$0 = 0 - \frac{\partial p}{\partial r} + \frac{\partial}{\partial z}\left(\eta \frac{\partial v_r}{\partial z}\right)$$

or

$$\frac{d^2 v_r}{dz^2} = \frac{1}{\eta} \frac{dp}{dr}$$

which can be integrated twice to give

$$v_r = \frac{1}{2\eta} \frac{dp}{dr}(hz - z^2) \qquad \text{(I-1)}$$

Constants of the above integrations are determined from a statement of the surface velocities of the solids bounding the film (no slip flow).

Volumetric flow per unit length in the radial direction:

$$q_r = \int_0^h v_r \, dz = - \frac{1}{2\eta} \frac{dp}{dr} \frac{h^3}{6} \qquad \text{(I-2)}$$

Total volumetric flow around the circumference of the bearing at radius r:

$$Q = 2\pi r q_r = - \frac{\pi r}{\eta} \cdot \frac{\frac{d}{dr}(p^2)}{2p} \cdot \frac{h^3}{6} \qquad \text{(I-3)}$$

In order to calculate film pressures, Reynolds equation is used. This basic equation of fluid film lubrication is derived from equations of motion and continuity. It represents conservation of mass for the fluid in the bearing and it states:

Poiseuille flow (pressure flow) =

= Couette flow (velocity flow) + squeeze flow + local compression flow.

Couette flow disappears when radial velocity components of solid bearing surfaces are zero. For steady-state problems resultant squeeze velocity and fluid density derivative with respect to time are zero so that both squeeze flow and local compression flow disappear. Reynolds equation therefore consists of pressure flow only. In cylindrical polar coordinates it is equal to:

$$\frac{\partial}{\partial r}\left(\frac{\rho h^3}{12\eta} r \frac{\partial p}{\partial r}\right) = 0 \qquad \text{(I-4)}$$

Following assumptions AI.1 and for a uniform film bearing, the above Reynold equation reduces to:

$$\frac{d}{dr}\left[r \frac{d}{dr}\left(p^2\right)\right] = 0 \qquad \text{(I-5)}$$

This equation describes the film pressure p of aerostatic thrust bearings in the bearing land, from port radius r_p where pressure $p = p_p$ to outer radius r_o where

pressure is ambient, $p = p_a$.

It is often advantageous to work in dimensionless form and the following definitions are introduced, see fig.I-1.

$$\left.\begin{aligned} R_p &= r_p/r_o \\ R &= r/r_o \\ P_p &= p_p/p_a \\ P &= p/p_a \end{aligned}\right\} \qquad (I\text{-}6)$$

By means of the above definitions Reynolds equation can be written as:

$$\frac{d}{dR}\left[R\,\frac{d}{dR}\left(P^2\right)\right] = 0 \qquad (I\text{-}7)$$

which can be integrated twice to give -

$$P^2 = 1 + \frac{P_p^2 - 1}{\ell n R_p}\,\ell n R \qquad (I\text{-}8)$$

Constants of the above integrations are evaluated from boundary conditions shown on fig.I-1.

From (I-8):

$$\frac{d}{dR}(P^2) = \frac{P_p^2 - 1}{\ell n R_p} \times \frac{1}{R} \qquad (I\text{-}9)$$

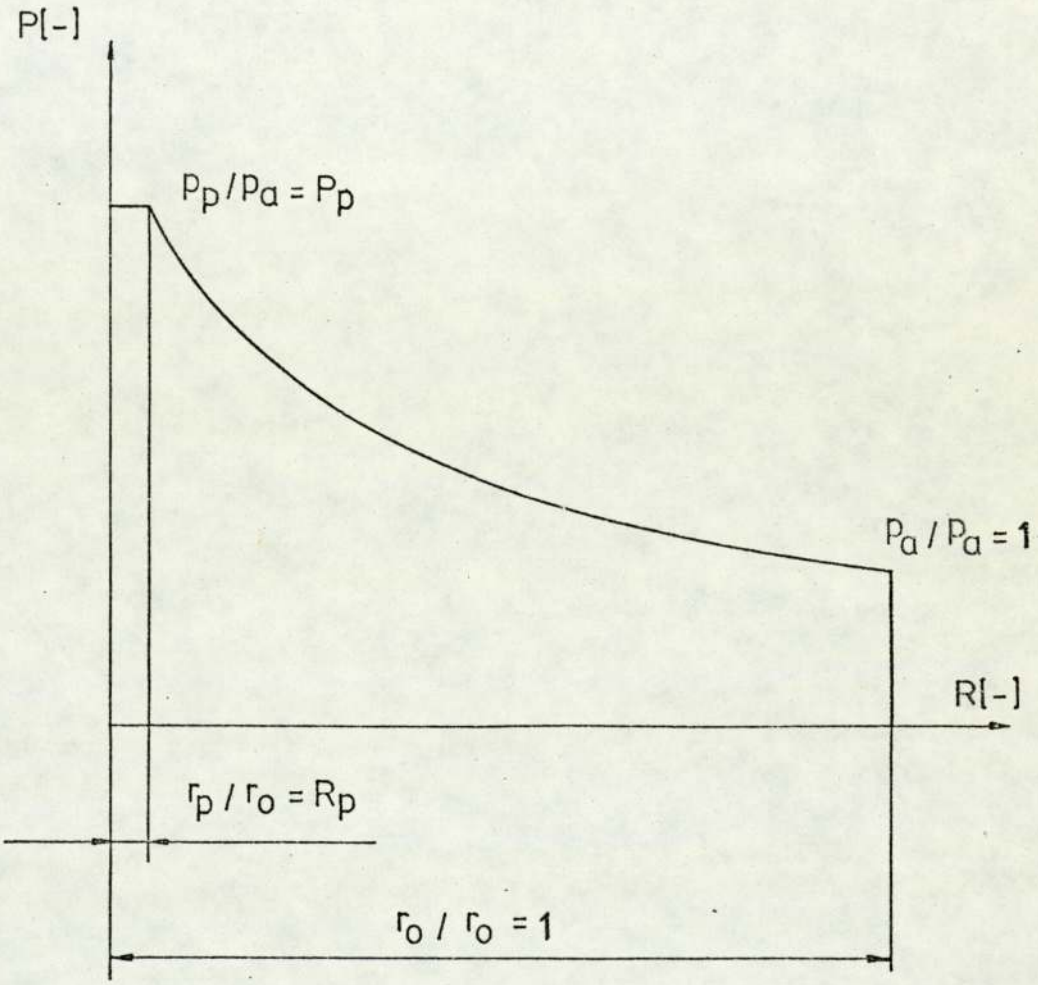

$P = 1$, $R = 1$

$P = P_p$, $R = R_p$

BOUNDARY CONDITIONS

FIG I-1

In dimensional form equations (I-8) and (I-9) become:

$$p^2 = p_a^2 + \frac{p_p^2 - p_a^2}{\ell n(r_p/r_o)} \ell n(r/r_o) \qquad \text{(I-10)}$$

$$\frac{d}{dr}(p^2) = \frac{p_p^2 - p_a^2}{\ell n(r_p/r_o)} \times \frac{1}{r} \qquad \text{(I-11)}$$

From equations (I-3) and (I-11), the volumetric flow becomes:

$$Q = - \frac{\pi}{12\eta p} h^3 \times \frac{p_p^2 - p_a^2}{\ell (r_p/r_o)} \qquad \text{(I-12)}$$

and mass flow

$$M = \frac{pQ}{R_a T_a} = - \frac{\pi}{12\eta R_a T_a} h^3 \frac{(p_p^2 - p_a^2)}{\ell n(r_p/r_o)} \qquad \text{(I-13)}$$

From equation (I-12) it is seen that the product of volumetric flow and film pressure does not depend upon bearing radius. This product can be taken at port radius and outer radius to give:

$$Q \times p = Q_p \times p_p = Q_a \times p_a$$

$$= - \frac{\pi h^3 (p_p^2 - p_a^2)}{12\eta \ell n(r_p/r_o)} \qquad \text{(I-14)}$$

From equation (I-13), for given ambient conditions and bearing geometry, mass flow depends upon the film thickness and port pressure.

Ambient conditions are taken from one of bearing tests and they are:

$$p_a = 1.0039 \quad \text{bar}$$
$$T_a = 294.15^{\circ}K$$

the bearing geometry is:

$$R_p = \frac{r_p}{r_o} = \frac{0.28575\text{mm}}{64.135\ \text{mm}} = 0.004455$$

Three typical values of port pressures corresponding to the bearing tests are chosen and mass flow is calculated for a range of film thickness up to 30μm, which is the range encountered during the rigid bearing experiments. Figures I-2 and I-3 represent plots of mass flow against film thickness and against port pressure respectively.

AI.3 Bearing Load

From equation (I-8), film pressure:

$$P = \frac{p}{p_a} = \left[1 + \frac{(p_p^2 - 1)}{\ell n\ R_p} \ell nR\right]^{\frac{1}{2}} \qquad \text{(I-15)}$$

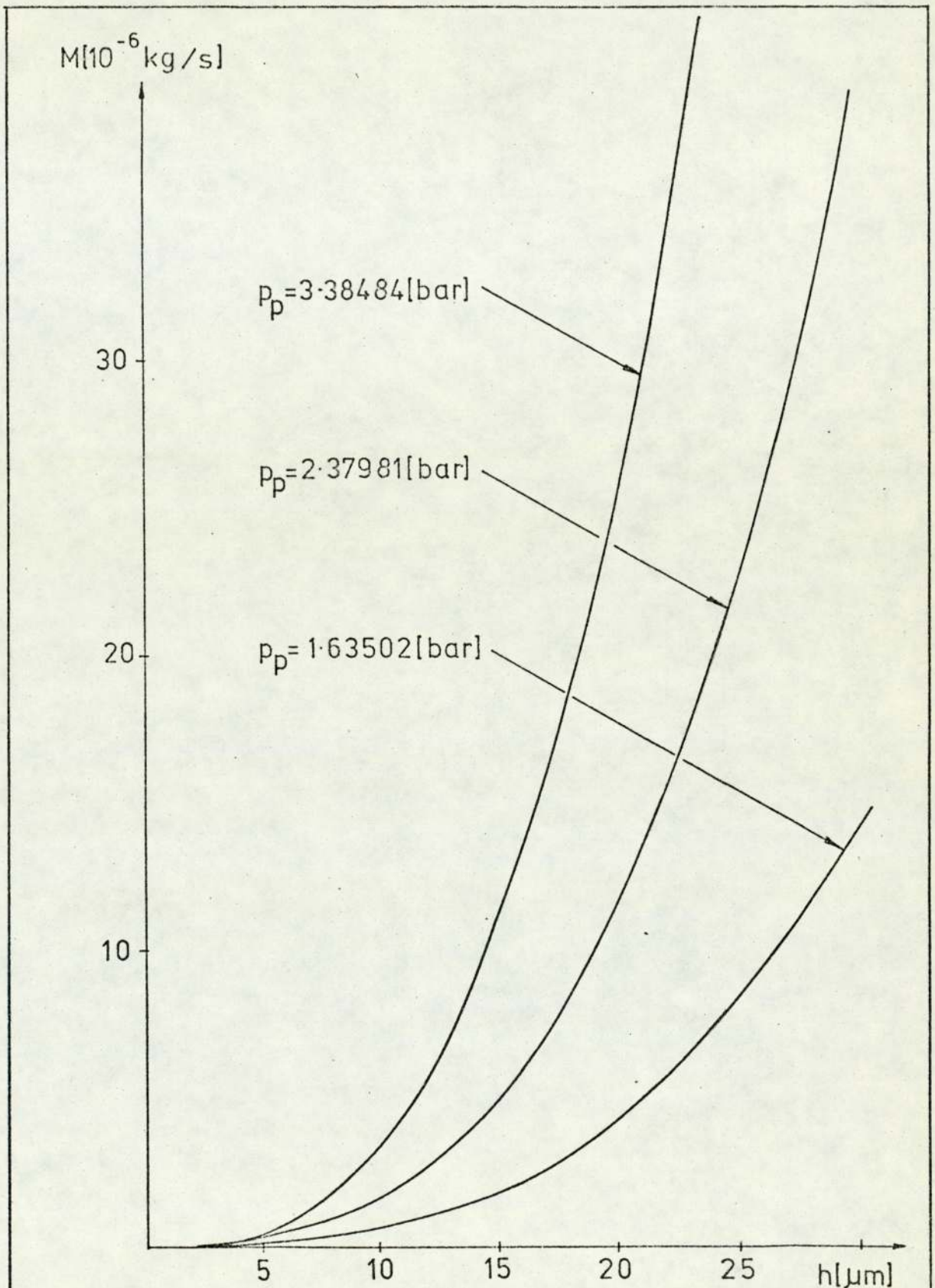

MASS FLOW V. FILM THICKNESS

FIG I-2

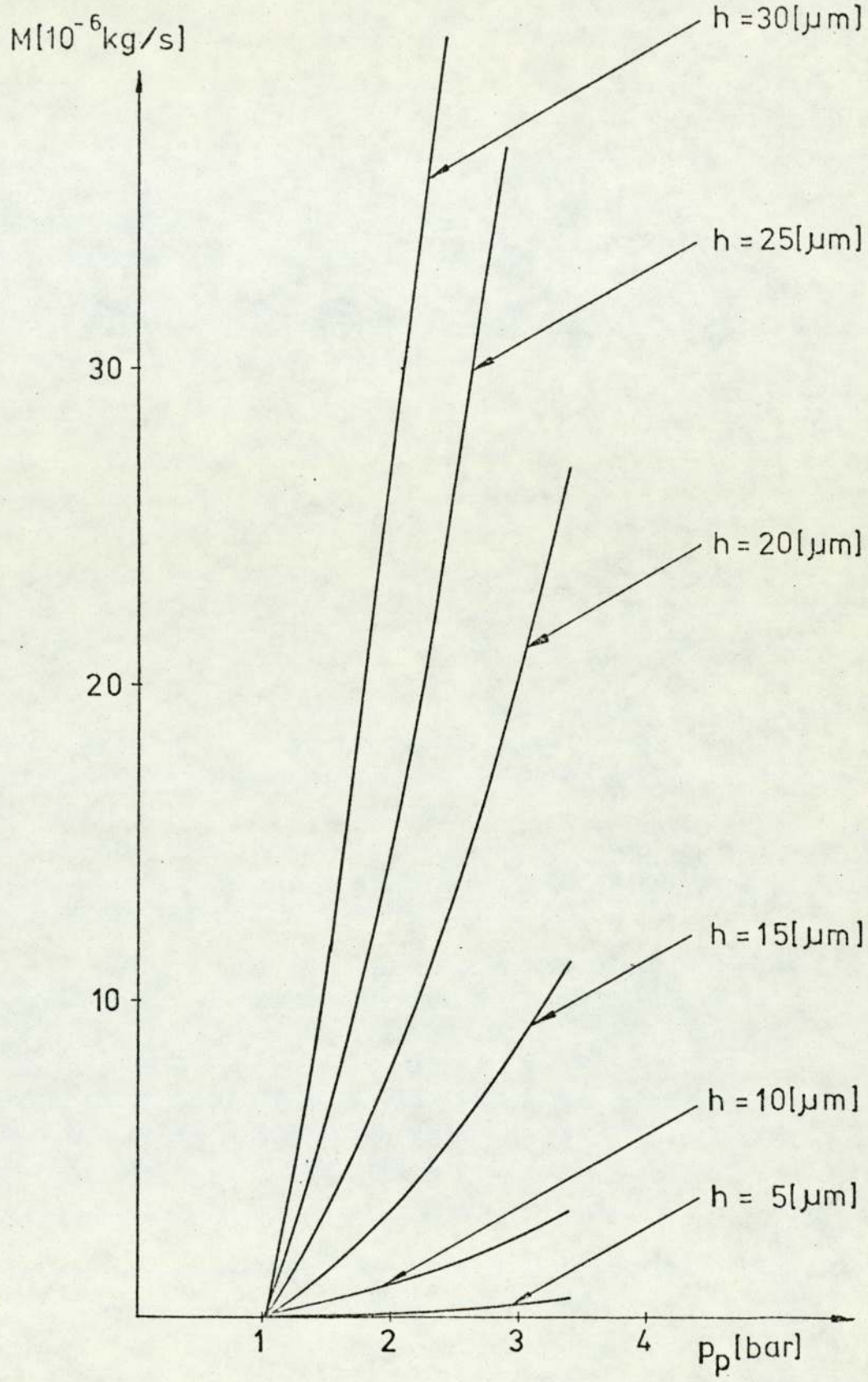

MASS FLOW V. PORT PRESSURE

FIG I-3

Load is given as:

$$W = \pi r_p^2 p_p + 2\pi \int_{r_p}^{r_o} pr\, dr - \pi r_o^2 p_a$$

$$= \pi r_p^2 p_p + 2\pi p_a r_o^2 \int_{R_p}^{1} PR\, dR - \pi r_o^2 p_a \qquad \text{(I-16)}$$

Consider dimensionless load defined as

$$\overline{W} = \frac{W}{\pi r_o^2 p_a} = \frac{r_p^2}{r_o^2}\frac{p_p}{p_a} + 2\int_{R_p}^{1} PR\, dR - 1$$

$$= R_p^2 P_p + 2\int_{R_p}^{1} PR\, dR - 1 \qquad \text{(I-17)}$$

Take

$$I = \int_{R_p}^{1} PR\, dR = \int_{R_p}^{1} \left(1 - \frac{1 - P_p^2}{\ell n R_p}\, \ell n R\right)^{\frac{1}{2}} R\, d\, R \qquad \text{(I-18)}$$

and

$$A_2^2 = \frac{1 - P_p^2}{2\ell n\, R_p} \quad . \qquad \text{(I-19)}$$

Take

$$A_2 \xi \equiv (1 - 2A_2^2 \ell n R)^{\frac{1}{2}}$$

so that

$$A_2^2\xi^2 = 1 - 2A_2^2 \ell nR \qquad \text{(I-20)}$$

and

$$\ell nR = \frac{1}{2A_2^2} - \frac{1}{2}\xi^2$$

then

$$dR = e^{\frac{1}{2A_2^2}} \times e^{-\frac{\xi^2}{2}} \times -\frac{2\xi}{2} d\xi$$

$$= -e^{\frac{1 - A_2^2\xi^2}{2A_2^2}} \xi d\xi$$

Limits ξ_1 and ξ_2 are calculated from:

$$R = R_p, \qquad \xi = \xi_1$$

$$R = 1, \qquad \xi = \xi_2$$

From (I-20)

$$A_2^2\xi_1^2 = 1 - \frac{1 - P_p^2}{\ell nR_p} \ell nR_p$$

so that

$$\xi_1 = \frac{P_p}{A_2} \qquad \text{(I-21)}$$

Similarly

$$\xi_2 = \frac{1}{A_2} \qquad \text{(I-22)}$$

Now

$$I = \int_{R_p}^{1} (1-2A_2^2 \ell nR)^{\frac{1}{2}} RdR$$

$$= \int_{\xi_1}^{\xi_2} A_2 \xi e^{\frac{1-A_2^2\xi^2}{2A_2^2}} \times - e^{\frac{1-A_2^2\xi^2}{2A_2^2}} \xi d\xi$$

$$= - A_2 e^{\frac{1}{A_2^2}} \int_{\xi_1}^{\xi_2} e^{-\xi^2} \xi^2 d\xi \qquad \text{(I-23)}$$

Equation (I-23) can be written slightly differently by considering

$$d(e^{-\xi^2}) = e^{-\xi^2} \times -2\xi d\xi,$$

so that:

$$I = \frac{A_2}{2} e^{\frac{1}{A_2^2}} \int_{\xi_1}^{\xi_2} \xi d(e^{-\xi^2}).$$

By integrating partially taking

$$\xi = u \qquad \text{and} \qquad d(e^{-\xi^2}) = dv$$

$$I = \frac{A_2}{2} e^{\frac{1}{A_2^2}} \left(\xi_2 e^{-\xi_2^2} - \xi_1 e^{-\xi_1^2} - \int_{\xi_1}^{\xi_2} e^{-\xi^2} d\xi \right) \qquad \text{(I-24)}$$

Error function between limits ξ_1 and ξ_2 is defined as:

$$\text{erf } \xi_2 - \text{erf } \xi_1 = \frac{2}{\sqrt{\pi}} \int_{\xi_1}^{\xi_2} e^{-\xi^2} d\xi$$

so that the last integral of (I-24) becomes:

$$\int_{\xi_1}^{\xi_2} e^{-\xi^2} d\xi = \frac{\sqrt{\pi}}{2}\left(\text{erf}\xi_2 - \text{erf}\xi_1\right) \qquad \text{(I-25)}$$

Now, from (I-21) and (I-22):

$$\xi_2 e^{-\xi_2^2} - \xi_1 e^{-\xi_1^2} = \frac{1}{A_2} e^{-\frac{1}{A_2^2}} - \frac{P_p}{A_2} e^{-\frac{P_p^2}{A_2^2}}$$

so that equation (I-24) reduces to:

$$I = \tfrac{1}{2} e^{\left(\frac{1}{A_2^2} - \frac{1}{A_2^2}\right)} - \frac{P_p}{2} e^{\left(\frac{1}{A_2^2} - \frac{P_p^2}{A_2^2}\right)}$$

$$- \frac{A_2}{2} e^{\frac{1}{A_2^2}} \frac{\sqrt{\pi}}{2}\left[\text{erf}\left(\frac{1}{A_2}\right) - \text{erf}\left(\frac{P_p}{A_2}\right)\right].$$

The second term of the above equation can be written as

$$\frac{P_p}{2} e^{\frac{1 - P_p^2}{A_2^2}} = \frac{P_p}{2} e^{\frac{(1-P_p^2) \times 2\ell n R_p}{(1-P_p^2)}}$$

$$= \frac{P_p}{2}\left(e^{\ell n R_p} \times e^{\ell n R_p}\right) = \frac{P_p}{2} R_p^2$$

Integral I originally given by equation (I-18) reduces to:

$$I = \tfrac{1}{2} - \frac{P_p}{2} R_p^2 + \frac{A_2}{2} e^{\frac{1}{A_2^2}} \frac{\sqrt{\pi}}{2} \left[\operatorname{erf}\left(\frac{P_p}{A_2}\right) - \operatorname{erf}\left(\frac{1}{A_2}\right) \right] \qquad \text{(I-26)}$$

Now dimensionless load:

$$\overline{W} = R_p^2 P_p + 2I - 1$$

$$= A_2 e^{\frac{1}{A_2^2}} \frac{\sqrt{\pi}}{2} \left[\operatorname{erf}\left(\frac{P_p}{A_2}\right) - \operatorname{erf}\left(\frac{1}{A_2}\right) \right] \qquad \text{(I-27)}$$

Clearly this equation contains the expression $e^{\frac{1}{A_2^2}}$ and this can be shown to equal $R_p^2 e^{(\frac{P_p}{A_2})^2}$ as follows

$$R_p^2 e^{\left(\frac{P_p}{A_2}\right)^2} = R_p^2 e^{\left(\frac{P_p^2 \times 2\ell n\, R_p}{1 - P_p^2}\right)} = e^{2\ell n R_p} \times e^{\frac{P_p^2 \times 2\ell n\, R_p}{1 - P_p^2}}$$

$$= e^{\frac{(1-P_p^2) \times 2\ell n R_p + P_p^2 \times 2\ell n R_p}{(1 - P_p^2)}}$$

$$= e^{\frac{2\ell n R_p}{(1-P_p^2)}} = e^{\frac{1}{A_2^2}} .$$

Therefore an alternative expression for the dimensionless load $\overline{W}$ is:

$$\overline{W} = R_p^2 e^{\left(\frac{P_p}{A_2}\right)^2} \times A_2 \frac{\sqrt{\pi}}{2} \left[\operatorname{erf}\left(\frac{P_p}{A_2}\right) - \operatorname{erf}\left(\frac{1}{A_2}\right) \right] \qquad \text{(I-28)}$$

as shown by Gross [108].

From (I-27) and (I-28) it can be seen that the bearing load is a function of port pressure. From (I-19), A_2 is a function of bearing geometry and port pressure. For a given bearing and a given port pressure $\left(\frac{P_p}{A_2}\right)$ and $\left(\frac{1}{A_2}\right)$ are known. Then, the probability or error functions of $\left(\frac{P_p}{A_2}\right)$ and $\left(\frac{1}{A_2}\right)$ can be either looked up in the tables or obtained through a computer by calling a corresponding library function. The disadvantage of the tables is that extrapolation can cause errors.

An alternative approach to determine bearing load is to start from the equation (I-17) and determine the integral I by means of Simpson's Rule. A small BASIC programme to do this is written and used on the departmental computer. Programme flow chart is as follows:

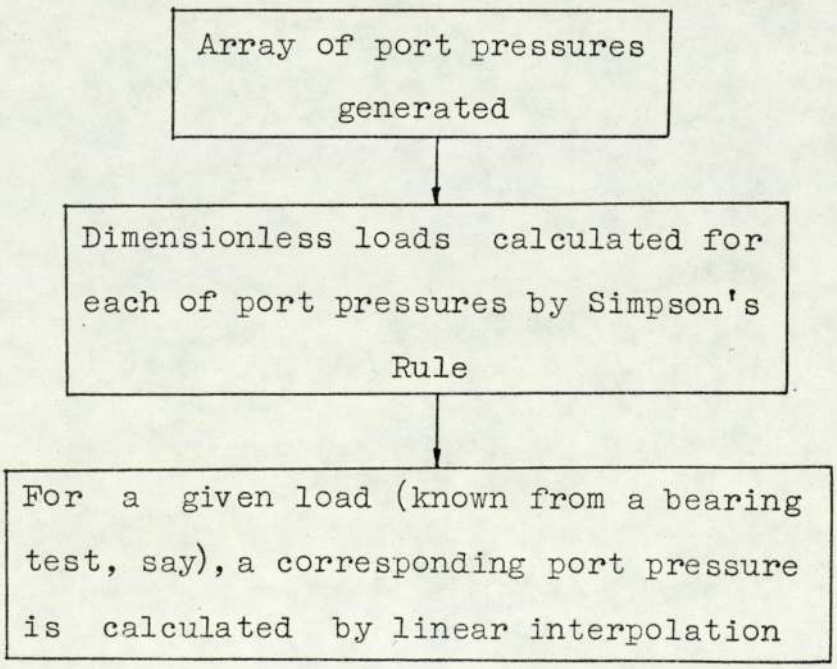

Linear interpolation is justified by figure I-4, 'Dimensionless load versus port pressure'. It is seen that this relationship is nearly a straight line. The bearing geometry is the same as for calculating flow rates on figures I-2 and I-3.

Three port pressures given on figure I-2 are typical values for a bearing experiment. These port pressures are calculated by means of the BASIC programme just described and they are used as an example throughout this appendix. The purpose of this example is to show that it is possible to obtain different expressions for load than given by equations (I-27) and (I-28), and that for the range of loads in the experiments $\mathrm{erf}(\frac{P_p}{A_2})$ can be taken as equal to unity. The following calculations are now performed to prove this point (erfc means a complementary error function); and they are shown in a table.

The error of substituting expression 'C' by a complementary error function in the expressions for load is small, as seen in Table AI-1. Clearly for the range of loads, i.e. port pressures encountered in the experiments, formulae (I-28) and (I-27) can be substituted by:

$$\bar{W} = R_p^2 \, e^{\left(\frac{P_p}{A_2}\right)^2} \times A_2 \, \frac{\sqrt{\pi}}{2} \, \mathrm{erfc}\left(\frac{1}{A_2}\right) \qquad \text{(I-29)}$$

$$\bar{W} = A_2 \, e^{\frac{1}{A_2^2}} \, \frac{\sqrt{\pi}}{2} \, \mathrm{erfc}\left(\frac{1}{A_2}\right) \qquad \text{(I-30)}$$

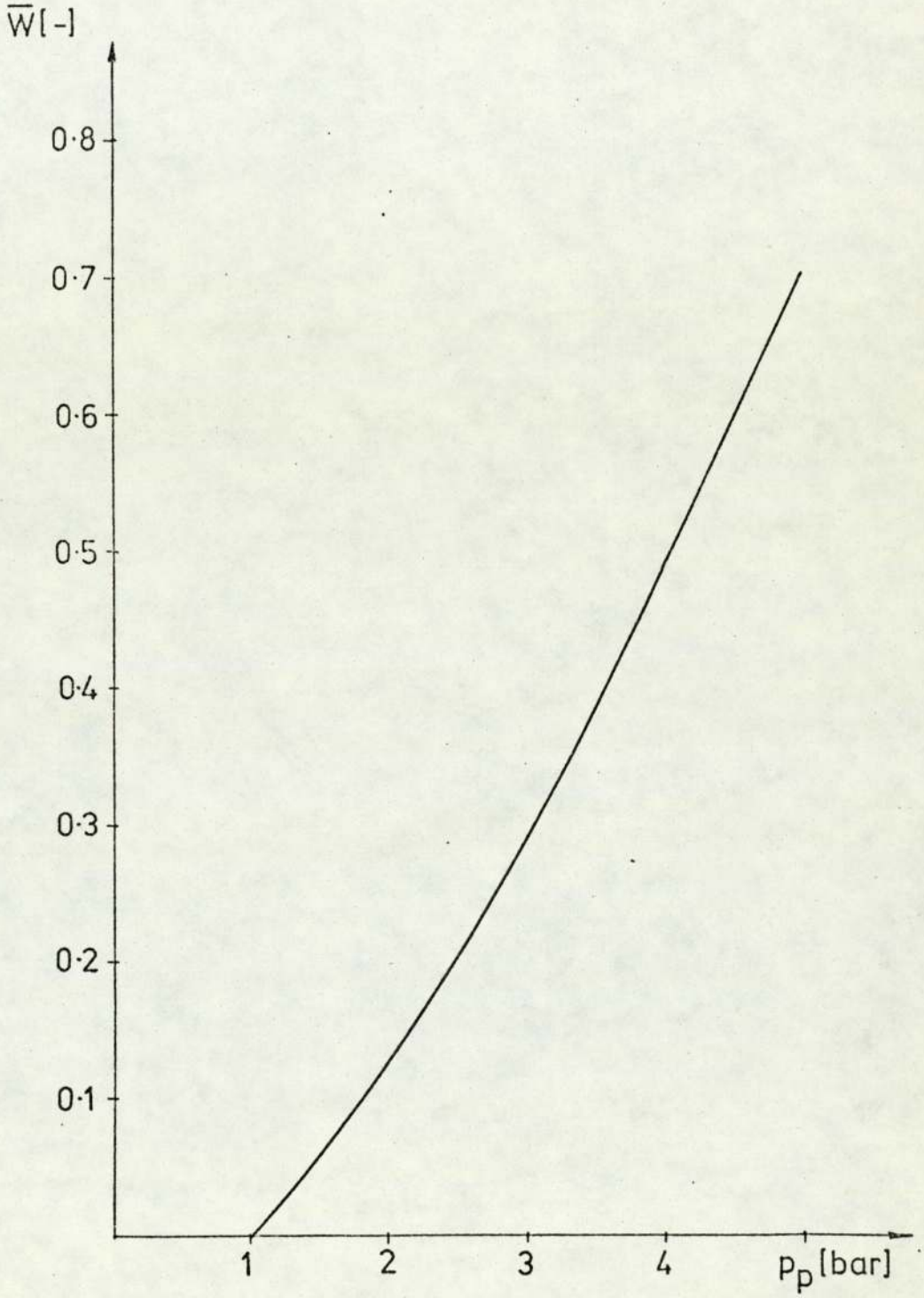

DIMENSIONLESS LOAD V. PORT PRESSURE

FIG I - 4

	I	II	III
p_p	1.6350	2.3798	3.3848
$P_p = \frac{p_p}{p_a}$	1.628644	2.370529	3.371632
$A_2^2 = \frac{1-P_p^2}{2\ell n R_p}$	0.152622	0.426646	0.957574
$\frac{1}{A_2}$	2.559712	1.530968	1.021913
$\frac{P_p}{A_2}$	4.168860	3.629204	3.445513
A_2	0.390669	0.653181	0.978557
$\mathrm{erf}\left(\frac{P_p}{A_2}\right)$	1.00000000	0.99999971	0.99999890
$\mathrm{erf}\left(\frac{1}{A_2}\right)$	0.99970537	0.96962117	0.85159919
$C = \mathrm{erf}\left(\frac{P_p}{A_2}\right) - \mathrm{erf}\left(\frac{1}{A_2}\right)$	0.00029463	0.03037854	0.14839971
$a = \mathrm{erfc}\left(\frac{1}{A_2}\right)$	0.000294626	0.030378825	0.148400810
$\frac{C-a}{a} \times 100$	+ 0.0012	- 0.0009	- 0.0007

Bearing with minimum possible load only ⟶ external load increasing

TABLE AI-I

This is convenient, because it is now possible to differentiate expressions (I-30) with respect to film thickness and obtain an analytic expression for stiffness in terms of dimensionless load $\bar{W}$ as shown later (section AI.5). It would not be possible to obtain an analytical expression for stiffness from the load $\bar{W}$, computed by numerical methods such as Simpson's Rule. Moreover, long and cumbersome expressions for stiffness would be obtained when differentiating equations (I-27) and (I-28) with respect to film thickness. The simplified equations (I-29) and (I-30) were found to be adequate by substituting unity for $\text{erf}(\frac{P_p}{A_2})$, as verified in Table AI-1.

In order to compare the values of load calculated by error function method and by Simpson's Rule, the following calculations are performed:

	I	II	III
$e^{\frac{1}{A_2^2}}$	700.732014	10.421417	2.841426
$A_2 \times e^{\frac{1}{A_2^2}}$	273.754275	6.807072	2.780498
$\bar{W}_e$	0.071479	0.183264	0.365682
$\bar{W}_s$	0.071436	0.183087	0.365365
$\frac{\bar{W}_e - \bar{W}_s}{\bar{W}_s} \times 100$	0.060	0.096	0.087

TABLE AI-2

Here $\bar{W}_e$ and $\bar{W}_s$ denote dimensionless loads calculated by means of error functions and by Simpson's Rule respectively. It can be seen that the differences involved are less than 0.1%. Subsequently values of load were calculated by Simpson's Rule.

AI.4 Flow and Load Parameters

For uniform film bearings lubricated by an incompressible fluid, non-dimensional flow and load can be conveniently expressed as:

$$q = \frac{Q\eta}{(p_p - p_a)h^3}$$

$$w_g = \frac{W}{A(p_p - p_a)}$$

For a circular step bearing

$$q = -\frac{\pi}{6\ell n(r_p/r_o)}$$

$$w_g = -\frac{[1-(r_p/r_o)^2]}{2\ell n(r_p/r_o)}$$

It can be seen that in the case of incompressible lubrication these basic parameters depend upon bearing geometry only.

For gas lubrication and for the same circular step geometry from (I-13) the flow parameter can be defined as

$$q = \frac{Q\eta p}{h^3(p_p^2 - p_a^2)} = \frac{M\eta R_a T_a}{h^3(p_p^2 - p_a^2)} \qquad \text{(I-31)}$$

This flow parameter also depends upon bearing geometry only and it is equal to:

$$q = \frac{-\pi}{12\ell n(r_p/r_o)} = -\frac{\pi}{12\ell n R_p} \qquad \text{(I-32)}$$

For the bearing geometry of the experiments:

$$q = 0.048359$$

Regarding a load parameter w_g, which is dependent upon the bearing geometry only,

defined by

$$w_g = R_p^2 \frac{\sqrt{\pi}}{2} = \left(\frac{r_p}{r_o}\right)^2 \frac{\sqrt{\pi}}{2} \qquad \text{(I-33)}$$

then through equations (I-29) and (I-17) it follows that the non-dimensional load is expressed as

$$w_g = \frac{W}{\pi r_o^2 p_a e^{\left(\frac{P_p}{A_2}\right)^2} \times A_2 \operatorname{erfc}\left(\frac{1}{A_2}\right)} \qquad \text{(I-34)}$$

For the bearing geometry of the experiments:

$$w_g = 0.0044552 \times \frac{\sqrt{\pi}}{2} = 0.1759 \times 10^{-4}$$

AI.5 Bearing Stiffness

Apart from bearing flow and bearing load, bearing stiffness is another important bearing parameter and it is defined as:

$$S = -\frac{dW}{dh} \qquad (I\text{-}35)$$

So far the analysis herewith has not included the bearing compensating element, shown in the sketch.

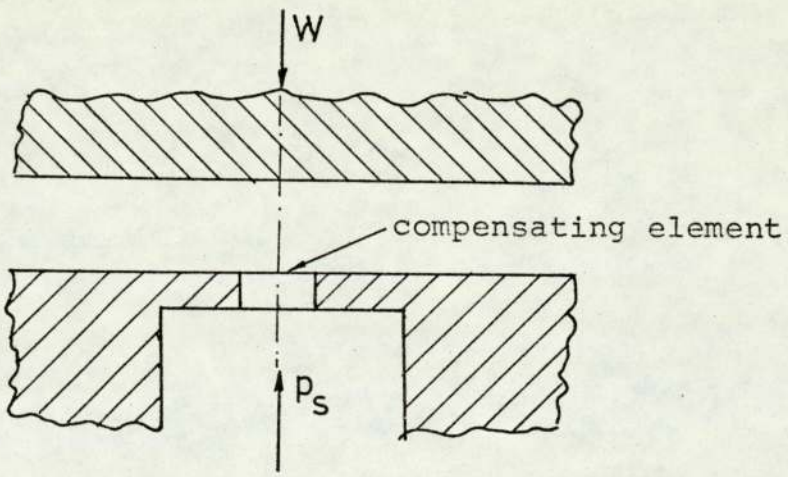

This element is included in bearing design so that the bearing can sustain a sudden change in load. If the bearing load is increased, the compensating element prevents the collapse of the bearing film. Alternatively, if the load is suddenly removed, the compensating element avoids excessive fluid flow.

Bearing stiffness depends upon the nature of this compensation and on the supply conditions.

Following (I-6) define further dimensionless quantities as

$$\left.\begin{aligned} P_s &= p_s/p_a \\ H &= h/r_p \end{aligned}\right\} \qquad \text{(I-36)}$$

From (I-13) the dimensionless mass flow can be defined as

$$\bar{M} = \frac{M\eta \bar{R}_a T_a}{q r_p^3 p_a^2} = H^3(P_p^2 - 1) \qquad \text{(I-37)}$$

From (I-17), (I-35) and (I-36) the dimensionless stiffness is expressed by:

$$\bar{S} = \frac{S r_p}{\pi r_o^2 p_a} = -\frac{d\bar{W}}{dH} \qquad \text{(I-38)}$$

From (I-37)

$$H = f(P_p, \bar{M}) \qquad \text{(I-39)}$$

Thus, a general expression for evaluating stiffness can be written as

$$\bar{S} = -\frac{d\bar{W}}{dH} = -\frac{d\bar{W}}{dP_p} \cdot \frac{\partial P_p}{\partial H} - \frac{d\bar{W}}{dM} \cdot \frac{\partial M}{\partial H} \qquad \text{(I-40)}$$

But from (I-17) and (I-29), $\bar{W} = f(P_p)$ only, so that

$$\bar{S} = -\frac{d\bar{W}}{dP_p} \cdot \frac{dP_p}{dH} \qquad \text{(I-41)}$$

$\frac{d\overline{W}}{dP_p}$ can be obtained from expressions for bearing load. From (I-22) and (I-30):

$$\overline{W} = \frac{1}{\xi_2} e^{\xi_2^2} \frac{\sqrt{\pi}}{2} \operatorname{erfc}(\xi_2) \qquad \text{(I-42)}$$

Remembering that

$$\operatorname{erfc}\xi_2 = 1 - \operatorname{erf}\xi_2 = 1 - \frac{2}{\sqrt{\pi}} \int_0^{\xi_2} e^{-\xi^2} d\xi$$

and (from reference [7], page 573)

$$\frac{d}{d\xi_2} \operatorname{erfc}(\xi_2) = - \frac{2}{\sqrt{\pi}} e^{-\xi_2^2},$$

it can be written:

$$\frac{d\overline{W}}{dP_p} = \frac{d\overline{W}}{d\xi_2} \times \frac{d\xi_2}{dA_2} \times \frac{dA_2}{dP_p} \qquad \text{(I-43)}$$

From (I-22) and (I-19)

$$\frac{d\xi_2}{A_2} \times \frac{dA_2}{dP_p} = \left(- \frac{1}{A_2^2}\right) \times \left(- \frac{P_p}{2\ell n R_p} \times \frac{1}{A_2}\right)$$

so that:

$$\frac{d\overline{W}}{dP_p} = \frac{d\overline{W}}{d\xi_2} \times \frac{1}{A_2^2} \frac{P_p}{2\ell n R_p} \times \frac{1}{A_2} \qquad \text{(I-44)}$$

From (I-42)

$$\frac{d\overline{W}}{d\xi_2} = \frac{d}{d\xi_2}\left(\frac{1}{\xi_2} e^{\xi_2^2}\right) \frac{\sqrt{\pi}}{2} \operatorname{erfc}\left(\xi_2\right) + \left(\frac{1}{\xi_2} e^{\xi_2^2}\right) \frac{d}{d\xi_2}\left[\frac{\sqrt{\pi}}{2}\operatorname{erfc}\left(\xi_2\right)\right]$$

$$= e^{\xi_2^2}\left(2 - \frac{1}{\xi_2^2}\right)\frac{\sqrt{\pi}}{2}\operatorname{erfc}\left(\xi_2\right) - \frac{1}{\xi_2} e^{\xi_2^2} \times e^{-\xi_2^2}$$

$$= e^{\frac{1}{A_2^2}}\left(2 - A_2^2\right) \times \frac{\sqrt{\pi}}{2}\operatorname{erfc}\left(\frac{1}{A_2}\right) - A_2$$

$$= \frac{\overline{W}(2 - A_2^2)}{A_2} - A_2 \qquad \text{(I-45)}$$

Now, from (I-44) and (I-45):

$$\frac{d\overline{W}}{dP_p} = \left[\overline{W}\left(\frac{2}{A_2^2} - 1\right) - 1\right] \times \frac{1}{A_2^2} \frac{P_p}{2\ell n R_p}$$

$$= \left[\overline{W}\left(\frac{4\ell n R_p}{1-P_p^2} - 1\right) - 1\right] \frac{2\ell n R_p}{(1-P_p^2)} \frac{P_p}{2\ell n R_p}$$

$$= -\left[\overline{W}\left(\frac{4\ell n R_p}{1-P_p^2} - 1\right) - 1\right] \frac{P_p}{P_p^2 - 1} \qquad \text{(I-46)}$$

From (I-41), dimensionless stiffness can be written as

$$\overline{S} = \left[\overline{W}\left(\frac{4\ell n R_p}{1-P_p^2} - 1\right) - 1\right] \frac{P_p}{P_p^2 - 1} \times \frac{dP_p}{dH} \qquad \text{(I-47)}$$

where $\frac{dP_p}{dH}$ depends upon the compensating element and the supply conditions. Three types of compensating elements

are used in gas lubrication - capillary, orifice and inherent compensation. For each type of compensating element (or restrictor) $\frac{dP_p}{dH}$ is calculated from the condition of continuity of mass through the restrictor and through the bearing.

(a) Capillary Restrictor

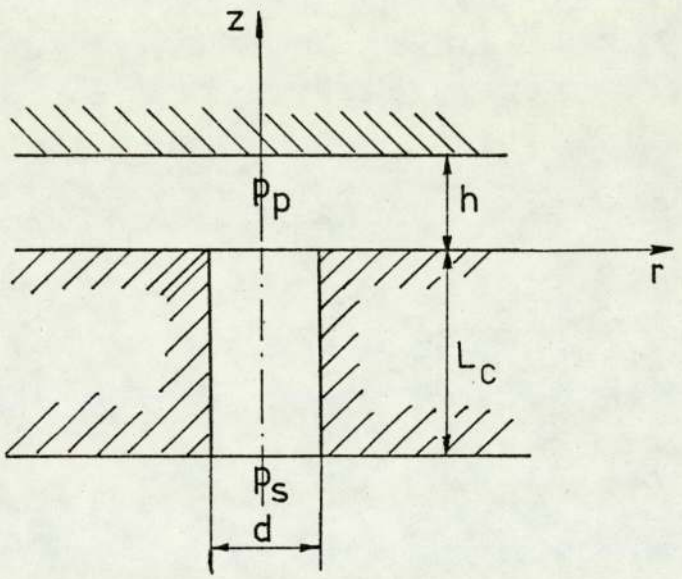

Assuming laminar feeding, then in accordance with the Poiseuille equation, the

flow through the capillary is given by:

$$Q = - \frac{\pi d^4}{128\eta} \frac{dp}{dz}$$

or

$$pQdz = - \frac{\pi d^4}{128\eta} pdp$$

As $pQ = p_s Q_s$, for isothermal flow of a perfect gas

then $$p_s Q_s \int_{-L_c}^{o} dz = \frac{-\pi d^4}{128\eta} \int_{p_s}^{p_p} pdp$$

or

$$p_s Q_s = \frac{\pi d^4}{128 L_c} \times \frac{1}{2\eta}(p_s^2 - p_p^2)$$

$$= \frac{k_c}{2\eta}(p_s^2 - p_p^2)$$

where k_c is the capillary coefficient. Mass flow through the capillary is then equal to:

$$M = \frac{k_c}{2\eta R_a T_a}(p_s^2 - p_p^2) \qquad \text{(I-48)}$$

Now equating (I-13) and (I-48) and also taking into consideration (I-32)

$$\frac{k_c(p_s^2 - p_p^2)}{2\eta R_a T_a} = \frac{qh^3(p_p^2 - p_a^2)}{\eta R_a T_a}$$

and in dimensionless form:

$$\frac{2qr_p^3}{k_c} \times H^3 = \frac{P_s^2 - P_p^2}{P_p^2 - 1} \qquad \text{(I-49)}$$

From (I-49):

$$\frac{2qr_p^3}{k_c} \times 3H^2 = \frac{-2(P_s^2 - 1)}{(P_p^2 - 1)^2} P_p \frac{dP_p}{dH}$$

Rearranging after substituting (I-49) again

$$\frac{dP_p}{dH} = -\frac{(P_s^2-p_p^2)(P_p^2-1)}{2(P_s^2-1)P_p} \times \frac{3}{H} \qquad \text{(I-50)}$$

then through equation (I-47)

the dimensionless stiffness for capillary compensated circular air bearings is given by :

$$\bar{S} = \left[1 - \bar{W}\left(\frac{4\ell nR_p}{1-P_p^2} - 1\right)\right] \frac{P_s^2-P_p^2}{2(P_s^2-1)} \times \frac{3}{H} \qquad \text{(I-51)}$$

(b) Orifice Restrictor

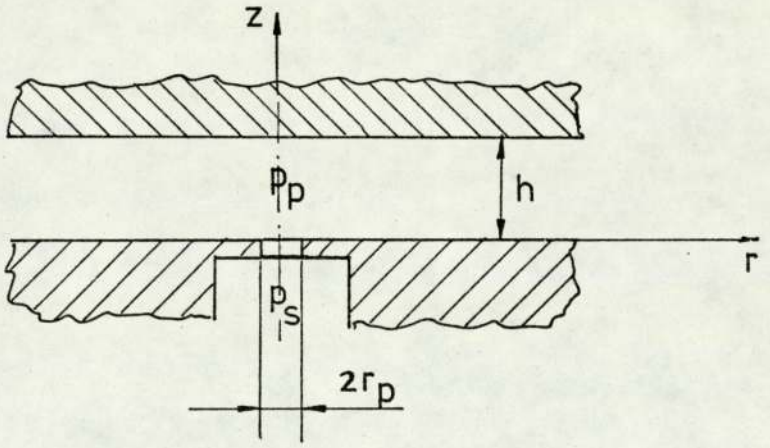

Mass flow through the orifice is given by

$$M = C_D \rho_p A v_z \qquad \text{where} \qquad A = \pi r_p^2$$

Assuming isentropic expansion through the orifice

[107]
$$\rho_p = \rho_s \left(\frac{p_p}{p_s}\right)^{\frac{1}{\gamma}} = \frac{p_s}{R_a T_a} \left(\frac{p_p}{p_s}\right)^{\frac{1}{\gamma}}$$

and

$$v_z^2 = \frac{2\gamma R_a T_a}{\gamma - 1}\left[1 - \left(\frac{p_p}{p_s}\right)^{\frac{\gamma-1}{\gamma}}\right]$$

so that

$$M^2 = C_D^2 \rho_p^2 A^2 v_z^2$$

$$= \frac{C_D^2 p_s^2}{R_a^2 T_a^2} \left(\frac{p_p}{p_s}\right)^{\frac{2}{\gamma}} \times A^2 \times \frac{2\gamma R_a T_a}{\gamma - 1}\left[1 - \left(\frac{p_p}{p_s}\right)^{\frac{\gamma-1}{\gamma}}\right] \qquad \text{(I-52)}$$

Equating squares of mass flow through orifice (I-52) and through bearing from (I-13) and (I-32) gives

$$\frac{q^2(\gamma-1)}{\eta^2 A^2 \times 2\gamma R_a T_a} h^6 = C_D^2 \frac{p_s^2 \left(\frac{p_p}{p_s}\right)^{\frac{2}{\gamma}}\left[1 - \left(\frac{p_p}{p_s}\right)^{\frac{\gamma-1}{\gamma}}\right]}{(p_p^2 - p_a^2)^2}$$

and in dimensionless form:

$$\frac{q^2(\gamma-1)p_a^2 r_p^6}{\eta^2 A^2 \times 2\gamma R_a T_a} H^6 = C_D^2 \left[\frac{\left\{ P_s^{2\left(\frac{\gamma-1}{\gamma}\right)} \times P_p^{\frac{2}{\gamma}} - P_s^{\frac{\gamma-1}{\gamma}} \times P_p^{\frac{\gamma+1}{\gamma}} \right\}}{(P_p^2 - 1)^2} \right]$$

(I-53)

Take:

$$N_o = \frac{q^2(\gamma-1)p_a^2 r_p^6}{\eta^2 A^2 \times 2\gamma R_a T_a} \qquad \text{(I-54)}$$

$$\{\ \} = P_s^{2\left(\frac{\gamma-1}{\gamma}\right)} \times P_p^{\left(\frac{2}{\gamma}\right)} - P_s^{\left(\frac{\gamma-1}{\gamma}\right)} \times P_p^{\left(\frac{\gamma+1}{\gamma}\right)} \qquad \text{(I-55)}$$

$$[\ ] = \frac{\{\ \}}{(P_p^2-1)^2} = \frac{N_o H^6}{C_D^2} \qquad \text{(I-56)}$$

Coefficient of discharge is a function of a pressure drop across the orifice. For a constant supply pressure, it is a function of port pressure, so it can be stated:

$$\frac{dC_D}{dH} = \frac{dC_D}{dP_p} \times \frac{dP_p}{dH} \qquad \text{(I-57)}$$

Now (I-53) can be written as

$$N_o H^6 = C_D^2 [\ ]$$

and differentiating

$$N_o \times 6H^5 = 2C_D \frac{dC_D}{dH} [\ ] + C_D^2 \frac{d}{dH} [\ ]$$

$$= 2C_D \frac{dC_D}{dP_p} \times \frac{dP_p}{dH} [\ ] + C_D^2 \frac{d}{dH} [\ ] \quad \text{(I-58)}$$

Now from equation (I-56)

$$\frac{d}{dH}[\ ] = \frac{\frac{d}{dH}\{\ \} \times (P_p^2-1)^2 - \{\ \} \times 2(P_p^2-1) \times 2P_p \frac{dP_p}{dH}}{(P_p^2 - 1)^4}$$

and from equation (I-55)

$$\frac{d}{dH}\{\ \} = 2P_p \left(\frac{P_s}{\gamma}^{2\left(\frac{\gamma-1}{\gamma}\right)} \times P_p^{-2\left(\frac{\gamma-1}{\gamma}\right)} - P_s^{\left(\frac{\gamma-1}{\gamma}\right)} \cdots\cdots \right.$$

$$\left. \cdots\cdots \times \left(\frac{\gamma+1}{2\gamma}\right) \times P_p^{-\left(\frac{\gamma-1}{\gamma}\right)} \right) \frac{dP_p}{dH}$$

$$= \left(\right) \times 2P_p \frac{dP_p}{dH}$$

and combining

$$\frac{d}{dH}[\ ] = \frac{(\ ) \times 2P_p \frac{dP_p}{dH} \times (P_p^2-1)^2 - \{\ \} \times 2(P_p^2-1) \times 2P_p \frac{dP_p}{dH}}{(P_p^2 - 1)^2 \times (P_p^2 - 1)^2}$$

Substituting in (I-58) and rearranging, there follows

taking into consideration (I-53).

$$C_D^2 \frac{d}{dH}[\ ] = \left(\frac{(\ )}{\{\ \}} - \frac{2}{(P_p^2-1)} \right) \times 2P_p \frac{dP_p}{dH} \times N_o H^6$$

$$= \left(\alpha - \frac{2}{(P_p^2-1)} \right) \times 2P_p \frac{dP_p}{dH} \times N_o H^6 \qquad \text{(I-59)}$$

where

$$\alpha = \frac{\frac{P_s}{\gamma}^{2\left(\frac{\gamma-1}{\gamma}\right)} \times P_p^{-2\left(\frac{\gamma-1}{\gamma}\right)} - P_s^{\left(\frac{\gamma-1}{\gamma}\right)} \times \left(\frac{\gamma+1}{2\gamma}\right) \times P_p^{-\left(\frac{\gamma-1}{\gamma}\right)}}{P_s^{2\left(\frac{\gamma-1}{\gamma}\right)} \times P_p^{\left(\frac{2}{\gamma}\right)} - P_s^{\left(\frac{\gamma-1}{\gamma}\right)} \times P_p^{\left(\frac{\gamma+1}{\gamma}\right)}}$$

$$= \frac{\left[\frac{\gamma+1}{2} - \left(\frac{P_s}{P_p}\right)^{\frac{\gamma-1}{\gamma}} \right]}{\gamma P_p^2 \left[1 - \left(\frac{P_s}{P_p}\right)^{\frac{\gamma-1}{\gamma}} \right]} \qquad \text{(I-60)}$$

Now from (I-58) and (I-56)

$$N_o \times 6H^5 = 2C_D \times \frac{1}{P_p} \frac{dC_D}{dP_p} \times P_p \frac{dP_p}{dH} \times \frac{N_o H^6}{C_D^2}$$

$$+ \left(\alpha - \frac{2}{(P_p^2-1)} \right) \times 2P_p \frac{dP_p}{dH} \times N_o H^6$$

$$= 2P_p \frac{dP_p}{dH} \left[\frac{1}{C_D P_p} \frac{dC_D}{dP_p} + \alpha - \frac{2}{P_p^2-1} \right] N_o H^6$$

so that for orifice compensation

$$\frac{dP_p}{dH} = - \frac{1}{P_p\left[\frac{2}{P_p^2-1} - \alpha - \frac{1}{C_D P_p}\frac{dC_D}{dP_p}\right]} \times \frac{3}{H} \qquad \text{(I-61)}$$

and the dimensionless stiffness becomes through equation (I-47)

$$\overline{S} = \frac{\left[1 - \overline{W}\left(\frac{4\ell nR_p}{1-P_p^2} - 1\right)\right]}{\left(P_p^2-1\right)\left[\frac{2}{P_p^2-1} - \alpha - \frac{1}{C_D}\frac{dC_D}{dP_p}\right]} \times \frac{3}{H} \qquad \text{(I-62)}$$

Where the variation of discharge coefficient with port pressure can be neglected, the stiffness reduces to:

$$\overline{S} = \frac{\left[1 - \overline{W}\left(\frac{4\ell nR_p}{1-P_p^2} - 1\right)\right]}{\left[2 - \alpha\left(P_p^2 - 1\right)\right]} \times \frac{3}{H} \qquad \text{(I-63)}$$

All this is valid for unchoked flow.

For choked conditions:

$$\frac{p_p}{p_s} = \frac{P_p}{P_s} = \left(\frac{2}{\gamma+1}\right)^{\frac{\gamma}{\gamma-1}}$$

as shown, for example, by Powell [107]. For $\gamma = 1.403$, $P_p/P_s = 0.528$. The normal operational range of these bearings is $P_p/P_s > 0.528$

If, however, bearings are operating at $P_p/P_s < 0.528$, i.e. choked flow region, the flow through the orifice and the stiffness of such bearings can be calculated by substituting the the actual value of P_p/P_s by 0.528, for example, in equations (I-52) and (I-60).

(c) Inherent Restrictor

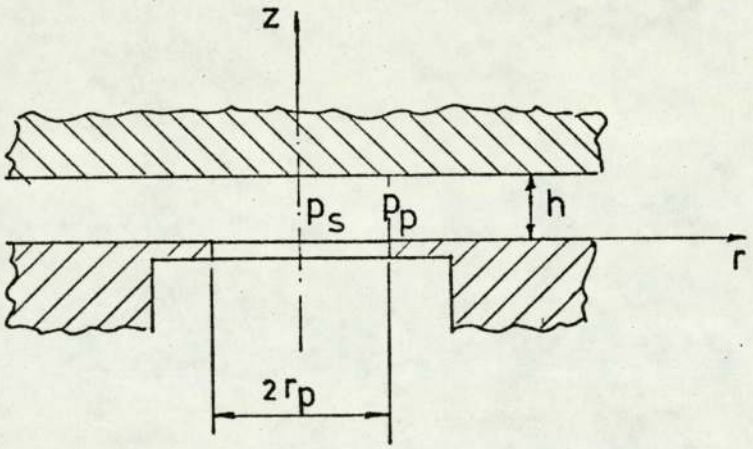

'Inherent area' is equal to $2\pi r_p h$ and orifice area to πr_p^2. Inherent restriction takes place when the inherent restriction area is smaller than the orifice area, i.e. when $h < \frac{r_p}{2}$. For the rigid bearing experiments, $r_p \simeq 0.286$mm and the film thickness h is always smaller than $\frac{r_p}{2}$(=0.143mm). Therefore inherent restriction takes place during bearing tests.

It will be assumed that the mass flow through this inherent restrictor can be described by the same expression as the mass flow through the orifice restrictor except that values of discharge coefficient C_D may be different. These values of C_D are determined experimentally by equating the mass flows squared through the inherent restrictor, given by orifice law and through the bearing (derived from Reynold's Equation). From (I-13), (I-32) and (I-52) with $A=2\pi r_p h$:

$$\frac{q^2(\gamma-1)}{\eta^2 \times 4\pi r_p^2 \times 2\gamma R_a T_a} h^4 = C_D^2 \frac{p_s^2 \left(\frac{p_p}{p_s}\right)^{\frac{2}{\gamma}} \times \left[1 - \left(\frac{p_p}{p_s}\right)^{\frac{\gamma-1}{\gamma}}\right]}{\left(p_p^2 - p_a^2\right)^2}$$

and in dimensionless form:

$$\frac{q^2 (\gamma-1) p_a^2 r_p^2}{\eta^2 \times 8\pi\gamma R_a T_a} H^4 = C_D^2 \left[\frac{\left\{P_s^{2\left(\frac{\gamma-1}{\gamma}\right)} \times P_p^{\left(\frac{2}{\gamma}\right)} - P_s^{\left(\frac{\gamma-1}{\gamma}\right)} \times P_p^{\left(\frac{\gamma+1}{\gamma}\right)}\right\}}{\left(P_p^2 - 1\right)^2}\right] \qquad \text{(I-64)}$$

Take:

$$N_i = \frac{q^2 (\gamma-1) p_a^2 r_p^2}{\eta^2 \times 8\pi\gamma R_a T_a} \qquad \text{(I-65)}$$

$$\{\ \} = P_s^{2\left(\frac{\gamma-1}{\gamma}\right)} P_p^{\left(\frac{2}{\gamma}\right)} - P_s^{\left(\frac{\gamma-1}{\gamma}\right)} \times P_p^{\left(\frac{\gamma+1}{\gamma}\right)} \qquad \text{(I-66)}$$

$$\text{and} \quad [\ ] = \frac{\{\ \}}{(P_p^2-1)^2} = \frac{N_i H^4}{C_D^2} \qquad \text{(I-67)}$$

A similar analysis as in the case of orifice restriction then gives:

$$\frac{dP_p}{dH} = - \frac{1}{P_p\left[\frac{2}{P_p^2-1} - \alpha - \frac{1}{C_D P_p}\frac{dC_D}{dP_p}\right]} \times \frac{2}{H} \qquad \text{(I-68)}$$

where α is given by (I-60).

and the dimensionless stiffness similar to (I-62) becomes:

$$\bar{S} = \frac{\left[1 - \bar{W}\ \frac{4\ell n R_p}{1-P_p^2} - 1\right]}{(P_p^2 - 1)\left[\frac{2}{P_p^2-1} - \alpha - \frac{1}{C_D}\frac{dC_D}{dP_p}\right]} \times \frac{2}{H} \qquad \text{(I-69)}$$

Clearly by comparison with equation (I-62) for orifice compensation it can be deduced that

$$\bar{S}_I = \frac{2}{3}\bar{S}_o \qquad \text{(I-70)}$$

In order to obtain experimentally the relationship of $\frac{dC_D}{dP_p}$ and port pressure, bearing load is kept constant and the supply pressure is varied; film thickness, supply pressure and bearing load are monitored. The plot of C_D with P_p/P_s

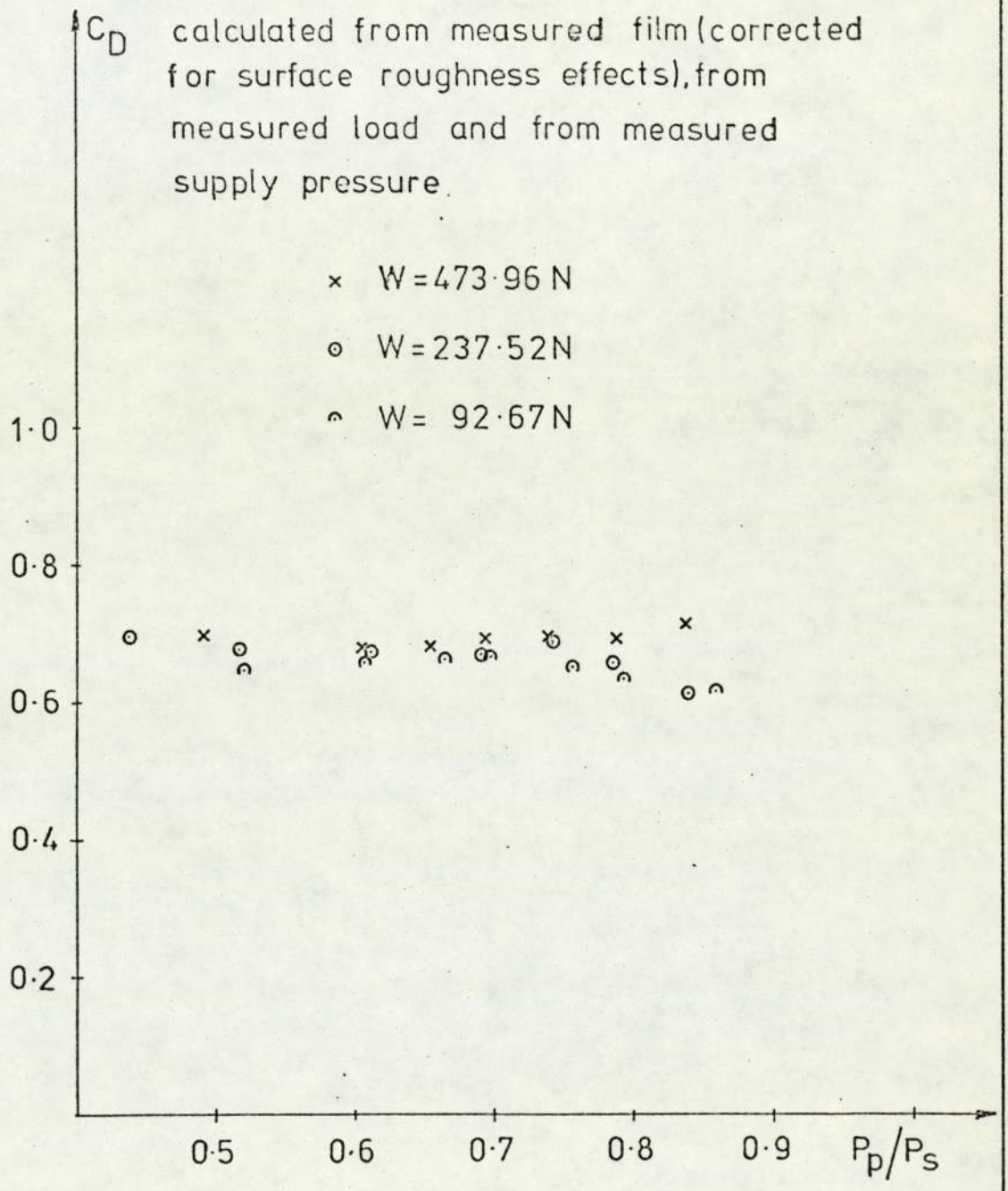

COEFFICIENT OF DISCHARGE V.

PORT/SUPPLY PRESSURE RATIO

FIG I-5

ratio is shown in fig. I-5 for three different loads. It is seen that the discharge coefficient C_D does not change with port pressure for values of P_p/P_s encountered during experiments. It is approximately equal to $C_D = 0.68$. Therefore, equation (I-68) can be simplified to read:

$$\frac{dP_p}{dH} = -P_p \left[\frac{1}{\frac{2}{P_p^2-1} - \alpha}\right] \times \frac{2}{H} \qquad \text{(I-71)}$$

Dimensionless stiffness of inherently compensated circular air bearings then becomes:

$$\bar{S} = \frac{\left[1 - \bar{W}\left(\frac{4\ell n\, R_p}{1-P_p^2} - 1\right)\right]}{\left[2 - \alpha(P_p^2 - 1)\right]} \times \frac{2}{H} \qquad \text{(I-72)}$$

APPENDIX II

STRESS-STRAIN RELATIONSHIPS FOR BEARING ELASTOMERS

In order to describe stresses acting on a body in equilibrium, generally three normal components of stress and six shearing components are necessary. In cartesian coordinates x, y, z the state of stress in the body can be represented by an array as follows:

$$\begin{bmatrix} \sigma_x & \tau_{xy} & \tau_{xz} \\ \tau_{yx} & \sigma_y & \tau_{yz} \\ \tau_{zx} & \tau_{zy} & \sigma_z \end{bmatrix}$$

In cylindrical polar coordinates r, θ, z, the array becomes

$$\begin{bmatrix} \sigma_r & \tau_{r\theta} & \tau_{rz} \\ \tau_{\theta r} & \sigma_\theta & \tau_{\theta z} \\ \tau_{zr} & \tau_{z\theta} & \sigma_z \end{bmatrix}$$

For the concise representation of general equations, the so called index or subscript notation is advantageous and often used, and so both of the above arrays can be represented by

$$\tau_{ij} = \begin{bmatrix} \tau_{11} & \tau_{12} & \tau_{13} \\ \tau_{21} & \tau_{22} & \tau_{23} \\ \tau_{31} & \tau_{32} & \tau_{33} \end{bmatrix}.$$

In the last array normal stresses are represented by τ_{11}, τ_{22} and τ_{33}, i.e. when subscript i is equal to subscript j. Shear stresses are represented by unequality τ_{ij} when $i \neq j$.

τ_{ij} represents a tensor of rank 2 because it has got $3^2 = 9$ components. A vector is a tensor of rank 1 and in the extreme a scalar is a tensor of rank 0.

For completion of the above statement scalars, vectors and tensors can be more rigorously differentiated according to how the components of the system are defined in the variables x_i and how they are transformed when the variables are changed to x_i'.

By introducing a summation convention:

$$\sum_{i=1}^{3} a_i x_i = a_1 x_1 + a_2 x_2 + a_3 x_3 = a_i x_i$$

it is seen that a repeated subscript i means summation with respect to that subscript over its range.

As an example for a transformation law of vectors a rotation of coordinates x_1, x_2 by an angle θ anticlockwise to coordinates x_1', x_2' can be described by $x_i' = \alpha_{ij} x_j$ where α_{ij} are the elements of the array:

$$\begin{bmatrix} \alpha_{11} & \alpha_{12} \\ \alpha_{21} & \alpha_{22} \end{bmatrix} = \begin{bmatrix} \cos\theta & \sin\theta \\ -\sin\theta & \cos\theta \end{bmatrix}$$

This law of transformation can be easily extended to three dimensions. Tensors transform according to [302]:

$$\tau_{\alpha\beta}' = \ell_{\alpha i}\, \ell_{\beta j}\, \tau_{ij}$$

where the summation is first for j and then for i. For example if we need τ_{12}', then

$$\begin{aligned}
\tau_{12}' &= \ell_{1i}\, \ell_{2j}\, \tau_{ij} \\
&= \ell_{1i}(\ell_{21}\tau_{1} + \ell_{22}\tau_{i2} + \ell_{23}\tau_{i3}) \\
&= \ell_{21}(\ell_{11}\tau_{11} + \ell_{12}\tau_{21} + \ell_{13}\tau_{31}) \\
&+ \ell_{22}(\ell_{11}\tau_{12} + \ell_{12}\tau_{22} + \ell_{13}\tau_{32}) \\
&+ \ell_{23}(\ell_{11}\tau_{13} + \ell_{12}\tau_{23} + \ell_{13}\tau_{33})
\end{aligned}$$

Consider stresses τ_{zr} and τ_{rz} acting on an element in the plane z, r.

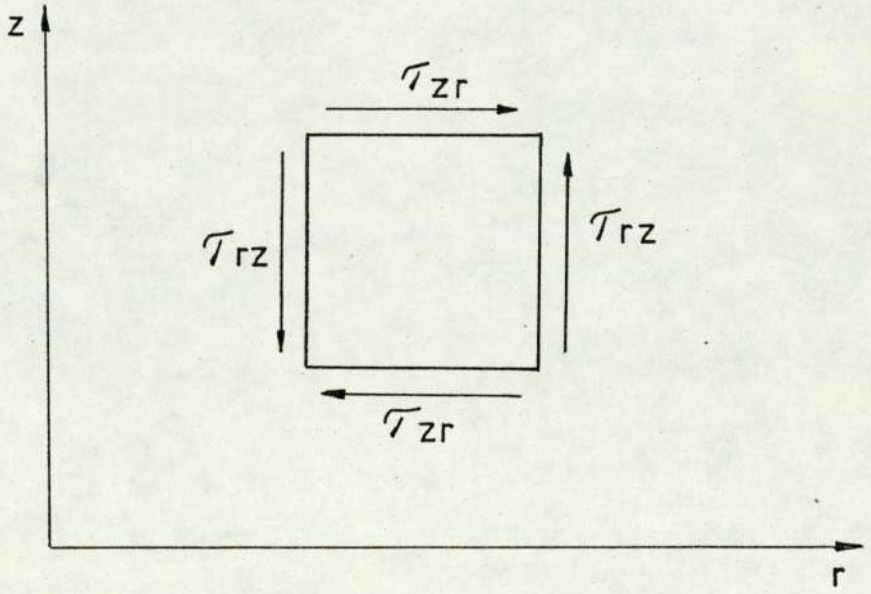

Because of the equilibrium of moments τ_{rz} must be equal to τ_{zr} and they are known as complementary shear stresses.

Similarly $\tau_{\theta r} = \tau_{r\theta}$ and $\tau_{\theta z} = \tau_{z\theta}$, so that a stress state of a body generally represented by nine components reduces to six independent ones.

Strains are also tensors of rank 2 and similarly because of symmetry the nine strain components reduce to six.

For materials which obey Hooke's law, stress tensor τ_{ij} is proportional to strain tensor e_{ij} [302], [314] and [315], and the relationship is given as:

$$\tau_{ij} = C_{ijk\ell}\, e_{k\ell} \qquad \text{(II-1)}$$

these materials are sometimes called Hookean elastic solids. A tensor of elastic constants or moduli $C_{ijk\ell}$ is a tensor of rank 4 and it has got $3^4 = 81$ elements. However because of $\tau_{ij} = \tau_{ji}$ and $e_{ij} = e_{ji}$, there are only six independent elements in the stress tensor and six in the strain tensor. If each element of τ_{ij} is linearly related to all elements of e_{ij} or vice versa, there will be six equations of six constants each, i.e. thirty-six constants in total. Therefore after symmetrization a tensor of elastic constants $C_{ijk\ell}$ reduces to thirty-six element from eighty-one. From energy considerations [313] in general there are only twenty-one constants.

Further reduction of elastic constants is caused by material symmetry and the number of elastic constants in most models of elastic solids is smaller than twenty-one. Elastic properties of isotropic materials are the same in all directions and for these materials the number of elastic constants reduces

to two from twenty-one.

Any state of stress can be thought of a superposition of pure shear and a uniform tension (or compression) all round. This leads to the idea of stress deviation which is the actual state of stress minus uniform stress all round.

$$\widehat{\tau}_{ij} = \tau_{ij} - \delta_{ij}\tau_{mean} \qquad \text{(II - 2)}$$

here δ_{ij} denotes the array

$$\delta_{ij} = \begin{bmatrix} 1 & 0 & 0 \\ 0 & 1 & 0 \\ 0 & 0 & 1 \end{bmatrix}$$

i.e. $\delta_{ij} = 1$ when $i = j$, otherwise it is equal to zero. Also

$$\begin{aligned} \tau_{mean} &= \tfrac{1}{3}(\sigma_x + \sigma_y + \sigma_z) \\ &= \tfrac{1}{3}(\sigma_r + \sigma_\theta + \sigma_z) \\ &= \tfrac{1}{3}(\tau_{11} + \tau_{22} + \tau_{33}) \\ &= \frac{\tau_{kk}}{3} \end{aligned} \qquad \text{(II - 3)}$$

The importance of the deviator is that it does not produce a change in volume.

Similarly, the strain deviator is defined as

$$\widehat{e}_{ij} = e_{ij} - \delta_{ij}e_{mean} \qquad \text{(II - 4)}$$

where:

$$e_{mean} = \frac{1}{3}(e_x + e_y + e_z)$$

$$= \frac{1}{3}(e_r + e_\theta + e_z)$$

$$= \frac{1}{3}(e_{11} + e_{22} + e_{33})$$

$$= \frac{e_{kk}}{3} \qquad \text{(II - 5)}$$

For isotropic materials Hooke's law may be stated in the form:

$$\tau_{kk} = 3K\, e_{kk} \qquad \text{(II - 6)}$$

$$\widehat{\tau}_{ij} = 2G\, \widehat{e}_{ij} \qquad \text{(II - 7)}$$

If the strain were infinitesimal, e_{kk} would be the change of volume per unit volume $e_{kk} = \frac{\Delta V}{V}$, so that equation (II - 6) states that the change of volume is proportional to the mean stress.

In the special case of hydrostatic compression

$$\tau_{11} = \tau_{22} = \tau_{33} = -p$$

and

$$\tau_{kk} = -3p$$

so that

$$-3p = 3K\, e_{kk}$$

and the volume strain

$$e_{kk} = -\frac{p}{K} = \frac{\Delta V}{V} = \frac{\tau_{kk}}{3K} = \frac{\tau_{mean}}{K} \qquad \text{(II - 8)}$$

where the elastic constant K is called bulk modulus of the material.

The strain deviator e_{ij} describes a deformation of shape without change of volume. In the special case where $e_{12} \neq 0$ and other strains are equal to zero

$$\tau_{12} = 2G\ e_{12}$$

the coefficient 2 in the above equation is included, because before the tensor concept was introduced it was customary to define engineering shear strain as $\gamma_{12} = 2e_{12}$. Elastic constant G is called the modulus of elasticity in shear or the modulus of rigidity.

If definitions (II - 2) and (II - 4) are substituted into (II - 7):

$$\tau_{ij} - \delta_{ij}\,\tau_{mean} = 2G(e_{ij} - \delta_{ij}\,e_{mean})$$

By using (II - 8) the stress state is given as:

$$\tau_{ij} = \delta_{ij}\,K\,e_{kk} - \frac{2}{3}G\,\delta_{ij}\,e_{kk} + 2G\,e_{ij}$$

and

$$\tau_{ij} = \lambda\,\delta_{ij}\,e_{kk} + 2G\,e_{ij} \qquad \text{(II - 9)}$$

where

$$\lambda = K - \frac{2}{3}G.$$

Alternatively the strain state is given as :

$$e_{ij} = \frac{\tau_{ij}}{2G} - \frac{\delta_{ij}}{3}\tau_{kk}\left(\frac{1}{2G} - \frac{1}{3K}\right) \qquad \text{(II - 10)}$$

Equations (II - 9) represent stresses in terms of strains and equations (II - 10) represent strains in terms of stresses.

Elastic constants λ and G are called Lamé's constants, E is modulus of elasticity or Young's modulus, ν is Poisson's ratio and K is bulk modulus. Four constants have dimensions of pressure whilst Poisson's ratio ν is dimensionless. Some of the more important interelationships between these constants are:

$$\left.\begin{aligned}
2G &= \frac{E}{1+\nu} = 3(K-\lambda) \\
3K &= \frac{E}{1-2\nu} = 3\lambda+2G \\
\frac{1}{2G} - \frac{1}{3K} &= \frac{3\lambda}{2G(3\lambda+2G)} \\
\nu &= \frac{\lambda}{3K-\lambda} = \frac{E}{2G} - 1 \\
\frac{G}{\lambda+G} &= 1-2\nu \\
\frac{\lambda}{\lambda+2G} &= \frac{\nu}{1-\nu} \\
\lambda &= \frac{2G\nu}{1-2\nu} = K - \frac{2}{3}G
\end{aligned}\right\} \qquad \text{(II - 11)}$$

APPENDIX III

STRESS-STRAIN RELATIONSHIPS FOR BEARING ELASTOMERS WHEN THEY ARE ALMOST COMPLETELY OR COMPLETELY INCOMPRESSIBLE

Equation for stress in terms of strain (II-9), Appendix II) contains

$$\lambda = \frac{E}{(1+\nu)} \qquad \frac{\nu}{(1-2\nu)}$$

which is very large when $\nu \to 0.5$ and for $\nu = 0.5$ it is not defined. Therefore, it is necessary to develop special relationships for stress in terms of strain when ν approaches 0.5.

The stress state in an elastomer including temperature effects (compare (II-9), Appendix II) is given as

$$\tau_{ij} = \lambda e_{kk} \delta_{ij} + 2Ge_{ij} - K \times 3\alpha \Delta T \delta_{ij} \qquad \text{(III-1)}$$

Taking $K = \frac{3\lambda + 2G}{3}$ and

adding to and subtracting from the equation (III-1) the quantity $3G\alpha\Delta T\delta_{ij}$, equation (III-1) can be written as:

$$\tau_{ij} = \delta_{ij} \left[\lambda(e_{kk} - 3\alpha\Delta T) - 3G\alpha\Delta T + G\alpha\Delta T\right] + 2Ge_{ij} \qquad \text{(III-2)}$$

Using the concept of the mean stress defined by (II-3), Appendix II

$$\tau_{mean} = \frac{\tau_{kk}}{3} \qquad \text{(III-3)}$$

Hooke's law including temperature effects can be written as

$$\tau_{mean} = K(e_{kk} - 3\alpha\Delta T) \qquad \text{(III-4)}$$

or

$$e_{kk} - 3\alpha\Delta T = \frac{3\nu\tau_{mean}}{\lambda(1+\nu)} \qquad \text{(III-5)}$$

so that

$$\tau_{ij} = \delta_{ij}\left[\lambda\frac{3\nu\tau_{mean}}{\lambda(1+\nu)} + G\left(\frac{3\nu\tau_{mean}}{\lambda(1+\nu)} - e_{kk}\right) + G\alpha\Delta T\right] +$$

$$+ 2Ge_{ij}$$

$$= \delta_{ij}\left[\frac{3\nu\tau_{mean}}{(1+\nu)}\quad\frac{\lambda + G}{\lambda} - Ge_{kk} + G\alpha\Delta T\right] + 2Ge_{ij} \qquad \text{(III-6)}$$

as $$\frac{\lambda + G}{\lambda} = \frac{1}{2\nu}$$

equation (III-6) reduces to

$$\tau_{ij} = \frac{3\tau_{mean}}{2(1+\nu)}\delta_{ij} - Ge_{kk}\delta_{ij} + G\alpha\Delta T\delta_{ij} + 2Ge_{ij} \qquad \text{(III-7)}$$

If the temperature effects can be neglected ($\Delta T=0$) and taking the equivalent mean pressure as

$$p_m = \frac{3\tau_{mean}}{2(1+\nu)} \qquad \text{(III-8)}$$

then the elastomer stress state becomes:

$$\tau_{ij} = p_m\delta_{ij} - Ge_{kk}\delta_{ij} + 2Ge_{ij} \qquad \text{(III-9)}$$

Equation (III-9) is valid for $0<\nu< 0.5$.

In order to discuss the situation when $\nu = 0.5$ consider equation of continuity of displacements u and w in cylindrical

polar coordinates, see sketch below:

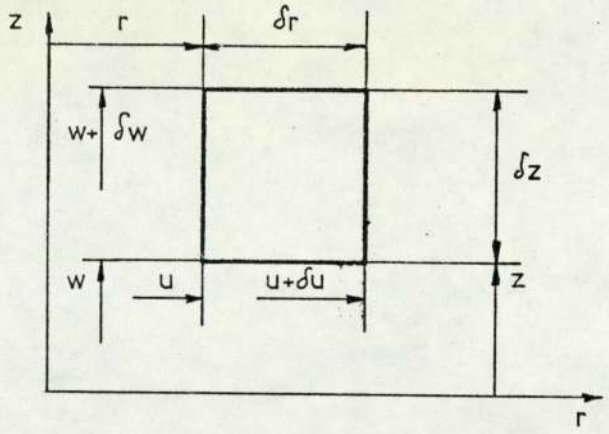

$$u\delta z \times 2\pi r - (u + \delta u)\ \delta z \times 2\pi(r + \delta r)$$
$$+ w\delta r \times 2\pi r - (w + \delta w)\ \delta r \times 2\pi r = 0 \qquad \text{(III-10)}$$

The term containing ($\delta u \delta r \delta z$) can be neglected as a small quantity when compared to other terms. Dividing the above equation by $\delta r \delta z$, it reduces to:

$$\frac{\partial u}{\partial r} + \frac{u}{r} + \frac{\partial w}{\partial z} = 0 \qquad \text{(III-11)}$$

which can also be written as

$$\frac{1}{r}\ \frac{\partial}{\partial r}(ur) + \frac{\partial w}{\partial z} = 0 \qquad \text{(III-12)}$$

In passing it can be noted that if the displacement vector is defined as

$$\vec{a} = u\vec{i} + v\vec{j} + w\vec{k}, \text{ then}$$
$$\text{div}\ \vec{a} = \frac{1}{r}\ \frac{\partial}{\partial r}(ru) + \frac{1}{r}\frac{\partial v}{\partial \theta} + \frac{\partial w}{\partial z}$$

which for axial symmetry reduces to:

$$\text{div}\ \vec{a} = \frac{1}{r}\ \frac{\partial}{\partial r}(ru) + \frac{\partial w}{\partial z}$$

so that the condition of incompressibility means that the divergance of a given vector is equal to zero.

The above means that in terms of strains the condition of incompressibility is satisfied when

$$e_{kk} = e_r + e_\theta + e_z = \frac{\partial u}{\partial r} + \frac{u}{r} + \frac{\partial w}{\partial z} = 0 \quad \text{(III-13)}$$

For Poisson's ratio $\nu = 0.5$, equation (III-9) reduces to:

$$\tau_{ij} = \tau_{mean}\, \delta_{ij} + 2Ge_{ij} \quad \text{(III-14)}$$

Equation (III-14) describes the stress state for an incompressible elastomer.

APPENDIX IV

COMPUTER PROGRAMMES

(consult Fig. 7)

1. Calculating axial displacements w.

```
      PROGRAM SON(INPUT,OUTPUT,RES,TAPE1=INPUT,
     1TAPE2=OUTPUT,TAPE4=RES)
      WRITE(2,100)
  100 FORMAT(13H ENTERING SON)
      CALL EPDE1
      STOP
      END


      SUBROUTINE USER1
      DIMENSION DUM(9)
      DIMENSION NT3(780),UT3(780),NT4(780),HT4(780,4),KT4(780),
     1NT5(390,2),UMAT(3250),NUMPT(2900),DIFCO(2900,5),P(12)
      COMMON C5,C95,NT3,UT3,NT4,HT4,KT4,NT5,NE3,NE4,NE5,NC,NR,KODBAS,
     1DX,DY,JOBNUM,UMAT,NEQU,NPIA,EWANT,BFINAL,NLITS,NBFREF,DUM,
     2DPM,BETA,BEEPR,EIGEN,NIT,NITP,NUMPT,DIFCO
      LEVEL 2,C5
      WRITE(2,105)NE3,NE4,NE5,(NT3(I),UT3(I),I=1,NE3)
      WRITE(2,106)(NT4(I),(HT4(I,J),J=1,4),KT4(I),I=1,NE4)
      WRITE(2,107)(NT5(I,1),NT5(I,2),I=1,NE5)
  105 FORMAT(///3I15///(I6,1PE15.7))
  106 FORMAT(///(I6,4F10.6,I6))
  107 FORMAT(///(2I6))
      END


      SUBROUTINE USER2
      STOP
      END
```

```
      SUBROUTINE GETCO(X,Y,HL,N,KODE,COFFT,JEQU)
      COMMON DUMMY,DX,DY
      DIMENSION HL(4),COFFT(5),DUMMY(/028)
      LEVEL 2,DUMMY,KODE,JEQU
C INTERIOR POINTS HAVE CODE 200
CPOINTS AT BOUNDARY ONE HAVE CODE 201
C POINTS AT BOUNDARY TWO HAVE CODE 203
CPOINTS AT Z AXIS HAVE CODE 205
C POINT(II,JJ)HAS CODE 202
CPOINT(1,JJ)HAS CODE 204
C INITIAL VALUES OF FILM PRESSURES
      AP=0.0
      BP=0.0
      CP=-0.635/(20.0*DX)/10.0
      DP=0.635/10.0
C G BARS/10  (N/MM**2)
      G=0.7
C EQUATION OF W
      IF(KODE-200)100,300,100
  300 CKAY=(2.0/DX+(HL(3)-HL(1))/X)/(HL(1)*HL(3)*DX)+
     12.0/(HL(2)*HL(4)*DY**2)
      COFFT(1)=((2.0/DX+HL(3)/X)/(HL(1)*(HL(1)+HL(3))*DX))/CKAY
      COFFT(2)=(2.0/(HL(2)*(HL(2)+HL(4))*DY**2))/CKAY
      COFFT(3)=((2.0/DX-HL(1)/X)/(HL(3)*(HL(1)+HL(3))*DX))/CKAY
      COFFT(4)=(2.0/(HL(4)*(HL(2)+HL(4))*DY**2))/CKAY
      COFFT(5)=0.0
      RETURN
C BOUNDARY ONE OF W
  100 IF(KODE-201)110,400,110
  400 CKAY=2.0/(HL(3)*DX)**2+2.0/(HL(2)*HL(4)*DY**2)
      COFFT(1)=0.0
      COFFT(2)=(2.0/(HL(2)*(HL(2)+HL(4))*DY**2))/CKAY
      COFFT(3)=(2.0/(HL(3)*DX)**2)/CKAY
      COFFT(4)=(2.0/(HL(4)*(HL(2)+HL(4))*DY**2))/CKAY
      COFFT(5)=0.0
      RETURN
C POINT(II,JJ)
  110 IF(KODE-202)120,340,120
  340 CKAY=2.0/(HL(3)*DX)**2+2.0/(HL(4)*DY)**2
      COFFT(1)=0.0
      COFFT(2)=0.0
      COFFT(3)=(2.0/(HL(3)*DX)**2)/CKAY
      COFFT(4)=(2.0/(HL(4)*DY)**2)/CKAY
      COFFT(5)=0.0
      RETURN
C BOUNDARY TWO OF W
  120 IF(KODE-203)130,380,130
  380 CKAY=(2.0/DX+(HL(3)-HL(1))/X)/(HL(1)*HL(3)*DX)+
     12.0/(HL(4)*DY)**2
      COFFT(1)=((2.0/DX+HL(3)/X)/(HL(1)*(HL(1)+HL(3))*DX))/CKAY
      COFFT(2)=0.0
      COFFT(3)=((2.0/DX-HL(1)/X)/(HL(3)*(HL(1)+HL(3))*DX))/CKAY
      COFFT(4)=(2.0/(HL(4)*DY)**2)/CKAY
      PG=AP*X**3+BP*X**2+CP*X+DP
      COFFT(5)=(-1.0)*PG/(G*HL(4)*DY)/CKAY
      RETURN
C POINT(1,JJ)
```

```
  130 IF(KODE-204)140,320,140
  320 CKAY=2.0/(HL(1)*DX)**2+2.0/(HL(4)*DY)**2
      COEFT(1)=(2.0/(HL(1)*DX)**2)/CKAY
      COEFT(2)=0.0
      COEFT(3)=0.0
      COEFT(4)=(2.0/(HL(4)*DY)**2)/CKAY
      PG=0.035/10.0
      COEFT(5)=(-1.0)*PG/(G*HL(4)*DY)/CKAY
      RETURN
C BOUNDARY THREE OF W
  140 IF(KODE-205)410,360,410
  360 CKAY=2.0/(HL(1)*DX)**2+2.0/(HL(2)*HL(4)*DY**2)
      COEFT(1)=(2.0/(HL(1)*DX)**2)/CKAY
      COEFT(2)=(2.0/(HL(2)*(HL(2)+HL(4))*DY**2))/CKAY
      COEFT(3)=0.0
      COEFT(4)=(2.0/(HL(4)*(HL(2)+HL(4))*DY**2))/CKAY
      COEFT(5)=0.0
      RETURN
C BOUNDARY FOUR W=0.0
  410 WRITE(2,420)M,KODE
      STOP
  420 FORMAT(7H0 POINT,I5,26H HAS UNDEFINED CODE NUMBER,I5)
      END
```

2. Calculating radial displacements u

```
      PROGRAM SON(INPUT,OUTPUT,RES,TAPE1=INPUT,
     1TAPE2=OUTPUT,TAPE4=RES)
      WRITE(2,100)
  100 FORMAT(13H ENTERING SON)
      CALL EPDE1
      STOP
      END



      SUBROUTINE USER1
      DIMENSION DUM(9)
      DIMENSION NT3(780),UT3(780),NT4(780),HT4(780,4),KT4(780),
     1NT5(390,2),UMAT(3250),NUMPT(2900),DIFCO(2900,5),P(12)
      COMMON C5,C95,NT3,UT3,NT4,HT4,KT4,NT5,NE3,NE4,NE5,NC,NR,KODBAS,
     1DX,DY,JOBNUM,UMAT,NEQU,NPIA,EWANT,BFINAL,NLITS,NBFREF,DUM,
     2OPM,BETA,BLEPR,EIGEN,NIT,NITP,NUMPT,DIFCO
      LEVEL 2,C5
      WRITE(2,105)NE3,NE4,NE5,(NT3(I),UT3(I),I=1,NE3)
      WRITE(2,106)(NT4(I),(HT4(I,J),J=1,4),KT4(I),I=1,NE4)
      WRITE(2,107)(NT5(I,1),NT5(I,2),I=1,NE5)
  105 FORMAT(///3115///(16,1PE15.7))
  106 FORMAT(///(I6,4F10.6,I6))
  107 FORMAT(///(2I6))
      END



      SUBROUTINE USER2
      STOP
      END
```

```
      SUBROUTINE GETCO(X,Y,HL,M,KODE,COFFT,JEQU)
      COMMON DUMMY,DX,DY
      DIMENSION HL(4),COFFT(5),DUMMY(7028)
      LLVEL 2,DUMMY,KODE,JEQU
C INTERIOR POINTS HAVE CODE 300
CPOINTS AT BOUNDARY ONE HAVE CODE 301
C POINTS AT BOUNDARY TWO HAVE CODE 303
C POINT(II,JJ)HAS CODE 302
      B3=0.000001603
      B2=-0.000159935
      B1=-0.00322589
C EQUATION OF U
      IF(KODE-300)510,500,510
  500 CKAY=(2.0/DX+(HL(3)-HL(1))/X)/(HL(1)*HL(3)*DX)+
     12.0/(HL(2)*HL(4)*DX**2)+1.0/X**2
      COFFT(1)=(2.0/DX+HL(3)/X)/(HL(1)*(HL(1)+HL(3))*DX)/CKAY
      COFFT(2)=2.0/(HL(2)*(HL(2)+HL(4))*DY**2)/CKAY
      COFFT(3)=(2.0/DX-HL(1)/X)/(HL(3)*(HL(1)+HL(3))*DX)/CKAY
      COFFT(4)=(2.0/(HL(4)*(HL(2)+HL(4))*DY**2))/CKAY
      COFFT(5)=0.0
      RETURN
C BOUNDARY ONE OF U
  510 IF(KODE-301)520,600,520
  600 CKAY=2.0/(HL(3)*DX)**2+2.0/(HL(2)*HL(4)*DY**2)+1.0/X**2
      COFFT(1)=0.0
      COFFT(2)=2.0/(HL(2)*(HL(2)+HL(4))*DY**2)/CKAY
      COFFT(3)=2.0/(HL(3)*DX)**2/CKAY
      COFFT(4)=2.0/(HL(4)*(HL(2)+HL(4))*DY**2)/CKAY
      COFFT(5)=0.0
      RETURN
C BOUNDARY TWO OF U
  520 IF(KODE-303)530,700,530
  700 CKAY=2.0/(HL(1)*HL(3)*DX**2)+2.0/(HL(4)*DY)**2+
     1(HL(3)-HL(1))/(HL(1)*HL(3)*DX)+1.0/X**2
      COFFT(1)=(2.0/DX+HL(3)/X)/(HL(1)*(HL(1)+HL(3))*DX)/CKAY
      COFFT(2)=0.0
      COFFT(3)=(2.0/DX-HL(1)/X)/(HL(3)*(HL(1)+HL(3))*DX)/CKAY
      COFFT(4)=2.0/(HL(4)*DY)**2/CKAY
      DEW=3.0*B3*X**2+2.0*B2*X+B1
      COFFT(5)=(-2.0*DEW/(HL(4)*DY))/CKAY
      RETURN
C BOUNDARY THREE U=0
C BOUNDARY FOUR U=0
C POINT(II,JJ)
  530 IF(KODE-302)540,800,540
  800 CKAY=2.0/(HL(3)*DX)**2+2.0/(HL(4)*DY)**2+1.0/X**2
      COFFT(1)=0.0
      COFFT(2)=0.0
      COFFT(3)=(2.0/(HL(3)*DX)**2)/CKAY
      COFFT(4)=(2.0/(HL(4)*DY)**2)/CKAY
      DEW=3.0*B3*X**2+2.0*B2*X+B1
      COFFT(5)=(-2.0*DEW/(HL(4)*DY))/CKAY
      RETURN
  540 WRITE(2,550)M,KODE
      STOP
  550 FORMAT(7H0 POINT,I5,26H HAS UNDEFINED CODE NUMBER,I5)
      END
```

3. Reynolds equation

```
DIM W[21],R[21],B[21],P[21],F[21]
REM FILE 12 REYNOLDS EQUATION
REM F PRES SQUARED,W AXIAL DISP
D=3.175
H=0.025
REM READING PRESSURES
FOR I=2 TO 8
READ P[I]
F[I]=P[I]*P[I]
 NEXT I
 FOR I=9 TO 15
 READ P[I]
 F[I]=P[I]*P[I]
 NEXT I
 FOR I=16 TO 20
 READ P[I]
 F[I]=P[I]*P[I]
 NEXT I
 P[1]=P[2]
 P[21]=0
 F[1]=F[2]
 F[21]=0
 REM READING DISPLACEMENTS
 FOR I=1 TO 7
 READ W[I]
 NEXT I
 FOR I=8 TO 14
 READ W[I]
 NEXT I
 FOR I=15 TO 21
 READ W[I]
 NEXT I
 FOR I=2 TO 20
 R[I]=D*(I-1)
 B[I]=3*(W[I+1]-W[I-1])/((H+W[I])*2*D)+1/R[I]
 F[I]=F[I+1]*(1+B[I]*D/2)/2+F[I-1]*(1-B[I]*D/2)/2
 P[I]=SQR(F[I])
 PRINT "P=";P[I]
 NEXT I
 P[1]=P[2]
 P[21]=0
 REMDATA FOR PRESSURES
 DATA 0.060325,0.05715,0.053975,0.0508,0.047625,0.04445,0.041275
 DATA 0.0381,0.034925,0.03175,0.028575,0.0254,0.022225,0.01905
 DATA 0.015875,0.0127,0.009525,0.00635,0.003175
 REM DATA FOR DISPLACEMENTS
 DATA 0.484041,0.473262,0.459228,0.441572,0.421242,0.398965,0.3752
 DATA 0.350552,0.325097,0.299138,0.272864,0.246449,0.22007,0.19392
 DATA 0.168239,0.143341,0.119667,0.09785,0.07883,0.064101,0.05645
 STOP
 END
```

LIST OF REFERENCES

GENERAL

1. O. Pinkus and B. Sternlicht, "Theory of Hydrodynamic Lubrication", McGraw Hill, New York, 1961.

2. M.D. Hersey, "Theory and Research in Lubrication", John Wiley & Sons Inc., New York, 1966.

3. F.P. Bowden and D. Tabor, "Friction and Lubrication", Methuen and Co. Ltd., London 1967.

4. B.S. 1134, "Method for the Assessment of Surface Texture", British Standards Institution, 1972

5. P. Anderton and P.H. Bigg, "Changing to the Metric System", National Physical Laboratory, Her Majesty's Stationery Office, London 1972.

6. B. Tower, "First and Second Report on Friction Experiments", Proc. I. Mech.E. 1883, pp. 632-659
1884, pp. 29-35
1885, pp. 58-70

7. K. Rektorys, "Survey of Applicable Mathematics", Iliffe Books Ltd. 1969.

8. D. Dowson, G.R. Higginson, "Elasto-Hydrodynamic Lubrication", Pergamon Press, Oxford, 1966.

9. P. Freeman, "Lubrication and Friction", Pitman, London, 1962.

10. C.M.M. Ettles, "A Comparison of some Instrumentation Methods for Hydrodynamic Bearings, "Proc. I. Mech. E., Vol. 182, 1967, pp. 53-55.

11. Wilhelm Flügge, "Viscoelasticity", Waltham, Massachusetts, 1967.

12. H. Hertz, "Miscellaneous Papers", Macmillan, London, 1896.

13. M. Neale, "Tribology Handbook", Butterworths, 1973.

14. I.N. Sneddon, "Fourier Transforms", McGraw-Hill, New York, 1951.

15. J.H. Michell, Proceedings of the London Mathematical Society, Vol. 31, 1899, p.100.

16. Machinery's Handbook (16th Edition), New York, 1959.

17. S.J. Peerless, "Basic Fluid Mechanics", Pergamon Press, 1967.

18. G.E. Forsythe and W.R. Wasow, "Finite Difference Methods for Partial Differential Equations", Wiley, 1960.

LIST OF REFERENCES

RIGID BEARINGS

101 D.D. Fuller, "Theory and Practice of Lubrication for Engineers", John Wiley and Sons Inc., New York, 1956.

102 R.C. Elwell and B. Sternlicht, "Theoretical and Experimental Analysis of Hydrostatic Thrust Bearings", Trans. ASME, Series D, Vol. 82, 1960, pp. 505-512.

103 R. Comolet, "Ecoulement d'un fluide entre deux plans parallèles. Contribution à l'étude des butées d'air", Service de documentation et d'information technique de l'aéronautique, Paris 1957.

104 I.C. Tang and W.A. Gross, "Analysis and Design of Externally Pressurized Gas Bearings", Trans. ASLE, Vol. 5, 1962, pp. 261-284.

105 B.J. Powell, M.H. Moye and P.R. Dwight, "Fundamental Theory and Experiments on Hydrostatic Air Bearings", Inst. Mech. Engrs., Lubrication and Wear Convention, 1963.

106 N.S. Grassom and J.W. Powell (Editors), "Gas Lubricated Bearings", Butterworths, London 1964.

107 J.W. Powell, "The Design of Aerostatic Bearings", The Machinery Publishing Co. Ltd., London 1970.

108 W.A. Gross, "Gas Film Lubrication", McGraw-Hill, New York, 1962.

109 Various Authors, "Design of Gas Bearings", Mechanical Technology Incorporated, New York, 1972.

110 I.R.G. Lowe, "A Study of Flow Phenomena in Externally Pressurized Gas Thrust Bearings", National Research Council of Canada, NRC, DME MT-61, 1970.

111 E.H. Dudgeon, "Performance Factors for Circular, Hydrostatic, Gas-lubricated, Thrust Bearings", National Research Council of Canada, NRC, DME MT-62, 1970.

112 E.H. Dudgeon and I.R.G. Lowe, "An Investigation of Centrally-fed, Circular, Inherently Compensated, Aerostatic, Thrust Bearings", paper 5, Gas Bearing Symposium, University of Southampton, 1971.

113 I.C. Tang, "Inertia Effects of Air in an Externally Pressurized Gas Bearing", Acta Mechanica, 5, 71-82 (1968)

114 H. Mori, "A Theoretical Investigation of Pressure Depression in Externally Pressurized Gas-Lubricated Circular Thrust Bearings", Trans. ASME, SERIES D, vol. 83, 1961, pp.201-208

115 H. Mori & Y. Miyamatsu, "Theoretical Flow Models for Externally Pressurized Gas Bearings", Trans. ASME, SERIES F, vol. 91, 1969, pp.181-193.

116 M. Poupard and G. Druin, "Theoretical and Experimental Pressure Distribution in Supersonic Domain for an Inherently Compensated Circular Thrust Bearing", Trans. ASME, series F, vol. 95, 1973, pp. 217-221.

117 H.G. Elrod and T.Y. Chu, "Inertia and Energy Effects in the Developing Gas Film between two Parallel Flat Plates", Trans. ASME, Series F, vol. 95, 1973, pp. 524-534.

118 D. Dowson, "Inertia Effects in Hydrostatic Thrust Bearings", Trans. ASME, series D, vol.83, 1961, pp. 227-234.

119 J.A. Coombs and D. Dowson, "An Experimental Investigation of the Effects Lubricant Inertia in a Hydrostatic Thrust Bearing", Proc. I.Mech.E., vol. 179, 1965, pp. 96-108.

120 E. Makay and R.R. Trumpler, "Inertia Effects in Fully Developed Axisymmetric Laminar Flow" Trans. ASME, series F, Vol. 93, July 1971, pp.408-414

121 G.K. Lewis, "The Steady-State Performance of Hydrostatic Oil Bearings", Technical Note, The University of Aston in Birmingham, 1967.

122 M.T.S. Ling, "On the Optimization of the Stiffness of Externally Pressurized Bearings", Trans. ASME, series D, vol. 84, 1962, pp.119-122.

123 S.B. Malonoski, A.M. Loeb, "The Effect of the Method of Compensation on Hydrostatic Bearing Stiffness", Trans. ASME, series D, vol. 83, 1961, pp. 179-187.

124 G.K. Lewis and J.C. Scouller, "Stiffness of Self-Compensated Hydrostatic Bearing Systems" Instn. Mech. Engrs. 1971.

125 H.L. Wunsch and C.A. Scoles, "Automatic load-compensation device for air bearings" NEL report No. 86, 1963.

126 G.T.F. Kilmister, "A Self-Compensating Flow Restrictor for Externally-Pressurized Bearings", paper 17, Gas Bearing Symposium, University of Southampton, 1971.

127 B.C. Majumdar and S. Ramchamdran, "Aerostatic Thrust Bearing using simple Orifice Restrictor", I.E. (I) Journal - ME, vol. 52, Nov. 1971.

128 G.K. Lewis and J.P. O'Donoghue, "Tapered Land Hydrostatic Oil Bearing", Tribology, Jan. 1968.

129 R.B. Howorth, "Effects of Tilt on the Performance of Hydrostatic Thrust Pads", Proc. I. Mech.E., vol. 185, 1971, pp. 717-723 + D. 285 - D 286.

130 M.E. Saloma, "The Effect of Macro-roughness on the Performance of Parallel Thrust Bearings", Proc. I. Mech.E., vol. 163, 1950, pp.149-161.

131 W. Bailey, "The Tribology of Precision Machines", Tribology Inrernational, volume 8, number 2, April 1975, pp. 73-76.

132 H. Christensen, "A Theory of Mixed Lubrication", Proc. I. Mech. E., vol. 186, 1972, pp. 421-430.

133 K. Tønder, H. Christensen, "Waviness and Roughness in Hydrodynamic Lubrication".
Proc. I. Mech. E., vol.186, 1972, pp 807-812

134 R.A. Burton, "Effect of Two-dimensional, Sinusoidal Roughness on the Load Support Characteristics of a Lubricant Film" Trans. ASME, series D, vol. 85, June 1963, pp. 258-264.

135 S.T. Tseng and E. Saibel, "Surface Roughness Effect on Slider Bearing Lubrication", Trans. ASLE vol. 10, 1967 pp. 334-338.

136 Christensen, H. and K Tønder, "The Hydrodynamic Lubrication of Rough Journal Bearings", Trans. ASME, series F, vol. 95, 1973, pp. 166-172.

137 Castelli, V. and Pirvics, J., "Equilibrium Characteristics of Axial Grooved Gas Lubricated Bearings", Trans. ASME, series F, vol. 89, 1967, pp. 177-196.

138 V. Castelli and J. Pirvics, "Review of Numerical Methods in Gas Bearing Film Analysis", Trans. ASME, series F, vol. 90, 1968, pp.777-803.

139 G.K. Lewis and R. Taylor, "Steady-state Solutions for an Aerostatic Thrust Bearing with an Elastic Porous Pad", paper C5, Gas Bearing Symposium, University of Southampton 1974.

140 B.D. Hobson and J.M. Lowrie, "A Method of Analysing the Effect of Inertia and Compressibility in an Externally Pressurized Gas Lubricated Thrust Bearing", Externally Pressurized Bearings, I.Mech. E., I Prod. E. 1971, pp. 368-381.

141 R. Taylor, Ph.D. Thesis, 1975, University of Aston.

142 R. Taylor, G.K. Lewis- "Experience Relating to the Steady Peformance of Aerostatic Porous Thrust Bearings", Proc. Instn. Mech. Engrs. Vol. 189, pp. 383-390, 1975.

143 D. Dowson, C.M. Taylor, "Turbulent Lubrication Theory - Application to Design", Trans. ASME, series F, pp. 36-47, Jan. 1974.

144 E. Dudgeon and I.R.G. Lowe, "A Simplified Method for the Design of Externally Pressurized Gas Lubricated Thrust Bearings, Transactions of the C.S.M.E., Vol. 1, No. 4, 1972, pp. 205-212.

LIST OF REFERENCES

COMPLIANT BEARINGS

201 D. Dowson and C.M. Taylor, "Elastohydrostatic Lubrication of Curcular Plate Thrust Bearings", Trans. ASME, series F, vol. 89, 1967, pp.237-244.

202 V. Castelli, G.K. Rightmire, D.D. Fuller, "On the Analytical and Experimental Investigation of a Hydrostatic Axisymmetric Compliant-Surface Thrust Bearing", Trans. ASME, vol. 89, 1967, pp. 510-520.

203 M.K. Benjamin, "Compliant Surface Bearings - An Analytic Investigation", Columbia University Lub. Res. Lab. Report No. 15, 1969.

204 M.K. Benjamin, V. Castelli, "A Theoretical Investigation of Compliant Surface Journal Bearings", Trans. ASME, series F, vol. 93, 1971, pp. 191-201.

205 M.K. Benjamin, G.K. Rightmire and V. Castelli, "Compliant-Surface, Fluid Film Bearings: Theory and Experiment for the Circular-Face Thrust-bearing, and Theory for the Journal Bearing", Rev. Roum. Sci. Techn. - Mec. Appl. Tome 16, No. 2, Bucarest, 1971, pp.427-458.

206 J. Pirvics and V. Castelli, "Characteristics of the Elastohydrostatic Gas Lubricated Axisymmetric Thrust Bearing", Columbia University Lub. Res. Lab. Report No. 8, 1966.

207 V. Castelli, G.K. Rightmire, M.K. Benjamin, D.D. Fuller, "Design Guide for Hydrostatic Axisymmetric Compliant-Surface Thrust Bearings", Columbia University Lub. Res. Lab. Report No. 16, 1969.

208 J. Pirvics and V. Castelli, "Elastomer Inertia Effects in Compliant Surface Bearings", Trans. ASME, series F, vol. 95, 1973, pp. 372-380.

209 J. Pirvics and V. Castelli, "Elastomer Viscoelasticity Effects in Compliant Surface Bearings", Trans. ASME, series F, vol. 95, 1973, pp. 363-371.

210 I.R.G. Lowe, "Characteristics of Externally Pressurized Thrust Bearings with one Compliant Surface", paper A4, 6th International Gas Bearing Symposium, University of Southampton, 1974.

211 I.R.G. Lowe, "Some Experimental Results from Compliant Air Lubricated Thrust Bearings", Trans. ASME, series F, vol. 96, 1974, pp. 547-553 and 560.

212 H. Lau and C.M. Harman, "Externally Pressurized Compliant Air Bearing Operating on a Rough Moving Surface", Trans. ASME, series F, vol. 97, 1975, pp. 63-68.

213 R.L. Smith and S.J. Calabrese, "Development Studies on Utilising the Self-Caging Spherical Bearing for Directional Gyroscopes", Report MTI-71TR 39, Mechanical Technology Inc., New York, 1971.

214 R.L. Smith and P.K. Gupta, "Development of Compliant Bearing Designs for Directional Control Gyroscope, " Report AD-762036, Mechanical Technology Inc., New York, 1973.

215 W.J.Anderson, "Analysis of an All-Metallic Resilient Pad Gas-Lubricated Thrust Bearing", Trans. ASME, Series F, vol. 97, 1975, pp.296-302

216 C. Dayson, "Flexible Stepped Thrust Bearings", Trans. ASLE, vol. 16, 1973, pp. 32-41

217 W.E. Schmidt, "Design, Testing and Performance of Elastomeric Bearings", preprint No. 883, American Helicopter Society, 30 East 42nd Street, New York, N.Y. 10017.

218 G.R. Higginson, "The Theoretical Effects of Elastic Deformation of the Bearing Liner on Journal Bearing Performance", Proc. Instn. Mech. Engrs. 1965-66, vol. 180, pp. 31-38.

219 P.K. Gupta, "Incipient Lift-off in Preloaded Plane Externally-Pressurized Compliant Surface Bearings", Proc. Instn. Mech. Engrs. vol. 188 42/74, pp. 447-455.

220 P. Meijers, "The Contact Problem of a Rigid Cylinder on an Elastic Layer", Appl. Sci. Res., Feb. 1968, pp. 353-383.

221 W.H. Kinsman, "Stesses in a Thin Disc subjected to Lateral Pressure" - private communication.

LIST OF REFERENCES

ELASTOMER PROPERTIES

301 S.P. Timoshenko and J.N. Goodier, "Theory of Elasticity", third edition, McGraw-Hill Book Company, Tokyo, 1970.

302 Y.C. Fung, "A First Course in Continuum Mechanics", Prentice-Hall, Inc., Englewood Cliffs, N.J. 1969.

303 K. Marguerre, "Ansätze zur Lösung der Grundgleichungen der Elastizitätstheorie", Z. angew. Math. Mech. Bd. 35 Nr. 6/7 Juni/Juli 1955, pp. 242-263.

304 W.W. Vogt and R.D. Evans, "Poisson's Ratio and Related Properties for Compounded Rubber", Industrial and Engineering Chemistry, 1923, pp. 1015-1018.

305 G.K. Rightmire, "An Experimental Method for Determining Poisson's Ratio of Elastomers", Trans. ASME, series F, vol. 92, pp. 381-388.

306 A.B. Davey and A.R. Payne, "An Introductory Survey of Rubber", Engineering Materials and Design, 1964, pp. 376-382 and 465-467.

307 P.B. Lindley, "Engineering Design with Natural Rubber", NR Technical Bulletin, 1970, Published by the Natural Rubber Producers' Research Association.

308 Various Authors, edited by L.R. Mernagh, "Rubbers Handbook", Morgan-Grampian (Publishers) Ltd., London, 1969.

309 British Standard BS903 - Methods of Testing Vulcanized Rubber (Parts A2, A4, A24, A26)

310 American Society for Testing Materials Standards ASTM (part 28)

311 R.C. Drutowski, "Contact Elasticity of Seal Elastomers", Trans. ASME, series F, vol. 1968, pp. 478-483.

312 E.F. Finkin, "The Determination of Young's Modulus from the Indentation of Rubber Sheets by Spherically Tipped Indentors", Wear, vol. 19, 1972, pp. 277-286.

313 Y.C. Fung, "Foundations of Solid Mechanics", Prentice-Hall, Inc., Englewood Cliffs, New Jersey, 1965.

314 I.S. Sokolnikoff, "Mathematical Theory of Elasticity", McGraw-Hill, New York 1956.

315 T.H. Richards, "Solid Mechanics" - M.Sc. Course Notes, University of Aston, 1973.

316 W. Edwards (Mrs.), "Dynamic Behaviour of Composite Structures Containing Viscoelastic Materials with Applications to Solid Fuel Rocket Motors", Ph.D. Thesis, University of Aston, 1975.

317 L.R. Hermann, "Elasticity Equations for Incompressible and Nearly Incompressible Materials by a Variational Theorem", AIAA Journal, Vol. 3, No. 10, October 1965, pp. 1896-1900.